2018

Master of Science Thesis

Numerical assessment of preloading strategies for jack-up vessels in cohesive soils

Joep Fila

TU Delft

Van Oord
Marine ingenuity

Numerical assessment of preloading strategies for jack-up vessels in cohesive soils

By

Joep Fila
Student number: 4141393

In partial fulfilment of the requirements for the degree of

Master of Science
In Geo-Engineering

At the Delft University of Technology,
to be defended on April 17, 2018.

Thesis Committee

Dr.ir. F. Pisanò	Offshore Engineering	TU Delft (chair)
Dr.ir. W. Broere	Geo-Engineering	TU Delft
Prof.dr. K.G. Gavin	Geo-Engineering	TU Delft
Ir. S. Brinkman	Geotechnical Engineer	Van Oord
Ir. G. Dantuma	Geotechnical Engineer	Van Oord

Table of Contents

Acknowledgements

I would like to express my gratitude to the people who have supported me throughout this thesis work.

First of all, the members of my graduation committee. I would like to thank Federico Pisanò, my daily university supervisor for his continuous support, patience, helpful discussions and the valuable feedback he provided. He always found time to answer all of my questions. Many thanks to my second university supervisor Wout Broere for his valuable input during the meetings.

I would like to thank my company supervisors, Sanne Brinkman and Gerrit Dantuma, for the thesis opportunity, motivation, critical reviews and their enthusiasm during my time at Van Oord. I gained much practical experience and improved my knowledge on (offshore) soil behaviour.

Finally, I would like to express my very gratitude to my parents and to my girlfriend for providing me with unfailing support and continuous encouragement throughout my years of study and through the process of researching and writing this thesis. This accomplishment would not have been possible without them. Thank you.

Joep Fila

Summary

As the demand for renewable energy is constantly rising, more offshore wind farms are being built at sea to meet European targets towards sustainable energy transition. Van Oord's offshore installation vessel Aeolus was purposely-built to transport and install foundations of offshore wind turbines. To ensure that the vessel remains competitive in a market that is changing rapidly, Van Oord decided to upgrade this vessel to expand its operational capabilities to work on soft soil seabed conditions.

Equipped with moveable legs, the mobile jack-up vessel is able to elevate its hull out of the water and provide a stable work platform. Prior to each installation, the soil is preloaded by penetrating the spudcan footings into the soil under the self-weight of the structure, followed by progressively pumping sea water into the ballast tanks until the target preload is reached. Offshore industry guidelines follow the conventional bearing capacity theory to assess jack-up procedures. However, these conventional procedures are inadequate in incorporating all relevant mechanisms that contribute to the preloading behaviour in cohesive soils. The effect of consolidation around the spudcan footings on the soil strength and the viscous strain rate-dependent soil strength are two important aspects which are poorly described in the current guidelines. Using numerical modelling, a better understanding of these mechanisms is aimed for in order to evaluate spudcan bearing capacity in cohesive soils in a more detailed design.

An axisymmetric finite element model of the spudcan foundation is constructed in PLAXIS 2D to assess the effects of consolidation and rate-dependence of soil strength on the use of different preloading strategies. As spudcan penetration is relatively fast and clay permeability is relatively low, consolidation effects are found to be insignificant during the preloading process. Contrary, viscous strain rate effects dominate the soil strength of clay in predominantly undrained conditions. Higher shear strengths are found for higher spudcan penetration rates. During the standard jacking process, when the target preload value is reached and the spudcan is stopped, a reduction of the leg load occurs due to decreasing viscous resistances, which must actively be brought back to the target preload value. In clay soils, this leads to further penetrations and multiple preload cycles are required before the spudcan response is stabilised. In terms of preloading duration, a rather slow spudcan penetration rate is therefore beneficial when using the standard jacking procedure.

Alternatively, a different jacking procedure is assessed numerically, which adapts for these viscous strain rate effects by overshooting the target preload value by 10-15%, in order to reach the stable spudcan response more quickly. In this way, the spudcan is brought to the depth, which would have been reached by the creep-like additional penetrations in the iterative preload cycles under the target preload value. Once the load is reduced from the overshoot to the target preload value, it is likely that the preload can be sustained without additional penetrations and preload cycles. The overshooting jacking procedure reduces the required preloading time considerably for both spudcan penetration rates. The largest time savings are gained for the largest penetration rates. However, using this method, larger leg penetration predictions compared to the standard jacking procedure are observed for decreasing spudcan penetration rates. That is because in the standard jacking procedure, less creep-like additional penetrations are present when using a slow spudcan penetration rate. The overshooting jacking procedure can thus be considered beneficial for relatively fast spudcan penetration rates, both in term of preloading duration and spudcan penetrations.

Abbreviations

B_{BD}	Bottom Boundary Distance
BD	Boundary Distance
CLS	Critical State Line
CPT	Cone Penetration Test
CPTu	Cone Penetration Test with pore pressure sensors (piezocone)
CS	Critical State
DC	Displacement-Controlled
EOP	End of Primary
EP	Elastic Plastic
ESP	Effective Stress Path
EVP	Elastic viscoplastic
FE	Finite Element
ISO	International Standard Organisation
JIP	Joint Industry-funded Project
L_{BD}	Lateral Boundary Distance
LC	Load-Controlled
LDFE	Large Deformation Finite Element
MC	Mohr-Coulomb
MCC	Modified Cam-Clay model
NC	Normally Consolidated
OC	Overconsolidated
OCR	Overconsolidation ratio
PR	Press-Replace
PSD	Particle Size Distribution
SHANSEP	Stress History and Normalised Soil Engineering Properties
SNAME	The Society of Naval Architects and Marine Engineers
SSA	Site Specific Assessment
SSC	Soft Soil Creep model
SSFE	Small Strain Finite Element
SSF-SBD	Surface Sand Formation – Seabed Depression Member
WIP	Wished-In-Place
WIS-MF	Western Irish Sea Formation – Mud Facies

1. Introduction

1.1 Problem description

Mobile jack-up vessels are widely used for installation of foundations and turbines during the construction of offshore wind farms. Equipped with moveable legs, these vessels are able to elevate their hull out of the water and provide a stable work platform. Since each location offers a new set of unique conditions, a site specific assessment (SSA) is required prior to each mobilisation. The SSA will identify any potential problems related to foundation conditions during installation, operation and extraction. During preloading, the legs are pushed into the ground until a stable condition is reached to execute the installation of the wind turbine. Preloading is aimed at subjecting the seabed to a significantly higher load than design storm load conditions to ensure that the soil resistance is sufficient to resist the maximum design loads during operational and survival conditions. The time required to complete the preload process is referred to as the preload duration.

The preloading duration is important for determining the total required installation time of offshore wind turbine foundations. Since the installation vessel can carry only a limited amount of material and needs to sail back and forth to the harbour to pick up new wind farm elements, the preloading duration is therefore essential in planning and cost estimation of the total project. In cohesionless materials like sand, preloading is relatively fast, in the order of one hour (Van Oord, 2017). Cohesive soils, which contain silt and clay, behave much different from cohesionless materials and are expected to require a longer preloading time.

Van Oord's offshore installation vessel Aeolus was purposely-built to construct wind parks at sea. Four giant legs, called spuds, with spudcan footings underneath to spread the load, allows the Aeolus to be jacked-up and provide a stable platform for the installation activities. Preloading is performed by lowering the legs to the seafloor and loading alternately diagonally opposing leg pairs by pumping water ballast on board in order to ensure that adequate bearing capacity is achieved. The preloading process is represented in figure 1.1. At point 1, the active leg pair (blue) is loaded until a predefined target preload value by releasing the weight on the opposite, passive leg pair (red). As the active leg pair penetrates into the soil, the complete vessel moves downwards until the passive leg pair starts taking over load from the active leg pair. During phase 1-2, reloading and load transfer continues in several cycles until a certain preload criterion is achieved. In this thesis, a preload criterion of 400 ton load reduction per 15 minutes is assumed. After this, the active and passive leg pairs are switched (phase 2-3) before starting the preloading cycles of the other leg pair (phase 3-4). After completion of the preload, the loads on all four legs are equalised and the deck can be safely raised.

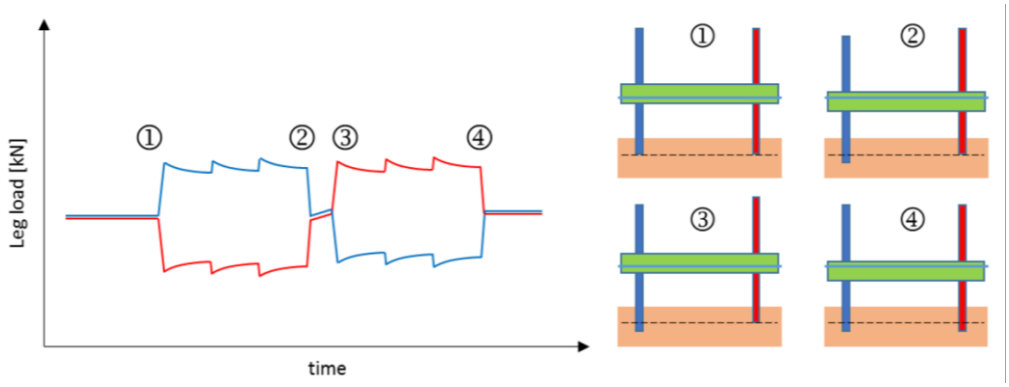

Figure 1.1 Preloading procedure (Cathie et al., 2017)

The offshore industry has published guidelines for site specific assessment of mobile jack-up units (SNAME, 2008), developed prediction guidelines for geotechnical performance of spudcan foundations during installation and removal of jack-up units (InSafeJIP, 2011) and the International Standard Organization has published ISO19905-1 (2012) in order to standardise jack-up assessment procedures. These guidelines adapt the framework for onshore application following conventional bearing capacity theory to assess spudcan penetration depth.

However, the conventional procedures described in the guidelines are inadequate in incorporating all relevant mechanisms that contribute to the preload time in cohesive soils. The effect of consolidation on the soil strength occurring during the preloading cycles and viscous strain rate effects as a result of spudcan penetration are two important aspects which are poorly described. Using numerical modelling, a better understanding of these mechanisms is aimed for in order to evaluate spudcan bearing capacity in soft soils in a more detailed design.

Offshore Wind farm project

Because the demand for renewable energy is rising constantly and onshore space is limited, more wind farms are being built at sea. Van Oord has been involved in many offshore wind projects in northwestern Europe during the past decade. Currently, an offshore wind project in the Irish Sea is being completed in order to deliver sustainable energy to approximately half a million extra households in the United Kingdom. It will contribute to governmental targets to ensure that, by 2020, fifteen percent of the UK's energy is being produced sustainably (UK Government, 2017). The installation work started in spring 2017 and is expected to be completed in 2018.

Figure 1.2 Map of Irish Sea

Description of the Aeolus
Van Oord was awarded the contract to transport and install all wind turbine foundations at the offshore wind farm project in the Irish Sea. The foundation type of the wind turbines consist of monopiles with an expected diameter of Ø7.4m -Ø8.2m, which will be installed by the Aeolus. The offshore installation vessel Aeolus was purposely-built for the construction of wind farms. Equipped with four giant legs, each measuring 85 meters in length, the ship can be jacked-up out of the water, resulting in a self-elevated platform with a full integration of hydraulic systems for lifting the monopoles. The ship can operate in water depths up to 45 meters deep. (Van Oord, 2017)

Figure 1.3 Offshore installation vessel Aeolus in jacked-up position.

1.2 Research objectives

To assess the behaviour of cohesive soils during preloading, a numerical model is required, which incorporates all relevant mechanisms that may contribute to the preload time.

Main objective
The main objective of this research is:
Performing a numerical assessment on the effect of different preloading strategies for jack-up vessels in cohesive soils.

An axisymmetric finite element analysis in PLAXIS 2D is used to investigate the spudcan penetration process of jacked spud legs subjected to vertical loading.

Sub-objectives
The following sub-objectives are considered, which act as a framework to construct the main objective.

- Interpretation site investigation data
  Determine design soil parameters, which represent the cohesive material present at the offshore wind farm construction site.
- Constitutive modelling
  - Select a soil constitutive model, which is able to capture essential features of soft soil behaviour.
  - Describe model possibilities and limitations.
  - Calibrate model parameters against design soil parameters.
- Implementation of finite element (FE) method
  - Define domain size and boundary conditions.

    - Investigate mesh density
    - Investigate effects of interface elements
- Investigate the suitability of the Press-Replace technique for modelling spudcan penetration compared to the Wished-in-Place method.
- Further understand the relevant mechanisms that contribute to preload time in cohesive soils and implement these mechanisms in a numerical model.
    - Investigate the effects of partial consolidation on the soil strength.
    - Investigate the effects of strain rate on the soil strength

This study only investigates spudcan penetration in a homogeneous clay layer. Layered soil configurations are not considered.

This study only focusses on the performance of spudcan penetration under vertical loading conditions. Other site specific assessments as mentioned below are not considered in the current research.

- Combined vertical, horizontal and moment loading due to environmental loading conditions from wind, waves and currents.
- Sliding check; horizontal shear forces acting at the interface of footing and soil are not checked against the maximum sliding resistance.

1.3 Thesis outline

This thesis consists of five parts:

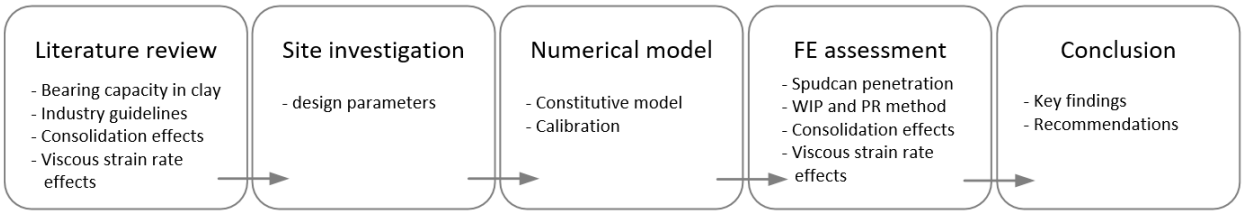

Figure 1.4 Thesis outline

The outline is structured as follows:

- In chapter 2, a literature study is presented on the different methods to determine the bearing capacity of clay. Other relevant aspects contributing to the preload time, like spudcan dimensions, consolidation and rate effects are discussed as well.
- Chapter 3 provides a geotechnical analysis of the offshore wind farm site conditions including the determination and interpretation of the design parameters used in the analytical and numerical models.
- In chapter 4, a suitable constitutive model is selected, which is able to capture essential features of soft soil behaviour. Model parameters are calibrated against the derived design parameters.
- Chapter 5 provides a FE assessment of spudcan penetration predictions on a homogeneous clay layer by comparing two modelling methods (Wished-in-Place and Press-Replace method). Additionally, a numerical investigation of partial consolidation effects and strain rate effects on the spudcan penetration resistance is performed.
- Finally, chapter 6 concludes the findings of this study and gives recommendations for future research.

2. Spudcan penetration in clay

2.1 General concept of bearing capacity

Spudcan penetration is generally predicted by considering the vertical bearing capacity of a series of 'wished-in-place' footings at different depths, from which a penetration curve can be constructed based on several independent calculations at different depths. Terzaghi (1943) published an analytical solution for the bearing capacity under a strip footing, in which the conventional failure mechanism of the sliding soil mass under the foundation is subdivided into three zones, as shown in figure 2.1. When the footing is loaded, the soil in zone I (elastic zone) is pushed down as a whole and pressed against the soil in zone II (radial shear zones), which moves outwards and upwards up to zone III (passive zone), where the horizontal stress is larger than the vertical stress. The boundary lines between these zones indicate slip planes along which shearing occurs under the foundation (Bowles, 1988).

Terzaghi (1943) extended the traditional bearing capacity theory of Prandtl (1921) by taking into account the weight of the soil and the effect of soil above the base of the foundation. Terzaghi's formula for ultimate bearing capacity is expressed in equation (2.1). The bearing capacity factors N_c, N_q and N_γ represent the contribution of cohesion, surcharge and soil unit weight to the ultimate bearing capacity, respectively. In undrained conditions ($\phi = 0$ condition), factor N_γ equals zero and hence, the bearing capacity of cohesive soils only depend on N_c and N_q, which are expressed as function of internal friction angle (ϕ). Additionally, if consolidation is taken into account in cohesive soils, excess pore water pressure will dissipate and bearing capacity is enhanced by an increase of the effective friction angle. Contrary, for cohesionless soils such as sand ($c = 0$), only N_q and N_γ are relevant for calculating the bearing capacity.

The traditional formula can be extended to account for different footing shapes, load inclinations and embedded foundations, for which several authors have proposed methods for obtaining the N-factors. Meyerhof (1963) proposed the bearing capacity equation (2.2) which includes shape, depth and inclination factors of the footing. Unlike N_c and N_q, several suggestions were made to calculate N_γ, for example by Hansen (1970) and Vesic (1975). The Vesić (1975) and Meyerhof (1963) procedure essentially uses the same method with select changes, which leads to slightly different expressions. A full overview of the different methods is given in Appendix A.

Terzaghi (1943)

$$q_u = cN_c + q'N_q + \frac{1}{2}\gamma B N_\gamma \qquad \textit{Eq. (2.1)}$$

Meyerhof (1963)

$$q_u = c \cdot s_c \cdot d_c \cdot i_c \cdot N_c + q' \cdot s_q \cdot d_q \cdot i_q \cdot N_q + \frac{1}{2} \cdot \gamma' \cdot B \cdot s_\gamma \cdot d_\gamma \cdot i_\gamma \cdot N_\gamma \qquad \textit{Eq. (2.2)}$$

In which

$c = cohesion$
$q' = effective\ overburden\ pressure$
$\gamma' = effective\ unit\ weight\ of\ soil$
$B = width\ of\ foundation$
$N_c, N_q, N_\gamma = bearing\ capacity\ factors$
$s_c, s_q, s_\gamma = shape\ factors$
$d_c, d_q, d_\gamma = depth\ factors$
$i_c, i_q, i_\gamma = load\ inclination\ factors$

The Terzaghi equation is widely used because of its simplicity, as all the extra shape, depth and other factors do not have to be computed. It is only suitable for a concentrically loaded footing on horizontal ground (on soils where $D/B \leq 1$) and can be used for a quick estimate of bearing capacity to compare with other models. It is not applicable for footings carrying moments or horizontal forces or on sloping grounds. Up to a depth of $D \approx B$, the Meyerhof solution is not greatly different from the Terzaghi value. The Hansen and Vesić method can be used when the base is tilted or in cases where $D/B \geq 1$.

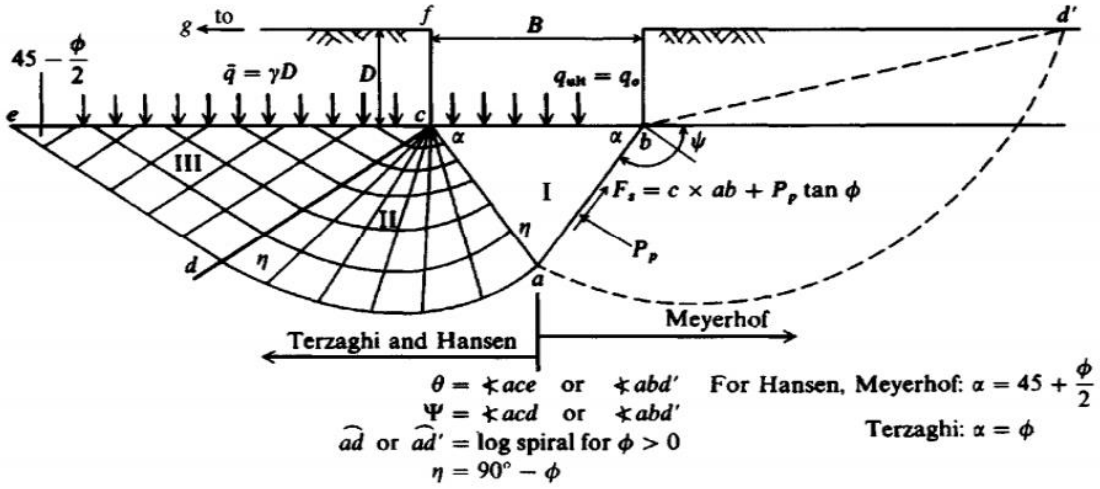

Figure 2.1 General footing-soil interaction for bearing capacity equations for strip footing (Bowles, 1988).

2.2 Bearing capacity methods for predicting spudcan penetration in cohesive soils

The maximum preload is assessed by calculating the ultimate vertical bearing capacity of a spudcan in cohesive soils. Different bearing capacity calculation methods exist to predict jack-up spudcan penetration in clays (undrained failure, $\phi = 0$). The methods include solutions based on SNAME (2008) recommendations, using bearing capacity formulations as proposed by Skempton (1951) and Hansen (1970), a method recommended by Houlsby and Martin (2003) and a method recommended by Hossain et al. (2006).

Skempton method

Most industry guidelines use the method of Skempton's bearing capacity, including shape and depth factors to determine the spudcan penetration in clay of uniform shear strength, s_u, as expressed in equation (2.3). The term p_0' is the effective overburden pressure at depth D. Skempton (1951) has shown that the bearing capacity factor N_c is a function of ratio (D/B) for $\phi = 0$ conditions. The spudcan geometry is idealised by a flat circular footing placed on the sea surface, for which the product $N_c \cdot s_u$ should be taken as 6.0 at sea surface level (figure 2.2). It is also assumed that the soil above the spudcan will backflow and completely fill the spudcan cavity. Complete soil backflow into the spudcan cavity is a reasonable assumption in normally consolidated clay soils.

Skempton (1951) $$Q_V = (s_u N_c s_c d_c + p_0')A \qquad \textit{Eq. (2.3)}$$

In which

$$s_c = 1 + 0.2\,(B/L)$$
$$d_c = 1 + 0.2\,(D/B) \leq 1.5$$
$$N_c \cdot s_c = 6.0;\ \ for\ circular\ footings$$

According to ISO 19905-1: 2012, the design undrained shear strength s_u should be selected based on the sampling method, the laboratory test type and the field experience regarding the prediction and observations of spudcan penetrations. Field measurements in the Gulf of Mexico have indicated that spudcan penetrations in clay are well predicted by selecting s_u as the average shear strength over a depth of half the spudcan diameter below the widest cross section.

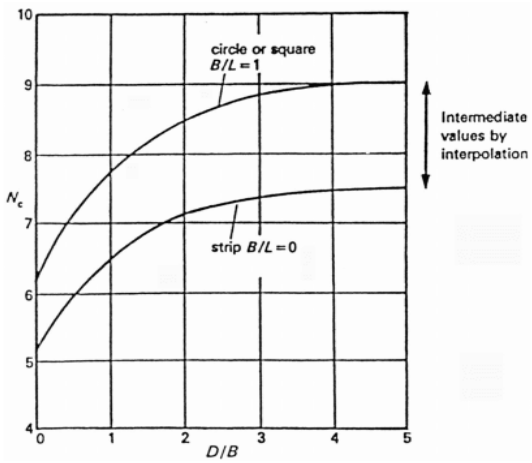

Figure 2.2 Skempton's bearing capacity factor Nc.

Houlsby & Martin method

An alternative bearing capacity factor N_c as proposed by Houlsby and Martin (2003) for shallow circular foundations can be used for lower bound solutions to the soil resistance, which incorporates the spudcan tip design features such as embedment (d), cone angle (β), rate of increase of strength with depth (k) and surface roughness of the foundation (α). The method was developed for sites with clay shear strength profile that increase linearly with increasing depth. This ISO-method assumes failure based on wished-in-place footings. Bearing capacity values proposed by Houlsby and Martin (2003) are indicated below.

Houlsby & Martin (2003)

$$N_c = N_{c0\alpha} + \frac{\alpha}{\tan\left(\frac{\beta}{2}\right)}\left[1 + \frac{1}{6\tan\left(\frac{\beta}{2}\right)}\frac{Bk}{s_{u0}}\right] \qquad \textit{Eq. (2.4)}$$

In which

$$N_{c0\alpha} = N_{c00}\left[1 + (0.212\alpha - 0.097\alpha^2)(1 - 0.53\frac{d}{B+d})\right] \qquad \textit{Eq. (2.5)}$$

$$N_{c00} = N_1 + N_2\frac{Bk}{s_{u0}} \qquad \textit{Eq. (2.6)}$$

$$N_1 = 5.69 + \left[1 - 0.21\cos\left(\frac{\beta}{2}\right)\right]\left(1 + \frac{d}{B}\right)^{0.34} \qquad \textit{Eq. (2.7)}$$

$$N_2 = 0.5 + 0.36\left[\frac{1}{\tan\left(\frac{\beta}{2}\right)}\right]^{1.5} - 0.4\left(\frac{d}{2}\right)^2 \qquad \textit{Eq. (2.8)}$$

Hossain et al., Method

Hossain et al. (2006) proposed new guidelines to calculate penetration resistance and cavity depth based on new backflow mechanisms above the spudcan. He identified soil flow mechanisms around the spudcan by using both centrifuge modelling and finite element modelling. The spudcan penetration response is elaborated by Hossain and Randolph (2009b) by presenting bearing capacity factors for spudcan penetration resistance on single layer homogeneous and non-homogeneous clay, with k as gradient of the undrained shear strength which is linear with depth. The spudcan base roughness was found to have a significant effect to the penetration resistance, for which different fits were made to the empirical data.

Homogeneous clay

$$N_{cd} = 5.69 + \frac{d}{0.22H}\left(1 - \frac{d}{5.8H}\right) \leq 12 \qquad smooth\ base \qquad \textit{Eq. (2.9)}$$

$$N_{cd} = 6.05 + \frac{d}{0.21H}\left(1 - \frac{d}{6.2H}\right) \leq 13.1 \qquad rough\ base \qquad \textit{Eq. (2.10)}$$

Non-homogenous clay

$$N_{c0k} = N_{c0}\left[1 + \frac{0.161\left(\frac{kd}{s_{u0}}\right)^{0.8}}{\left(1+\frac{d}{B}\right)^{2}}\right] \qquad smooth\ base \qquad \textit{Eq. (2.11)}$$

$$N_{c0k} = N_{c0}\left[1 + \frac{0.191\left(\frac{kd}{s_{u0}}\right)^{0.8}}{\left(1+\frac{d}{B}\right)^{1.5}}\right] \qquad rough\ base \qquad \textit{Eq. (2.12)}$$

Current best-practice

Owing to a lack of solutions for continuous penetration, the SNAME guidelines, suggesting a recommended practice for site specific assessment of mobile jack-up units, adapt the framework used for onshore foundations considering the bearing capacity of a series of wished-in-place spudcans at increasing depths, from which a penetration curve can be progressively constructed from independent calculations at different depths.

SNAME recommends two sets of formulas for calculating penetration resistance for penetration with and without backfill, i.e. equation (2.13) and (2.14). The originally developed bearing capacity factors for a flat surface strip footing by Prandtl (1921) were modified for shape and embedment depth following the approaches of Skempton (1951) and Brinch Hansen (1970). An average value of undrained shear strength, s_u, over an arbitrary depth below the spudcan level is applied to account for any variations in soil strength. Typically, a distance of $0.5 - 1D$ below the maximum spudcan diameter is taken.

The major drawback of the SNAME (2008) and other guidelines is that the recommended bearing capacity calculation procedures do not account for the effects of consolidation and viscous strain rate on the soil strength of clay. These aspects are mentioned, but no further calculation approaches are proposed. As a result, the current suggested design approaches in the guidelines tend to be fairly conservative. Yet, accurate rather than conservative estimates of spudcan penetration is desired for an efficient design.

2.3 Soil backfill mechanism

Soil backfill, composed of backflow and infill, is an important mechanism to consider when estimating the penetration of the spudcan during preloading. The backflow mechanism, where soil flowing from beneath the spudcan, around the sides and onto the top, is more likely to occur in clays than in sands. The degree of backflow is also more likely to increase at deeper penetrations as investigated by Hossain and Randolph (2009b). Complete soil backflow into the spudcan cavity is a reasonable assumption in very soft clays. In firm to stiff clays and granular materials, where spudcan penetration is expected to be small, the possibility of backflow scales down (ISO19905-1, 2012).

Infill is the soil on top of the spudcan that results from cavity wall collapse or sediment transport and is more likely to occur in granular materials. Cavity wall collapse can occur during or after preloading, whereas sediment transport is only of importance after preloading. Cavity wall collapse can occur slowly or suddenly. If it occurs suddenly during preloading, it can cause a rapid increase in penetration. In places where moving sandbanks occur, the spudcan cavity can be filled up with sediment over time, which can cause a slow increase in penetration.

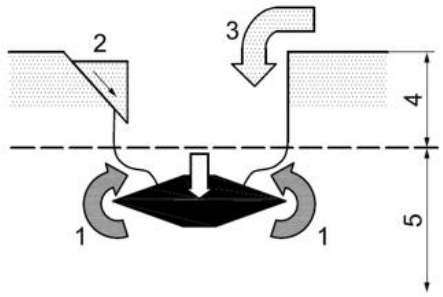

Key
1 backflow
2 infill - wall failure
3 infill - sediment transport
4 region subject to infill processes
5 region subject to backflow
NOTE Backfill includes backflow and infill.

Figure 2.3 Backflow and infill (ISO19905-1, 2012).

The submerged weight of the backfill material provides additional weight on top of the spudcan, which results in additional penetration. As a result, the soil will reach failure earlier compared to spudcan penetration without backfill. The backfill weight depends on the limiting cavity depth, which is the part of the cavity that remains open above the spudcan during penetration. At maximum preload, the ultimate bearing capacity, Q_V, under the spudcan is equal to the preload reaction, V_L, plus the submerged weight of any backfill onto the spudcan, W_{BF}, minus the soil buoyancy of the spudcan below the bearing area, B_S. This last term represents the submerged weight of soil displaced by the spudcan below the greatest depth of maximum cross section.

Ultimate bearing capacity	$Q_V = V_L$	*No backfill*	*Eq. (2.13)*
	$Q_V = V_L + W_{BF} - B_S$	*With backfill*	*Eq. (2.14)*
In which	$B_S = \gamma' \cdot V$		*Eq. (2.15)*

Based on geotechnical centrifuge experiments, Hossain and Randolph (2009b) underlined three distinctive mechanisms of soil flow around the spudcan, as indicated in figure 2.4: (a) outward and upward flow leading to surface heave and formation of a cavity above the spudcan; (b) gradual flow back into the cavity; and (c) fully localised flow around the embedded spudcan. At a certain penetration depth, soil backflow is initiated, which limits the cavity depth. Empirical equations for estimating the cavity depth are given in ISO 19905-1:2012, based on the experiments by Hossain and Randolph (2009b). Distinction is made between material with a uniform and linearly increasing undrained shear strength with depth.

Uniform shear strength	$\frac{H_{cav}}{B} = S^{0.55} - \frac{S}{4}$	*Eq. (2.16)*
	$S = \left(\frac{s_u}{\gamma' B}\right)^{\left(1-\frac{\rho}{\gamma'}\right)}$	*Eq. (2.17)*
Multi-layer clays with moderate changes of strength	$\frac{H_{cav}}{B} = \left(\frac{s_u H}{\gamma' B}\right)^{0.55} - \frac{1}{4}\left(\frac{s_u H}{\gamma' B}\right)$	*Eq. (2.18)*

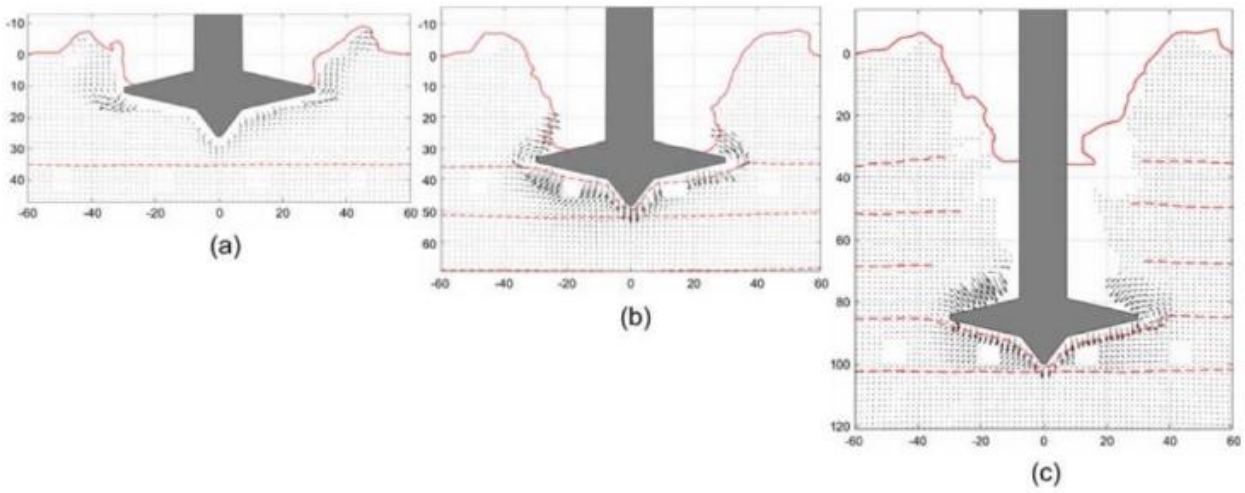

Figure 2.4 Flow mechanism for spudcan penetration in clay (Hossain and Randolph, 2009b).

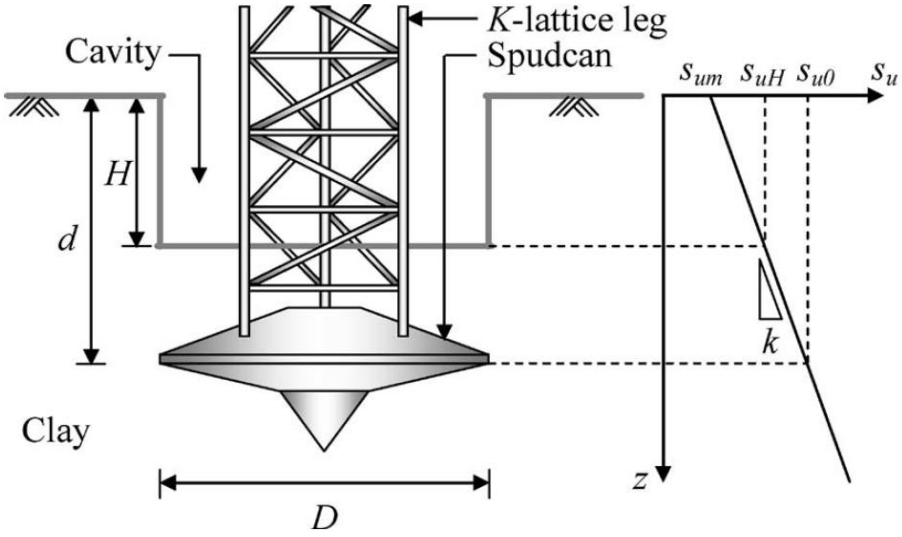

Figure 2.5 Schematic view of embedded spudcan foundation showing idealized open cavity.

2.4 Punch-through

Punch-through is an installation risk in layered strata with significant strength differences. Rapid, uncontrolled vertical leg movement can occur when spudcan footings penetrate through strong overlying weak soils, for instance spudcan penetrating in sand overlying clay or stiff clay overlying soft clay. This normally involves rapid footing penetration of several meters in seconds. Punch-through failures can be extremely dangerous and costly, both for the personnel on board and in lost time and repair costs. If one leg breaks through a strong zone, it puts the other legs in a large bending moment, causing them to buckle which may lead to toppling of the whole jack-up unit.

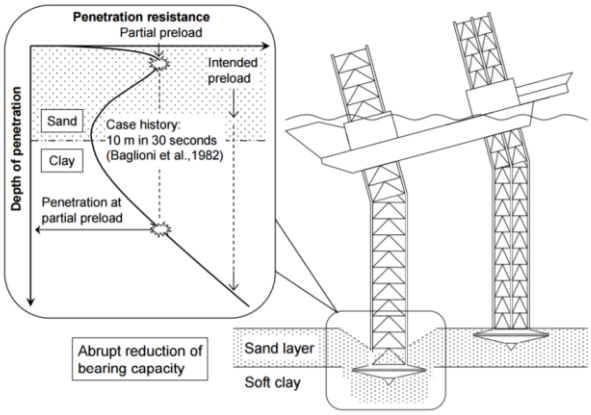

Figure 2.6 Illustration of punch-through failure during preload (Lee, 2009).

Figure 2.7 Photograph showing a jack-up failure due to a punch-through event in 2002 (Hunt and Marsh, 2004).

In the preload check, the punch-through potential is assessed by evaluating the footing bearing capacity at increasing penetration depth. The response of leg loads versus footing penetration is measured during important preloading stages, namely ship plus variable load, V_1, (as the hull lifts out of the water) and full preload, V_p. Figure 2.8**Error! Reference source not found.** shows leg load-enetration curves in different conditions. In graph (a), punch-through occurs before the hull is clear of the water, which causes little concern. However, if the punch-through is likely to occur during the preloading phase, as illustrated in graph (b), then the installation procedures need careful reflection. Graph (c) represents the case in which punch-through is unlikely to occur at full preload and installation should be safe. In order to avoid unexpected punch-through failure, accurate rather than conservative estimate of spudcan penetration resistance profile is required.

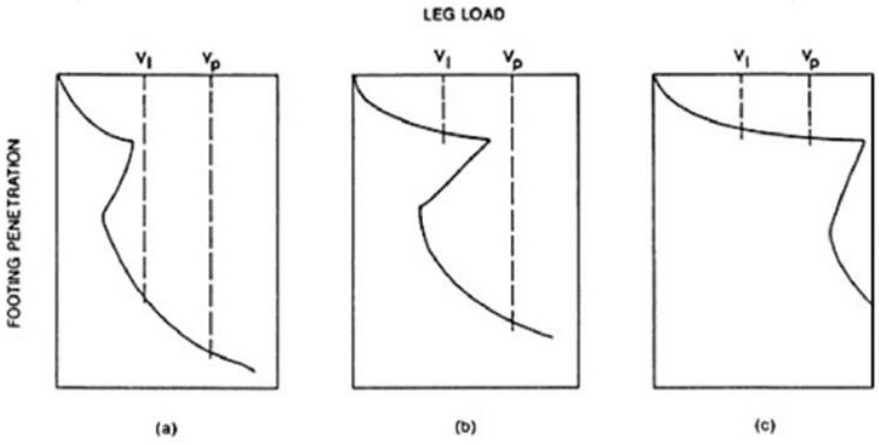

Figure 2.8 Leg-load penetration curves indicating punch-through in different conditions.

2.5 Spudcan design

Each leg of the jack-up platform is supported on the sea floor by a large inverted conical foundation, known as a spudcan, which contributes to the pressure exerted on the sea floor by the legs. The spudcan is designed to spread the load in order to prevent the rig from sinking deep into the seabed. In general, the geometry of the spudcan is approximately circular (hexagonal or octagonal) in plan with a shallow conical underside and a sharp protruding spigot. The spigot feature is designed to facilitate initial positioning and to provide enough sliding resistance. Some designs are more suitable to specific seabed conditions than others. For instance, the use of detachable spudcans makes it easy to adapt for specific seabed characteristics. Different footings can be fitted to the legs for operations in different conditions. Some examples of typical spudcan shapes are shown in figure 2.10.

Currently, the Aeolus is being modified as part of a total rebuild to make the vessel suitable for present-day operations. As the weight of the vessel is increased, it also needs larger spudcans to support the load. The spudcan diameter is enlarged from 8 meter to 13 meter in order to gain more bearing capacity in clay at shallower depths. When applying load, the soil reaction force equals the integration of vertical stresses in the soil directly below the footing. By increasing the spudcan diameter, a larger reaction force is obtained as more soil is being mobilised underneath.

A cross sectional area of the Aeolus extended spudcan geometry can be seen in figure 2.9. The cascaded design points out that most of the current spudcan is maintained, only the bottom base is removed and enlarged in size.

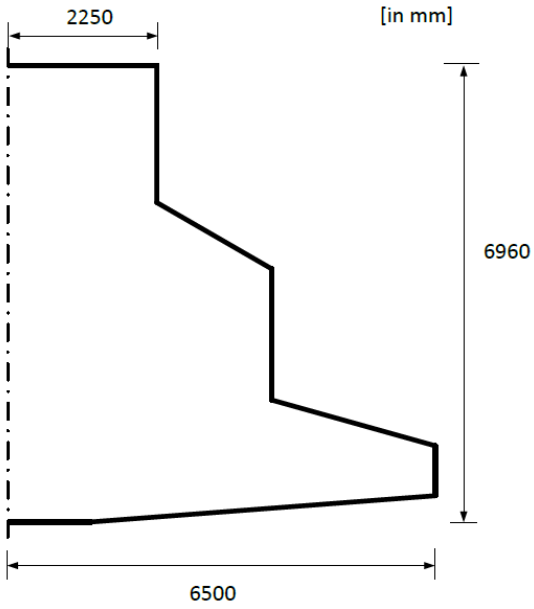

Figure 2.9 Aeolus extended spudcan geometry

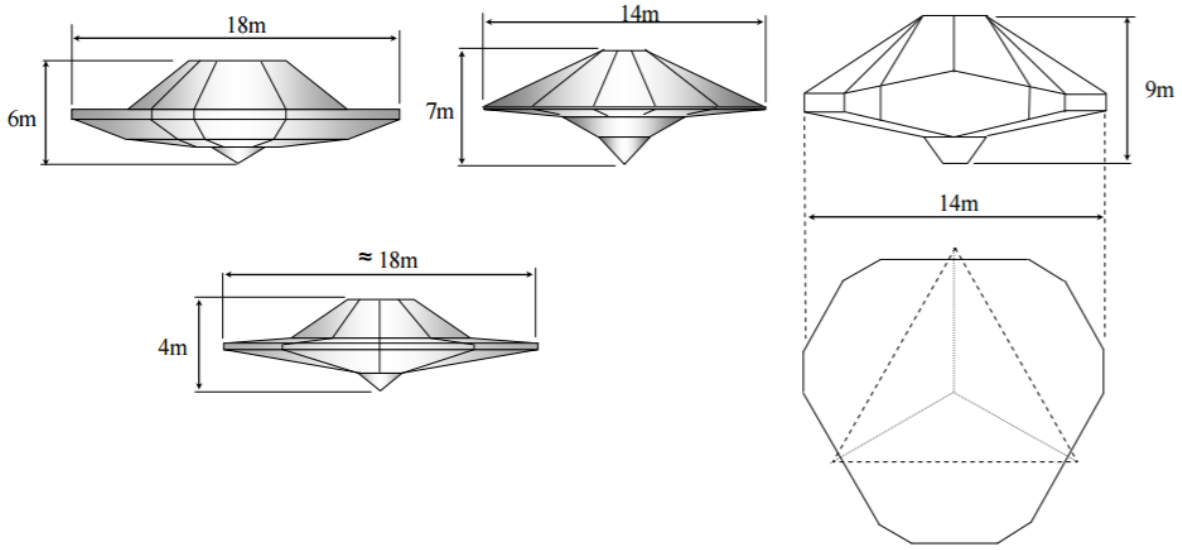

Figure 2.10 Examples of spudcan geometries (Teh, 2007)

2.6 Consolidation effects

Partial consolidation

Besides in layered soil strata, punch-through potential can also arise in a uniform soil as a result of soil consolidation during load-hold periods in the preloading cycles. The effects are even worse in case the preloading is interrupted by unplanned delays due to inclement weather, equipment malfunction or other causes. During these pauses, the soil below the footing is subjected to significant loads, causing partial consolidation of the soil around the spudcan due to the dissipation of excess pore pressures. This results in a zone of increased strength and stiffness of the soil and enhancement of bearing capacity of the spudcan at that depth. This effect of increased effective stress is only present in the area surrounding the spudcan. Applying additional load afterwards may lead to the spudcan punching through this strengthened zone. In offshore practice, even relatively short consolidation periods of approximately 3-4 hours were reported to have resulted in punch-through failure (Brennan et al., 2006).

The effects of discontinuous spudcan penetration on the soil response was investigated experimentally by Bienen and Cassidy (2013). Figure 2.11 schematically illustrates the effect of consolidation on the load-penetration curve of a spudcan footing. At the stage where preloading is stopped, settlement will occur due to the dissipation of pore pressures. Once preloading is restarted, a stiffened soil response is observed as a result of overconsolidation. It was demonstrated that the peak resistance as well as the extent of the strengthened soil zone depends on the length of the consolidation period. Besides the magnitude of the peak resistance, the response following the peak also contributes to the punch-through risk. The post peak behaviour is described by the (negative) gradient of penetration resistance, which indicates the reduction in bearing pressure until no further effect of consolidation is evident and the gradient of the penetration curve returns to be parallel to the reference case of continuous penetration.

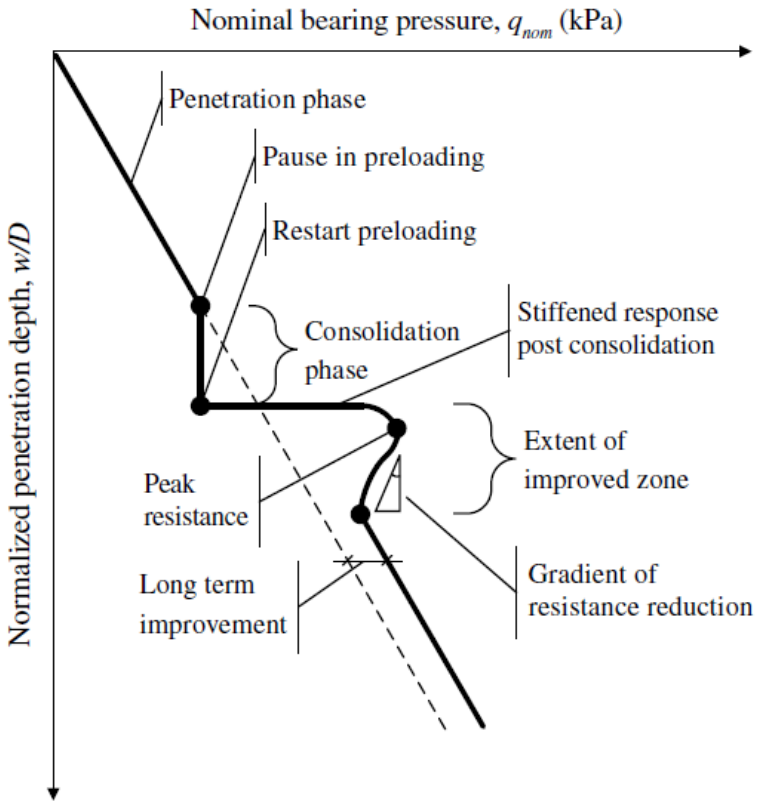

Figure 2.11 Effect of consolidation on the load-penetration curve of a spudcan footing (Bienen and Cassidy, 2013).

2.7 Viscous strain rate effects

Traditional bearing capacity design approaches were developed based on idealised rate-independent soils, in which the soil strength is characterised by static shear stress resistance due to friction and particle interlocking. However, the rate of spudcan penetration, i.e. the speed of which deformation occurs, seems also to have an effect on the shear strength of clay.

Casagrande and Wilson (1951) were among the first to investigate the effect of strain rate on measured shear strength in clay. From that point onward, this subject has been the focal point of numerous investigations (Skempton and Bishop, 1954, Crawford, 1960, Akai et al., 1962, Richardson and Whitman, 1963, Berre and Bjerrum, 1973, Kimura and Saitoh, 1983). There is a general agreement that shear strength of clays is highly strain rate dependent. Typical curves relating the undrained shear strength with the strain rate are shown in figure 2.12 (Skempton and Bishop, 1954).

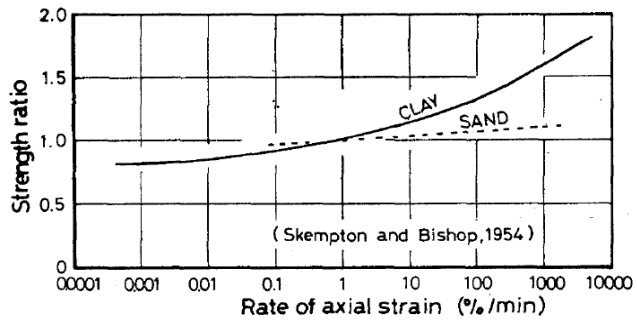

Figure 2.12 Typical curves relating shear strength with shear strain (fully undrained conditions).

As seen in the figure, the strength of sand is almost independent of the strain rate, but the strength of clay is more sensitive to the strain rate. The strength of clay typically increases by 5-20% for each order of magnitude increase in shear strain rate. In addition, in fully undrained conditions, there seems an indication that a further reduction of strain rate would produce little, if any, further decrease in the soil strength.

Based on the investigations of strain rate dependency of the stress–strain behaviour, it was concluded that the rate effect upon strength is caused by a change in the excess pore water pressures generated during the shear process. At small strain rates, consolidation causes an increase in resistance in terms of effective stress. At the faster strain rates, the increase in resistance seems to result from decreased excess pore pressures. Richardson and Whitman (1963) conducted triaxial compression tests on normally consolidated clay specimens, in which the strain rate was suddenly increased. Results plotting the deviator stress and excess pore water pressure versus strain from tests with sudden increase in strain rate can be seen in figure 2.13. The behaviour of the pore pressure following a sudden increase in the strain rate shows that there is fundamentally an inverse relationship between strain rate and excess pore pressure. Consider the condition at point A, once the strain rate increases, the excess pore water pressure decreases (after a small transient increase).

In conclusion, at large strains, the relationship between void ratio and effective stress apparently is strain rate dependent. That means, as the strain rate is increased, a larger effective stress is required to hold the soil at any given void ratio. At the faster strain rates, adjacent soil particles find it more difficult to move relatively, and, unless restrained by increased effective stress, will tend to ride up over one another. The effect can be thought of either as an increased resistance to compression or as an increased tendency to dilate. In either case the result in the same: increasing the strain rate applied to a saturated soil means larger effective stresses and consequently greater shear resistances.

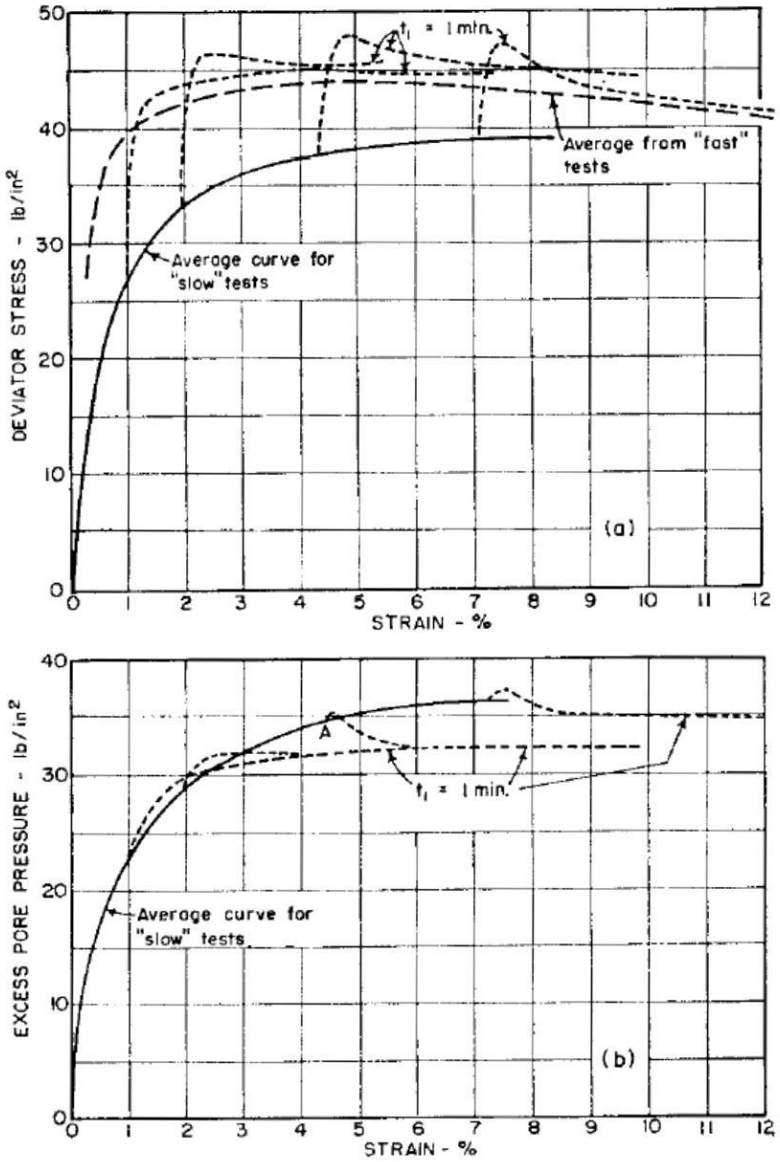

Figure 2.13 Deviator stress and excess pore water pressure vs. strain from tests with change in strain rate (Richardson and Whitman, 1963).

Viscous effects on penetrating shafts

When a rigid footing, such as a spudcan, penetrates into soft soil, the soil mass at and near the tip is subjected to large shearing forces which causes high stresses and strains. Here, the soil mass fails and reaches critical state (CS), as indicated in figure 2.14. Under a constant vertical (normal) effective stress, the soil tends to reach an approximately constant shear stress and constant void ratio for continued shearing, i.e. the critical state frictional shear stress, τ_f. If applied stress on a soil at CS exceeds the yield value, the soil will flow like a viscous fluid in its post-failure response. During continuous penetration, the material below the footing will then flow outward and upward along the shaft, as illustrated in figure 2.15(a). Besides the shear strength due to friction and particle interlocking, the soil flow will offer an additional resistance to the moving shaft. The total resistance, τ, of a shaft during penetration is then the combination of both a frictional shear stress resistance component, τ_f, and an additional term for the viscous stress of the soil, τ_v.

$$\tau = \tau_f + \tau_v \qquad \textit{Eq. (2.19)}$$

The frictional shear stress term is constant and is independent of the penetration rate. However, the viscous component will be influenced by the spudcan penetration rate. For a shaft at rest (penetration rate = 0), the viscous resistance will not act and the total resistance will be equal to the static component solely.

Due to penetration of the shaft, the soil in its path fails and is displaced outwards during its advancement. A region of soil around the surface of the shaft is disturbed, as illustrated in figure 2.15(b). According to Zeevaert (1948), the disturbed zone is classified into different sub zones according to the created intensity of disturbance. Three zones around the pile shaft were identified based on observations of shaft penetration in the subsoil of Mexico City clay. Zone I, or the critical state zone, consists of soil that is subjected to excessive disturbance, as this is located directly adjacent to the pile shaft. The soil in this zone reaches CS and is at a post-failure state. If no soil is squeezed out to the ground surface, the volume of the CS zone is at least equal to the soil volume displaced by the occupied shaft volume. The extent of this zone according to Zeevaert (1948) is 1.4 times the shaft radius measured from the centre of the shaft.

Zone II, or the influence zone, is a disturbed zone with a lesser degree of disturbance. The soil in this zone is usually at a pre-failure state. This zone, according to Zeevaert (1948), extends to about 3 times the shaft radius measured from the centre of the shaft (Appendix B). Beyond the influence zone, the soil is undisturbed and unaffected by the penetrating shaft.

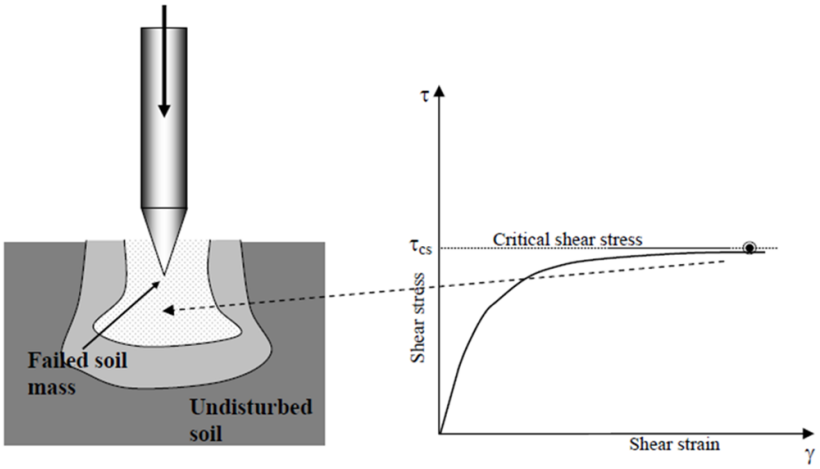

Figure 2.14. Soil state at the tip of the penetrating shaft (Cooke and Price, 1973).

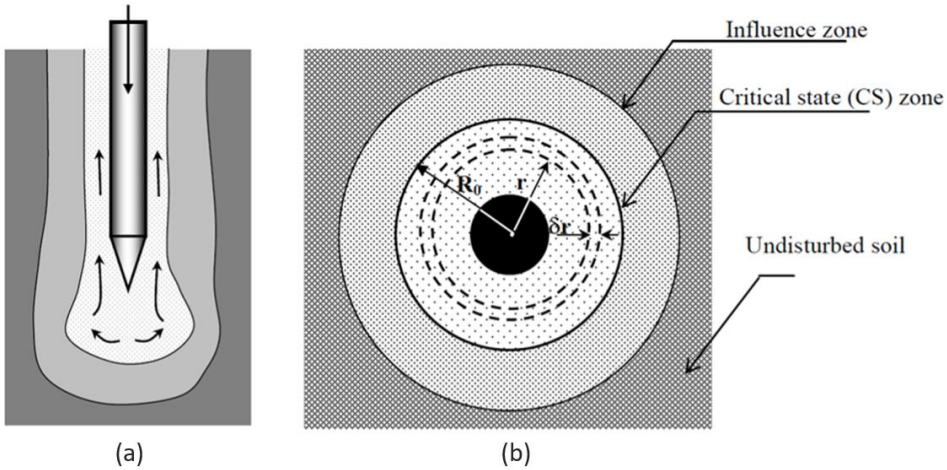

Figure 2.15 (a) Soil flow around the penetrating shaft. (b) Soil zone of influence around penetrating shaft (Cooke and Price, 1973)

Relative importance of consolidation and viscous effects on spudcan penetrating resistance

The rate dependence of the T-bar and ball penetrometer resistance in kaolin clay was investigated in centrifuge tests at the University of Western Australia (UWA) (Lehane et al., 2009). The tests, which involved either a 10 mm diameter cone or a 5 mm diameter T-bar, where conducted in normally consolidated kaolin for penetrometer velocities varying over multiple order of magnitudes. Test results show a consistent trend of normalised soil resistance over the full penetration velocity range, as indicated in figure 2.16. The graph can be subdivided into two regions, i.e. the partially drained region, where both consolidation and viscous effects are of importance and the fully undrained region, where the viscous effects dominate the consolidation effects.

Regarding the partially drained region, it is well known that penetration resistance in clay increases with reduced penetrometer velocity as more time for consolidation around the penetrometer is possible. Dimensional analysis shows that the degree of partial consolidation during continuous penetration is controlled by the normalised velocity. The normalised velocity, V, is equivalent to the ratio of the time for a given fraction of diameter penetration ($= vt/d$) to the time for a given fraction of consolidation ($c_h t/d^2$). The normalised velocity is defined as:

$$V = \frac{vd}{c_h} \qquad \textit{Eq. (2.20)}$$

Where v is the penetrometer velocity, d is the diameter of the penetrometer and c_h is the coefficient of consolidation of the soil. In the graph, it is seen that the minimum normalised q/σ'_v resistance ratio occurs at a normalised velocity V_t. As the penetration velocity reduces, partially drained conditions apply and the soil resistance increases until a resistance about 2.5 times larger is reached. This trend is attributed to the increased degree of consolidation occurring at lower velocities. At even lower velocities in the fully drained range ($V \approx 0.01$), the viscous effects are negligible and penetration resistance is independent of V. Here, the resistance is limited to a maximum value equal to the drained penetration resistance.

After reaching a minimum, the penetration resistance increases again with velocity. Exceeding V_t, the conditions are predominantly undrained. Penetration velocity is assumed fast and therefore, hardly any time for consolidation around the penetrometer is possible. The increase in soil resistance is because positive viscous effects dominate over reductions in resistance owing to lower levels of consolidation. The larger the penetration velocity, the larger will be the viscous drag component.

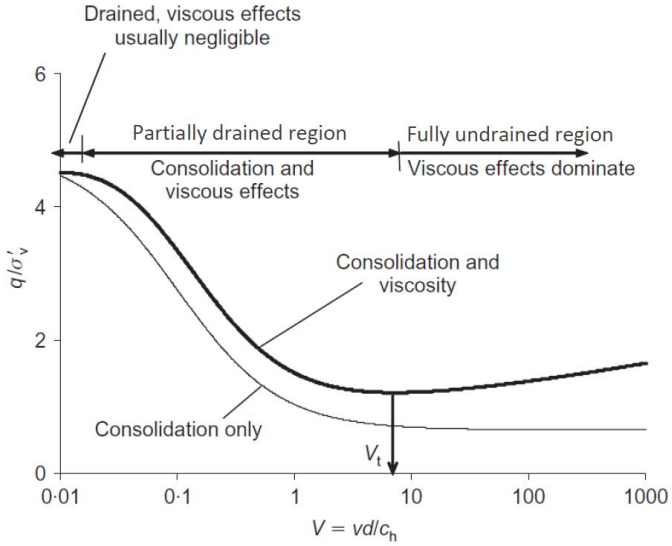

Figure 2.16 Combined influence of consolidation and viscous effects on penetrating soil resistance in clay (Lehane et al., 2009).

2.8 Alternative jacking procedure

InSafeJIP (2011) guidelines state that, as clays show some viscous increase in strength, the shearing resistance would be slightly higher during rapid spudcan penetrations than in the case for very slowly applied loads. The shearing resistance is high during spudcan penetration, but can quickly reduce when jacking is stopped and the load on the spuds is kept constant. In the default preloading procedure, as described in the introduction, many preload-hold cycles may be required in order reach the preload criterion of 400 ton load reduction in 15 minutes, which adds up to considerable preloading times. Alternatively, an overshooting preloading procedure is introduced, which may result in significant time savings.

Isotache behaviour in clay

The concept of isotache behaviour is based on two important consequences of the viscous behaviour in clays, namely creep and stress relaxation. During creep, the soil deforms over time, while subjected to a constant load. The inverse phenomenon, termed stress relaxation, is a reduction in stress over time after a soil is subjected to a constant strain level. A unique relationship holds between stress, strain and strain rate (or time), which is denoted as isotache behaviour (Augustesen et al., 2004). In general, the viscous response is not present in sands, and therefore, their behaviour is termed non-isotache. Both models are illustrated in figure 2.17.

Experimental research by Hossain and Randolph (2009a) shows that at stresses approaching the strength of the material, the creep strain rate becomes very large and signals the onset of failure (figure 2.18). In other words, the larger the applied load, the larger the creep strain rates of the material. Conversely, this implies rapid relaxation rates at shear stresses close to failure.

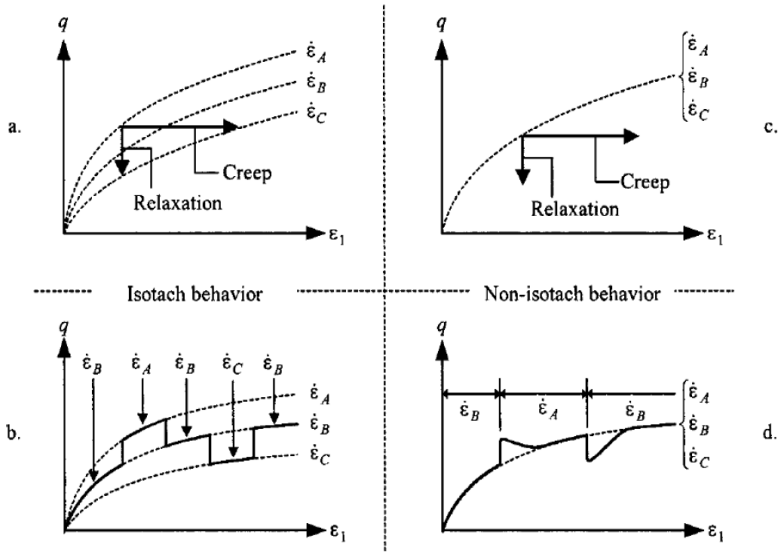

Figure 2.17 Isotache behaviour observed in clay for (a) creep and relaxation and (b) stepwise change in rate. Non-isotache behaviour observed in sand for (c) creep and relaxation rate and (d) stepwise change is rate.

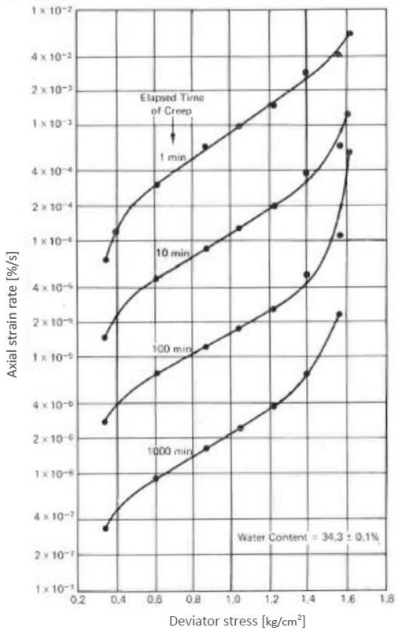

Figure 2.18 Evolution of creep strain rates (and inversely relaxation rates) as function of deviator stress.

Application to the jacking procedure

The isotache behaviour has an effect on the preloading response of cohesive soils. Figure 2.19 shows the difference in jacking procedures between the standard (default) and overshooting preload strategy[1]. Using the standard jacking procedure, the spudcan is stopped once the target preload is reached (see section A – B). As the strain rate reduces to zero, this gives rise to quite rapid load relaxation of the soil, which the operator corrects by increasing the load on the spudcan again. This process results in a creep-like additional spudcan penetration, and it may take a long time before the spudcan response is stabilised (section B – C). In sands, the rate dependency is negligible and additional penetration is generally not noted.

An alternative jacking procedure is proposed by Cathie et al. (2017), which states that if the required target preload is overshot by 10-15% (point D), then the spudcan is brought to the depth which would have been reached by the creep-like additional penetration under the target preload value. This alternative jacking procedure is sketched by the blue lines in figure 2.19. This makes it possible to reach the end point (point C) of the standard procedure more quickly. Once the load is reduced from the overshoot to the target preload (section D – C), it is likely that the preload can be sustained without additional penetration (and load cycles), as it is now located on the quasi-static leg penetration curve.

The overshooting procedure in clay is promising, as the amount of preload cycles can be reduced by following this alternative loading path. However, this method does require a loading capacity which is higher than the target preload, which is not always available. In layered soils, it could also lead to excessive penetration when the peak punch-through load is exceeded unintentionally during overshooting. The required amount of overshooting needs to be determined on a site-specific basis.

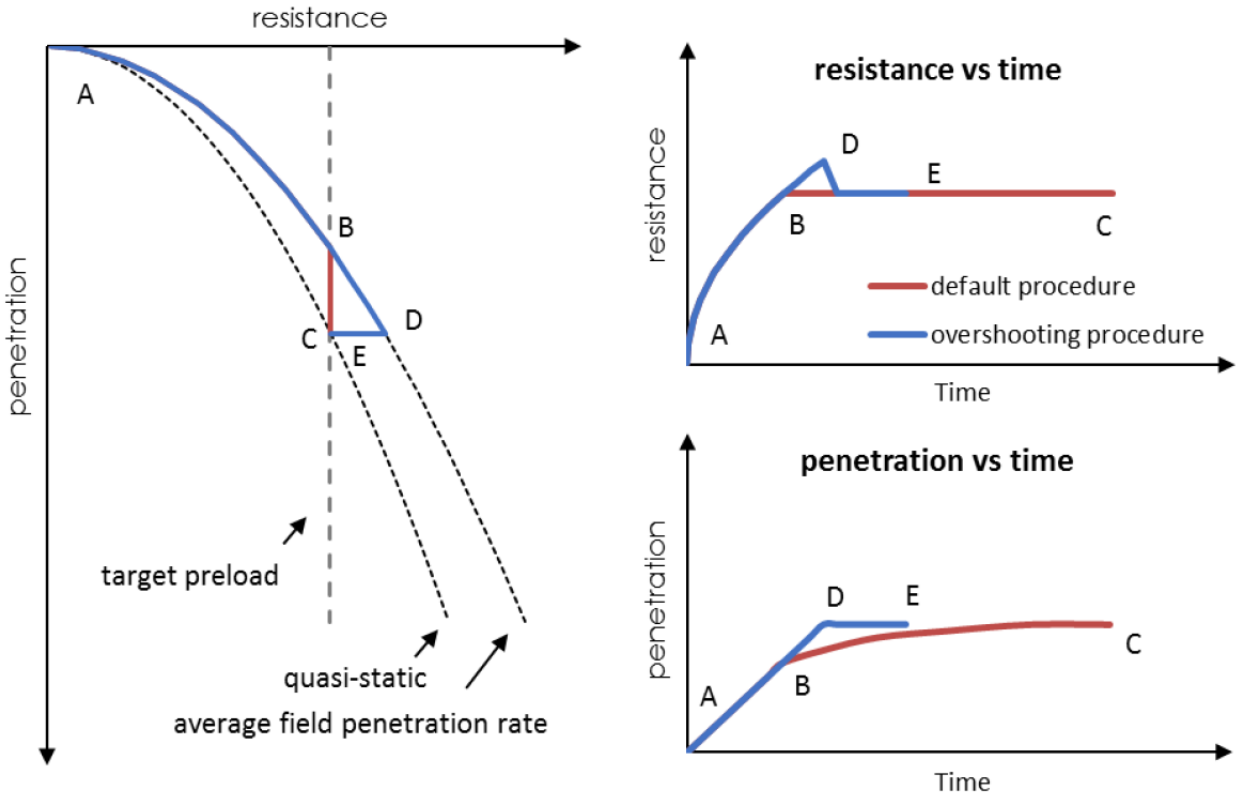

Figure 2.19 Spudcan penetration and resistance - default and overshooting procedure (Cathie et al., 2017)

[1] Note that this is a simplified representation as the soil behaviour exhibits purely creep and stress relaxation in sections B-C and D-E, respectively. In reality, both mechanisms will occur simultaneously.

3. Interpretation of site investigation data

3.1 Geotechnical site investigation

Exploitation of offshore resources requires knowledge of the mechanical properties of the seabed sediments, which determine the material behaviour under certain loading conditions. Marine soil investigation includes both in-situ tests and laboratory tests on selected soil samples. The geotechnical properties obtained from the field investigation and subsequent laboratory work provide the basis for the engineering parameters required for design of foundations and other offshore infrastructure.

A geotechnical site investigation is performed by specialised equipment from a purposely-built platform or vessel. The choice of a suitable platform depends on the water depth at the site. Some of the possible investigation platforms are shown in figure 3.1. Jack-up rigs, like the Aeolus vessel, are applicable in water depths ranging from 20 – 120 meter (Randolph and Gourvenec, 2011). Due to the executional difficulty and high mobilisation costs of specialised vessels, the costs of site investigation in the offshore environment are orders of magnitude greater than the corresponding costs on land. Extracting information for geotechnical site investigation is often constrained by high costs and should be considered wisely. Geophysical surveys can help to give a better understanding of geological features and to select possible locations of the proposed foundations. Afterwards, interpretation of the geotechnical site investigation data is required to determine the design soil parameters.

For the offshore wind project, a geotechnical site investigation was performed by Fugro (2013) to provide soil information about the proposed location of the Offshore Wind Farm in the Irish Sea. The report presents information based on the results of all in-situ and laboratory testing and the data obtained from the fieldwork. The following section describes the interpretation of soil investigation data, from which the required design soil parameters are derived for the model input.

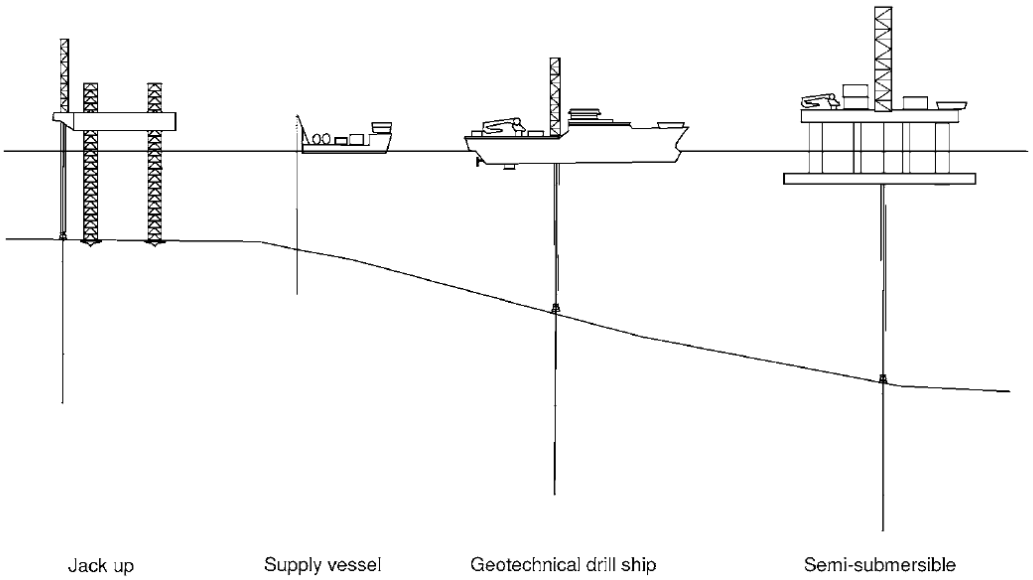

Figure 3.1 Alternative investigation platforms for increasing water depth (Randolph and Gourvenec, 2011).

3.2 Geology

3.2.1 Soil layering

Geotechnical logs for the Offshore Wind Farm locations were compiled based upon laboratory test results and in-situ test data. Soil descriptions made offshore were checked and updated as necessary based on the results of onshore testing. Each log is different due to the lateral variation in layering across the site. A selection of the geotechnical logs can be found in Appendix C (Fugro, 2013). Three characteristic geotechnical profiles can be identified, which are depicted in figure 3.2 on the right hand side.

From the top, a loose sandy surface layer of 1 or 2 m thick covers a dense sandy subsoil, which ranges from 10 to 25 m thickness. Below, a clay layer of intermediate strength is found before reaching the stiff clay layer at larger depths (>35m). The first two profiles are characterised by taking limiting layer boundaries between these strata; one with a smaller sand layer relative to the intermediate clay layer and vice versa. The third profile is characterised by a soft clay layer at the upper side of the soil column, right between the surface layer and the dense sand.

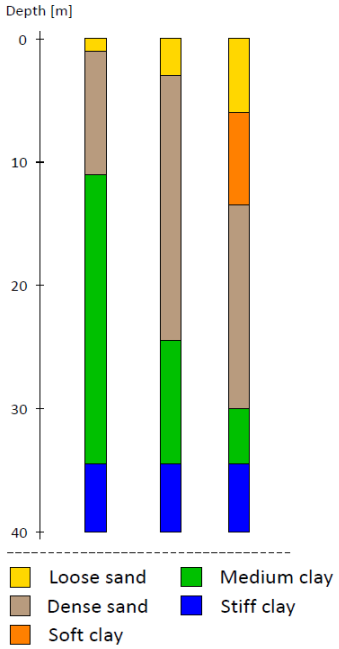

Figure 3.2 Characteristic geotechnical profiles at the offshore wind farm site

3.2.2 Geological description of soil formations

A geological model including eleven different soil formations was formed for the offshore wind farm location based on geotechnical data collected by Fugro Geoconsulting Ltd (2012-2014). As this thesis study focusses on spudcan penetration in soft soil only, just two of the geological formations were classified as a clay and are selected for engineering design. One soft (SSF-SBD) and one slightly stiffer clay (WIS-MF) formation. Both of the clay formations will be discussed further within this report. The geological model and description of the selected clay formations are presented in table 3.1 and 3.2, respectively.

Table 3.1 Geological model for selected clay formation.

Period	Epoch	Formation	Member/unit
Quaternary	Holocene	Surface Sands Formation	Seabed Depression Member (SSF-SBD)
	Pleistocene	Western Irish Sea Formation	Mud Facies (WIS-MF)

Table 3.2 Geological description for selected clay formation members.

Formation member	Description
SSF-SBD	Very soft to soft locally slightly sandy CLAY with few shell fragments.
WIS-MF	Firm to stiff sandy CLAY, with occasional silty laminations and shells.

3.3 Soil classification parameters

3.3.1 Particle size distribution

The particle size distribution (PSD) of the selected soft soil members at the site were determined from laboratory sieving analysis. The division of the grain size classification is presented, adopting limits from the British Soil Classification System given by the British Standards Institute (2004). A point on the curve gives the percentage by weight of material smaller in size than that at the given point on the graph. The grading curves of both the SSF-SBD and WIS-MF soil units are given in figure 3.3 and 3.4 below.

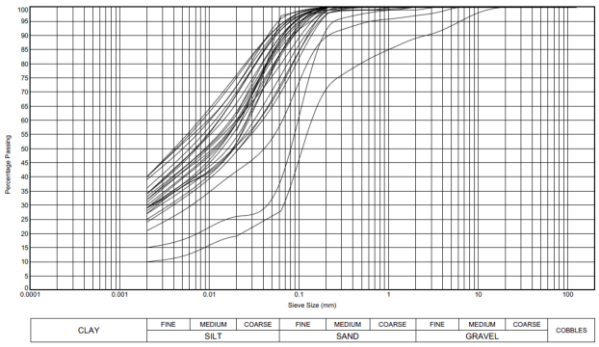

Figure 3.3 PSD grading curves for SSF-SBD

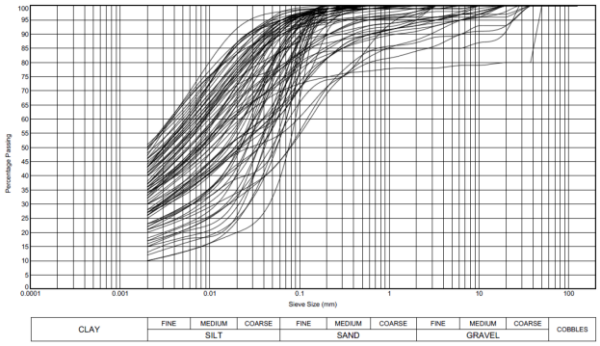

Figure 3.4 PSD grading curves for WIS-MF

Median particle size

When comparing the grain sizes of the particle size distribution of both samples, the median diameter is often used, which represents the target grain size by a single numerical value. The median particle size (d_{50}) is defined as the midpoint of the PSD, i.e. the particle diameter at which the cumulative distribution curve intersects the vertical axis at 50%. In other words, 50% (by weight) of the sediment is coarser and 50% is finer than the median particle size. A summary of the representative d_{50}-values of both soil units is presented in table 3.3.

Table 3.3 Summary of the representative median particle size

Soil unit	Median particle size, d_{50} (mm)	
	Characteristic range	Representative
SSF-SBD	0.005 to 0.020	0.010
WIS-MF	0.002 to 0.050	0.015

Clay and fines content

According to the classification system presented in BS EN ISO 14688-2:2004 (British Standards Institute, 2004), particles less than 0.06 mm in size are characterised as fine soils (clay +silt). Above is characterised as coarse soils. Pure clays contain particles less than 0.002 mm in size. A summary of the characteristic soil classification and clay and fines content for both soil units is presented in table 3.4.

From the distribution curves, it is noted that the WIS-MF soil unit has a larger variation in particle sizes compared to the SSF-SBD soil unit, as is has a wider curve. Yet, the averaged d_{50}, clay and fines contents are more or less comparable. As the WIS-MF soil unit contains a higher degree of coarser particles, it is therefore expected to behave somewhat stiffer when compressed, compared to the SSF-SBD soil unit.

Table 3.4 Summary of soil classification and clay and fines content from PSD.

Soil unit	Soil classification	Clay content (%)		Fines content (%)	
		Range	Representative	Range	Representative
SSF-SBD	Medium graded silty clay	20 to 40	30	70 to 95	90
WIS-MF	Medium graded silty clay to clay, some parts sandy	15 to 50	35	55 to 95	85

3.3.2 Atterberg limits

Natural moisture content

The natural moisture content of each of the fine-grained soil units at the site was determined from laboratory wet and dry mass readings. It is defined as the weight percent of moisture compared to the mass of the solids. When compared to the Atterberg limits, the natural moisture content of clay indicates the consistency of the clay and provides a useful indication of certain engineering characteristics. A summary of natural moisture content for each clay unit is presented in table 3.5. It is noted that the youngest geological unit has a higher moisture content value associated, which is expected as they are typically closer to the seabed level and will therefore were subjected to lower overburden pressures by soils above.

Table 3.5 Natural moisture content

Soil unit	Natural moisture content [%]	
	Range	Representative
SSF-SBD	30 to 45	35
WIS-MF	15 to 40	25

Plasticity

Plastic behaviour of each soil unit was determined from laboratory Atterberg limit tests and the interpretation method proposed by Casagrande (1932). The Atterberg limits are defined by moisture content and provide data for the identification and engineering classification of clays. With increasing moisture content, the behaviour of the clay goes from plastic to liquid. The moisture content at this point is known as the liquid limit (LL). With further removal of water from the clay, the material remains in the plastic state, while stiffness increases, until it loses its plasticity and becomes brittle or begins to crumble. The moisture content at this point is known as the plastic limit (PL) and with further drying the clay behaves as a solid. The differences between these moisture content values is known as the plasticity index, ($PI = LL - PL$). A summary of the plasticity index for both clay units is presented below.

Table 3.6 Plasticity behaviour

Soil unit	Plasticity index [%]		Anticipated engineering behaviour
	Range	Representative	
SSF-SBD	15 to 25	20	Low to intermediate plasticity clay
WIS-MF	10 to 25	20	Low to intermediate plasticity clay

3.3.3 Cone penetrometer test soil behaviour types

Besides laboratory soil classification systems based on physical (textural) characteristic such as grain size and plasticity, soils should ideally be classified based on fundamental behaviour characteristics that have a strong link to in-situ behaviour. This is done by using piezocone penetration test (CPTu) measurements, based on behaviour characteristics, which is often referred to as a soil behaviour type (SBT) classification system. Interpretation of the in-situ CPTu piezocone data as proposed by Robertson (1990) was done to characterise the nature of each geological unit.

Robertson (1990) proposed that SBT could be characterised based on the relationship between corrected cone resistance, q_t, and friction ratio, R_f, and between corrected cone resistance and pore pressure ratio, B_q. Based on these relationships, Robertson constructed classification charts to classify the different units encountered during CPTu testing (Robertson et al., 1986). The chart is subdivided into 12 regions, which are stated at the right hand side of figure 3.5 and 3.6.

Composite plots for all geological units, showing the relationships between q_t and R_f and q_t and B_q are presented in figure 3.5 and 3.6, respectively. It can be clearly seen that all SBD samples lie within the 'clay' region (3). The WIS-MF soil unit is spread out more, covering region 3 to 6, ranging from 'clay' to 'sandy silt'. Since the WIS-MF soil unit contains larger degree of coarser particles, it is expected to behave stiffer compared to the SSF-SBD soil unit. This narrow and wider spreading was also previously seen in the particle size distributions of both soil units.

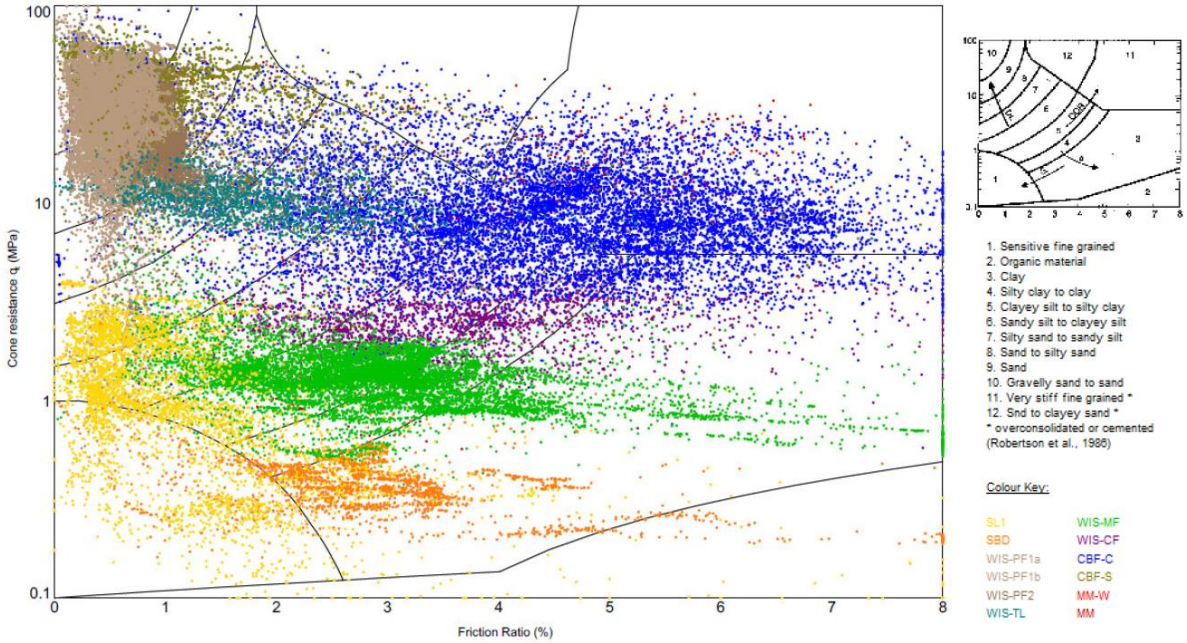

Figure 3.5 SBT classification chart based on q_t and R_f for all geological units

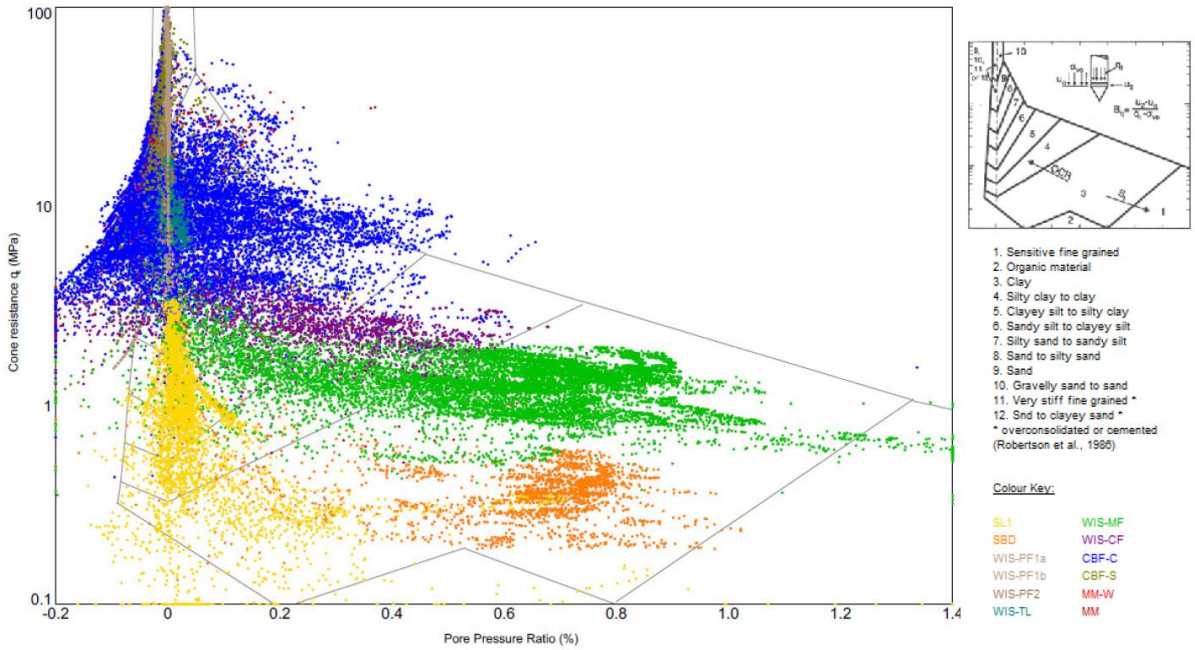

Figure 3.6 SBT classification chart based on q_t and B_q for all geological units.

3.4 Design parameters

3.4.1 Effective unit weight

Effective unit weight, γ', is determined from bulk unit weight, γ_{bulk}, which for undisturbed fine grained soils is assumed to be equal to the saturated unit weight, γ_{sat}. The bulk unit weight of each soil unit has been determined from laboratory tests by weighing the undisturbed soil mass per unit volume. The effective unit weight, which is defined as the difference between the saturated unit weight and the unit weight of water, is often used in the calculation of the effective stresses in the soil. The following relations were adopted:

$$\gamma_{sat} = \gamma_{bulk} \qquad \textit{Eq. (3.1)}$$

$$\gamma' = \gamma_{sat} - \gamma_w \qquad \textit{Eq. (3.2)}$$

Where γ_w is the unit weight of water, assumed as $9.81\ kN/m^3$.
A summary of the interpreted effective unit weight for each of the fine grained soil units is presented in table 3.7. The results of the individual samples are shown in figure 3.7 and 3.8.

Table 3.7 Effective unit weight of fine grained soil units

Soil unit	Effective unit weight [kN/m^3]	
	Range	Representative
SSF-SBD	7.6 to 9.4	8.6
WIS-MF	8.2 to 12.4	10.1

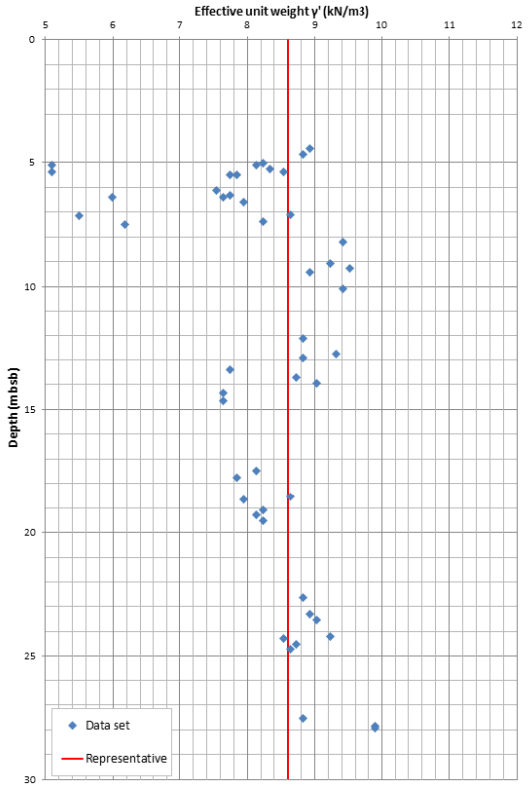

Figure 3.7 Effective unit weight for SSF-SBD

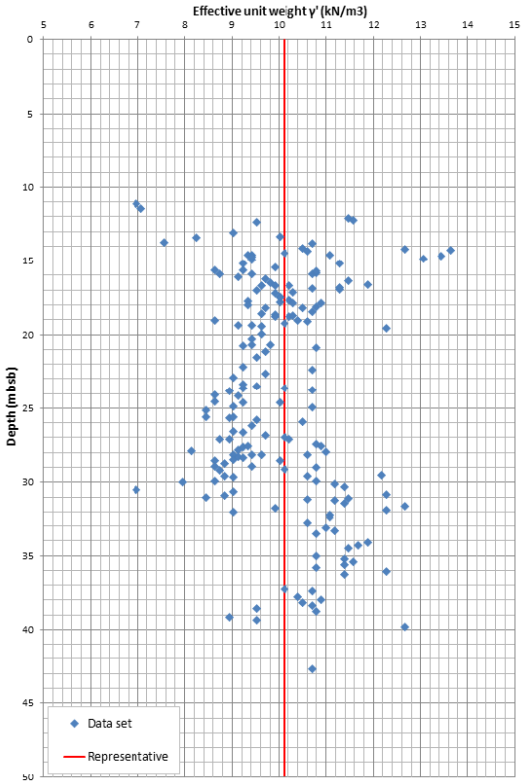

Figure 3.8 Effective unit weight for WIS-MF

3.4.2 Void ratio

The void ratio is an important design parameter in soft soils for the evaluation of soil behaviour. When a soil layer is subjected to vertical stress under drained conditions, volume change can take place through rearrangement of soil grains. As the volume of solids remains constant, the change in total volume is caused by a change in water volume. In saturated soils, this can only happen if water is pushed out of the voids. As a result, compaction occurs and the material becomes stiffer.

For a given soil, a relationship exists between void ratio and unit weight. The unit weight of a soil aggregate is defined as the weight of the aggregate (solids plus water) per unit of volume. It depends on the unit weight of the solid constituents, the porosity and the degree of saturation. For a fully saturated soil, the saturated unit weight is computed as follows. Using relations for porosity, n, and specific gravity, G_s, equation (3.3) can be rewritten as:

$$\gamma_{sat} = (1-n)\gamma_s + n\gamma_w \qquad \textit{Eq. (3.3)}$$

$$\textit{In which} \quad n = e/(1+e)$$

$$\gamma_s = G_s \cdot \gamma_w$$

$$\gamma_{sat} = \frac{G_s + e}{1+e} \cdot \gamma_w$$

The specific gravity of the mineral grains, G_s, is the ratio of the unit weight of solids relative to the unit weight of water. For the SSF-SBD and WIS-MF units, a representative value for particle density is found to be $2.72\ Mg/m^3$ and $2.74\ Mg/m^3$, respectively. Using equation (3.3) above, the void ratio for both fine grained soil units can be computed. A summary is presented in table 3.8.

Table 3.8 Void ratio

Soil unit	Void ratio [-]
	Representative
SSF-SBD	0.962
WIS-MF	0.690

3.4.3 Poisson's ratio

When a material is subjected to compression or tension in one direction, it usually tends to expand or contract in the other directions perpendicular to the applied force. Mathematically, this negative ratio of transverse to axial strain is known as the Poisson's ratio, ν. Isotropic materials must have a Poisson's ratio of $-1 < \nu < 0.5$. Typical isotropic engineering materials have a Poisson's ratio of $0.2 < \nu < 0.5$. The upper limit value of 0.5 is typically associated with a perfectly incompressible material (Mott and Roland, 2009).

In the case of undrained soil behaviour, no volume change is allowed to occur and thus, the soil is assumed to be incompressible. However, this approach leads to certain numerical difficulties in carrying out stress computations in the finite element analysis. A value of 0.5 exactly is not possible, since this would lead to singularity of the stiffness matrix. Thereby, an undrained Poisson's ratio close to 0.5 is selected, typically $\nu_u = 0.495$ (Brinkgreve and Vermeer, 2016). This value of Poisson's ratio is sufficiently high to give minimal volumetric strains, while maintaining numerical stability.

3.4.4 Soil stiffness parameters

Undisturbed incremental and continuous rate of strain (CRS) oedometer tests were performed on clay specimens to determine the soil stiffness parameters. For soft soils, the stiffness parameters can be calculated from the compression (c_c) and swelling (c_s) indices. The relationship between these parameters and the actual stiffness is given in table 3.9. The consolidation test results include the presentation of stress - void ratio in a semi-logarithmic scale. According to Koppula (1981), the compression index, c_c, is derived from the linear part of the curve. The slope of the unloading/reloading curve is called the swelling index, c_s, and is calculated using the same procedure. An example of an actual 1D compression test, in which the c_c and c_s indices are derived, can be found in Appendix D.

Typical values of compression index, c_c	
Soil type	c_c
Dense sand	0.0005 – 0.01
Loose sand	0.025 – 0.05
Firm clay	0.03 – 0.06
Stiff clay	0.06 – 0.15
Medium – soft clay	0.15-1.0
Organic soil	1.0 – 4.5
Rock	0

Table 3.9 Typical values of compression index, cc, according to Koppula (1981).

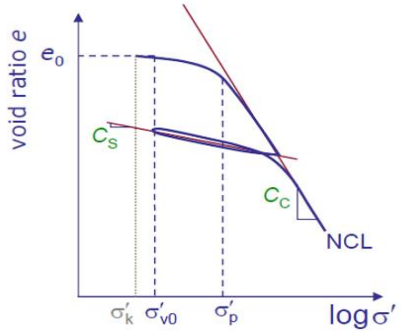

Figure 3.9 Void ratio - effective stress curve

In soft soil conditions, spudcans are expected to penetrate up to 2-3 diameters below the seabed before sufficient bearing resistance has been mobilised (Yi et al., 2012). Therefore, the compression and swelling indices from 25 clay specimens were determined up to a depth of 20 meters below seabed. The results are plotted in figure 3.10. From the graph, it is noted that the compression index shows a large variation. Thus, it would be inaccurate to just take one single characteristic value to represent the soil. Plotting a frequency histogram with bins according to the Koppula (1981) compression index values shows clearly that the clayey material present at the offshore wind farm site location can be classified in two groups; stiff clay and medium-soft clay.

Considering the frequency distribution in more detail, it is assumed that the stiff clay can be characterised by a compression index value of 0.12, based on the relatively large peak at this point. The medium-soft clay is characterised by the right tail of the frequency distribution, as this gives a lower bound for the soil stiffness. The highest compression index value of 0.30 is chosen, as this represents the lowest stiffness in the material. The final model input values are presented below.

Table 3.10 Estimated model input for compression and swelling indices for both clay groups

Soil unit	c_c [-]	c_s [-]
Stiff clay (WIS-MF)	0.12	0.024
Medium-soft clay (SSF-SBD)	0.30	0.050

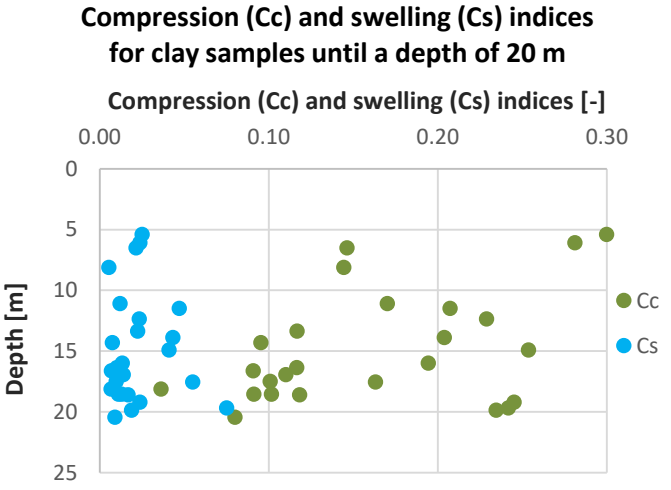

Figure 3.10 Compression (Cc) and swelling (Cs) indices for clay samples until a depth of 20 m

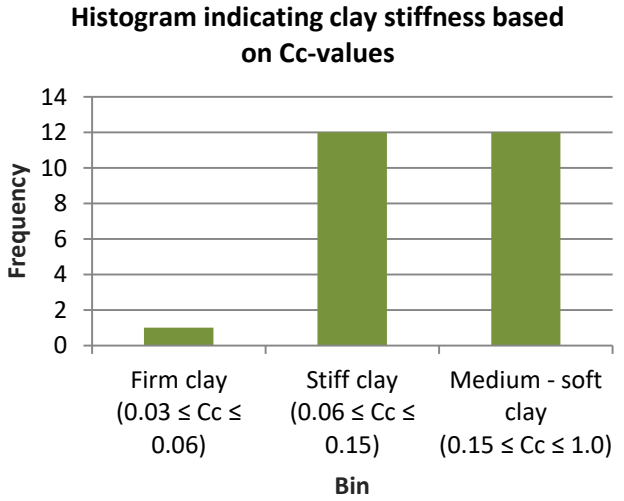

Figure 3.11 Histogram indicating clay stiffness based on Cc-values according to Koppula (1981).

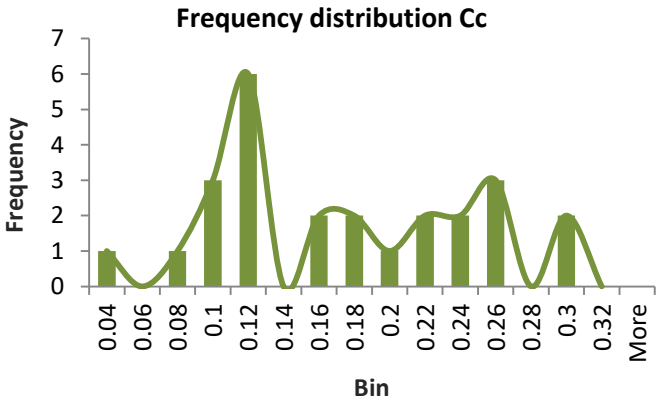

Figure 3.12 Frequency distribution for compression index

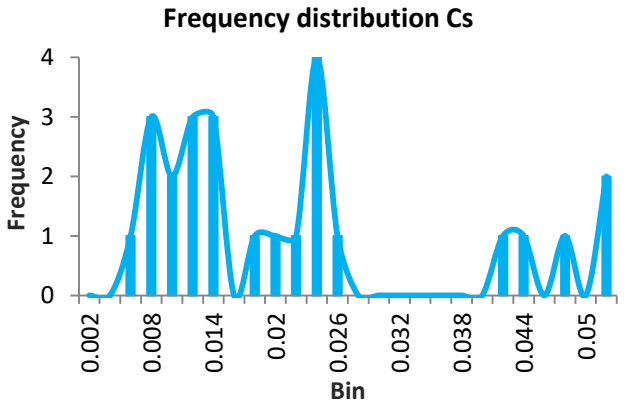

Figure 3.13 Frequency distribution for swelling index

3.4.5 Effective strength parameters

In undrained conditions, a change in total mean stress gives rise to excess pore water pressures. Therefore, to model this correctly, an undrained effective stress analysis with effective strength parameters is required in order to provide the right effective stress path in undrained loading. A problem is that for undrained materials, effective strength parameters are usually not available from soil investigation data. In this section, the effective strength parameters ϕ' and c' are derived from consolidated undrained triaxial tests on cohesive soil specimens.

Effective strength parameters (ϕ', c')

A series of consolidated undrained (CU) triaxial test were performed on cohesive soil specimens at different confining pressures. Since the generated excess pore pressures are measured in this test, we know the change in pore pressure at failure. By knowing both the total stresses and the pore pressures at failure, also the effective stresses at failure can be calculated. Failure is assumed to occur at peak principal effective stress ratio, because the major principal stress increases until failure and reduces after failure as the material no longer offers shear resistance. The effective stress Mohr's circles of both low strength clay (SSF-SBD) and medium strength clay (WIS-MF) are plotted in figure 3.14 and figure 3.15, respectively. Failure envelopes are drawn against the Mohr's circles, which indicate the effective friction angles. As there is a large variation in Mohr's circles for the medium strength clay, it is difficult to draw a clear failure envelope against it. Instead, a best estimate failure envelope is drawn in red against the available data. The results are summarised in the table below.

Table 3.11 Effective strength parameters

Effective strength parameters estimates		
Soil unit	**Effective cohesion** $c'[kPa]$	**Effective friction angle** $\phi'[°]$
Low strength clay (SSF-SBD)	8.0	28.4
Medium strength clay (WIS-MF)	5.0	30.3

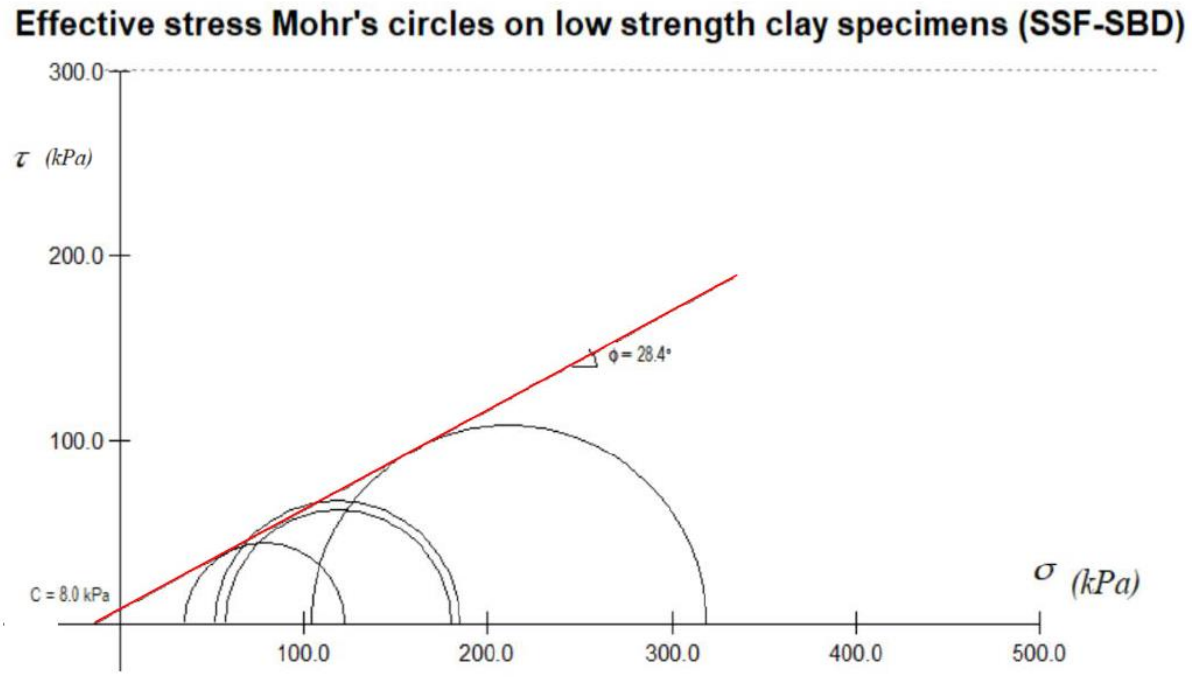

Figure 3.14 Effective stress Mohr's circles on low strength clay specimens (or SSF-SBD soil unit).

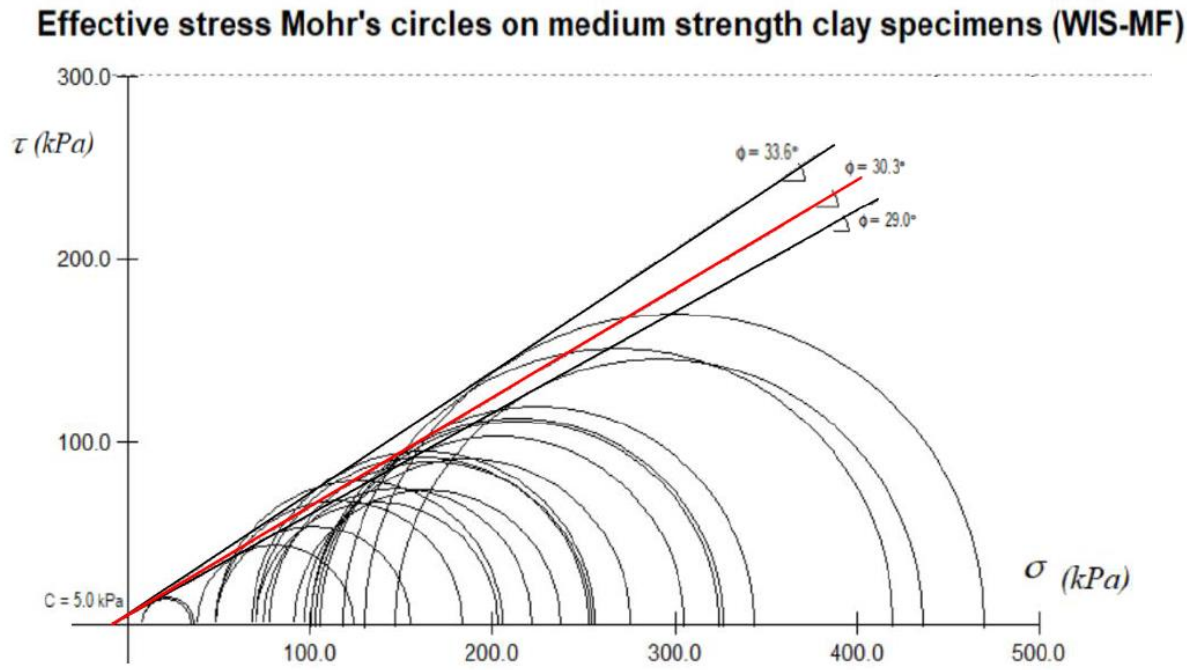

Figure 3.15 Effective stress Mohr's circles on medium strength clay specimens (or WIS-MF soil unit). Best estimate failure envelope shown in red.

Modelling limitation

As will be further explained in chapter 4, the soil will be modelled using the Modified Cam-Clay model. Considering cohesion, a small note must be made regarding the limitations of this soil constitutive model. That is:

Although in reality, some cohesion may be present in soils that have a certain degree of clay content, the PLAXIS implementation of the Cam-Clay model does not allow for a cohesion term in its calculations. Setting the same friction angle with $c' = 0$ could lead the model results a bit away from the actual experimental results. The soil's shear strength, which is a combination of a cohesion term and an internal friction angle term, would be underestimated if the cohesion term is neglected. For the sake of subsequent numerical modelling, an alternative interpretation of the effective strength parameters is adopted, in which c' is constrained to be zero and only ϕ' is fitted to data. As a result, a slightly higher ϕ' is obtained, which in turn, compensates the absence of the cohesion term. The results of the effective parameters used for modelling input are summarised in the table below.

Table 3.12 Effective strength design parameters

Effective strength parameters estimates for modelling input		
Soil unit	**Effective cohesion** $\boldsymbol{c'[kPa]}$	**Effective friction angle** $\boldsymbol{\phi'[°]}$
Low strength clay (SSF-SBD)	0	30.6
Medium strength clay (WIS-MF)	0	32.0

Correlation between Atterberg limits and strength parameters

Effective stress strength parameters (c', ϕ') depend principally on the clay's composition, mineralogy, structure and density. Experiments from different researches show empirical correlations between the friction angle and plasticity index for different types of clay materials, as shown in figure 3.16. The correlations are represented by a decreasing trend of the effective friction angle with increasing plasticity index (Holt, 1962, Wesley, 1977, Terzaghi et al., 1996).

At the offshore wind farm site, both the low strength (SSF-SBD) and medium strength (WIS-MF) clay units have a representative plasticity index of 20%. At first sight, the derived friction angles of $28.4°$ and $30.3°$ seem to be fairly high for clean clays and are typically related to more sandy materials (table E.1 in Appendix E). However, the SSF-SBD and WIS-MF soil units are not clean clays, as its clay content is only 30% and 35%, respectively. Considering the grading curves of both materials, the remaining parts are composed of silt and even sand particles, which may increase the overall friction angle of the mixture. Based on the correlation in figure 3.16, it is suggested that clays with low plasticity (PI = 20%) are expected to show relatively higher angles of internal friction. Especially considering the large variation between different clay types tested, even friction angles up to roughly $35°$ are possible. It is therefore concluded that the derived friction angles of $28.4°$ and $30.3°$ can be considered as proper representative values for the SSF-SBD and WIS-MF soil mixtures, respectively.

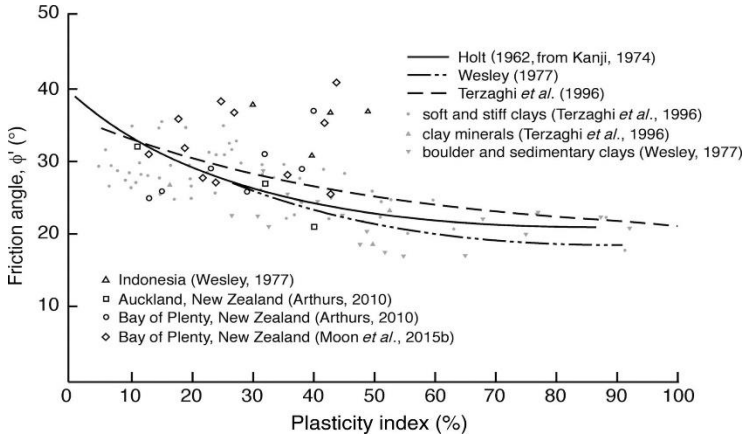

Figure 3.16 Correlation between effective friction angle and plasticity index (Holt, 1962, Wesley, 1977, Terzaghi et al., 1996)

3.4.6 Permeability

During consolidation, excess pore water in the voids is allowed to dissipate, reducing the volume of the soil and hence causing settlement. The rate of drainage of the water from the soil depends on the permeability and the locations of free draining boundary surfaces. Permeability tests on a few specimens indicate the permeability as function of vertical effective stress. An example of a test result can be found in Appendix F. The permeability is derived in a realistic vertical effective stress range, which is assumed to be in the range of $100 - 400\ kPa$. An average value of $6.6 \cdot 10^{-5}\ m/day$ is estimated, which corresponds to typical values found in literature (Waltham, 2009).

Table 3.13 Estimated model input for permeability of clay

Estimated permeability of clay	
k	$6.6 \cdot 10^{-5}\ m/day$

3.4.7 Overconsolidation ratio

The overconsolidation ratio (OCR) is an important parameter in soil deformation behaviour. It defines the formation of soils and is described as the ratio of the preconsolidation pressure over the current effective stress level. Oedometer testing was conducted in order to identify the pre-consolidation stress. Tests were performed using both incremental loading setup and constant rate of strain. If OCR=1 the soil is normally consolidated (NC), if OCR>1 the soil is over consolidated (OC). Soil deformation is higher in normally consolidated soil than it is over consolidated soil.

$$OCR = \frac{\sigma'_p}{\sigma'_{v0}} \qquad \textit{Eq. (3.4)}$$

All preconsolidation pressures were evaluated individually using the Casagrande interpretation method. Figure 3.17 presents the derived overconsolidation ratios as function of depth for the fine grained soil units CBF-C, WIS-MF, WIS-CF and SSF-SBD. Test results indicate that representative OCR values for both the SSF-SBD and WIS-MF soil unit are assumed to be equal to 1, which means that both units can be considered as normally consolidated clays.

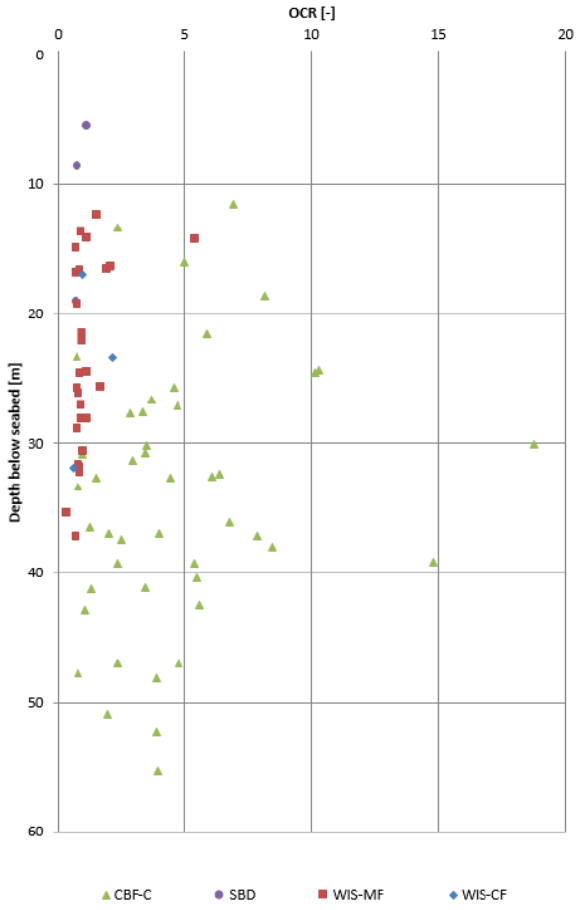

Figure 3.17. OCR values with depth for each formation.

3.5 Shear strength properties of soil

3.5.1 Effect of stress history on the strength of clay

The undrained shear strength of a soil mass, s_u, is an important parameter in design practice. It is defined as the internal resistance per unit area that the soil mass can offer to resist failure and sliding along any plane inside it. Failure from shear will occur when a shear stress on a plane reaches a given critical value. The maximum shear stress that soil can withstand depends on the stress history, i.e. the past and present consolidation stress state. It depends whether the soil is normally consolidated or overconsolidated. In general, higher preconsolidation pressure corresponds to higher relative density, and higher relative density corresponds to higher undrained shear strength.

The OCR can be used to generate the undrained shear strength with depth. Prediction of s_u was accomplished using the SHANSEP (Stress History and Normalised Soil Engineering Properties) procedure and the critical state model. The SHANSEP model was first introduced by Ladd and Foott (1974), in which a soil parameter is normalised by reducing it to a dimensionless number. Here, a normalised parameter is obtained by dividing s_u by the current vertical effective stress, σ'_{v0}. In this method, stress history, which is represented by the overconsolidation ratio OCR, has a great influence on the strength of the soil. The normalised relation is given as follows:

$$\frac{s_u}{\sigma'_{v0}} = \frac{1}{2}\sin(\phi') \cdot OCR^{\Lambda} \qquad \textit{Eq. (3.5)}$$

Where $\Lambda = 1 - c_s/c_c$ is the plastic volumetric strain potential, c_s is the swelling index and c_c is the compression index of the material. If the compression indices and ϕ' are not known with confidence, a recommended default form based on three decades of experimental laboratory work was proposed by Jamiolkowski et al. (1985), which is clearly a subset of the critical state soil mechanics equation where $\phi' = 26°$ and $\Lambda = 0.80$.

$$\frac{s_u}{\sigma'_{v0}} = 0.22\ OCR^{0.80} \qquad \textit{Eq. (3.6)}$$

According to the normalised soil parameter concept, figure 3.18 illustrates data from Ladd and Foott (1974) which shows the variation s_u normalised over σ'_{v0} against the overconsolidation ratio, OCR, for five cohesive soils. All soils show a similar trend of increasing s_u/σ'_{v0} with OCR.

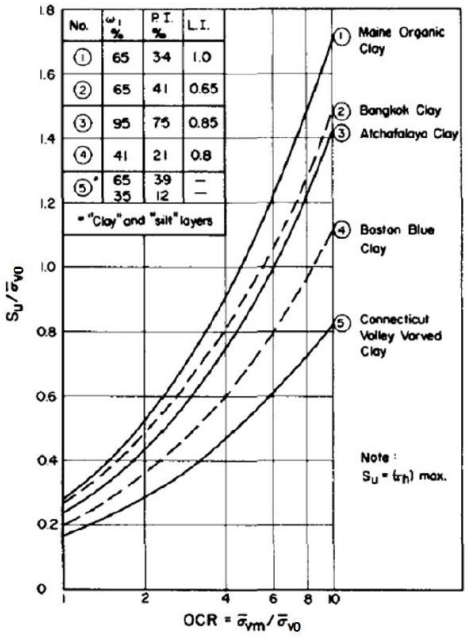

Figure 3.18 Variation of s_u/σ'_{v0} with OCR for five different clays (Ladd and Foott, 1974)

Considering both soil units (SSF-SBD and WIS-MF) have an OCR equal to 1.0, the undrained shear strength can be given as function of the vertical effective stress. Knowing the effective unit weight of both soil units, the s_u-profile as function of depth, z, can be constructed. The results are summarised in table 3.14.

$$s_u = \frac{1}{2}\sin(\phi') \cdot \sigma'_{v0} \qquad \textit{Eq. (3.7)}$$
$$s_u = \frac{1}{2}\sin(\phi') \cdot \gamma' \cdot z$$

Table 3.14 Estimated s_u- profile as function of depth

Soil unit	s_u-profile as function of depth
SSF-SBD	$s_u(z) = 2.19 \cdot z$
WIS-MF	$s_u(z) = 2.68 \cdot z$

3.5.2 Correlation between strength tests and CPTu measurements

Su-profile for WIS-MF soil unit

In order to establish a continuous strength profile at each depth, the s_u-profile is typically determined from CPTu net tip resistance, q_{net}, using the following relationship based on bearing capacity theory as proposed by Terzaghi (1943):

$$s_u^{CU} = \frac{q_{net}}{N_{kt}} = \frac{(q_t - \sigma_{v0})}{N_{kt}} \qquad \textit{Eq.(3.8)}$$

where s_u^{CU} is the undrained shear strength from consolidated undrained triaxial compression tests, q_t is the tip cone resistance, σ_{v0} is the initial vertical stress and N_{kt} is the empirical cone factor relating the undrained shear strength to the cone resistance. For each given s_u derived in the lab, the corresponding cone factor, N_{kt}, is derived based on q_{net} readings in the field. Pore pressure effects, cone geometry and overburden stresses significantly affect measured CPTu tip resistance in soft cohesive soils. All of which must be corrected for prior to calculating s_u and can be a considerable source of error and variability. The correction of the measured tip cone resistance, q_c, to the corrected tip cone resistance, q_t, is given by Lunne et al. (1997), where α is the area ratio, i.e. ratio of the area at the shoulder of the cone (not acted on by pore pressure) to the total cross sectional area of the cone shaft and u_2 is the water pressure at a certain depth.

$$q_t = q_c + (1 - \alpha)u_2 \qquad \textit{Eq. (3.9)}$$

The correlation between strength tests and CPTu measurements is determined in the lab by performing consolidated undrained (CU) and unconsolidated undrained (UU) triaxial compression test on many retrieved samples to determine the undrained shear strength. The general experience with UU-tests for clays with a plasticity index lower than 30-40% is that the UU-shear strength is lower than that found by corresponding CU-test (Fugro Geoconsulting Ltd, 2012-2014). Since the material's representative plasticity index is equal to 20%, a correction factor, k, is applied in order to relate the strengths to s_u^{CU}. To describe the in-situ behaviour best, the UU-tests are corrected to the results of the CU-tests by a factor k of 0.65 in the following manner (Fugro, 2013).

$$s_u^{CU} = \frac{s_u^{UU}}{k} \qquad \textit{Eq. (3.10)}$$

For the WIS-MF soil unit, figure 3.19 shows the results of the undrained shear strengths against the depth below seabed, assuming a representative effective unit weight of $10.1\ kN/m^3$ in the soil above. The derivation of the effective unit weight can be found in section 3.4.1 – Effective unit weight. From the s_u versus depth plot, several design lines can be drawn based on a statistical approach with an average value and standard deviation assuming normally distributed data. For determining the best estimate value, the mean value, μ, is selected, as indicated with the bold black line , whereas the other lines are derived based on ± 0.5 and ± 1.5 standard deviation.

Considering soil mechanics, it can be seen that the SHANSEP approach for determining the s_u-profile with depth as described by Ladd and Foott (1974) matches the statistical data very well. This s_u-profile is assumed to be equal to the in-situ undrained shear strength profile and used in the next chapter to calibrate the Modified Cam-Clay model parameters.

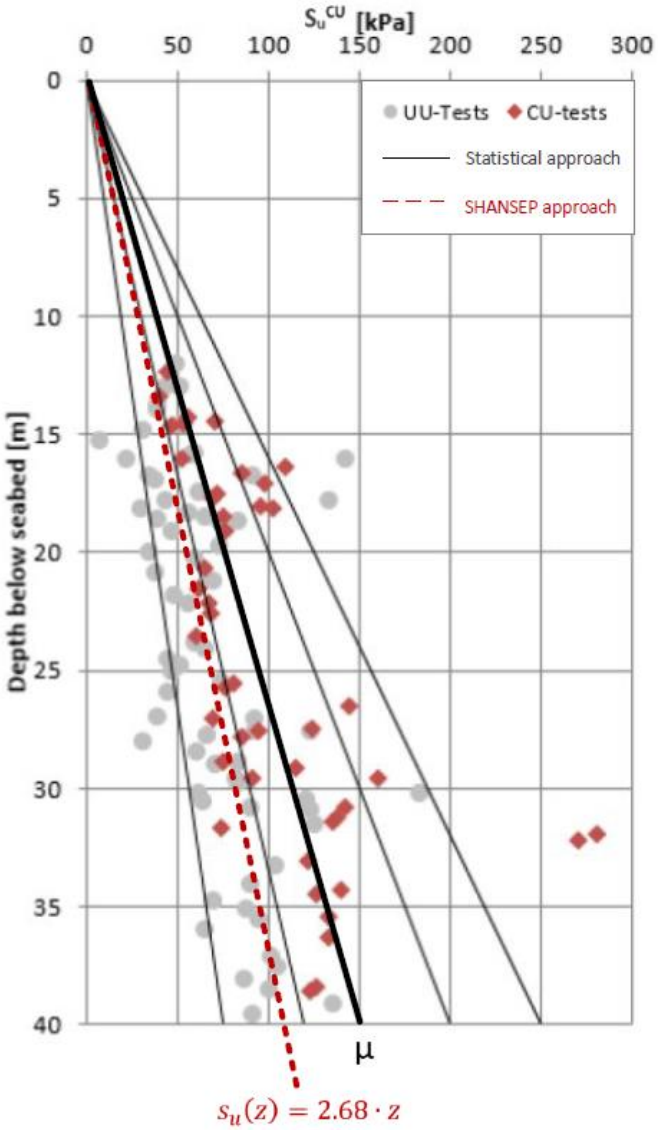

Figure 3.19 S_u-profile as function of depth for WIS-MF soil unit

The above shear strength profile of the normally consolidated WIS-MF soil unit can be defined as an initial strength with linearly increasing shear strength with depth, given by:

$$s_u = s_{um} + k_{su} \cdot z \qquad \textit{Eq. (3.11)}$$

where s_u represents the shear strength of the soil at depth z, s_{um} represents the shear strength at the mudline, which is linearly increased by the shear strength gradient k_{su}. The increase of undrained shear strength with depth is caused by the fact that larger effective stress states of the soil correspond to a higher shear stresses at failure. Since data from CU-triaxial tests are only available using a certain confining pressure, no tests results are available representing stress states up to a depth of roughly ten meters. Based on a linearly increasing undrained shear strength trend, the s_u-profile is extrapolated up to zero at the seabed. At the seabed, the undrained shear strength equals to zero, because the effective stress level at the mudline equals to zero. With a shear strength gradient of $2.68\ kPa/m$, an undrained shear strength of $107.2\ kPa$ is reached at a depth of 40m below the seabed. The shear strength profile for the WIS-MF soil unit can be defined as:

$$s_u = 2.68 \cdot z \qquad \textit{Eq. (3.12)}$$

Su-profile for SSF-SBD soil unit

For SBD, a very soft and low strength material, the N_{kt} approach is found inappropriate for describing the strength distribution. The measured q_c values are relatively small and the excess pore pressure may become very high. Even small errors in measured tip cone resistance can influence the results significantly, which introduces uncertainty to the estimated values of s_u. For this reason, Lunne et al. (1997) recommended the use of excess pore pressure instead of q_{net} to derive the undrained shear strength profile for very soft soils.

$$s_u^{CU} = \frac{\Delta u}{N_{\Delta u}} = \frac{u_2 - u_0}{N_{\Delta u}} \qquad \textit{Eq. (3.13)}$$

Where u_0 is the hydrostatic pore water pressure, u_2 is the pore pressure measured and $N_{\Delta u}$ is the empirical cone factor relating the undrained shear strength to the excess pore water pressure measured. The cone factor is based on correlation results of the various compression tests done by Fugro Geoconsulting Ltd (2012-2014). For each given s_u derived in the lab, the corresponding cone factor, $N_{\Delta u}$, is derived based on measured excess pore water pressures in the field. The test results are focussed on the CU-tests, as these test results are considered more representative for the in-situ state than the UU-tests results. Figure 3.20 shows the undrained shear strengths plotted versus depth, including some statistically derived design lines, assuming a representative effective unit weight of $8.6\ kN/m^3$ in the soil above (Effective unit weight derived according to method described in section 3.4.1 – Effective unit weight). Similarly, due to lack of CU-tests at very low confining pressure, the linear s_u-profile is extrapolated up to zero at the seabed. The resulting shear strength profile for the SSF-SBD soil unit can be defined as:

$$s_u(z) = 2.19 \cdot z \qquad \textit{Eq. (3.14)}$$

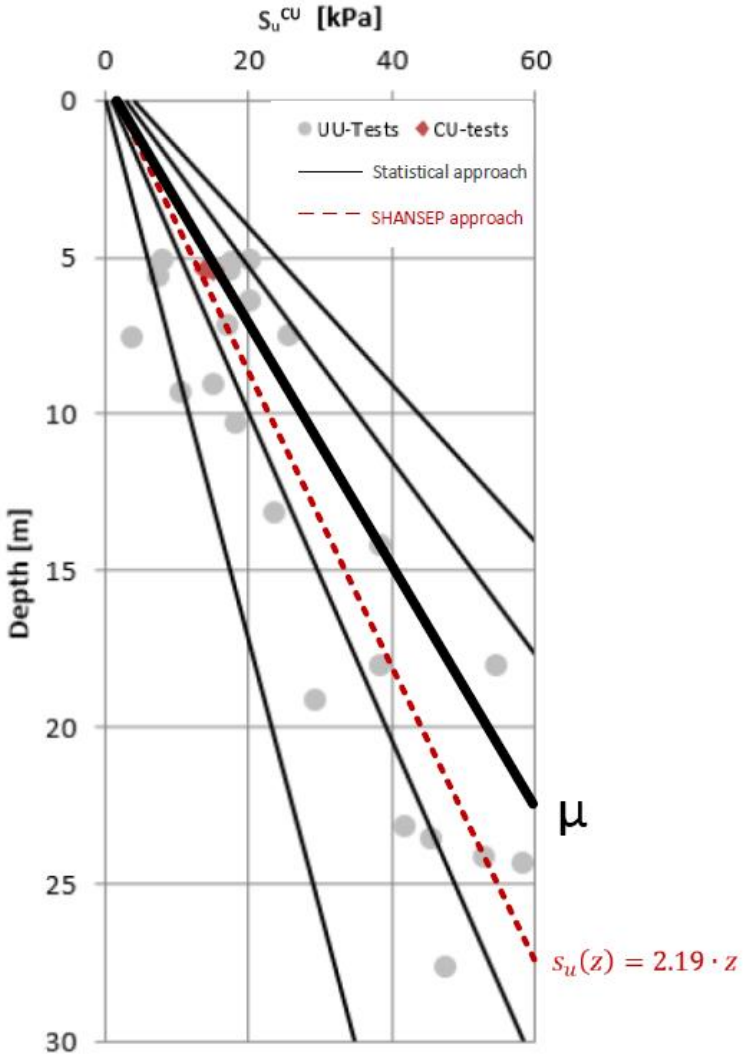

Figure 3.20 s_u-profile as function of depth for SSF-SBD soil unit

4. Constitutive modelling

4.1 Introduction

Numerical analysis has become one of the most important tools for predicting soil behaviour. The mechanical behaviour of soils may be modelled at various degrees of accuracy. Numerous constitutive models were developed over the past few years, each having different capabilities and shortcomings. A key problem in numerical analysis is to select proper soil constitutive models and their corresponding parameters for a particular task. According to the PLAXIS Material Models Manual (2016), the selection of a proper soil constitutive model depends not only on the soil type, but also on the type of application and type of loading of the soil. An overview of the applicability of different soil models is given in Appendix G.

In the case of offshore spudcan penetration at the offshore wind farm site, the subsoil consists of weak, silty-clay material which generally governs the material behaviour. First order approximation of practical analyses of geotechnical problems often assume material behaviour to be linear elastic, which is modelled by the Mohr-Coulomb model. However, soft soils do not simply behave linear elastically. Soft soil behaviour is highly non-linear, with both strength and stiffness depending on stress and strain levels. For realistic predictions, a more complex constitutive model is therefore required.

Due to the complexity of real soil behaviour, a single constitutive model that can describe all features of behaviour, with a reasonable number of input parameters, does not exist. Each model has different advantages and disadvantages. Regarding the loading type, in this case, the soil behaviour is considered to be undrained, because load is applied fast to a low permeable material in offshore conditions. During preloading, both primary compression of normally consolidated material and recompression of (lightly) overconsolidated materials might occur. Moreover, in a more practical way, the availability and quality of information from soil investigation data plays also an important role in selecting a suitable soil model.

The Modified Cam-Clay (MCC) material model is used in the model calculations, as this is based on critical state soil mechanics. Critical state soil mechanics is based on the observation that soils ultimately reach critical state at large strains, and at critical state there is a unique relationship between shear stress, normal effective stress, and void ratio. Since critical state is independent of the initial state, the parameters that define critical state depend only on the nature of the grains of the soils and can be linked to basic soil classification (Atkinson, 2007). In fine-grained soils, the current in-situ state is defined in terms of overconsolidation ratio (OCR), which is related to the normal compression line. In the Modified Cam-Clay model, stress paths are allowed to go beyond the failure line and touch the elliptical locus to then give rise to strain softening of (lightly) overconsolidated soils, whereas the Soft Soil or Hardening Soil models are not capable in doing so as the stress paths cannot go beyond the Mohr-Coulomb failure line and only strain hardening is able to occur (no strain softening). This phenomenon is further explained in detail in the next section.

4.2 (Modified) Cam-Clay model

The Cam-Clay model was developed by researchers of the University of Cambridge (hence its name) in the 1950s-1960s (Roscoe et al., 1958). It is considered as the most influential soil model ever proposed, because many of the more sophisticated models proposed in the recent years adopt the Cam-Clay model as their backbone.

Normal consolidation line and Swelling Lines

The model assumes that when a soft soil sample is slowly compressed under isotropic stress conditions ($\sigma_1' = \sigma_2' = \sigma_3' = p'$) and under drained conditions, a linear relationship holds between the specific volume, v, and the natural logarithm of the mean effective stress, p', as shown in figure 4.1. The straight line with inclination λ indicates primary loading and is called the isotropic normal consolidation line (iso-NCL). This line shows that an increase in mean effective stress leads to a reduction of void ratio. The straight line with inclination κ indicates unloading and reloading. This line can start anywhere from the normal consolidation line depending on the preconsolidation pressure, p_0. Any stress level before the preconsolidation pressure will follow a line parallel to the κ-line. Upon primary loading, the soil will memorise the new maximum stress level and so the preconsolidation pressure will increase. If the current state of a soil is on the normal consolidation line, the soil is described as being normally consolidated. The soil becomes overconsolidated when the stress state is described by the κ-line.

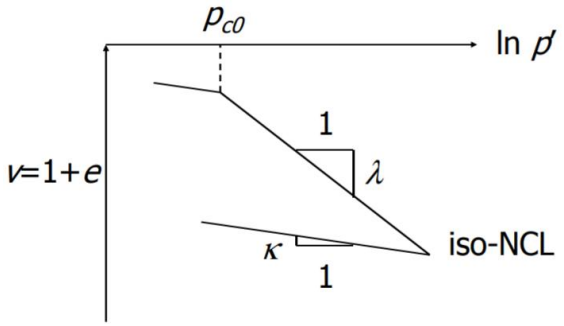

Figure 4.1 Linear relationship between specific volume and natural logarithm of mean effective stress.

Primary loading:

$$e_0 - e = \lambda \ln\left(\frac{p'}{p_0}\right) \qquad \textit{Eq. (4.1)}$$

Unloading / reloading:

$$e_0 - e = \kappa \ln\left(\frac{p'}{p_0}\right) \qquad \textit{Eq. (4.2)}$$

The Critical State Line

The Cam-Clay model is a critical state model for describing the behaviour of soft soils. The concept of critical state is that it is not just a state of failure, but it is defined as the situation in which there is no further change of volume as a soil sample is continuously sheared ($\psi = 0$). This state is called the critical state and is characterised by the critical state line (CSL). In the (p', q)-plane, the CSL is a straight line passing through the origin with slope equal to M. The critical state parameter M is considered a material constant, which determines the shape of the yield surface (height of ellipse) and is related to the friction angle. For initial compression stress states, the slope of the critical state line is approximated as:

$$M = \frac{6 \sin \phi'}{3 - \sin \phi'} \qquad \textit{Eq. (4.3)}$$

Yield functions

For the original Cam-Clay model, the yield contour is given by the following yield function:

$$f = \frac{q}{p'} - M \ln\left(\frac{p_c}{p'}\right) \qquad \textit{Eq. (4.4)}$$

Following a compressive stress that tends to pass the yield contour will lead to an increase in preconsolidation stress. As a result, the yield contour will expand (hardening) such that it keeps up with the current stress state. During expansion of the yield contour, the top of the contour remains at the critical state line. The increase of preconsolidation stress is associated with plastic compaction.

In the original Cam-Clay model, the plastic potential function, g, is equal to the yield function, f (associated plasticity: $g = f$). Since the plastic potential function is equal to the yield function, the plastic strain directions are also perpendicular to the yield contour. The magnitude and direction of the plastic strain increment vector is calculated with the flow rule, as described in equation (4.5). In here, the hardening rule expresses the change of plastic volumetric strain as function of the change of preconsolidation stress. This involves the compression and swelling parameters as described above. The compression index, λ, is associated with primary loading, which involves both elastic and plastic strain, whereas the swelling index, κ, is associated with unloading and reloading, which involves only elastic strain. The difference between λ and κ is thus associated with plastic strain. Moreover, it can be seen when integrating the hardening rule in differential form, a logarithmic stress-strain relation is obtained, which is consistent with equations (4.1) and (4.2).

Flow rule $$\frac{d\varepsilon_v^p}{d\varepsilon_s^p} = \frac{\partial g/\partial p'}{\partial g/\partial q} = M - \frac{q}{p'} \qquad \textit{Eq. (4.5)}$$

Hardening rule $$d\varepsilon_v^p = \frac{\lambda - \kappa}{v}\frac{dp_c}{|p_c|} \qquad \textit{Eq. (4.6)}$$

Now, having a closer look at the yield contour around the critical state line (figure 4.2), three distinctive stress states can be identified.

- For stress states right from the CSL, where $q < Mp'$, it follows from the flow rule that the increment in plastic volumetric strain is negative (which is compaction), and consequently from the hardening rule that the increment in pre-consolidation stress is negative. Since pre-consolidation stress is negative for compression, a negative increment results in a further increase of the pre-consolidation stress in absolute sense. This gives an expansion of the yield contour, which is hardening behaviour. This side of the yield surface is known as the wet side.
- For stress states left from the CSL, where $q > Mp'$, it follows from the flow rule that the increment in plastic volumetric strain is positive (which is expansion or dilatancy), and consequently from the hardening rule that the increment in pre-consolidation stress is positive. Since pre-consolidation stress is negative for compression, a positive increment results in a decrease of the pre-consolidation stress in absolute sense. This gives shrinkage of the yield contour, which is softening behaviour. This side of the yield surface is known as the dry side.
- For stress states on the CSL, located at the top of the yield contour, where $q = Mp'$, it follows from the flow rule that the increment in volumetric plastic strain is zero, and consequently from the hardening rule that the increment of preconsolidation stress is zero. In this case, there is no hardening or softening.

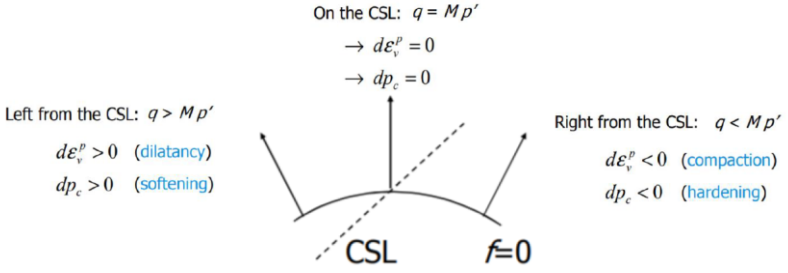

Figure 4.2 Stress states in Cam-Clay model

Modified Cam-Clay model

In the original Cam-Clay model, the yield surface has a logarithmic spiral shape. This shape was theoretically derived based on an energy equation. However, it is an inconvenient shape, as it has a pointly tip at point $(p', q) = (p_0, 0)$. Consequently, numerical troubles arise when the associated flow rule is applied, because discontinuity is encountered on the gradient of the yield surface. The direction of the plastic strain is not properly defined at the corner point. The singularity at this point causes the model to predict unrealistic plastic strain increments against isotropic compression.

The singularity at the corner of the original Cam-Clay model has triggered researches to come up with a slightly different formulation: the Modified Cam-Clay model (MCC). The only difference between the original Cam-Clay model and the Modified Cam-Clay model is the shape of the yield surfaces. The yield function of the Modified Cam-Clay model represents an ellipse in (p', q)-stress space. The top of the ellipse is located at the critical state line. The yield function of the Modified Cam-Clay model and the modified flow rule are give as:

Yield function $$f = \frac{q^2}{M^2} + p'(p' - p_c) \qquad \textit{Eq. (4.7)}$$

Flow rule $$\frac{d\varepsilon_v^p}{d\varepsilon_s^p} = \frac{\partial g/\partial p'}{\partial g/\partial q} = \frac{M^2 - q^2/p'^2}{2q/p'} \qquad \textit{Eq. (4.8)}$$

All other features of the Modified Cam-Clay model are similar to the original Cam-Clay model. The hardening rule is similar in both models, which makes the logarithmic stress-strain relationship in the Modified Cam-Clay model also valid. However, note that at the corner point of the elliptic yield surface, the plastic strain increment vector, which is perpendicular to the yield surface, is horizontal, and hence no plastic shear strain increment takes place $(d\varepsilon_s^p = 0)$ for a change in mean effective stress.

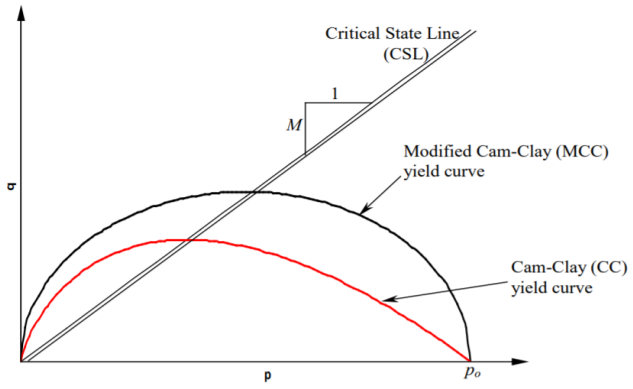

Figure 4.3 Difference between original Cam-Clay and Modified Cam-Clay model.

Parameters of the Modified Cam-Clay model

The Modified Cam-Clay model is based on five parameters. An overview is given in table 4.1. The derivation and interpretation of these input parameters are defined in detail in section 4.4 – Calibration of soil model.

Table 4.1 Input parameters MCC-model

Input parameters Modified Cam-Clay model			
Stiffness	λ	Cam-Clay compression index	[–]
	κ	Cam-Clay swelling index	[–]
	ν'_{ur}	Poisson's ratio for unloading/reloading	[–]
	e_{init}	Initial void ratio	[–]
Strength	M	Tangent of Critical State Line	[–]

4.3 Modelling undrained behaviour

The concept of undrained behaviour is the condition under which there is no flow of water into or out a mass of soil when the soil is subjected to a change of load. As a result, excess pore pressures are built up. Undrained analysis is appropriate in short-term behaviour when permeability is low or the loading rate is high. These conditions apply in the case of offshore spudcan penetration. PLAXIS offers different modelling schemes, which depend on the selection of the drainage type parameter, i.e. Undrained (A), (B) or (C). An overview and consequences of a particular selection of the drainage type parameter for undrained soil behaviour is given below. (PLAXIS Reference Manual 2017; PLAXIS Material Model Manual 2016)

Undrained (A)
The drainage type Undrained (A) enables modelling of undrained behaviour using effective parameters for stiffness and strength. Undrained effective stress analysis can be used in combination with effective strength parameters ϕ' and c' to model the material's undrained shear strength. PLAXIS automatically adds the stiffness of water to the stiffness matrix in order to distinguish between effective stresses and excess pore pressures. In this case, the development of the pore pressure plays a crucial role in generating the right effective stress path that leads to failure at a realistic value of undrained shear strength. However, most soil models are not capable of providing the right effective stress path in undrained loading. This is because the effective stress path followed in an undrained analysis may deviate from reality, due to limitations of the applied soil model. As a result, wrong output of undrained shear strength is produced if the material's strength is specified on the basis of effective strength parameters. It is therefore important to carefully calibrate the model outcome against the actual in-situ undrained shear strength profile, as done in the previous chapter. The advantage of using effective strength parameters in undrained loading conditions is that a qualitatively increased shear strength is obtained after consolidation. Yet, note that this increased shear strength could also be quantitatively wrong as it might deviate from reality.

Regarding the Modified Cam-Clay model, figure 4.4 (a) and (b) represents the situation of an undrained triaxial test considering normally consolidated material behaviour (Wood, 1990). The undrained test conditions prevent any volumetric strain to occur, which results in a constant void ratio or specific volume and hence, a horizontal path in the (v, p')-diagram, as shown in figure 4.4 (b). However, excess pore pressure will be generated instead and distinction is made between the total stress path (TSP) and the effective stress path (ESP). Isotropic elastic behaviour gives a TSP inclination (dq/dp') of 3:1 for triaxial compression. The ESP follows a curved line, bending towards the left in the (p', q)-diagram of fig 4.4 (a), starting from point A to B, C, D, E and finally towards F on the critical state line. The difference between TSP and ESP is the pore pressure, Δu. The bending of the ESP is explained as follows. Due to undrained behaviour, there is no net volumetric strain. However, since the yield contour will expand due to hardening, inevitable plastic volumetric strains (compaction) will be generated at the wet side of the CSL. These plastic volumetric strains need to be compensated by elastic expansion. According to the elastic part of the model, elastic expansion is associated with a reduction of mean effective stress, which explains why the ESP bends towards the left. The hardening process continues until the CSL is reached.

In the situation of an undrained test considering lightly overconsolidated material behaviour, the initial yield contour is beyond the initial stress state $(p_c > p')$, as shown in figure 4.4 (c). This means that during the first part of deviatoric loading, the behaviour is purely elastic $(dp' = 0)$ until the stress path reaches the initial yield contour at point B. From point B onwards, the hardening process starts, leading to a reduction of the mean effective stress, similar as in the previous case.

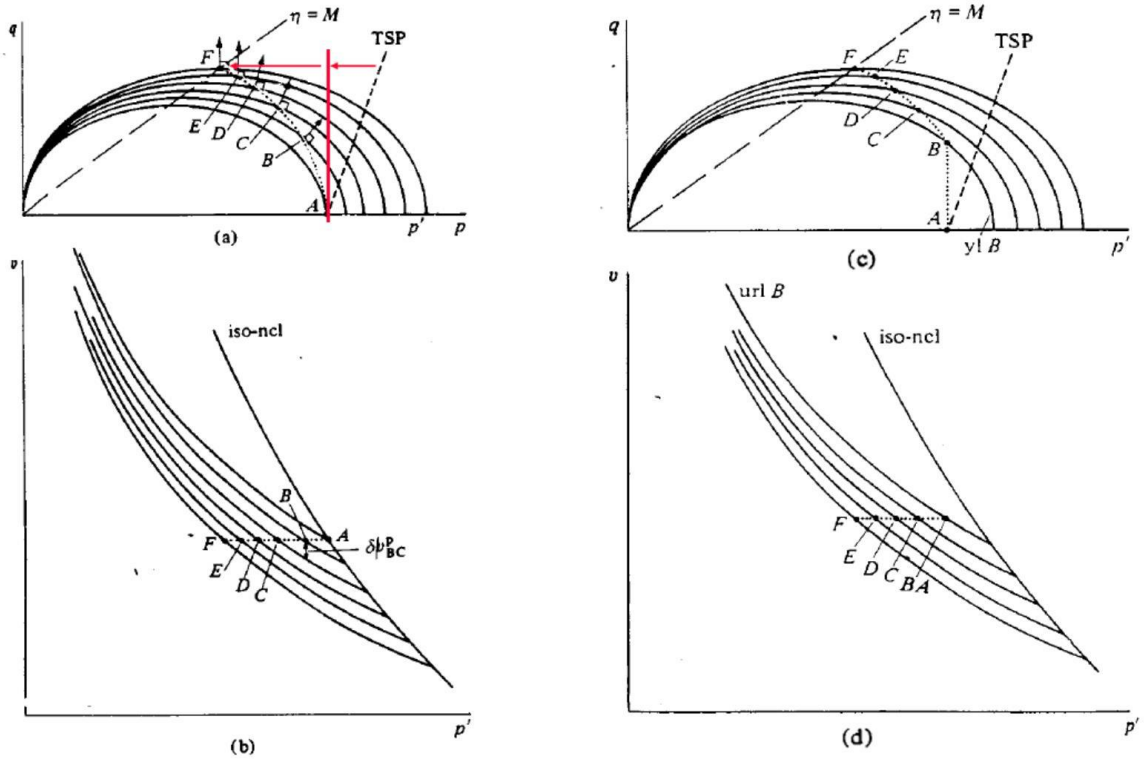

Normally consolidated Lightly overconsolidated

Figure 4.4 Total and effective stress paths followed considering normally consolidated (left) and lightly over-consolidated material behaviour using the Modified Cam-Clay material model. (Wood, 1990)

In summary, the characteristic features of the Undrained (A) method are:

- Undrained calculations are performed as effective stress analysis, using effective stiffness and strength parameters.
- Pore pressures are generated, but may be inaccurate. Effective stress path in the model may deviate from reality.
- Undrained shear strength is not an input parameter, but outcome of the constitutive model. Check resulting shear strength against known data.
- Consolidation analysis can be performed after the undrained analysis, without manually update the undrained shear strength.

Undrained (B)

In order to control the undrained shear strength directly, PLAXIS allows for an undrained effective stress analysis with direct input of the undrained shear strength. The drainage type should then be set to Undrained (B). A disadvantage of the undrained (B) approach is that a direct input of undrained shear strength does not automatically give an increase of undrained shear strength with consolidation. In a consolidation analysis, the undrained shear strength needs to be manually updated, which is time consuming and prone to error.

The drainage type Undrained (B) enables modelling of undrained behaviour using effective parameters for stiffness and undrained total parameters for strength. PLAXIS offers for some models an undrained effective stress analysis with direct input of the undrained shear strength. This option is only available for the Mohr-Coulomb model, the Hardening Soil model, the HS small model and NGI-ADP model. It is not available for the Modified Cam-Clay model. Therefore, it will not be further discussed.

Undrained (C)
Drainage type Undrained (C) enables simulation of undrained behaviour using a total stress analysis with undrained parameters. The disadvantage of this approach is that no distinction is made between effective stresses and pore pressures. Hence, all output referring to effective stresses should now be interpreted as total stresses as no pore pressures are generated. This approach cannot be used when modelling consolidation. Therefore, it will not be further discussed.

4.4 Calibration of soil model

In order to make reliable predictions of field performance, the model input parameters of the Modified Cam-Clay model should be calibrated against the actual soil properties. When using the undrained (A) approach in modelling undrained soil behaviour, the undrained shear strength is an output of the model calculations. Calibration is then performed by selecting the Modified Cam-Clay parameters in such a way that the resulting undrained shear strength profile approximates the in-situ undrained shear strength profile. According to the Geotechnical Interpretative Report (2015), two calibration cases can be identified based on the in-situ s_u-profiles of the SSF-SBD and WIS-MF soil unit. The calibration method of both cases are elaborated below.

4.4.1 Case 1: Calibration of MCC-parameters according to SSF-SBD soil unit

Soil constitutive models establish the relationship between applied stresses and strains. Material elastic, hardening law, yield criterion, and plastic potential parameters are required to mathematically formulate the soil constitutive relationships. For the Modified Cam-Clay model, the input parameters are calibrated such that the undrained shear strength profile as defined in section 3.5 is approximated as best as possible.

Tangent of the critical state line (M)
The angle of shearing resistance at critical state, or conventionally known as critical state friction angle, ϕ'_{cv}, is a key parameter in formulating constitutive models in the framework of critical state soil mechanics. In triaxial compressive stress states, the tangent of the CSL is defined by:

$$M = \frac{6 \sin \phi'_{cv}}{3 - \sin \phi'_{cv}} \qquad \textit{Eq. (4.9)}$$

Varying the stress ratio, M, may affect the yield surface and flow rule and hence the overall stress–strain behaviour, as shown in the Cam-Clay-type models. Laboratory CU-triaxial compression tests are used to obtain a value for the effective friction angle. The methodology and results are elaborated in section 3.4.5 – Effective strength parameters. Since the Cam-Clay model does not allow for a cohesion term in its calculations, the effective friction angle used as model input ($\phi' = 30.6°$) is higher than the actual ϕ' as measured in triaxial tests ($\phi' = 28.4°$). For soft soil, this is considered to be a relatively high angle of internal friction. As can be seen further in this section, the effective friction angle will be reduced by $3°$ in order to fit the model outcome more closely to the actual s_u-profile. The tangent of the CSL is found to be equal to $M = 1.0$.

Figure 4.5 shows the expanding yield surface during isotropic consolidation of the Modified Cam-Clay model in (p', q)-stress space for different stress states. The top of the yield surface crosses the CLS, which has an inclination of $M = 1.0$. However, the actual soil as present in the field does not exhibit isotropic compression. Typically, for normally consolidated soils, the horizontal stress is computed from the vertical stress using the coefficient of earth pressure at rest, $K_0^{NC} = \sigma_h{}'/\sigma_v{}'$, where σ'_h and $\sigma_v{}'$ are effective horizontal and vertical stresses, respectively. When loading the soil, shearing starts from an anisotropic stress state on the K_0^{NC}-line, following anisotropic consolidation until failure.

Since the material is assumed to be normally consolidated, only strain hardening behaviour occurs by expanding the yield surface as p' is increased beyond the preconsolidation stress, p'_c. The associated stress paths will always approach the CSL from the right side (wet side) in the (p', q)-plane. For normally consolidated soils, strain softening will never happen and therefore, the effective stress paths will not go beyond the CSL. If the material is overconsolidated, the MCC-model will allow for stress paths to go beyond the CSL and touch the elliptical locus to then give rise to strain softening. This model is thus able to model both NC and OC soils.

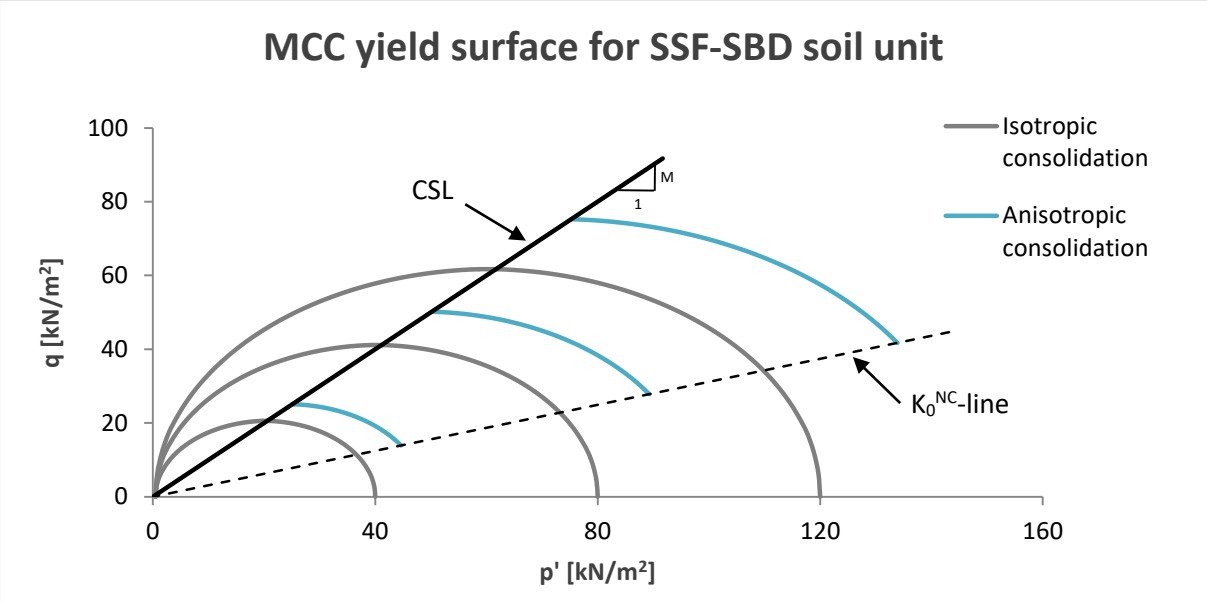

Figure 4.5 MCC yield surface for SSF-SBD soil unit.

Initial void ratio (e_{init})

The void ratio is an important parameter in relation to the soil behaviour. Generally, the lower the void ratio, the more dense the material and the higher its strength and stiffness. The initial void ratio is considered to be equal to the in-situ void ratio of the soil body in the field. For the SSF-SBD soil unit, an initial void ratio $e_{init} = 0.962$ is found.

The void ratio is a state parameter, which means that it evolves as function of the plastic strain. By combining the yield contour of the MCC-model in (p', q)-stress space for different values of the preconsolidation stress with the logarithmic stress-strain relationship in the (p', v)-space, a three dimensional diagram results showing the MCC yield surface in the p, q, v-space. This diagram links the stress state to the density. The void ratio is required by the MCC-model to estimate the soil volumetric strain deformations. The initial void ratio is the parameter that defines the initial volume state of the soil and is related to a mean effective stress state of $p' = 1\ kPa$.

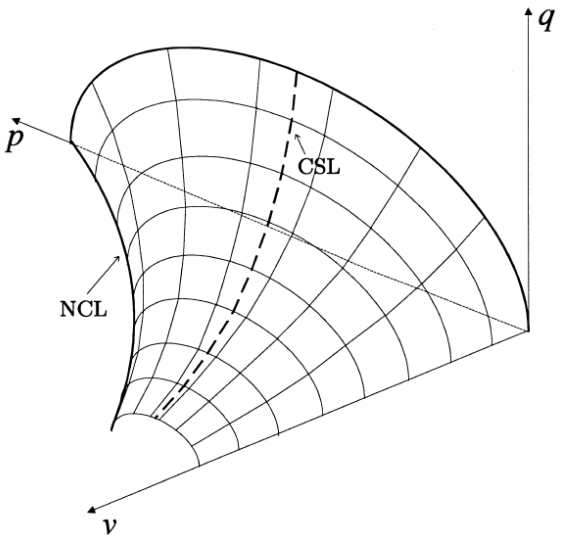

Figure 4.6 MCC yield surface in (p,q,v)-space.

Poisson's ratio (ν'_{ur})
The Poisson's ratio for unloading/reloading is an elastic parameter needed to describe deformation properties of a soil. According to the PLAXIS Material Models Manual (2016), its value will usually be in the range between 0.1 and 0.2. An average value of $\nu'_{ur} = 0.15$ is used.

Compression (λ) and swelling (κ) index
These parameters can be obtained from isotropic compression tests including isotropic unloading, as explained in section 4.2 – (Modified) Cam-Clay model. The values of the compression and swelling indices should be chosen in such a way that the in-situ s_u-profile is approximated as best as possible.

As a first estimate, the slopes of the normal compression line (λ) and swelling line (κ) in $v, ln(p')$-space are related to the slopes of the primary compression line (c_c) and the unloading/reloading line (c_s) in graphs of void ratio versus log effective stress, using equations (4.10) and (4.11) (Brinkgreve and Vermeer, 1998). Often, κ if found to be in the range of $\lambda/3$ to $\lambda/5$.

$$\lambda = \frac{c_c}{\ln(10)} \qquad \textit{Eq. (4.10)}$$

$$\kappa = \frac{c_s}{\ln(10)} \qquad \textit{Eq. (4.11)}$$

The values $\lambda = 0.13$ and $\kappa = 0.022$ are found. From the results of 'calibration 1' in figure 4.7, it can be seen that there is a large deviation from the assumed in-situ shear strength profile. The shear strength gradient obtained from this approach is much larger compared to the in-situ profile.

A second calibration is done by changing the values of λ and κ such that a best estimate is found, in which the difference between the shear strength gradients of the in-situ profile and model outcome is as small as possible. With $\lambda = 0.05$ and $\kappa = 0.002$, the in-situ s_u-profile is approximated more closely. Yet, still a deviation of 17% is present, which may be caused by the relatively high effective friction angle of the material. Due to uncertainties in the derivation of the effective friction angle, it is decided to adopt a conservative approach in which ϕ' is reduced until the model outcome matches the in-situ undrained shear strength profile. This approach is allowed since s_u is the main important factor for deriving the soil strength and thus, the model is expected to generate an identical s_u-profile as present in the field.

In the third calibration, it can be seen that reducing the actual derived effective friction angle from $\phi' = 28.4°$ to $\phi' = 25.4°$, while keeping λ and κ the same, results in a model output which matches the in-situ undrained shear strength profile very well. The tangent of the Critical State Line becomes $M = 1.0$. The final, calibrated MCC-parameters representing the SBD soil unit are summarised in table 4.2.

Table 4.2 Calibrated input parameters MCC-model for SSF-SBD soil

Calibrated input parameters for Modified Cam-Clay model for SSF-SBD			
Stiffness	λ	0.05	[−]
	κ	0.002	[−]
	ν'_{ur}	0.15	[−]
	e_{init}	0.962	[−]
Strength	M	1.0	[−]

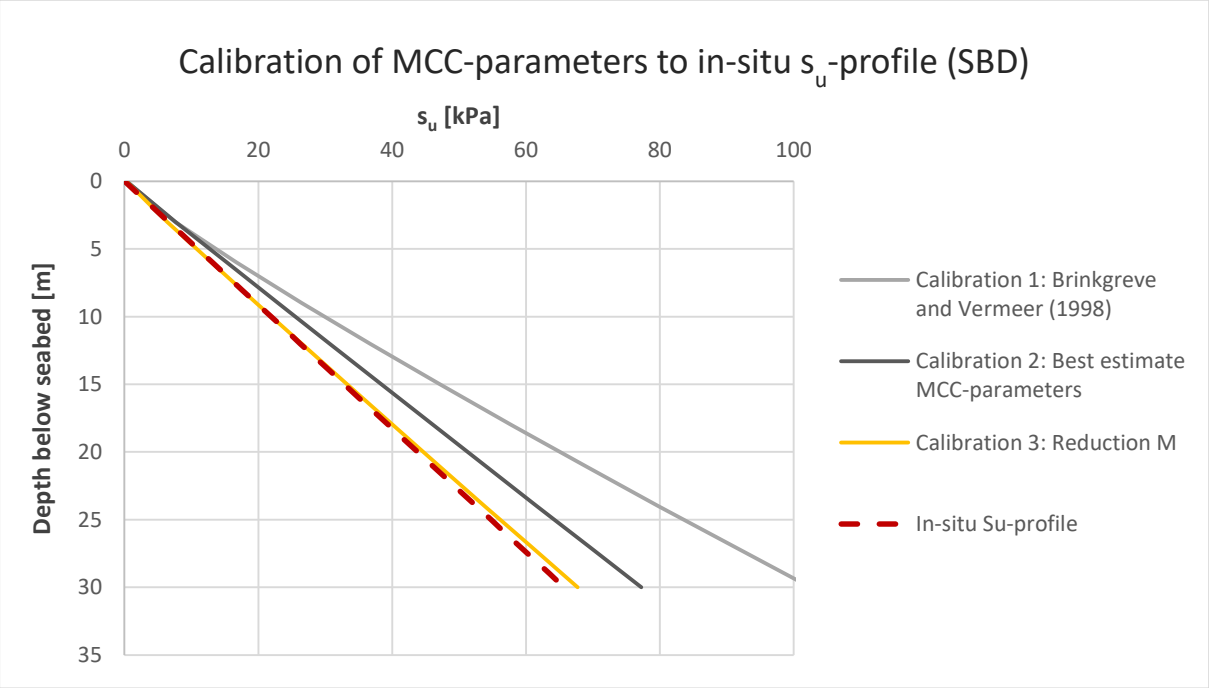

Figure 4.7 Calibration of MCC-parameters to in-situ s_u-profile for SBD soil.

4.4.2 Case 2: Calibration of MCC-parameters according to WIS-MF soil unit

Tangent of the critical state line (M)

For the WIS-MF soil unit, the angle of internal friction is also reduced by 3° to $\phi' = 27.3°$ in order to fit the model outcome to the actual s_u-profile. This results in a value for the tangent of the Critical State Line of $M = 1.08$. The expanding yield surface in both isotropic and anisotropic consolidation is shown in figure 4.8 below.

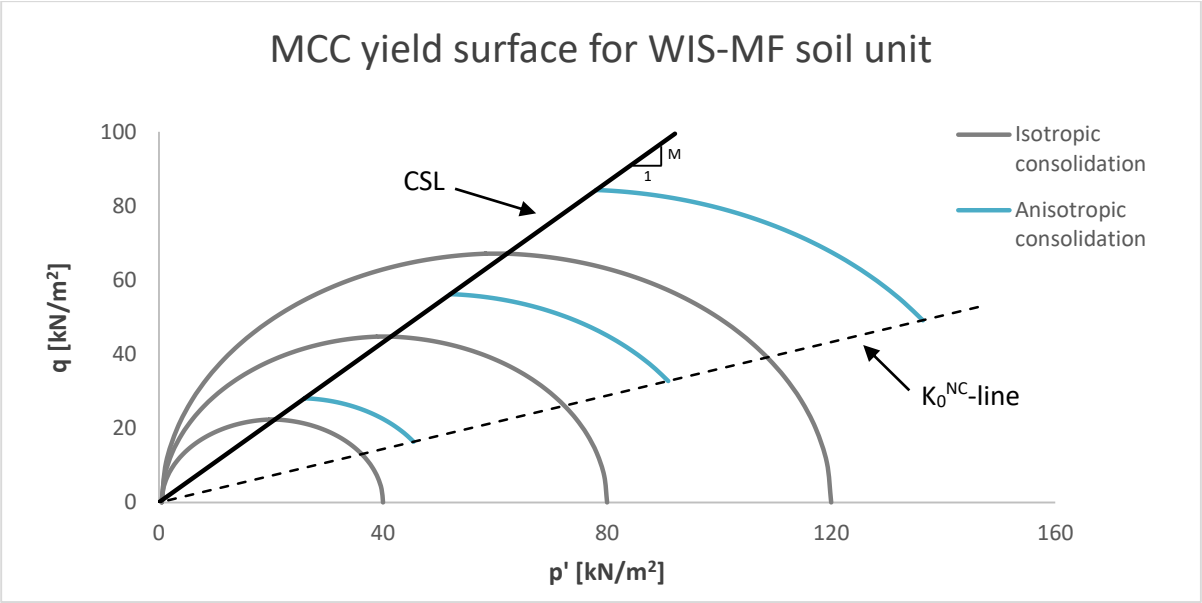

Figure 4.8 MCC yield surface for WIS-MF soil unit.

Initial void ratio (e_{init})
As derived in section 3.4.2, the initial void ratio of this material can be calculated based on a relationship between the unit weight of the solids, the porosity and unit weight of the water. An initial void ratio equal to $e_{init} = 0.690$ is found.

Poisson's ratio (ν'_{ur})
The Poisson's ratio for unloading/reloading is an elastic parameter needed to describe deformation properties of a soil. According to the PLAXIS Material Models Manual (2016), its value will usually be in the range between 0.1 and 0.2. Also here, an average value of $\nu'_{ur} = 0.15$ is used.

Compression (λ) and swelling (κ) index
Similar to the calibration approach in case 1, as a first estimate, the undrained shear strength profile as output of the Modified Cam-Clay model is estimated using the relations in equation (4.10) and (4.11), as described by Brinkgreve and Vermeer (1998). The values $\lambda = 0.052$ and $\kappa = 0.010$ are found. The results of this first calibration are compared to the undrained shear strength profile as derived based of triaxial compression tests. Also here, these values overpredict the undrained shear strength as function of depth, as seen in figure 4.9.

A second calibration is done by changing the values of λ and κ such that a best estimate is found, in which the difference between the shear strength gradients of the in-situ profile and model outcome is as small as possible. Since the WIS-MF material is stiffer, a slightly smaller value of the compression and swelling indices are found, relative to the SBD-soil unit. With $\lambda = 0.02$ and $\kappa = 0.001$, the in-situ s_u-profile is approximated more closely. Yet, still a deviation of 18% is present. Following the same approach by reducing the effective friction angle until the model result approximates the in-situ s_u-profile leads to the fully calibrated MCC parameters for this soil unit. The final, calibrated MCC-parameters are summarised in table 4.3.

Table 4.3 Calibrated input parameters MCC-model

Calibrated input parameters for Modified Cam-Clay model for WIS-MF			
Stiffness	λ	0.02	[−]
	κ	0.001	[−]
	ν'_{ur}	0.15	[−]
	e_{init}	0.690	[−]
Strength	M	1.08	[−]

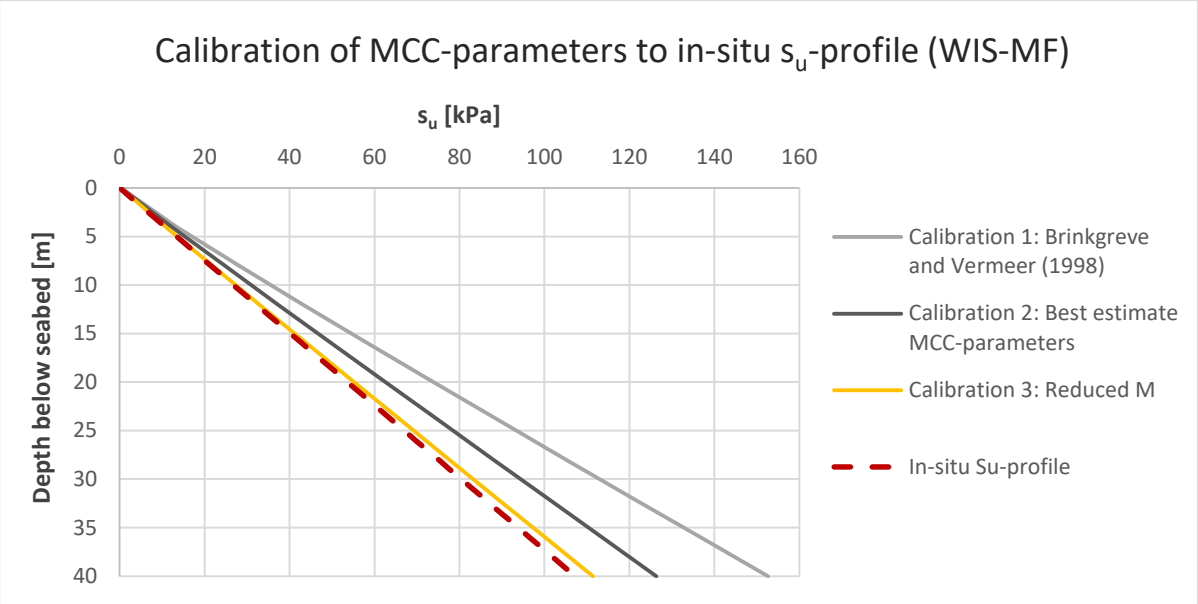

Figure 4.9 Calibration of MCC-parameters to in-situ s_u-profile for WIS-MF soil.

4.4.3 Summary: soil properties used in finite-element analysis

The final set of parameters for describing the clayey soil materials (SSF-SBD and WIS-MF) as present at the offshore wind farm site are modelled using the following Modified Cam-Clay parameters.

Table 4.4. Summary of MCC-model input parameters

Summary of MCC-model input parameters				
		SSF-SBD	WIS-MF	
Stiffness	λ	0.05	0.02	[−]
	κ	0.002	0.001	[−]
	ν'_{ur}	0.15	0.15	[−]
	e_{init}	0.962	0.690	[−]
Strength	M	1.0	1.08	[−]

4.5 Soft Soil Creep model

4.5.1 Application of Soft Soil Creep model

The Soft Soil Creep (SSC) model is an advanced soil constitutive model in PLAXIS, which is used to model the behaviour of compressible soft soils. As an advanced soil model, the SSC-model possesses an important feature of generating time-dependent deformations, which is also known as secondary compression or creep. The SSC-model incorporates the isotache concept, as seen in figure 4.10 (Bjerrum, 1967). The initial soil state is given by point A and the end of primary (EOP) consolidation by point B. In order to reach point B, the SSC-model assumes that the elastic strain will occur at time equal to zero and the viscoplastic strain will develop during the entire period. The latter time-dependent viscoplastic strain term is important to consider when considering spudcan penetration problems in soft soils.

Strain rate dependency of soft soil compressibility is an important concept for better understanding the viscous behaviour of soft soils. The Modified Cam-Clay model is used to model the elastoplastic behaviour of soils under compression. However, this model is rate-insensitive as there is no time dependency involved in its model calculations. In the Modified Cam-Clay model, the yield surface expands instantaneously if an increase in the load causes the stress state the fall outside the current yield surface. In the Soft Soil Creep model, this shift needs time. If a higher load is applied, the cap will not follow immediately, but will take time to adapt to the new stress state.

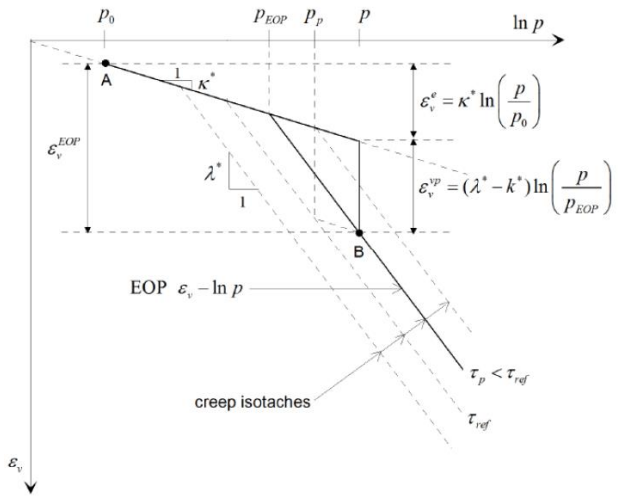

Figure 4.10 The isotache concept as used in SSC (Bjerrum, 1967).

4.5.2 Basic model formulations

Formulation of elastic strain

Similar as in elastoplastic theory, the total strain in an elastic-viscoplastic formulation (ε_v) can be decomposed into an elastic (ε_v^e) and inelastic (ε_v^{VP}) component. The elastic component is assumed to occur instantaneously, whereas the inelastic component of strain is irreversible and requires time. In this model, all inelastic strains are assumed to be time-dependent, i.e. purely viscous (Stolle et al., 1997, Vermeer and Neher, 1999). The total strain is given as:

$$\varepsilon_v = \varepsilon_v^e + \varepsilon_v^{VP} \qquad \textit{Eq. (4.12)}$$

In which the elastic strain component is given as:

$$\varepsilon_v^e = \kappa^* \ln\left(\frac{p}{p_0}\right) \qquad \textit{Eq. (4.13)}$$

Formulation of inelastic viscoplastic strain

The Soft-Soil Creep model is an elastic-viscoplastic formulation that incorporates a time dependent state variable to estimate viscoplastic deformation (Brinkgreve and Vermeer, 2016). Elastic-viscoplasticity (EVP) theory describes the rate dependent behaviour of soils, in which the deformation of a material depends on the rate at which loads are applied. Although both rate independent models and EVP models exhibit permanent deformations after application of the load, the latter undergoes additional creep flow as function of time. In the Soft Soil Creep model, creep is defined based on the theory of viscoplasticity. The viscoplastic volumetric strain increment for a specific soil over a period Δt is given by:

$$\Delta\varepsilon_v^{VP} = \mu^* \ln\left[1 + \frac{\Delta t}{1\ day}\left(\frac{p_{eq}}{p_{c0}}\right)^{\frac{\lambda^*-\kappa^*}{\mu^*}}\right] \qquad \textit{Eq. (4.14)}$$

In which λ^* is the modified compression index, κ^* is the modified swelling index and μ^* is the modified creep index parameter. The modified creep index specifies the creep rate after a reference time of 1 day. This value of 1 day is an arbitrarily chosen value used in the SSC model and cannot be varied by the user. The change of the creep rate in time is defined by the combination of parameters λ^*, κ^* and μ^*. For stress states within the current yield surface ($p_{eq} < p_{c0}$), the creep rate is negligible. For stress states outside the current yield surface ($p_{eq} > p_{c0}$), time dependent deformation is of more significance. These parameters of the Soft Soil Creep model are explained in more detail below.

Formulation of failure condition

The creep formulation does not include failure. Therefore, a Mohr-Coulomb type failure criterion, formulated in a perfect-plasticity framework, is added to the Soft Soil Creep model, which generates viscoplastic strains as soon as the failure condition is met. This failure condition takes into account soil parameters associated with the Mohr-Coulomb failure criterion, i.e. cohesion, friction angle and dilatancy angle.

4.5.3 Conversion to SSC-model

The Soft Soil Creep model can be seen as an advanced soil model, which incorporates the concepts of Modified Cam-Clay and viscoplasticity. The design parameters of the MCC-model are closely related to the SSC parameters and are used to construct the input parameters for the viscoplastic Soft Soil Creep analyses. The Soft Soil Creep model requires the following parameters:

Table 4.5 Input parameters for Soft Soil Creep model.

Input parameters for Soft Soil Creep model		
Failure parameters as in the Mohr-Coulomb model		
c	Effective cohesion	$[kN/m^2]$
ϕ'	Friction angle	[°]
ψ	Dilatancy angle	[°]
Basic stiffness parameters		
λ^*	Modified compression index	[−]
κ^*	Modified swelling index	[−]
μ^*	Modified creep index	[−]
Advanced parameters		
ν_{ur}	Poisson's ratio for unloading-reloading (default 0.15)	[−]
K_0^{NC}	$\sigma'_{xx}/\sigma'_{yy}$ stress ratio in a state of normal consolidation	[−]
M	K_0^{NC}-related parameter	[−]

Modified compression and swelling indices

The parameters of the Soft Soil Creep model include modified compression (λ^*) and swelling (κ^*) indices, which are related to the original Cam-Clay parameters λ and κ. The soft soil parameters are defined in terms of terms of volumetric strain ε_v, whereas the Cam-Clay parameters are defined in terms of void ratio, e. The relationship to the Cam-Clay parameters is given as:

SSC-model

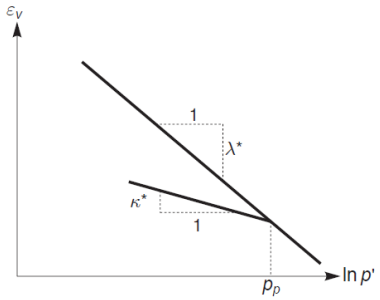

Figure 4.11 Logarithmic relation between volumetric strain and mean stress

Cam-Clay model

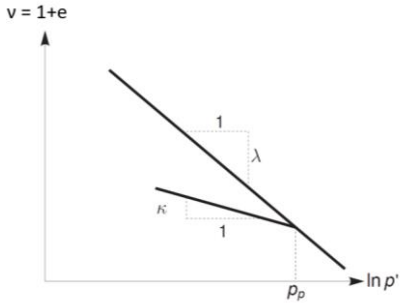

Figure 4.12 Logarithmic relation between void ratio and mean stress

Relationship to Cam-Clay parameters

$$\lambda^* = \frac{\lambda}{1+e} \qquad \textit{Eq. (4.15)}$$

$$\kappa * = \frac{\kappa}{1+e} \qquad \textit{Eq. (4.16)}$$

Modified creep index μ^* and the OCR

In order to properly model the creep behaviour, two main parameters are needed for the initial situation at $t = 0$. These are the location of the cap and its expansion velocity. These parameters cannot be entered directly by the user, but must be specified by means of the parameters μ^* and the OCR. The change of the creep rate in time is defined by the combination of parameters λ*, κ* and μ* where the modified creep index specifies the creep rate after 1 day. For a rough estimate, the ratio λ^*/μ^* should be in the range between 15 to 25 (Brinkgreve and Vermeer, 2016).

In the SSC-model, the position of the yield surface is time dependent, so a proper value of OCR should be applied that represents the history of the soil. For normally consolidated soft soil deposits in practice, it would seem logical to set the initial OCR value to 1.0. However, in the SSC-model this would mean that there has been creep for only one day. In other words, it would mean that the soil has just been deposited for just one day, whereas the geological history of the subsoil is much larger in reality. An OCR equal to 1.0 would lead to unrealistic large creep strain rates due to the initial stresses, without even considering additional loading. Consider the model equation for creep strain rate to be defined as:

$$\dot{\varepsilon}_v^c = \frac{\mu^*}{1\ day}\left(\frac{p_{eq}}{p_{c0}}\right)^{\frac{\lambda^*-\kappa^*}{\mu^*}} = \frac{\mu^*}{1\ day}\left(\frac{1}{OCR}\right)^{\frac{\lambda^*-\kappa^*}{\mu^*}} \qquad \textit{Eq. (4.17)}$$

The ratio of the effective stress state over the initial preconsolidation stress can be rewritten in terms of overconsolidation ratio. As the creep ratio, $\frac{\lambda^*-\kappa^*}{\mu^*}$, is relatively high (denominator is relatively small compared to numerator), increasing values of OCR will cause a decrease in creep strain rate. The actual degree of overconsolidation of a soil depends on the geological elapsed time since the soil was deposited. It is possible to estimate the OCR for soils assuming the last load step was primary (or virgin) loading and the overburden is constant ever since. In this case the OCR can be estimated using:

$$OCR \cong e^{\frac{\mu^*}{\lambda^*-\kappa^*}\ln(\Delta t)} \qquad \textit{Eq. (4.18)}$$

In this formula, Δt is the time in days that has elapsed since the last primary loading step, which is typically assumed as the time since the material was deposited. The evolution of OCR and creep strain rate as function of time is plotted in figure 4.13. It is clearly seen that the creep strain rate is large for

OCR equal to 1.0. In order to avoid these unrealistic creep strain rates, a proper OCR value should be assigned to represent the history of the soil. It is recommended to set the initial OCR value larger than 1.0, which means that the soil has aged since its deposition in geological history. According to the PLAXIS material model manual, a value in the order of 1.2-1.4 will generally work (Brinkgreve and Vermeer, 2016). In this range, the creep strain rates are more or less constant.

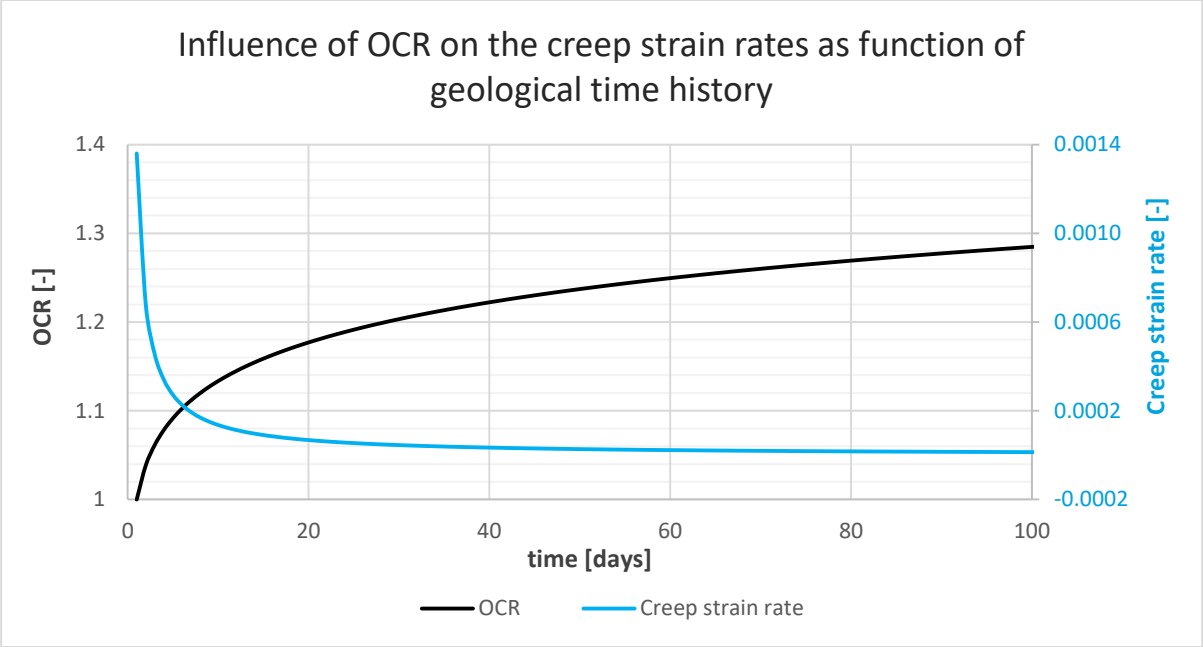

Figure 4.13 Influence of OCR on the creep strain rates as function of geological time history.

K_0^{NC}-parameter

By default, M is automatically determined based on the coefficient of lateral earth pressure in normally consolidated condition. Hence, the user cannot enter directly a value for M. Instead, a value for K_0^{NC} can be chosen. In order to match the same yield ellipses as in the Modified Cam-Clay model, the value of K_0^{NC} should be chosen such that the M-line in the SSC-model equals the critical state line of the MCC model., The Mohr-Coulomb failure criterion should then be located directly on this CSL by specifying its strength parameter equal to the critical state effective friction angle, ϕ'_{cv} .

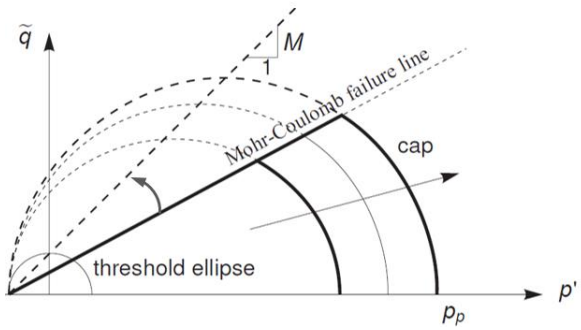

Figure 4.14 Yield surface of SSC-model

Final set of parameters

Using the Modified Cam-Clay parameters, a final set of input parameters for the Soft Soil Creep model can be derived for both soil units. Since the SSF-SBD soil unit represents the weakest material (less stiffness and strength), this material is used in the following FE calculations to investigate the viscous strain rate effect on the shear strength of clay. Given the ratio λ^*/μ^* should be in the range between 15 to 25 (Brinkgreve and Vermeer, 2016), an average value of the modified creep index, μ^*, is presented. The effect of μ^* is investigated later.

Table 4.6 Input parameters SSC

Soft Soil Creep model input parameters				
		SSF-SBD	WIS-MF	
Stiffness	λ^*	0.026	0.012	$[-]$
	κ^*	0.0010	0.0006	$[-]$
	μ^*	0.00136	0.00063	$[-]$
	e_{init}	0.962	0.690	$[-]$
Strength	c	0	0	$[kN/m^2]$
	ϕ'	25.4	27.3	$[°]$
	ψ	0	0	$[°]$
Advanced	K_0^{NC}	0.7419	0.7085	$[-]$
	M	1.0	1.08	$[-]$
	ν'_{ur}	0.15	0.15	$[-]$
	OCR	1.3	1.3	$[-]$

4.5.4 Concept of time dependent behaviour in SSC-model

Traditional penetration resistance design approaches were developed based on idealised rate independent soils, in which only the static frictional term is considered. In order to evaluate the effect of strain rate on the undrained shear characteristics of normally consolidated cohesive soils, a PLAXIS implementation with the SSC model is used to capture the viscous resistance component on the soil resistance.

Yield surface
The Soft Soil Creep model contains the same elliptic yield surface as the Modified Cam-Clay model, as introduced by Roscoe and Burland (1968). The only difference is that a stress paths can never go beyond the Mohr-Coulomb failure line in the SSC-model, i.e. only hardening of the material is allowed to occur (no softening behaviour in SSC-model).

During strain hardening, the material gains in strength as the elliptic yield surface increase in size. When load is applied in undrained conditions, excess pore water pressures are generated, causing the effective stress path (ESP) to bend towards the left, until it reaches the failure line. As indicated in figure 4.15, the initial yield surface increases, which leads to an increase of the soil strength. It is recognised that the rate of shearing has a significant influence on the undrained shear strength of saturated soils (Casagrande and Wilson, 1951, Skempton and Bishop, 1954, Crawford, 1960, Akai et al., 1962, Richardson and Whitman, 1963, Berre and Bjerrum, 1973, Kimura and Saitoh, 1983). According to Richardson and Whitman (1963), a faster shearing rate induces an increased tendency to dilate, as explained in section 2.7 – Viscous strain rate effects. This causes the effective stresses to increase and consequently, greater shear resistances are found. This is also referred to as the viscous effects on soil resistance. A graphical representation of this effect is shown in figure 4.16.

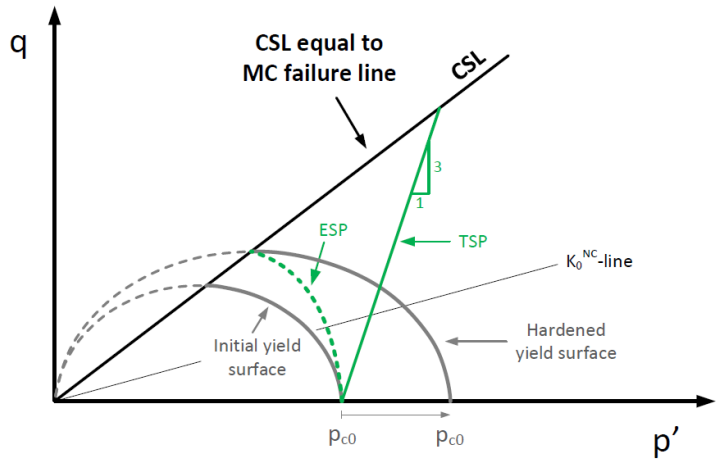

Figure 4.15 Yield surface of Soft Soil Creep model; strain hardening.

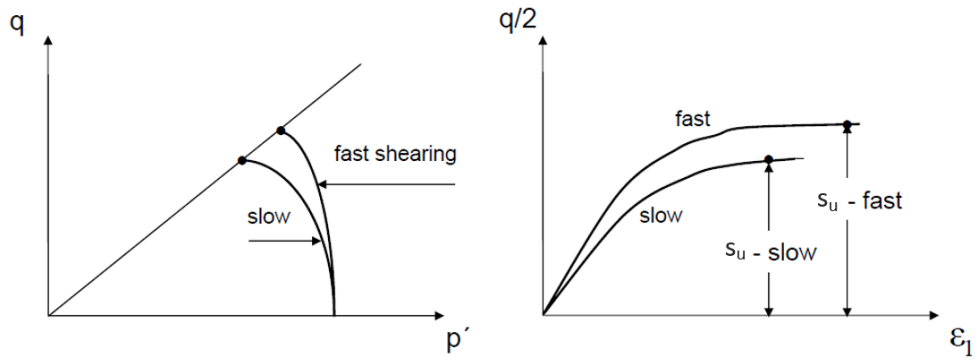

Figure 4.16 Effect of shearing rate on soil strength (Richardson and Whitman, 1963).

4.6 Conclusion and discussion

Modified Cam-Clay model

From the calibrations, it is noted that the first estimate of λ and κ based on the c_c and c_s parameters shows a significant deviation in shear strength gradient with depth. The second calibration is aimed at finding best estimates for the MCC-parameters to approximate the SHANSEP undrained shear strength profile as present in the field. Still, a deviation of approximately 17% is present between the model outcome and the actual s_u-profile**.** This deviation is caused by the relatively high derived effective friction angle for both materials. Correspondingly, the tangent of the CSL is relatively high as well, which leads to higher undrained shear strengths during shearing of the soil, because of the increased internal resistance. In order to fit the model outcome to the SHANSEP undrained shear strength profile, the derived effective friction angles are reduced slightly by 3 °, which lowers the CSL and thus, a slightly lower undrained shear strength is found.

Soft Soil Creep model

The elastoplastic MCC-model is not suitable for capturing the viscous strain rate effects in clay, as this model is rate-insensitive. Instead, the elastic-viscoplastic SSC-model is used, which incorporates the rate dependent behaviour of soils. The SSC-model is calibrated based on relations with the MCC-model. This model is only used when modelling the viscous strain rate effects during spudcan penetration into clay, as described in section 5.4 – Modelling viscous strain rate effects.

5. FEM Modelling

5.1 Introduction

PLAXIS is a special purpose 2D or 3D finite element (FE) computer program used to perform deformation and stability analysis for various types of geotechnical applications. All finite element analyses in this study are performed using PLAXIS 2D 2016.

5.1.1 General

Axisymmetric model

In this study, the FE analyses are carried out using a 2-dimensional axisymmetric model. An axisymmetric model is used for circular structures with a uniform radial cross section and loading scheme around the central y-axis, where the deformation and stress state are assumed to be identical in radial direction. A spudcan foundation can be represented as such and is only loaded vertically. Horizontal loading is neglected in this study. Axisymmetric element formulation is beneficial, because it saves considerable computation time compared to a 3D analysis as only one plane needs to be calculated. All other planes in radial direction are assumed to be identical (Brinkgreve et al., 2017).

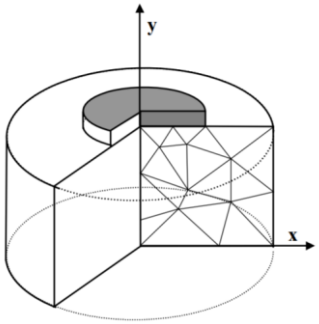

Figure 5.1 Illustration of axisymmetric model (Brinkgreve et al., 2017).

Elements

Two types of elements are available in PLAXIS to model soil layers and other volume clusters, either the 6-node or 15-node triangular elements. It is recommended to use 15-node elements in axisymmetric analyses, because these elements are more accurate compared to 6-node elements. Especially in situations where failure plays a role, for example in a bearing capacity calculation, high quality stress results are required. The elements consists of nodes and stress points, as shown in figure 5.2. The displacements are calculated in the nodes and the stresses and strains are calculated in the stress points. (Brinkgreve et al., 2017)

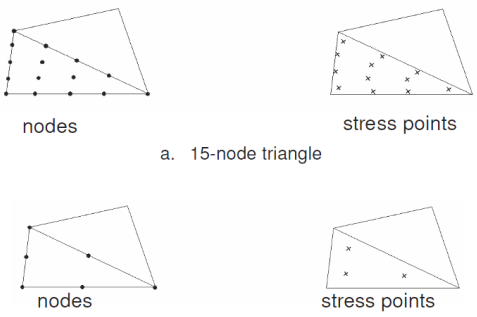

Figure 5.2 The triangular element in PLAXIS 2D with (a) 15-node and (b) 6-node triangular elements

5.1.2 Model accuracy

Boundary conditions

The 2D axisymmetric boundary domain is fixed at the bottom boundary by rigid supports. This means that this boundary is restrained both in rotation and translation. The lateral boundaries are constrained by roller supports, which are free to translate along the vertical direction. In this way, the soil body is able to move upwards and downwards under vertical loading, which allows for vertical settlements. All horizontal movement is fixed.

The spudcan footing is represented as a rigid body with a single load reference point located at the centre of the spudcan. The properties of the plate material is given in table 5.1. The footing is considered to be very stiff relative to the soil. As there is no flexibility in the footing, all displacements and stresses calculated can be directly attributed to the soil behaviour. Structural forces and deflection behaviour of the footing are neglected. Note that in reality the footing is not infinitely stiff and will bend during loading, which will reduce the contact stresses at the footing edges and consequently, a part of the load is taken by the structure. However, structural forces and deflection behaviour of the footing is outside the scope of this study and therefore not taken into account.

As for groundwater flow, only the top boundary is considered as free draining boundary. All other boundaries are closed. During consolidation, excess pore water pressure can only dissipate through the surface. A schematic overview of the boundary domain is given below.

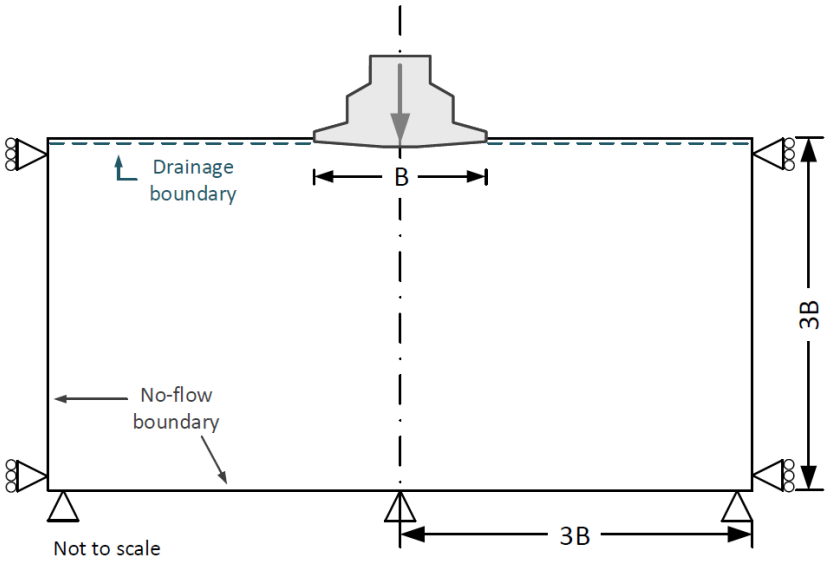

Figure 5.3 Schematic representation of the boundary domain.

Table 5.1 Properties of plate material

Properties of plate material - steel		
EA	10.0E12	kN/m
EI	250.0E9	$kN/m^2/m$

Boundary distance effect

An important part of the model design is to make sure the boundaries of the domain are located far enough away that the occurring effects do not arrive at the boundaries. If simulation effects from under the footing reach a model boundary, an artificial gradient will be created between the model boundary and the nodes within the model domain, which can force the model to produce an inappropriate result. The distribution of the plastic points gives an indication of the extent to which the failure mechanism is developing throughout the domain[2]. The red points in figure 5.4 indicate the plastic zone where the stress states of the soil elements are at failure. The blue points indicate soil elements which exhibit hardening behaviour (yielding and generating plastic strains). From figure 5.4, it can be seen that a too close lateral boundary distance intersects the developing failure mechanism and alters the numerical results. Thus, an appropriate boundary distance needs to be investigated.

A suitable lateral boundary distance (L_{BD}) is determined numerically by setting the boundary further away until convergence of the solution is found. As can be seen in figure 5.5, setting the lateral boundary at a distance of two times the spudcan diameter from the model axis ($L_{BD} = 2B$) is already far enough away without having significant effects of boundary conditions on the penetrating response. From the plastic points graph, however, it is noted that, especially at deep penetrations, a small amount of cap hardening points are located outside the domain of $L_{BD} = 2B$, which may result in a small deviation at larger depths. To ensure that all cap hardening points are always located within the boundary domain, a lateral boundary distance of $L_{BD} = 3B$ is taken. In addition, the bottom boundary distance (B_{BD}) should also be located far enough away in order to not disturb the model results. For practical reasons, the bottom boundary distance is set to be equal to the lateral boundary distance ($B_{BD} = L_{BD} = 3B$).

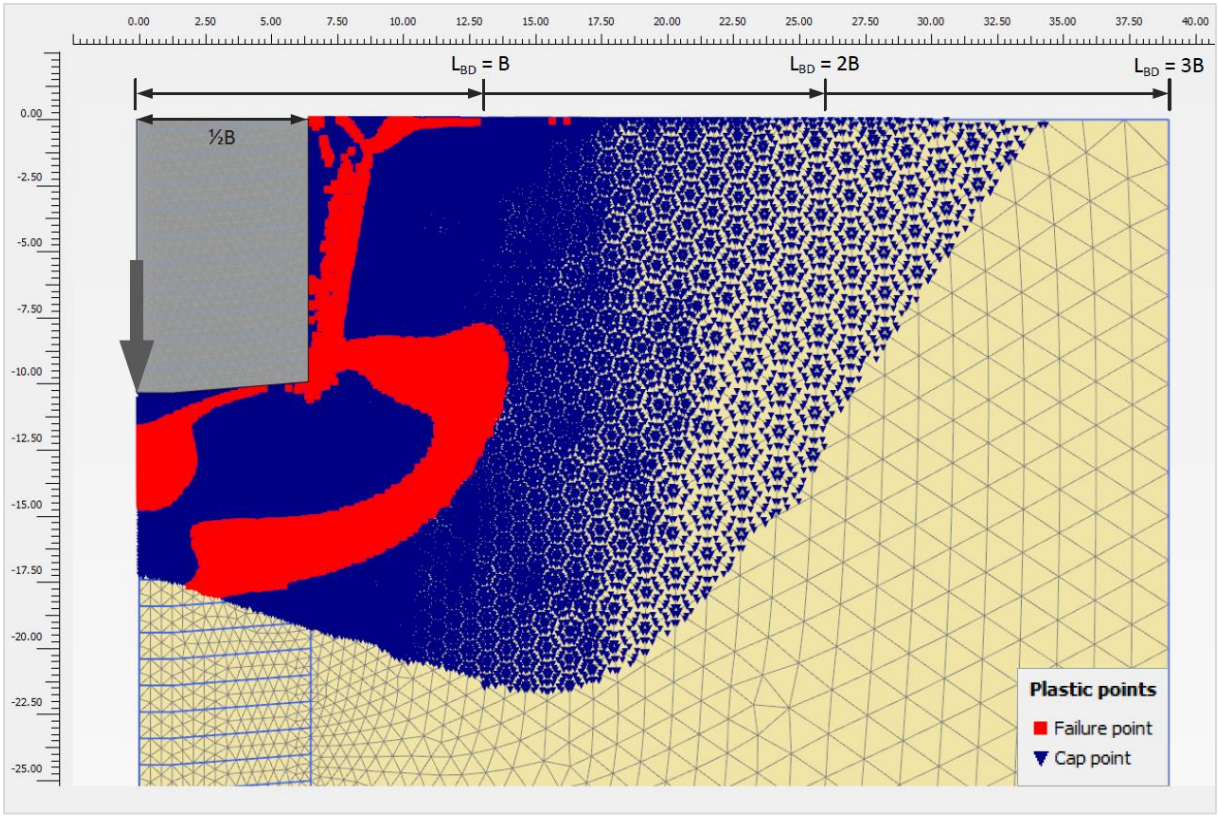

Figure 5.4 Plastic points indicating soil at failure (failure point) and hardening behaviour (cap point).

[2] Note that the distance at which plastic or cap points occur depends on soil type. SSF-SBD soil used in this analysis.

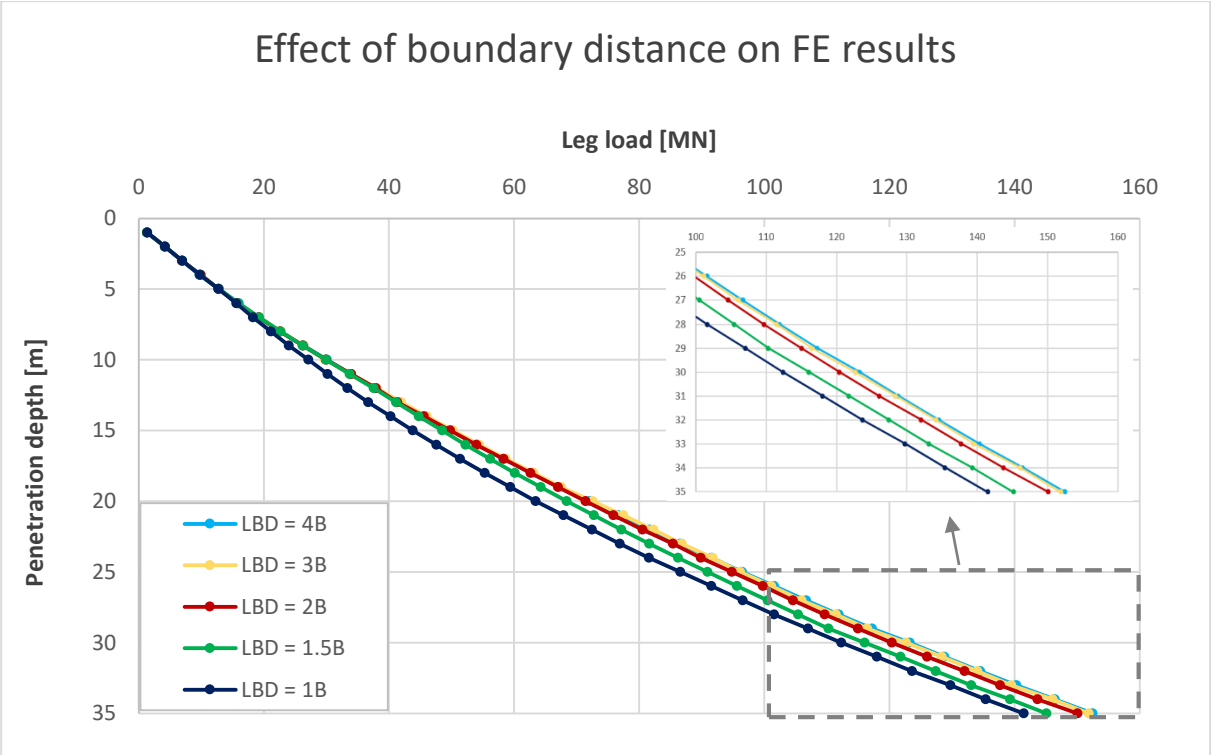

Figure 5.5 Boundary distance effect in FE model results

Mesh density

In finite element analysis, mesh density is a critical issue which is directly related to the accuracy of the finite element model. The effect of mesh density on the numerical results is analysed by discretising the axisymmetric soil domain in space by defining different grids with increasing mesh densities. The FE mesh is used to subdivide the model into smaller domains, i.e. elements, over which a set of equations is solved. As these elements are made smaller and smaller, the mesh is refined and the computed solution will approach the real solution. On the other hand, a high resolution mesh requires significantly more computational effort, which increases the complexity and computational time. Therefore, an optimal balance between mesh density and computational time is aimed for.

A very coarse, coarse, medium, fine and very fine triangular mesh element grid is used in PLAXIS to simulate the settlement of a circular footing into the soil. From the load-displacement graph in figure 5.6, it can be concluded that all numerical results are relatively closely together. It is also noted that the very coarse mesh produces some slightly deviating results. The elements are too widely spaced, which is reflected in the accuracy of the results. The other mesh densities converge towards a similar solution. Based on these results, the medium mesh is selected to be used in all numerical analyses.

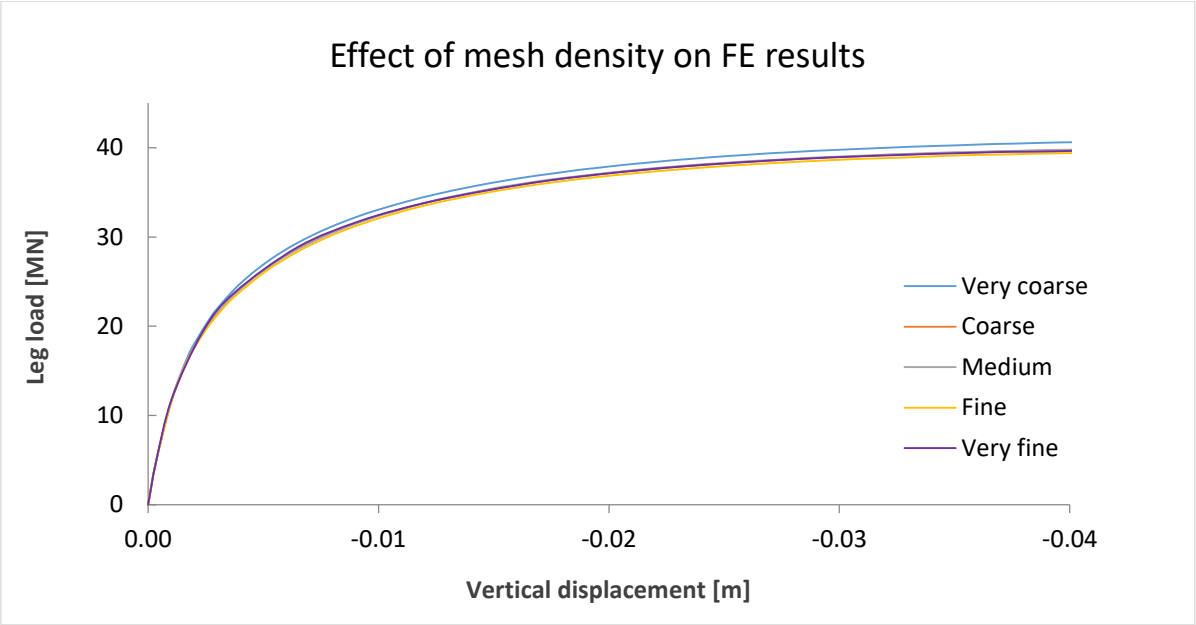

Figure 5.6 Load-displacement graph showing the effect of mesh density on FE results.

5.1.3 Singularities and stress concentrations in FEM

Singular plasticity points

When modelling soil behaviour, the relationship between the displacements and their derivatives, i.e. the stresses, provides the basis of proper calculations. However, at some points in the mesh, for instance at the appliance of a point load, at sharp re-entrant corners or corner of bodies in contact with other material, the strains can become unbounded, which will cause the stresses to become infinite. Such a point is called a numerical singularity, in which the solution is non-convergent with mesh refinement (Van Langen and Vermeer, 1991). This means that these locations are incapable of predicting accurate results even with accurate input data and a very fine mesh. The concept of singularity is elaborated below in terms of spudcan penetration.

Consider the indentation of a rigid footing into a purely cohesive material. The limit state of stress and deformation can be solved by using the method of slip line fields, as investigated first by Prandtl (1921) and later by Hill (1950). Figure 5.7 (a) shows Hill's field of slip lines at surface penetration. The material between OPR slides downwards and sidewards along OP and the triangle RQS slides upwards along QS. The material in the centre section PRQ does not move as a rigid block, which causes a singularity at R. The velocity field at this point is plotted in figure 5.7 (b) and describes a fan radiating in different directions. Such a singularity cannot be modelled by a FE computation which involves regular displacements for all nodal points.

The effect of singular plasticity points becomes more severe when considering embedded structures in deep penetration problems. Here, the material below the footing does not slip to the sides but only moves down and the material along the shaft moves up. Hence, a strong displacement discontinuity occurs at the edges, as indicated in figure 5.8. As a result, high stress concentrations occur locally at the edges, which makes the numerical collapse load much too high.

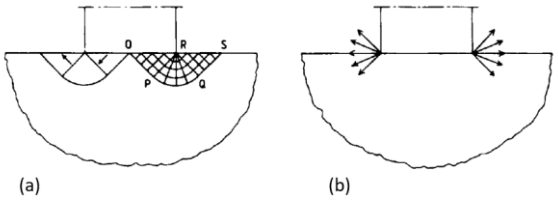

Figure 5.7 Theoretical slip line solution for surface penetration: (a) slip line field; (b) singular velocity at corner point. (Hill, 1950).

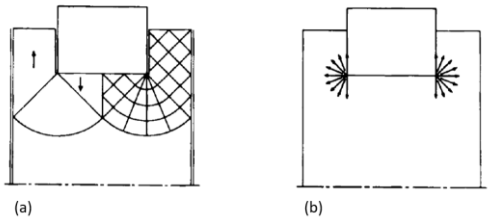

Figure 5.8 Theoretical slip line solution for deep penetration: (a) slip line field; (b) singular velocity at corner point. (Hill, 1950).

Dealing with singularity

Stress singularity and stress concentrations are common occurrences in FEM. There are three situations where it is acceptable to have singularity in the model (Van Langen and Vermeer, 1991):

- *When not evaluating solution at singularity, but some distance away.*
  One approach to dealing with singularity is to just ignore them. Locally, the predicted stresses in the above model are incorrect, but the stress solution does converge at a small distance away from the singularity. If interested in the stresses away from the singularity, the presence of the singularity does not pollute the predictions elsewhere.
- *When not evaluating the derivative of the solution.*
  It is also important to realise that singularity only occurs when taking the derivative of the solution field. The displacement field, u, is used to compute the stresses from the strains, $[\sigma] = [C] \cdot [\varepsilon]$, where strain is defined in terms of the gradient of the displacement field, $\varepsilon = \frac{1}{2}[\nabla u + (\nabla u)^T]$. Since the strains become unbounded at a singular point, it becomes clear why the solution for the stresses goes to infinity at a sharp corner. However, if only interested in the displacement field, u, the solution is not singular and does converge with mesh refinement.
- *When evaluating the integral around the singularity*
  Singularity is acceptable when interested in an integral quantity as output of the model. If a solution is evaluated with an integral of stresses over the singularity region, the output is convergent with mesh refinement, even though the integrand is non-convergent at the singular point inside the domain.

In other cases, where stress singularity or stress concentration is of importance, then:

- The mesh must be locally refined by inserting more elements at regions where the error is estimated to be large.
- Typical geometric induced singularities such as sharp re-entrant corners can be avoided by rounding off the sharp corners by using a Fillet node; applying a corner with a suitable radius. Effectively, the stress singularity becomes a stress concentration.
- Finally, to overcome the effect of singular plasticity points as described in the example above, some potential slip lines can be incorporated in the material domain to enhance the flexibility of the FE mesh in order to prevent non-physical stress results. These slip lines are represented by using interface elements.

Interface elements

Interface elements are used to model proper interaction between soil and structure. Especially problems of soil-structure interaction at corner points of the spudcan may require special attention. Corners in stiff structures and an abrupt change in boundary condition may lead to high peaks in the stresses and strains. Volume elements are not capable of reproducing these sharp peaks and will, as a

result, produce non-physical stress oscillations. This problem can be solved by introducing interface elements. As suggested by Van Langen and Vermeer (1991), it is recommended to extend the interface elements slightly into the soil, as shown in figure 5.9.

In the PLAXIS model, there is a small singularity at the end of the plate under loading conditions, as can be seen in figure 5.10. Here, at one side the soil elements are loaded and at the other side the elements are under free surface conditions. At the boundary, elements are party loaded and partly under free surface conditions. Consequently, interpolation of the stresses and strains using the shape functions within the elements could give two extreme values within one element. This will be difficult to solve numerically. Applying interface elements at this boundary makes sure that the elements are described such that they are fully loaded or fully under free surface conditions. This is done by drawing a vertical line with an interface into the FE mesh from the singular point down into the soil, as illustrated in figure 5.9 (a). The interface makes sure that the left and right hand side are not rigidly connected, but allow for some flexibility with a potential slip line along an artificial cut in the FE mesh (b).

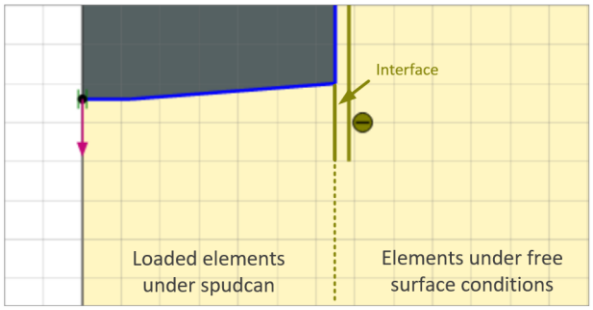

Figure 5.9 (a) Interface at soil-structure interaction

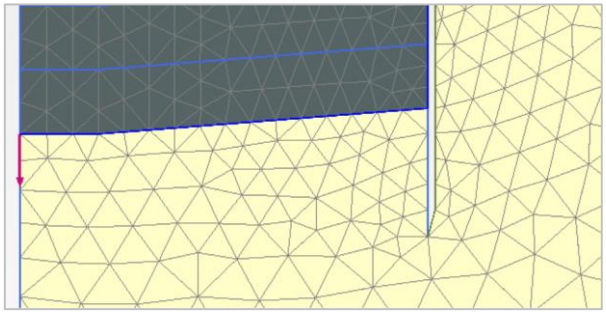

(b) Artificial cut in FE mesh

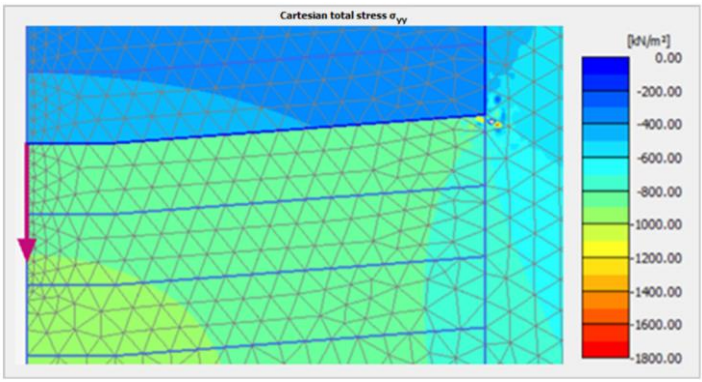

Figure 5.10 Singularity at end of spudcan bottom plate

The effect of interface elements on the soil reaction force is investigated numerically by considering a WIP analysis at a depth of 5 meters. Vertical interface elements are applied between the spudcan shaft and the soil, extending to 1 m depth below the spudcan outer edge. Different interface material properties in terms of effective friction angle, ϕ', are applied to investigate the effect on the soil reaction force directly beneath the footing. A small interface cohesion of $1.0\ kN/m^2$ is applied to improve calculation performance. From figure 5.11, it is noted that applying an interface has a reduced effect on the soil reaction force, even when the interface internal friction angle is set equal to the material's friction angle ($\phi'_{interface} = \phi'_{soil} = 25.4°$ for SSF-SBD soil). This is caused by the fact that the vertical potential slip line cuts through the FE mesh, which has a direct impact on the rigidity of the soil mass, leading to a 5.4% lower vertical bearing capacity. Reducing the interface material strength property even more, to $\phi' = 15°$ and $5°$, results in a further reduction of vertical bearing capacity.

The effect of applying interface elements on the vertical bearing capacity increases with depth, as shown in figure 5.12. Considering a WIP analysis at 10 m depth, the difference in soil reaction force with and without using an interface is then 10.5%.

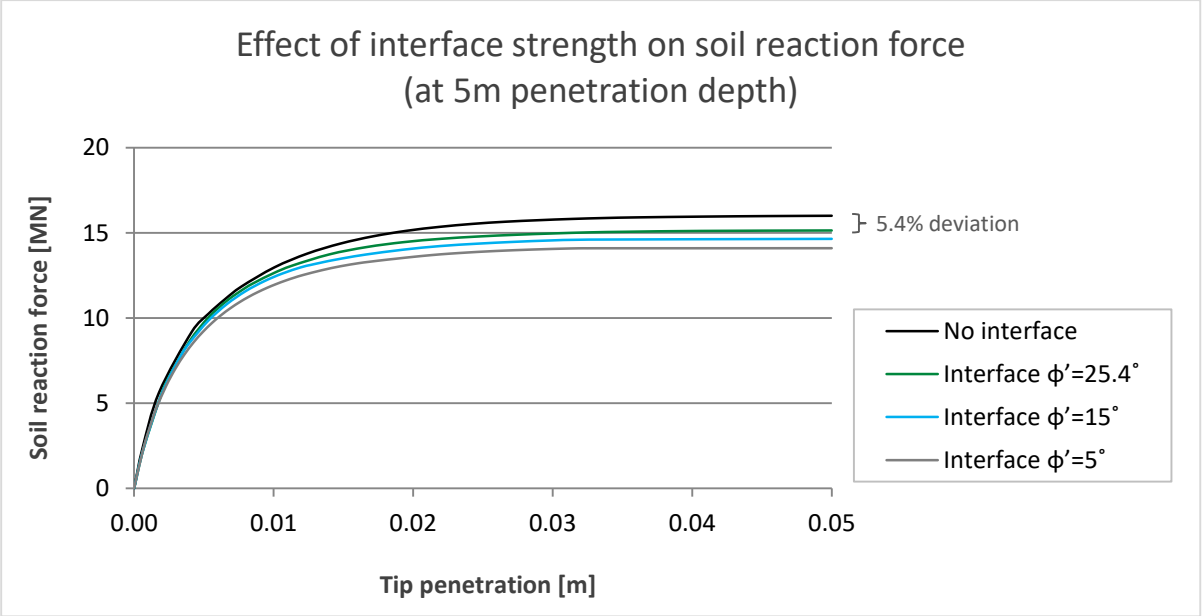

Figure 5.11 Effect of interface strength on soil reaction force at 5m penetration depth.

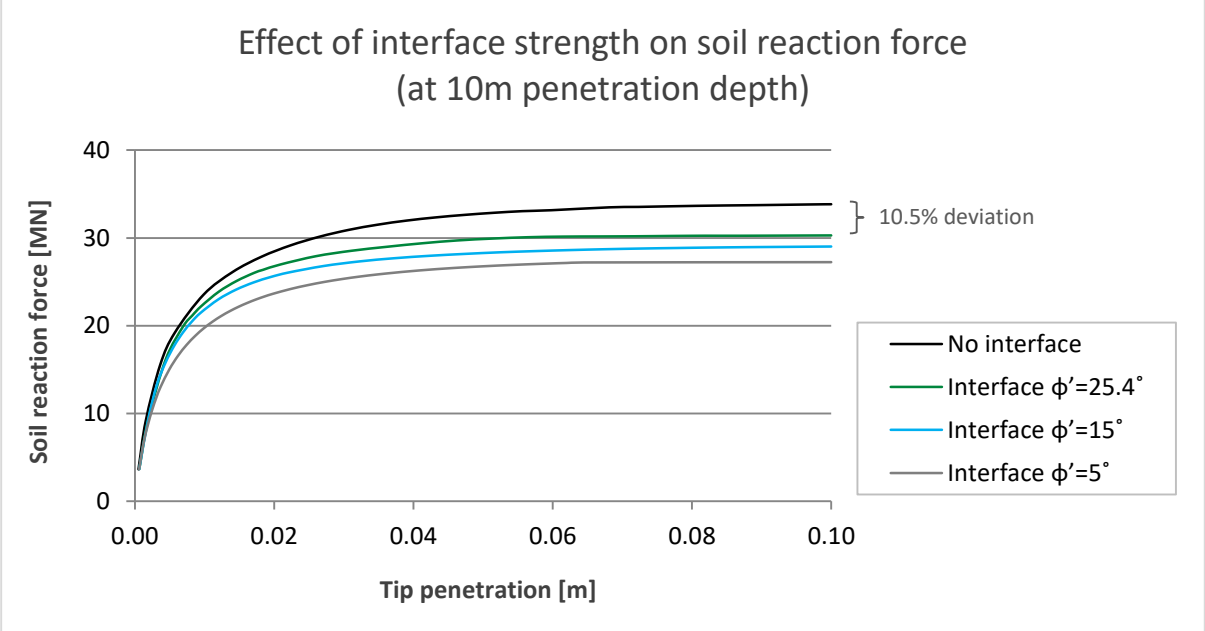

Figure 5.12 Effect of interface strength on soil reaction force at 10m penetration depth.

Concluding remarks

In the model, a small singularity is present at the outer end of the spudcan footing. Theoretically, the stress concentration in this point would predict a slightly higher numerical collapse load than would be in reality. However, since the total soil reaction force under the footing is evaluated by integrating the soil stresses over the full spudcan area, the singularity is acceptable and has a negligible effect on the derived total reaction force.

Considering WIP analyses, applying interface elements at the side of the spudcan has a reduced effect on the vertical soil reaction force under the footing. The difference in vertical bearing capacity with and without using interface elements increases with penetration depth. At ten meters penetration, the difference is calculated to be 10.5%, which is considered to be a significant deviation and cannot be just neglected. Disregarding interface elements would overpredict the leg penetration predictions.

However, when applying interfaces completely around the spudcan with flexible corner points (extending interfaces around singularities) would give unstable results. The combination of large deformations and relatively weak material does not seem to work properly. Especially when using an updated mesh approach (PR instead of a simple WIP analysis), in which the spudcan geometry is stepwise updated into the FE mesh, the interface at the singularity causes numerical instability of the model. That is, the numerical collapse load cannot be calculated properly. In order to be able to compare the WIP and PR approaches, interface elements are not applied in both cases. In this way, the WIP and PR approaches can be compared using similar model properties. A side note should thus be taken into account that applying interface elements would lower soil resistance slightly.

5.1.4 Modelling pore pressure effects

Pore pressure effects have to be considered when the soil is fully saturated and the loading is fast enough to cause undrained behaviour of the soil. Especially for consolidation analyses, the pore pressure generation and dissipation is required in order to model spudcan jacking in cohesive soils. The generation of pore water pressure around the spudcan footing is a crucial aspect for determining the required preload time, because the rate of pore pressure dissipation during consolidation is related to the preload requirement (400 tons load reduction per 15 min). For realistic prediction of spudcan bearing capacity, it is important to take into account the pore pressure effects of displaced spudcans during installation. In the case of displaced spudcans, the installation process causes a considerable amount of soil displacement and high levels of reaction stresses. An accurate accumulation of excess pore pressure under the footing during installation is therefore crucial when considering consolidation analyses afterwards.

It is expected that a more realistic behaviour and therefore an improved design would be achieved by considering pore pressure accumulations during spudcan penetration. Using the Wished-In-Place (WIP) method the initial pore pressure under the footing is assumed to be hydrostatic and only start increasing when load is applied. Since the pore pressure accumulation of previous loading steps is disregarded in a WIP approach, this method is expected to underestimate the amount of pore pressures being build up. Contrary, a continuous penetration is desired in which excess pore pressures are accumulated after the initial penetration. However, when modelling continuous penetration using FEM, large deformations occur that cause high stress concentrations and distortion of the mesh, which makes the model unstable. Large deformation effects require change of geometry due to spudcan penetration. To overcome this problem in a standard FE code, the Press-Replace (PR) technique was introduced, which benefits the use of a simple and robust small deformation formulation by modelling the large deformation effects (e.g. the penetration process) by using updated geometry.

In Appendix H, the model performances of both the WIP and PR technique are compared to investigate the suitability of these methods to correctly model the pore pressure effects. In conclusion, it is noted that the WIP and PR method show substantially similar results. Therefore, the more simple WIP method will be used in all further numerical analyses.

5.2 Wished-In-Place method

5.2.1 Leg penetration predictions

The load-penetration curve of the spudcan footing in clay is based on WIP analysis results conducted at different depths. In the model, the footing is installed at each consecutive meter depth after which the vertical prescribed displacements are increased until failure. The reached collapse load equals the vertical bearing capacity of the given soil. In figure 5.13, this analysis is represented by the dark blue lines. Note that no interface elements are used here. Due to the conical spudcan geometry, the bearing capacity is derived at the depth of spudcan maximum bearing area. The analysis results are reported at the tip, which is 0.4m below the spudcan maximum bearing area. For the SSF-SBD soil, it can be seen that the bearing capacity increases linearly with depth until it reaches the target bearing preload criterion of 120 MN at a depth of 28 meter. At this depth, the undrained shear strength is large enough to support full leg load.

Introducing interface elements between the soil and spudcan shows that the computed vertical bearing capacity is smaller compared to the case without interface elements, as represented by the light blue line in figure 5.13. That is because when introducing interface elements, the rigidity of the soil mass is reduced by constructing potential slip planes in the soil body, which allows for some flexibility in terms of deformation of soil elements directly under the footing, as indicted in figure 5.9. In this case, the target preload of 120 MN is reached at a depth of 33 meter and the difference in computed leg load is advanced up to 25.1%, compared to the case without interface elements.

Finally, the FE results are checked against the analytical solution for ultimate vertical bearing capacity in clays as defined by the ISO guideline 19905-1 (2012). The analytical expression is formulated in equation (2.3) of section 2.2. This expression increases linearly with depth and matches the FE results quite accurately up to a penetration depth of 10 meters. At deeper spudcan penetrations, the analytical solution starts to underpredict the bearing capacity in the case without interface elements and overpredict the bearing capacity in the case including interface elements. The ISO guideline is found to be in the middle of the finite element predictions and is therefore particularly suitable for quick and simple first order approximations of the soil bearing capacity.

Considering the same analysis for the WIS-MF soil (figure 5.14), the numerical prediction including interface elements balances around the analytical solution for determining the vertical bearing capacity. The ISO guideline is considered as an accurate match. Sufficient bearing capacity is reached at a spudcan penetration depth of 27 meters. Similarly to the SSF-SBD soil, the numerical prediction of the WIS-MF soil reaction force is considerably overestimated in the case without using interface elements (dark blue lines). For more accurate FE results, interface elements should be included in the numerical calculations.

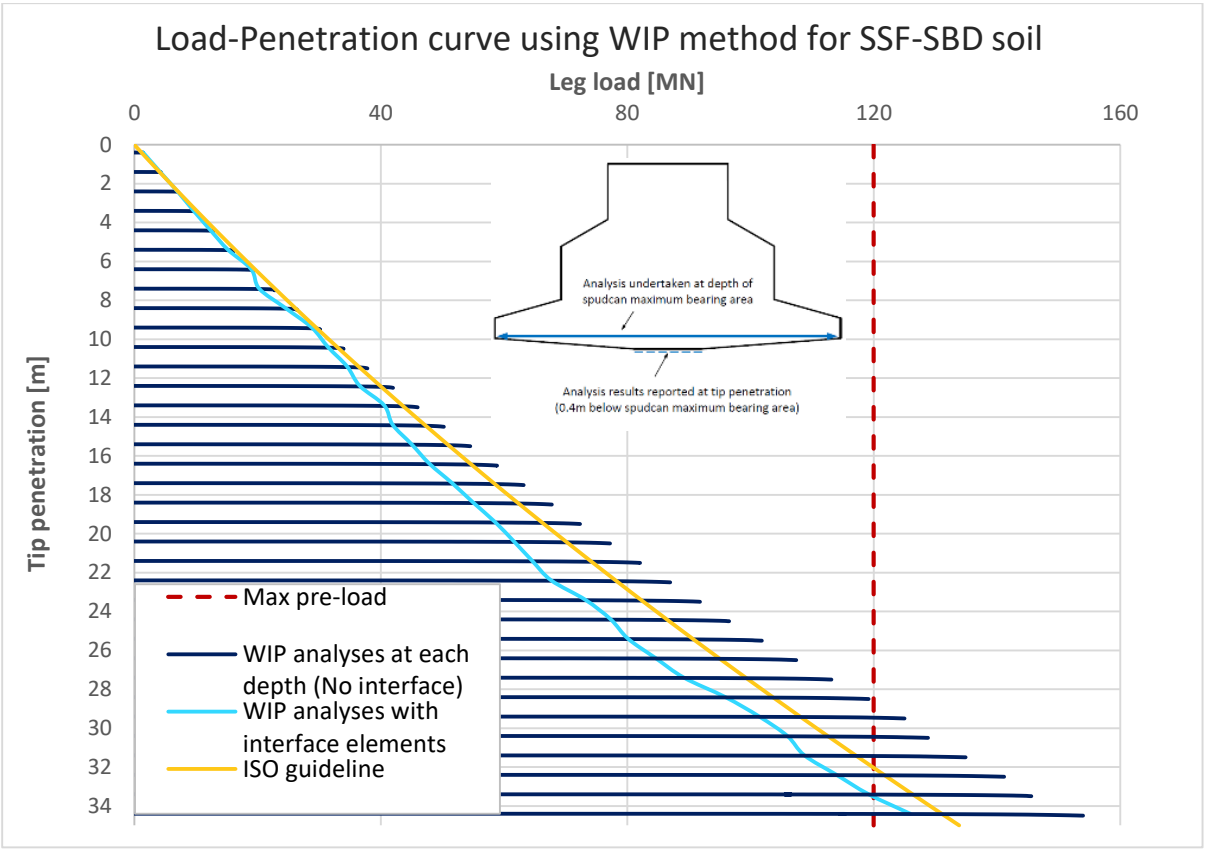

Figure 5.13 Load-Penetration curve using WIP method for SBD soil.

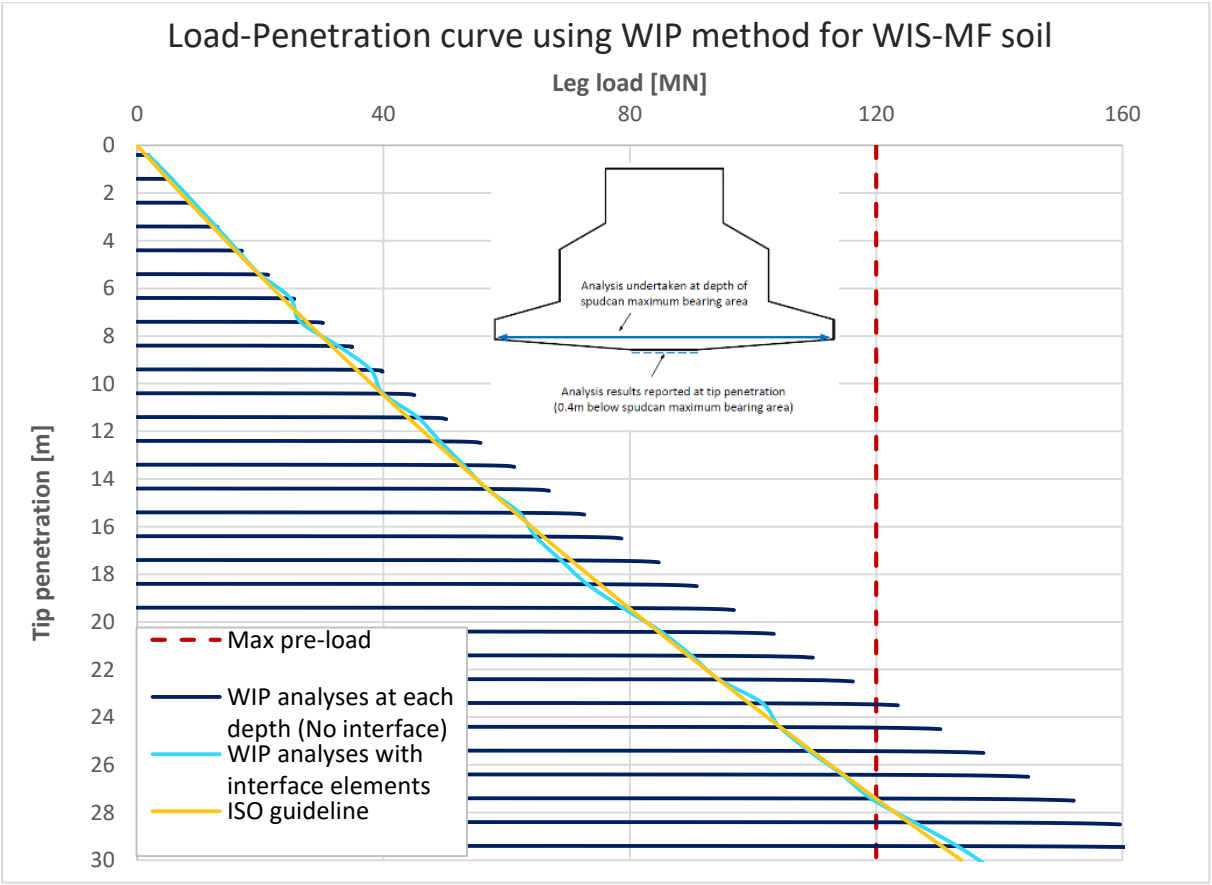

Figure 5.14 Load-Penetration curve using WIP method for WIS-MF soil.

5.2.2 Failure mechanism

Soil flow

Figure 5.16 (a-d) shows the deformation of the soil domain and velocity vectors as the spudcan is penetrated to depths of 1, 2, 4 and 8 meter. As figure 5.16 (a) shows, initial penetration of the spudcan pushes the soil near the spudcan edge outwards and upwards, resulting in surface heave just outside the spudcan edge. Beneath the spudcan, soil movement is directed mainly downward and outward to make way for the advancing spudcan. This pattern of soil flow is similar to that of a 'surface failure' reported by Hossain et al. (2006). At a penetration depth of 2m (fig 5.16 (b)), there is considerable rotation of the velocity vectors around the spudcan. Zooming in on this area (figure 5.15) shows that soil velocity vectors along the cavity face are displaced radially inward, wanting to close the cavity. This effect marks the onset of backflow, which corresponds to the critical depth of the cavity at which soil backflow initiates, as described in section 2.3 – Soil backfill mechanism. Hossain et al. (2006) proposed that the critical depth, H, which is the maximum cavity depth just before the onset of backflow, can be related to the shear strength, $s_{u,H}$, at depth H and strength gradient, k, via the following relation. For the SSF-SBD and WIS-MF soil units, a critical depth of $H = 2.13\,m$ and $H = 2.23\,m$ is found, respectively.

$$\frac{H}{B} = \left(\frac{s_{u,H}}{\gamma' B}\right)^{0.55} - \frac{1}{4}\left(\frac{s_{u,H}}{\gamma' B}\right) \qquad \textit{Eq. (5.1)}$$

In which

$$\frac{s_{u,H}}{\gamma' B} = \frac{s_{um}}{\gamma' B} + \frac{k}{\gamma'}\frac{H}{B} \qquad \textit{Eq. (5.2)}$$

With further penetration, backflow of soil covers the spudcan, leading to a reduction in surface heave, figure 5.16 (c). At large penetrations (figure 5.16 (d)) the soil backflow reaches a steady pattern, characterised by localised rotational movement of soil around the spudcan edge, while the soil near the ground surface is largely unaffected. This type of localised deep failure is similar to the 'flow failure' from Hossain et al.'s centrifuge model tests.

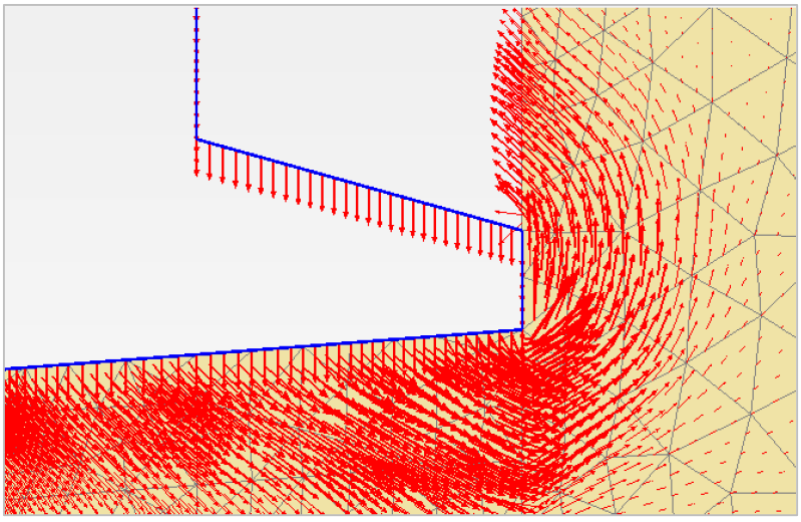

Figure 5.15 Soil flow around the penetrating spudcan.

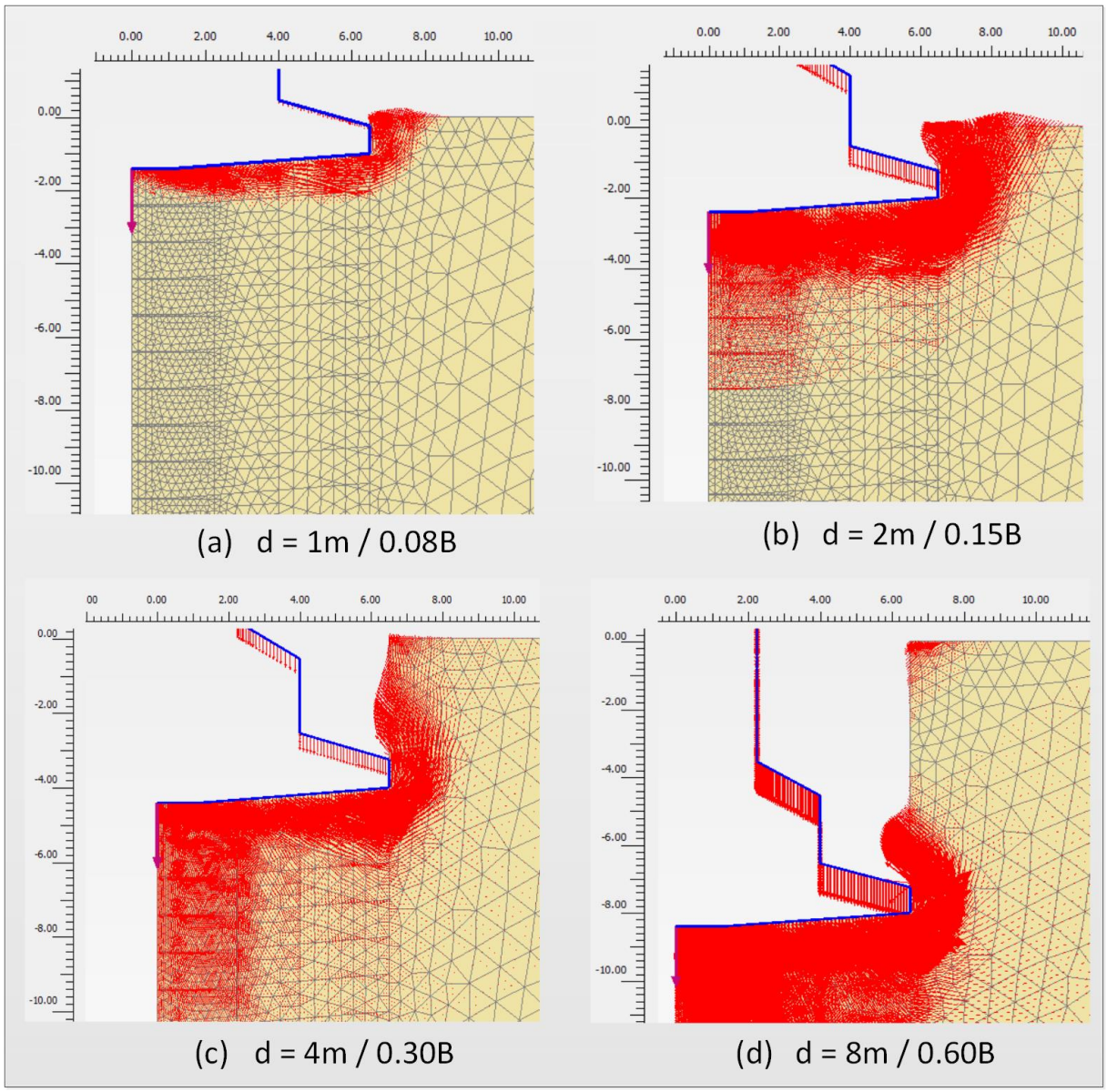

Figure 5.16 Soil velocity vectors at different penetration depths.

Material flow computational limitations

Regarding model stability, PLAXIS does not have material flow computational capabilities since it does not permit Eulerian and Lagrangian domains to be present in the same analysis. Material cannot be pushed out of the Eulerian domain and therefore, soil flow around the spudcan onto the top cannot be modelled. Modelling performances in this form with an open cavity are unstable and consequently, calculations cannot be executed. This stability issue is solved by changing the spudcan geometry in such a way that the shape of bottom side is kept intact, while the cavity is closed by remaining its maximum spudcan diameter over the full depth of penetration, as shown in figure 5.17. In this way, the surface heave at ground surface will not be reduced at deeper penetrations and soil is expected to move more radially outwards as penetration advances. This soil movement is shown by plotting the displacement contours.

Displacement contour

The failure mechanism developed during the WIP analyses is illustrated in figure 5.17 as displacement contours. As the footing is penetrating into the soil, a radial displacement pattern is observed, which is comparable to the shape of the failure surface as assumed by Terzaghi (1943). It should be noted that this displacement pattern depends on the soil type and soil layering. In a uniform soil body (as this is), the radial displacement pattern can be identified quite neatly. In the case of stiffer layers crossing the soil body, a different failure mechanism may occur. However, considering multiple soil stratification is outside the scope of this thesis and only uniform soil deposits are taken into account.

According to Terzaghi (1943), a wedge shaped body of soil (zone I) located directly under the footing can be identified. The soil in zone I moves down as a whole until the pressure exerted onto its inclined boundaries becomes equal to the passive resistance of the surrounding soil. This failure mechanism is more clearly explained in section 2.1 of this report. A schematic representation of the failure mechanism can be seen in figure 5.17 below. As the passive resistance increases with depth, the wedge shaped body of soil becomes larger. Hence, the radial shear zone and the passive zone are pushed up and more sideways as the spudcan penetrates into the soil.

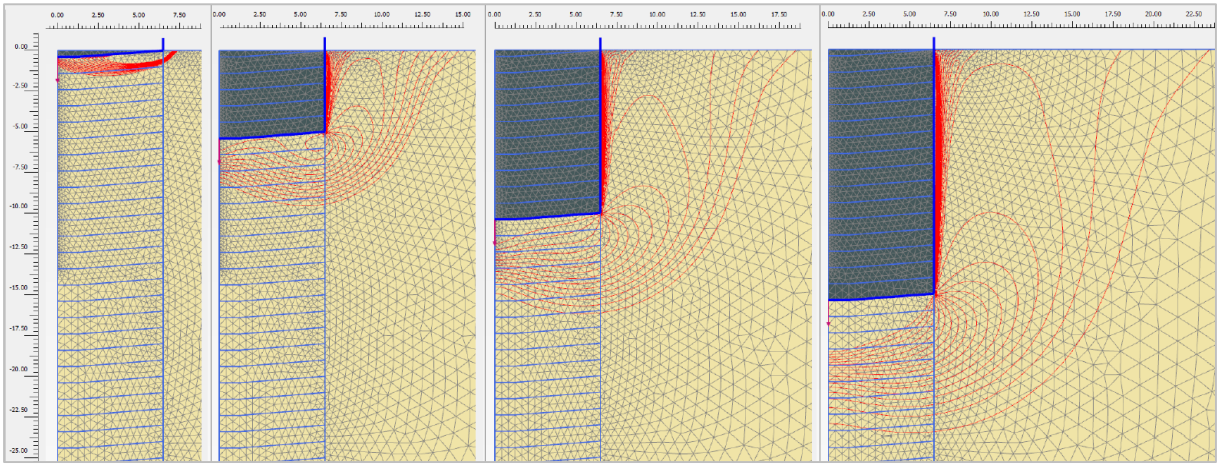

Figure 5.17 Displacement contours during WIP analyses

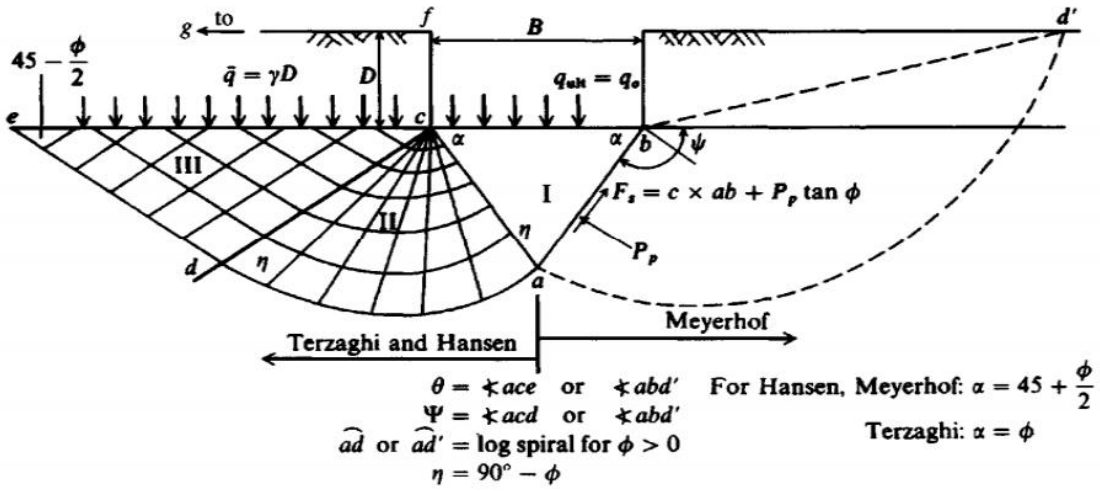

Figure 5.18 General footing-soil interaction for bearing capacity equations for strip footing (Bowles, 1988)

5.2.3 Excess pore water pressure

Using the WIP method, the spudcan footing is placed at different depths into the soil, where at each depth, a vertical prescribed displacement, u_y is applied until the collapse load is reached. As a result of loading, excess pore water pressures will be generated below the footing. Using WIP analyses at each meter depth, z, the excess pore water pressure is computed at the centre point, 0.5 m below the footing, as indicated in figure 5.19. The results are plotted in figure 5.20 against the percentage of the applied load at each calculations phase, $\sum M_{stage}$. Using the WIP method, spudcan penetration is modelled discontinuously by first positioning the footing at a certain depth and subsequently initiate a displacement. Therefore, the excess pore water pressure starts at zero at each consecutive depth and increases until an equilibrium solution.

Displacement-controlled modelling scheme

It can be seen that the excess pore water pressure, which refers to the difference between the total increased pore pressure due to rapidly applied loading conditions and the total hydrostatic pressure, becomes larger at deeper penetration depths. This is because the analysis is performed using a displacement-controlled modelling scheme. Each prescribed displacement is equal, but due to a linearly increasing s_u-profile, a larger soil strength is encountered at larger depths and thus, a larger force has to be applied in order to reach the collapse load. Consequently, the excess pore water pressure becomes larger. Since the strength increase is linear, the difference in excess pore water pressure increase is equal at each penetration depth. This concept can also be shown illustratively, as the excess pore water pressure contours will increase at larger penetration depths, as seen in figure 5.21.

Figure 5.22 shows the excess pore pressure contours along a radial section of the spudcan at different penetration depths. An excess pore pressure bulb develops as the spudcan penetrates into the soil. This bulb extends laterally outwards to approximately 2 radii from the edge of the spudcan. Above the spudcan, the excess pore pressures are much lower. In fact, at shallow penetration depths (fig 5.22 (a) and (b)), there is little to no excess pore pressures generated above the level of the spudcan tip. At larger penetration depths (c) and (d), the excess pore pressure bulb extends upwards, caused mainly by the remoulding of the soil.

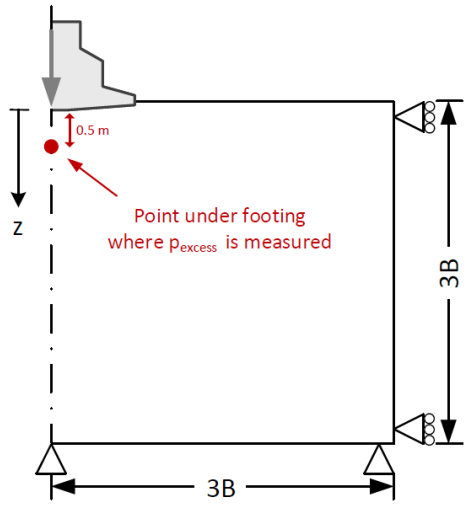

Figure 5.19 At each depth, p_{excess} is computed directly under the footing.

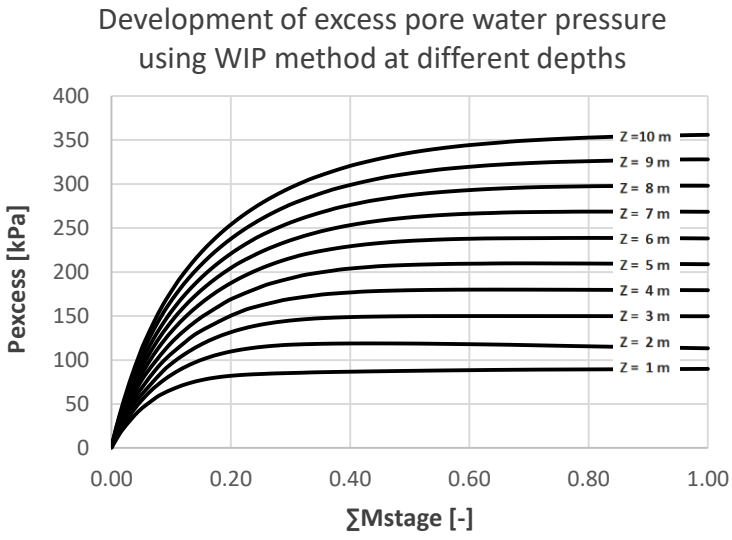

Figure 5.20 Development of p_{excess} using WIP method at different depths.

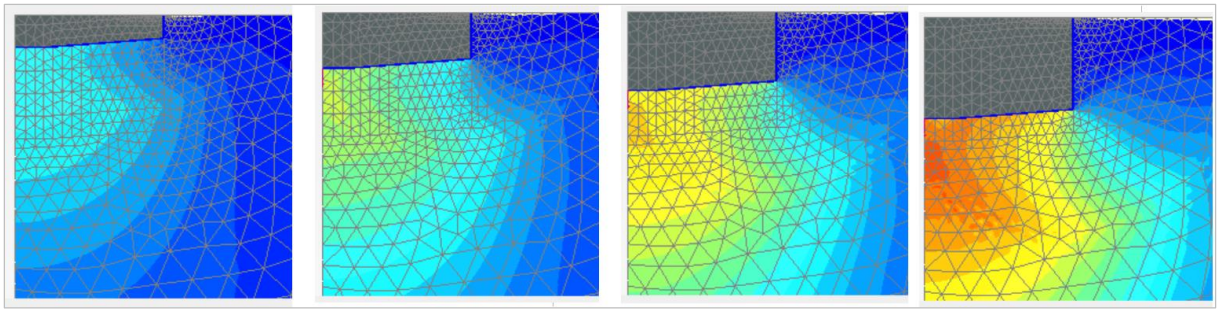

Figure 5.21 Increasing p_{excess} contours using a displacement-controlled modelling scheme.

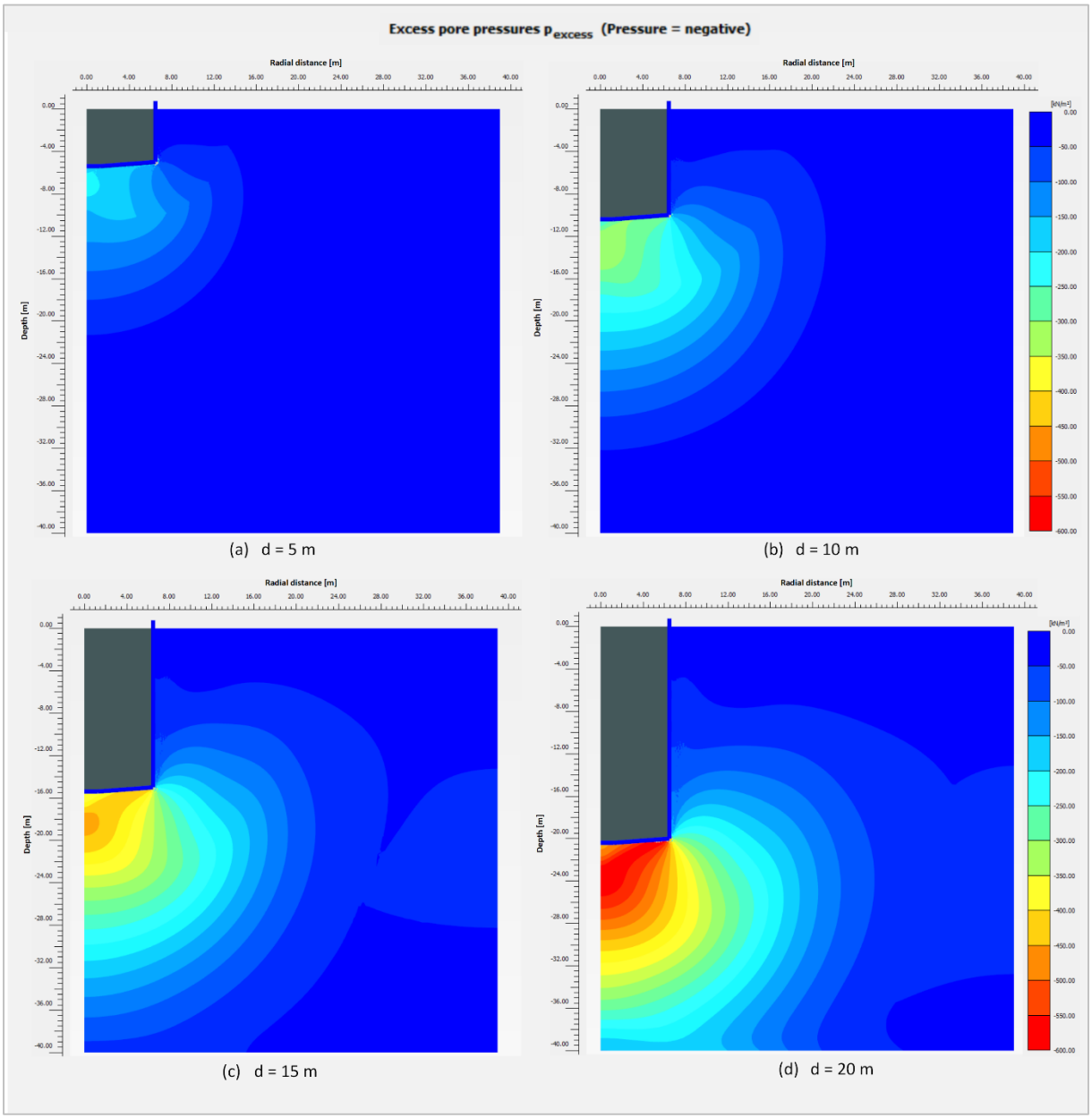

Figure 5.22. Excess pore water pressure contours at different penetration depths using displacement-controlled modelling scheme

Load-controlled modelling scheme
Contrary, when using a load-controlled modelling scheme, the applied force remains equal at each loading stage. Although the soil strength increases with depth, this is not reflected in the generation of excess pore water pressure, because the load remains constant and does not advances until failure. As a result, the excess pore water pressure contours remain more or less constant at increasing spudcan penetrations, as shown in figure 5.23. A constant 10 MN of force is applied at each depth.

However, it is noted that within the diagonal shear band directly below the footing, the magnitude of the excess pore water pressure is reducing at increasing spudcan penetration depths. Since the soil strength increases linearly with depth, a larger effective stress is found at deeper penetrations. As the load increment remains the same, the plastic deformations within the soil will reduce with depth and thus, the shear induces pore water pressures in the shear band will reduce as well.

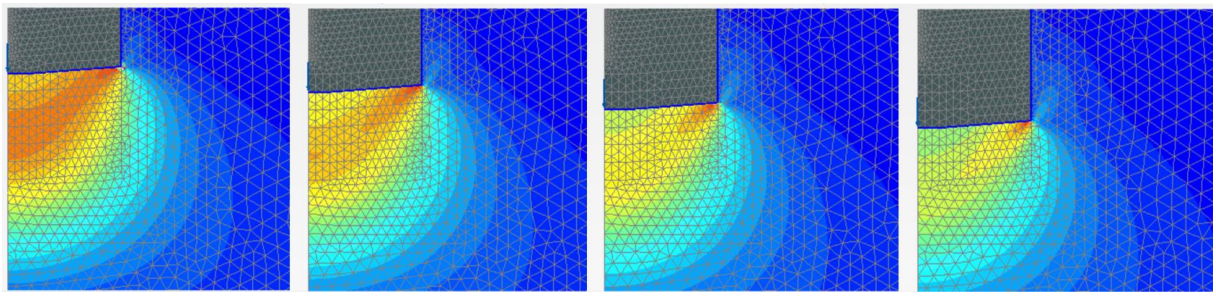

Figure 5.23 Increasing p_{excess} contours using a force-controlled modelling scheme.

Conclusion
Since we are interested in the maximum load the soil can resist at each depth, the displacement-controlled modelling scheme is used to calculate the excess pore water pressures at the collapsed load. Due to a linearly increasing soil strength with depth, a larger force needs to be applied at deeper penetrations to reach the collapse load. As a result, the excess pore water pressure generated below the footing increases with penetration depth.

5.3 Modelling consolidation effects

5.3.1 Modelling scheme

Consolidation analyses can be modelled using two modelling schemes, i.e. displacement-controlled and load-controlled modelling scheme. Each resulting in different model output. Both modelling schemes are elaborated below.

Displacement-controlled modelling scheme
In a displacement-controlled (DC) modelling scheme, displacements are prescribed initially and stresses are model output. At first, the soil below the spudcan footing is pushed down by prescribing a vertical displacement. Consequently, the stresses within the soil are increased by mobilising the material, which leads to certain reaction stresses of the soil. In undrained conditions, excess pore water pressures are generated. Using the WIP method, spudcan penetration is modelled until a target soil reaction force is reached. At that point, the vertical prescribed displacement is fixed and consolidation is initiated by allowing drainage through the soil surface boundary. As excess pore water pressure dissipates from the soil, total stresses decrease which leads to a reduction in soil reaction force.

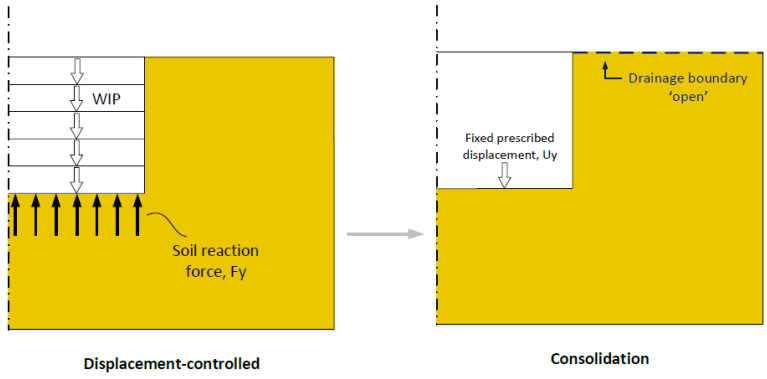

Figure 5.24 Displacement-controlled modelling scheme.

Load-controlled modelling scheme

In a load-controlled (LC) modelling scheme, calculations are reversed, which means that stresses are applied first and deformations are model output. To find the settlements during consolidation, the soil first has to be loaded by applying a force. The maximum collapse load is computed in a displacement controlled manner by loading the soil until failure and integrating the total soil stresses beneath the footing at a certain depth. Next, the resultant force is put on top of a rigid spudcan footing. As the soil reaction force and the resultant force are equal, the system is in equilibrium and no settlement occur during this stage. When opening the drainage boundary afterwards, excess pore water pressure is allowed to dissipate, causing settlement of the spudcan until a new equilibrium is reached.

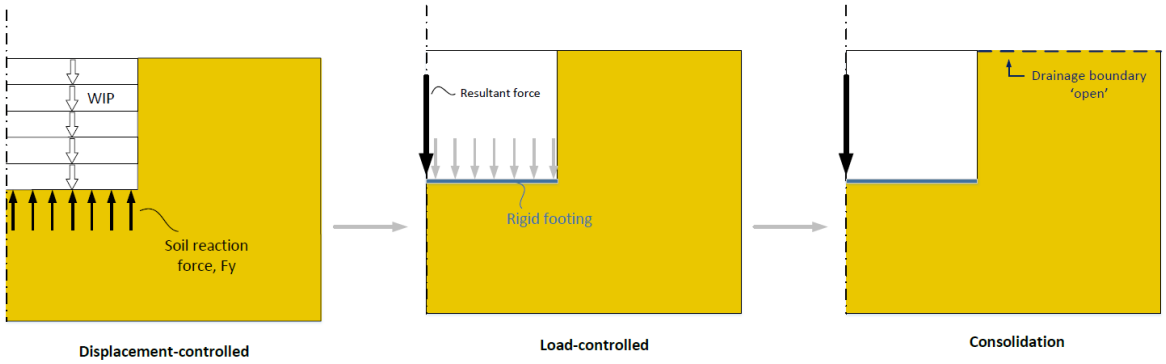

Figure 5.25 Load-controlled modelling scheme.

5.3.2 Change of permeability

Change of permeability parameter

When a soil is subjected to vertical stress, a reduction in volume takes place by expulsion of water under long term static loading. When soil is loaded in undrained conditions, the pore pressure increases. The excess pore pressure is dissipated by squeezing water out of the pore spaces, which leads to settlement. This process takes time and is controlled by the permeability of the soil and the locations of the free draining boundary surfaces. The change of permeability parameter, c_k, takes account of the fact that the permeability of a soil will reduce as it consolidates. Consequently, the rate of settlement during consolidation decreases over time.

The change of permeability during a consolidation analysis can be properly modelled by specifying a proper value for the change of permeability parameter, c_k. Taylor (1948) proposed the following empirical relationship between the logarithm of permeability and the change in void ratio. For clay soils, the permeability is found to change according to the following relationship:

$$log\left(\frac{k}{k_0}\right) = \frac{\Delta e}{c_k} \qquad \textit{Eq. (5.3)}$$

Where Δe is the change in void ratio, k is the variable permeability in the calculation and k_0 is the initial input value of the permeability in the data set. The permeability change index, c_k, determines the degree of reduction in soil permeability as function of compressibility. According to the PLAXIS 2D Reference Manual (Brinkgreve and Post, 2013), it is recommended to use a changing permeability only in combination with the Hardening Soil model, Hardening Soil model with small-strain stiffness, Soft Soil model or the Soft Soil Creep model, because those models describe the elastic behaviour of soils very well, which is important in terms of settlements. In that case the c_k-value is generally in the order of the compression index c_c. For all other models, the c_k-value should be left to its default value of 10^{15}.

From the one-dimensional consolidation tests on clay samples, the change in void ratio is derived by the difference between the void ratio at the beginning and end of the test. The magnitude of changing permeability is derived by selecting the right k-value at its corresponding effective stress level at the end of the consolidation test. The change of permeability parameter is calculated for multiple clay samples. An average result of $c_k = 0.12$ is found. This value is indeed in the order of the derived compression indices, as elaborated in section 3.4.4 – Soil stiffness parameters.

Table 5.2 Estimated model input for c_k.

Estimated change of permeability parameter (c_k)	
c_k	0.12

Modified Cam-Clay model

Calculations using the Modified Cam-Clay model are performed with a constant permeability. That means that a change of permeability during consolidation is not taken into account. As the consolidation duration is relatively small (the total installation time required for the Aeolus at each location is limited to approximately one day), the reduction of excess pore water pressure during this relatively short duration is very small, as shown in figure 5.26. From the PLAXIS calculations, it follows that after one day of consolidation, the degree of consolidation is just 3.1%, as indicated in figure 5.27. Therefore, the change of permeability during the first day of consolidation can be assumed as negligible and thus, the c_k-parameter is assumed not to be relevant during this short consolidation period.

Contrary, the change of permeability would play a role for longer consolidation durations. As water dissipates from the soil, the material is compressed, which leads to a reduction in void ratio over time. Due to the smaller available pore spaces for water to flow through, there would be an increase in flow resistance over time and the change of permeability would matter. However, in a relative small consolidation duration of just 1 day, this effect would not be relevant.

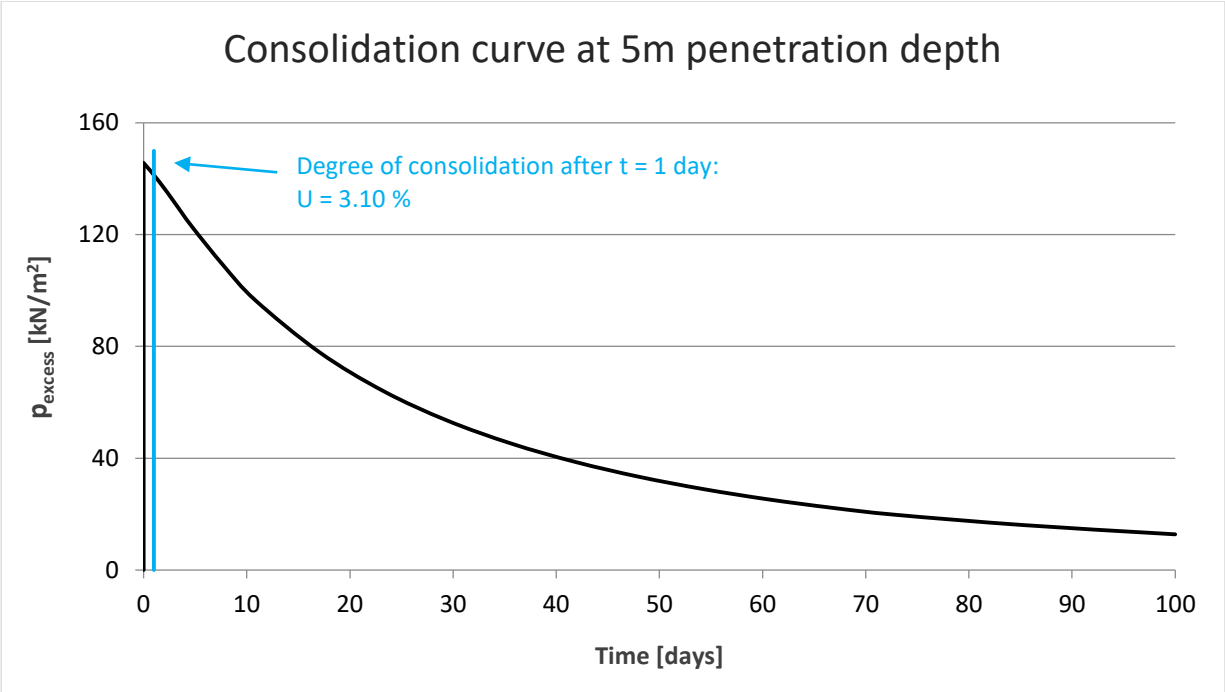

Figure 5.26 Consolidation curve

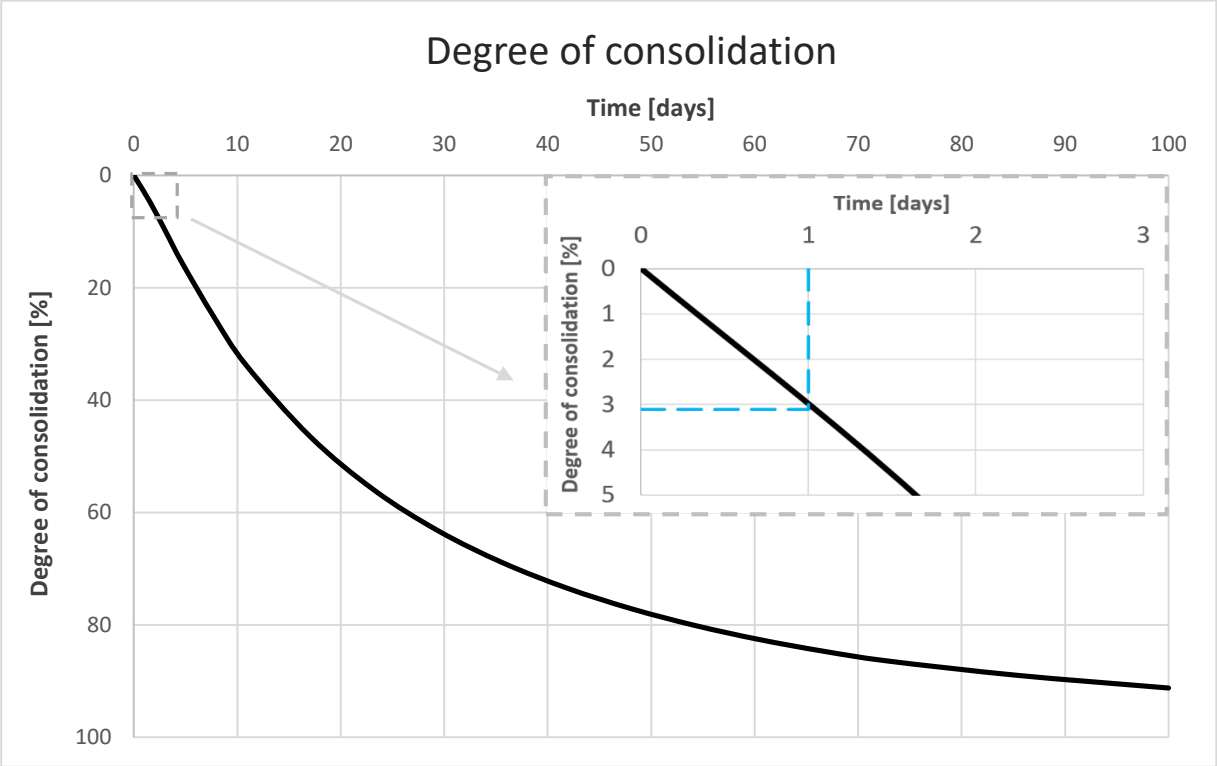

Figure 5.27 Degree of consolidation curve

5.3.3 Post consolidation load-penetration response

Settlements

During consolidation, soil particles will be packed more closely together over a period of time under the application of continued pressure, i.e. static loading. It is achieved by gradual drainage of water from the soil pore spaces (Terzaghi, 1943). In figure 5.28, the time settlement curve of a spudcan at 5 m penetration depth is shown under its maximum collapse loading conditions at this depth. The settlements are derived based on a load-controlled modelling scheme. From the graph, it is seen that initially, during the first few days of consolidation, settlements occur relatively fast after application of the load, which is mainly due to immediate compression of the soil layer under undrained conditions. Since the permeability is very low ($k = 6.6 \cdot 10^{-5}\ m/day$), excess pore water pressures have not been able to dissipate in just one day. Thus, the effect of one day of consolidation is assumed not to impact the spudcan penetration resistance. The increase in effective stress is thus also negligible.

After the immediate settlements, primary consolidation settlements dominate in a slower rate. As time progresses, expulsion of pore water from the void spaces can take place for a longer period, which will reduce the excess pore pressures and simultaneously increase the effective stresses below the spudcan footing. For a longer consolidation during, for instance in the order of 100 days, it is likely that consolidation effects can increase the soil resistance. However, in this study, jack-up durations of the Aeolus vessel are considered to be in the order of maximum one day (Van Oord, 2017). During this relatively short consolidation period, the effect of water dissipation and effective strength increase is negligible. Only immediate settlements are important for determining the penetration rate into the soil. Since the rate of immediate settlements are relatively fast, other effects such as the viscous effects are more likely to dominate the soil behaviour. The time dependent soil behaviour and strain rate effects on the viscous stress-strain behaviour is investigated in section 5.4 – Modelling strain rate effects.

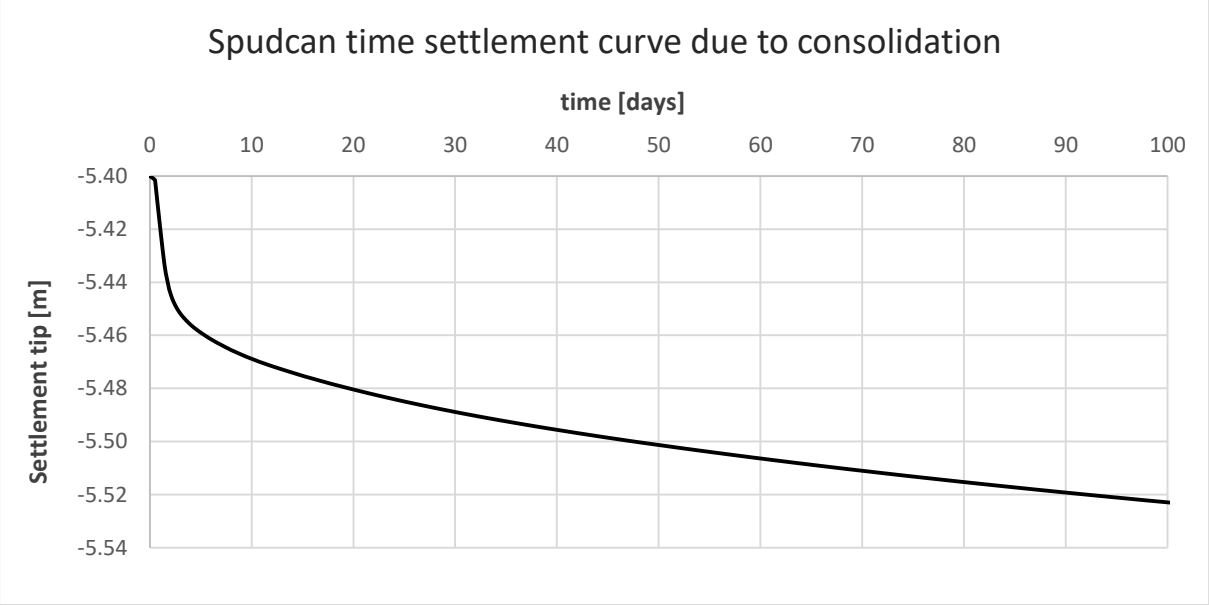

Figure 5.28 Time settlement curve for spudcan at 5m penetration depth

Increased mechanical strength

When soil is loaded in undrained conditions, the excess pore water pressure increases. Settlements take place as the excess pore pressures dissipate and water leaves the soil. This process takes time, and the rate of settlement decreases over time, as shown in figure 5.28. In cohesive soils, seepage is relatively slow due to low permeability. As a result of consolidation, the soil directly under the spudcan

footing is compressed and undergoes reduction in void ratio, after which its mechanical strength is increased due to particle interaction. The affected soil volume around the spudcan footing is known as the consolidation-induced zone of increased undrained shear strength. The effect of consolidation on the soil strength is investigated numerically by loading a spudcan footing at 5m penetration depth up to its collapse load, both before and after a consolidation period of 1 and 10 days, respectively.

In figure 5.29 and 5.30, the first vertical upward line represents the initial leg load which can be supported by the soil at $t = 0$. Next, a consolidation period of 1 and 10 days, respectively, are introduced, after which the soil is loaded again until its collapse load. It can be seen the soil strength is slightly increased in the (re)loading part after consolidation. As already mentioned before, the soil strength enhancement is only marginal ($\Delta F_y = 0.03\ MN$, which is an increase of 0.16%) and is assumed to be negligible compared to the soil strength before consolidation. Even for a consolidation duration of 10 days, the soil strength enhancement is still very small (+1.69%). Therefore, it can be concluded that a relatively short consolidation duration of 1 day (or even 10 days) does not have a significant effect on the mechanical strength increase of the soil directly below the footing.

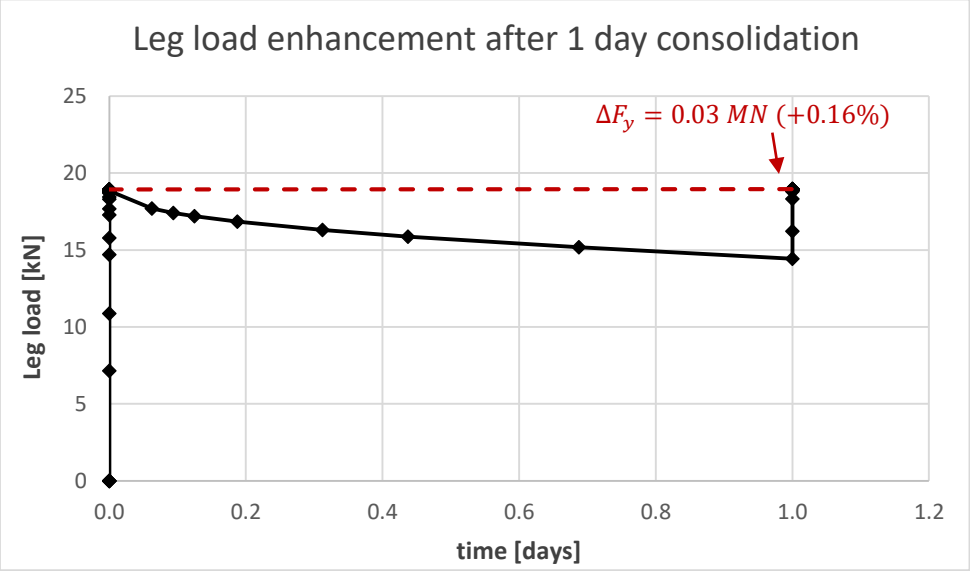

Figure 5.29 Leg load enhancement after 1 day consolidation

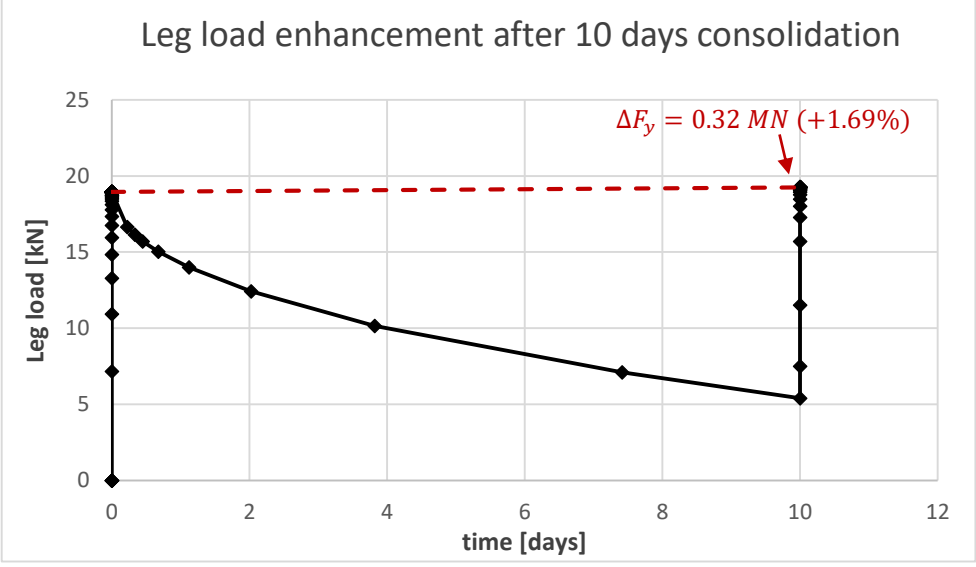

Figure 5.30 Leg load enhancement after 10 days consolidation

5.3.4 Conclusion

The required jack-up duration for the Aeolus vessel at each wind turbine location is approximately one day. During this relatively short period of time, water dissipation from the pore spaces is hardly possible as the drainage is slow due to a very small permeability of the clayey material ($k = 6.6 \cdot 10^{-5}\ m/day$). Inherently, only a marginal reduction of excess pore water pressure can take place, i.e. the degree of consolidation after one day is just 3.1%. The process of gradual transfer of stress from the pore water pressure to effective stress can also hardly take place, which is demonstrated by a marginal 0.16% increase of undrained shear strength of the soil post consolidation of one day. This increase in soil resistance is assumed to be negligible. It can therefore be concluded that the effect of consolidation, which takes place during one day, does not affect the soil resistance post consolidation.

5.4 Modelling viscous strain rate effects

In order to investigate the effects of strain rates on the viscous behaviour of clays, the Soft Soil Creep model is used to facilitate a better understanding of the effect of spudcan penetration rate on the soil penetration resistance. The viscoplastic Soft Soil Creep model is only used in this section to investigate the viscous strain rate effects of spudcan penetration problems.

5.4.1 Relative importance of strain rate effects

First of all, in order to know the relative importance of the consolidation and viscous effects on the soil resistance, it is required to estimate the normalised velocity for the case of spudcan penetration in the soft material as present at the offshore wind site. In general, engineering practice has indicated that for spudcan diameters of 10-20 m, penetration rates of 1 – 3 m/h are found (Hossain and Randolph, 2009a). Unfortunately, actual penetration of the spudcans over time has not been measured at the this project. Therefore, the actual spudcan penetration rate cannot be determined. For this thesis, a jacking rate of 1 m/h assumed.

The normalised velocity is expressed in equation (5.4). The coefficient of consolidation is a measure of the rate at which the consolidation process proceeds and is determined using 1D consolidation tests on soil specimens. At a reference effective stress level of $100\ kPa$, an average value of $c_h = 7.90\ m^2/yr$ is assumed for both the SSF-SBD and WIS-MF soil unit (Fugro Geoconsulting Ltd, 2012-2014). As the soil is modelled as a uniform material, the permeability in vertical direction is assumed equal to the permeability in horizontal direction. Inherently, the coefficient of consolidation is also assumed to be equal in vertical and horizontal direction. With a maximum spudcan diameter of 13 m, the normalised velocity becomes:

$$V = \frac{vd}{c_h} = \frac{1 \cdot 13}{7.90/(24 \cdot 365)} = 14{,}415 \quad [-] \qquad \textit{Eq. (5.4)}$$

Looking at the soil resistance curve as function of strain rate (figure 5.31), it noted that a normalised spudcan penetration velocity as found above is located far on the right hand side where fully undrained conditions prevail. Even with an uncertainty of $\pm 25\%$ for the coefficient of consolidation, the normalised velocity falls within a range of $11{,}530 - 19220$, which is still considered relatively high. The normalised velocity increases even more for higher spudcan penetration velocities.

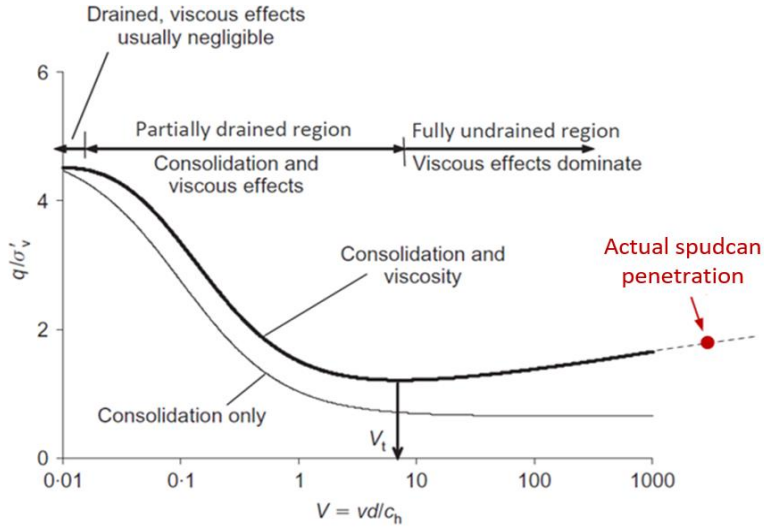

Figure 5.31. Combined influence of consolidation and viscous effects on penetrating soil resistance in clay (Lehane et al., 2009).

5.4.2 Simulation of triaxial tests

Effect of shearing rate on clay strength

To demonstrate the viscous effect of time dependent loading on the soil resistance, the general soil test facility in PLAXIS is used to simulate undrained triaxial compression tests during different loading durations. The resulting effective stress paths are shown in the (p',q)-plot in figure 5.32. First, samples are consolidated isotropically up to an initial effective stress of $100\ kN/m^2$ and then sheared until failure.

The soil samples are sheared until failure in different time intervals, ranging from $\Delta t = 0.001\ days$ to $\Delta t = 1000\ days$. The strain rate is computed by dividing the observed strain ($\varepsilon = 0.10\%$) over this time interval. From figure 5.32, it is clearly seen that higher effective stress paths are followed at faster shearing rates. At the faster shearing rates, adjacent soil particles find it more difficult to move relatively, and, unless restrained by increased effective stress, will tend to ride up over one another. The effect can be thought of either as an increased resistance to compression or as an increased tendency to dilate. In either case the result in the same: increasing the loading rate applied to a saturated soil means larger effective stresses and consequently greater shear resistances. This strength increase is demonstrated by plotting the undrained shear strength versus axial strain for different loading durations (figure 5.33). It is clearly seen that the undrained shear strength of the soil becomes larger for higher loading rates.

The green lines in figure 5.32 and 5.33 represent the effective stress path and undrained shear strength of the soil, respectively, for soil samples modelled using the Modified Cam-Clay model. This model is assumed to be rate-insensitive, as no time-dependent behaviour is incorporated. The yield surface of the MCC-model increases instantaneously for stress states outside the yield surface. Therefore, the effect of loading rate is not reflected in the model outcome. The stress path thus remains at one certain location, regardless of the loading rate.

The rate-insensitive MCC-model is assumed to be the time-independent lower limit of the rate-sensitive Soft Soil Creep model. For very small shearing rates, the undrained shear strength is considered to be independent of strain rate. Here, only the frictional resistance term is present (no additional viscous resistances). However, the model also produces stress states below this time-independent limit, which are assumed to be incorrect and should not be taken into account. A detailed overview of this modelling limitation is explained is Appendix I.

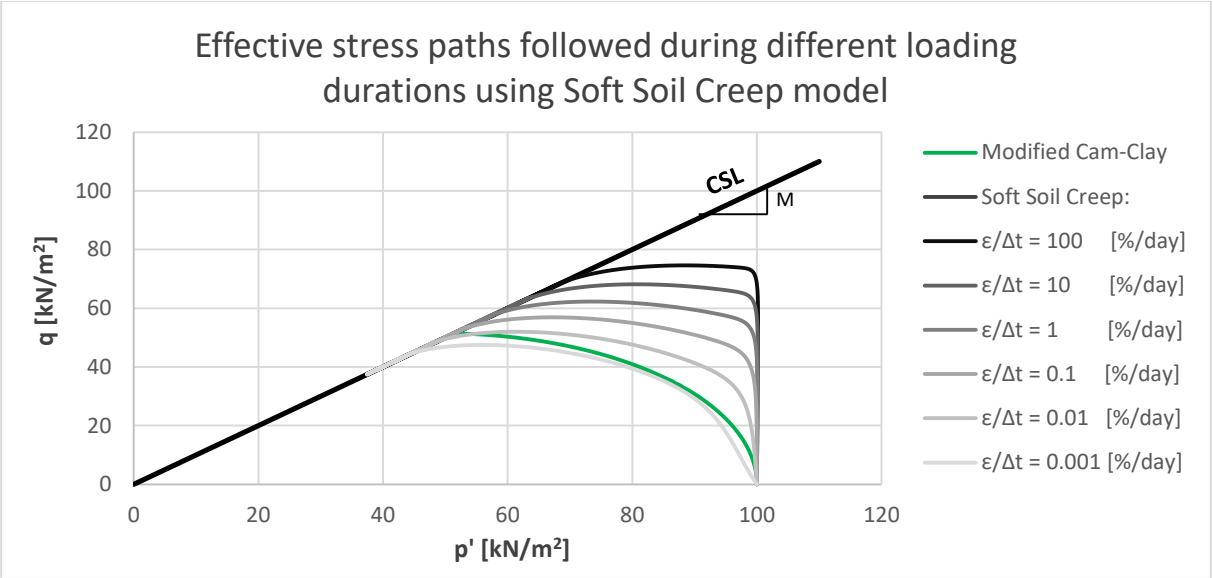

Figure 5.32 Effective stress paths followed for different shearing durations using Soft Soil Creep model.

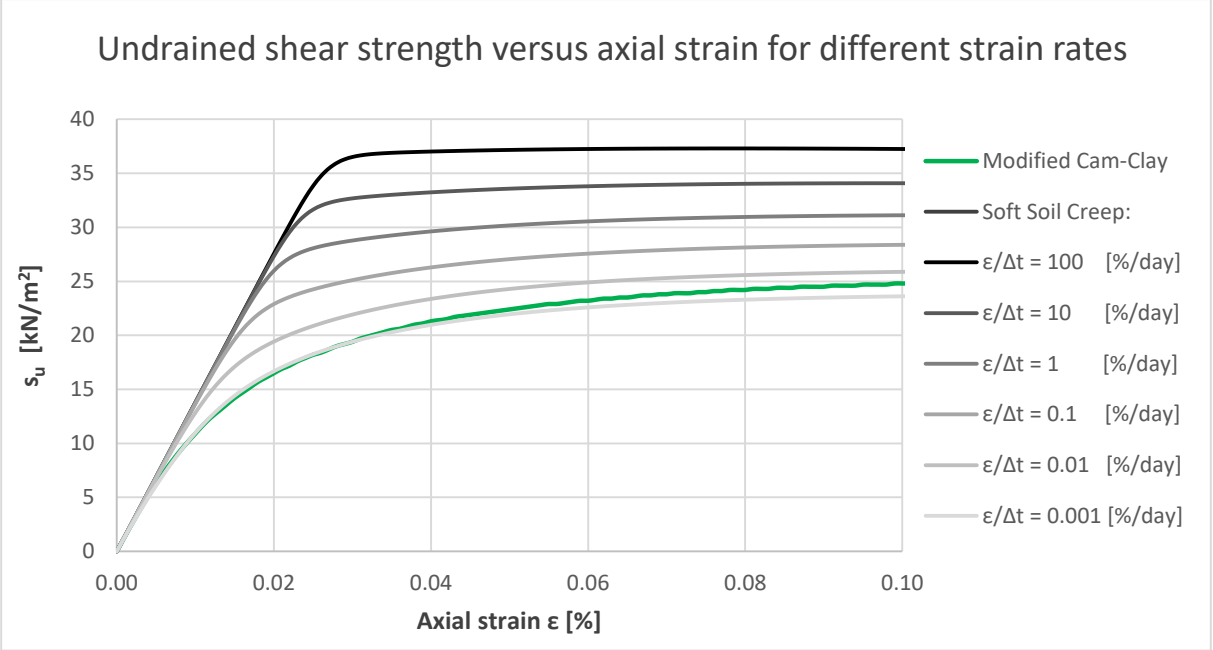

Figure 5.33 Undrained shear strength versus axial strain for different strain rates.

Effect of modified creep index parameter μ^*

The modified creep index parameter, μ^*, is related to the settlements caused by the secondary compression. It specifies the creep rate after 1 day. The change of the creep rate in time is defined by the combination of parameters λ*, κ* and μ*. For a rough estimate, the ratio λ^*/μ^* should be in the range between 15 to 25 (Brinkgreve and Vermeer, 2016). For the SBD soil, upper and lower limits of the creep index can be derived based on the its modified compression index parameter, λ^*.

Lower limit

$$\mu^* = \frac{\lambda^*}{25} = \frac{0.026}{25} = 0.0010 \quad [-] \qquad \textit{Eq. (5.5)}$$

Upper limit

$$\mu^* = \frac{\lambda^*}{15} = \frac{0.026}{15} = 0.0017 \quad [-] \qquad \textit{Eq. (5.6)}$$

The effect of the modified creep index parameter is investigated by plotting the effective stress paths for different values of μ^* in a (p',q)-plot, as shown in figure 5.34. It is seen that higher effective stress paths, and thus higher soil strengths, are found for higher creep indices. Considering clayey soils, a higher soil plasticity leads to more creep as the adsorbed water in the clay particles allows the particles to slip over one another. As a result, higher strain rates occur, which causes viscous resistances in the soil. In conclusion, for increasing soil plasticity, the modified creep index parameter is higher and thus an increased soil strength is observed.

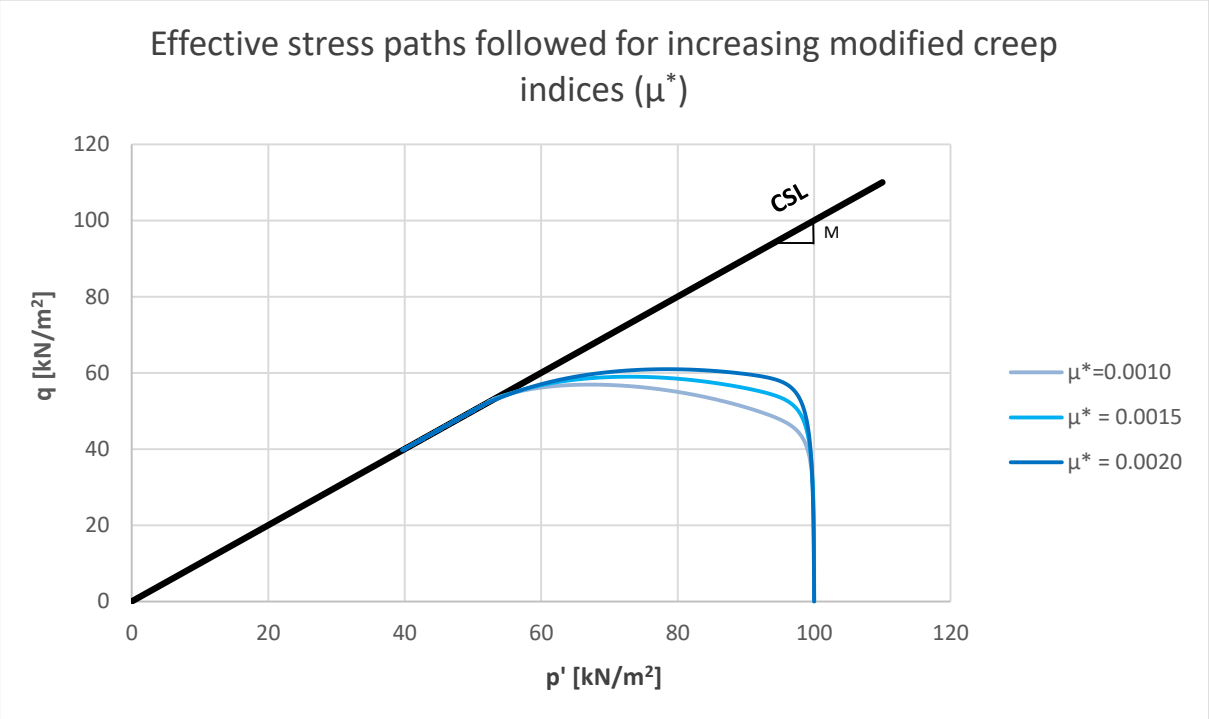

Figure 5.34 Effect of modified creep index on the soil strength

5.4.3 Coupling of viscoplastic modelling results to empirical relation

Empirical relation

Hossain and Randolph (2009a) investigated the effect of rate dependency on the penetration resistance of spudcan foundations on clay. Large deformation finite element analyses were constructed based on the framework of experimental full-flow penetrometer testing as performed by Lehane et al. (2009). These tests indicated that the undrained shear strength increases for larger strain rates. The soil strength is found to increase with strain rate by approximately 5-20% per log cycle of increasing strain rate. This can be expressed as:

$$s_u = s_{u,ref}\left[1 + \mu \log\left(\frac{\dot{\varepsilon}}{\dot{\varepsilon}_{ref}}\right)\right] \qquad \textit{Eq. (5.7)}$$

Where $s_{u,ref}$ is the soil shear strength at the reference strain rate $\dot{\varepsilon}_{ref}$ of $0.00001\,\%/s$. The expression follows a logarithmic law with rate parameter μ taken in the range of $0.05 - 0.2$ for normally consolidated clays. For very small strain rates, no strength increase is observed. There seems to be a threshold strain rate ($\dot{\varepsilon}_{ref}$) for which the undrained shear strength may be considered independent of strain rate. That is the case for $\dot{\varepsilon} < \dot{\varepsilon}_{ref}$.

In order to capture the rate dependent strength increase in the numerical model, each affected Gauss point should be modified according to the updated undrained shear strength response. Equation (5.7) can be rewritten in a dimensionless undrained shear strength ratio, given by:

$$\frac{s_u}{s_{u,ref}} = 1 + \mu \log\left(\frac{\dot{\varepsilon}}{\dot{\varepsilon}_{ref}}\right) \qquad \textit{Eq. (5.8)}$$

For a given reference s_u-profile, this ratio indicates the amount of undrained shear strength increase at each strain rate. The logarithmic curve representing the undrained shear strength ratio of equation (5.8) is plotted in figure 5.35. This curve appears as a straight line on a semi-logarithmic scale, as shown in figure 5.36. Taking the s_u-profile as originally determined using the SHANSEP approach (see section 3.5 – Shear strength properties of soil) as the reference undrained shear strength, $s_{u,ref}$, the increase in shear strength can then be calculated by means of the shear strength ratio, for each axial strain rate. These results are shown in figure 5.37. It can be seen that the larger the strain rate, the larger the increase in undrained shear strength.

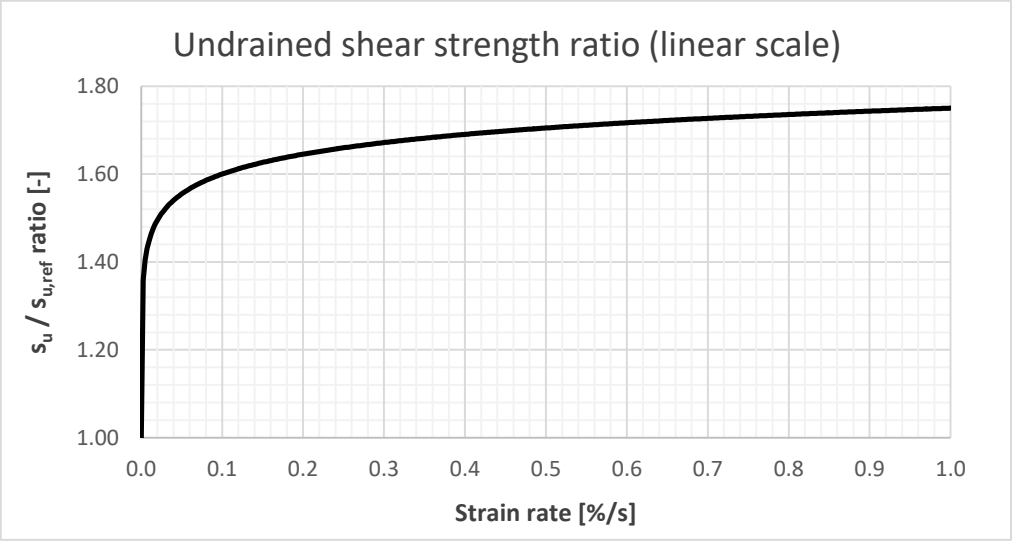

Figure 5.35 Undrained shear strength ratio (linear scale).

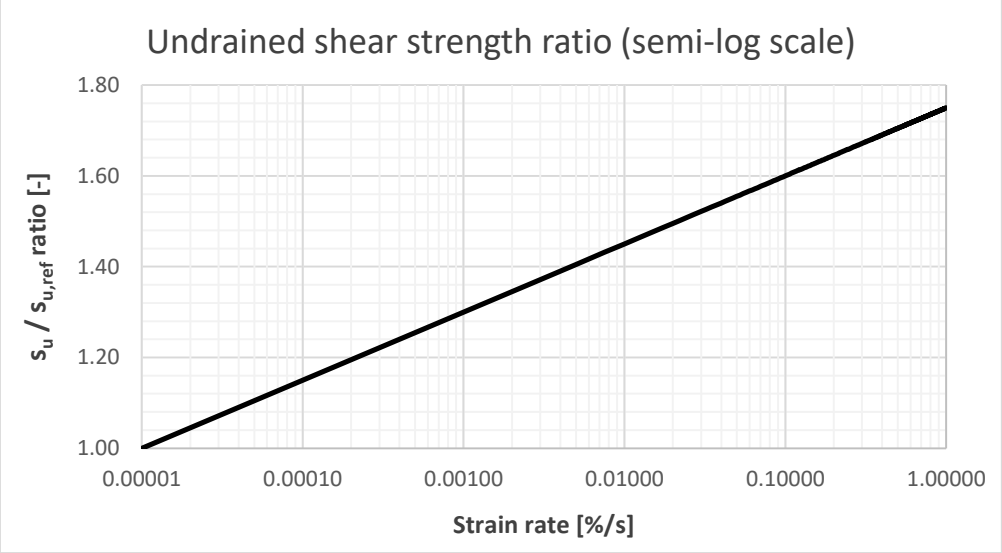

Figure 5.36 Undrained shear strength ratio (semi-log scale).

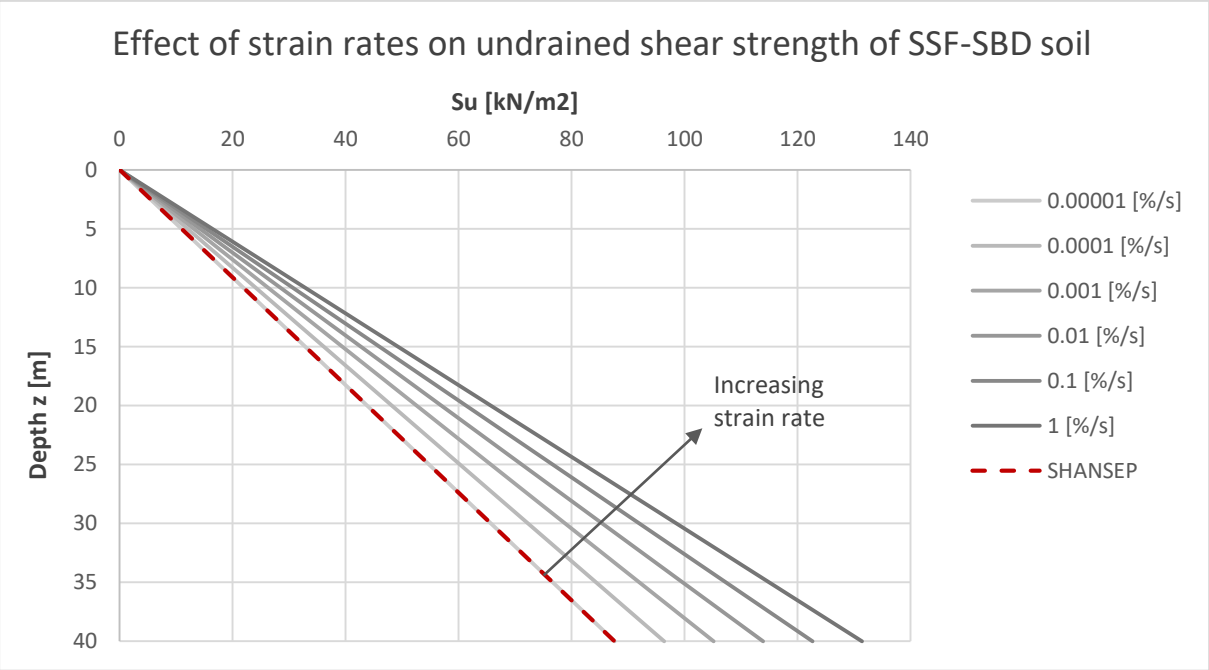

Figure 5.37 Effect of strain rates on undrained shear strength of SSF-SBD soil.

Viscoplastic FE modelling results

The model performance in terms of strain rate dependent soil strength is compared to the empirical relation as introduced by Hossain and Randolph (2009a). Simulations of triaxial tests in the PLAXIS Soil Test facility are used to derive the strain rates at which the samples are sheared until failure. The corresponding undrained shear strengths from the model are then checked against the soil strength found in the empirical equation.

Figure 5.38 shows the undrained shear strength as function of axial strain for different shearing durations, as computed with the Soft Soil Creep model. It is seen that the maximum s_u is obtained at an axial strain ε of 0.10%. This strain is then divided over the time duration, in which the sample is sheared to failure in order to find the corresponding strain rate, according to:

$$\dot{\varepsilon} = \frac{d\varepsilon}{dt} \qquad \textit{Eq. (5.9)}$$

Since the MCC model result (green line in figure 5.38) is assumed to be the time-independent limit of the viscoplastic model, the reference strain rate, $\dot{\varepsilon}_{ref}$, is found by shearing a sample with such a strain rate that its maximum value of s_u equals the maximum undrained shear strength found in the rate insensitive MCC model. This occurs when the sample is sheared until failure in 166 minutes, which corresponds to a reference strain rate of $0.10/(166 \cdot 60) \approx 1.004 \cdot 10^{-5}$ $\%/s$.

In figure 5.39, a comparison is made between the empirical relation and the viscoplastic model results by plotting the undrained shear strength as function of strain rate. It can be concluded that the strain rate dependent soil strength as calculated with the SSC model is compatible with the empirical relation described by Hossain and Randolph (2009a).

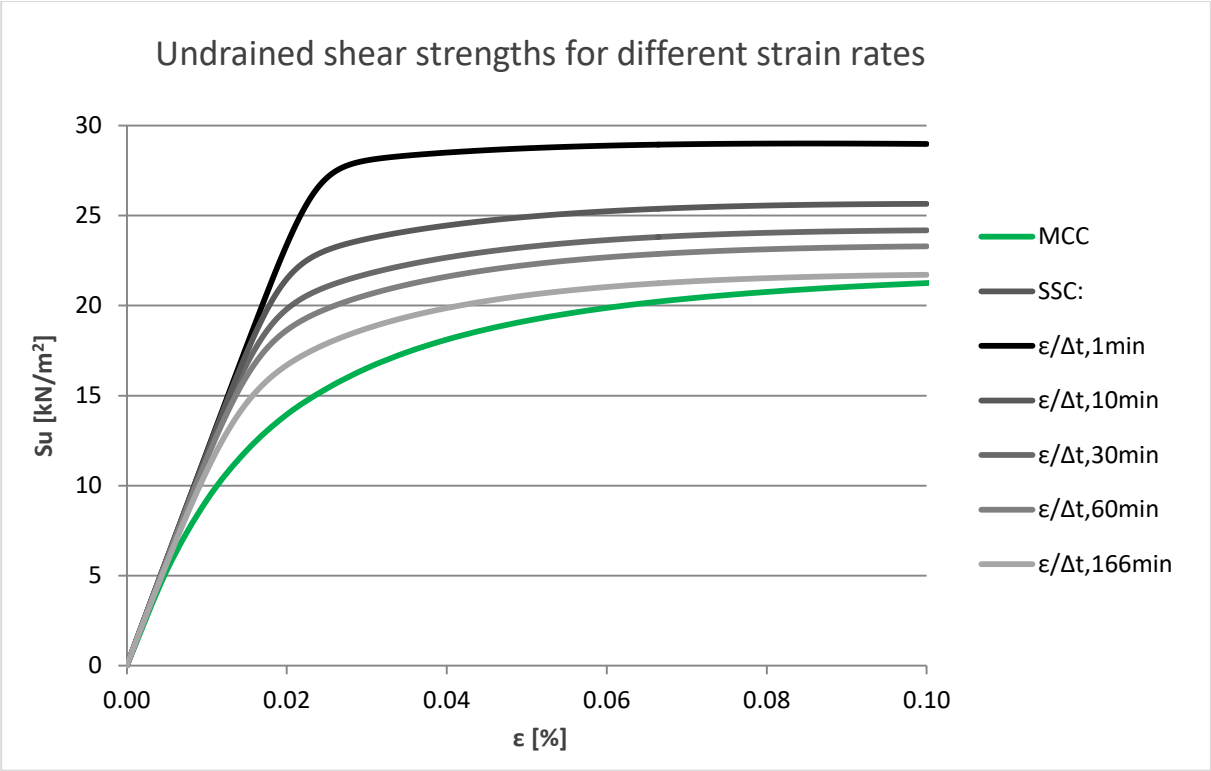

Figure 5.38 Undrained shear strengths for different strain rates

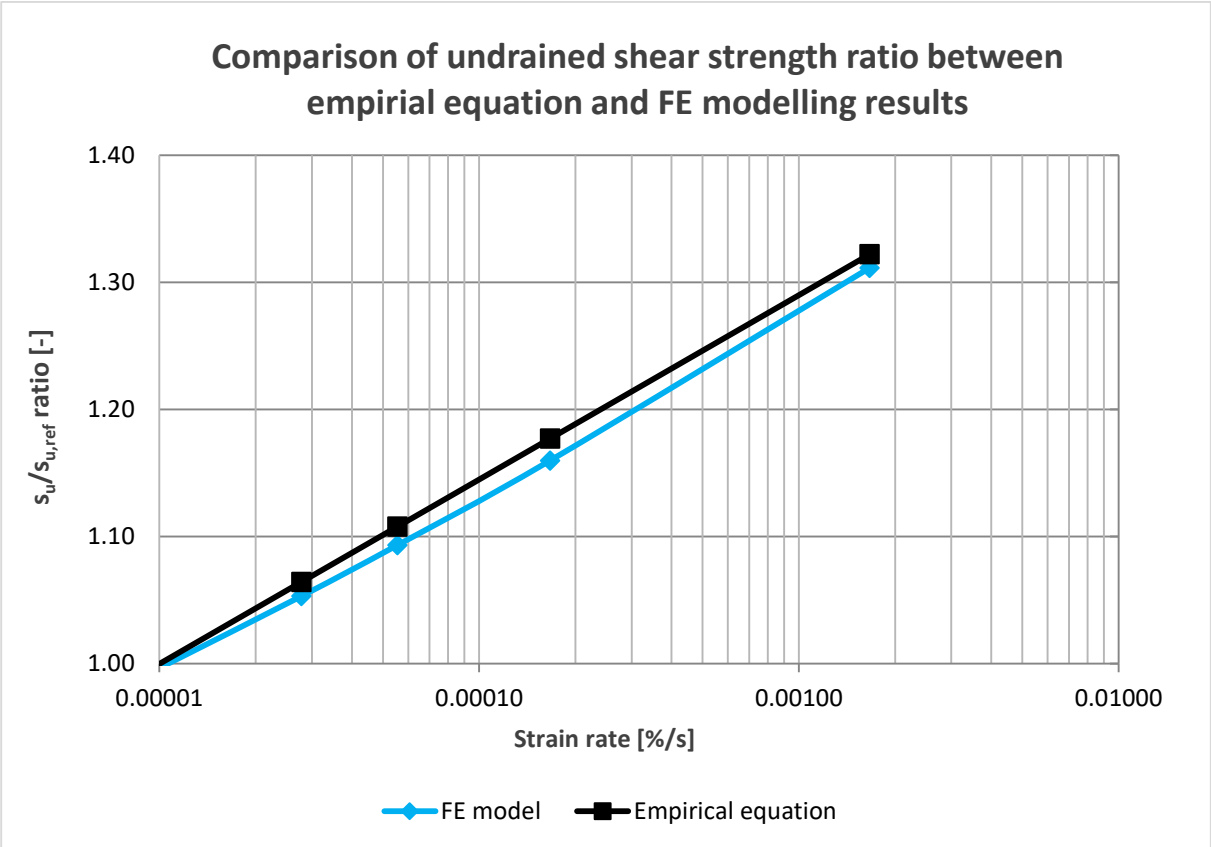

Figure 5.39 Comparison empirical relation with viscoplastic model results

5.4.4 Spudcan penetration time-dependent viscoplastic effects

To investigate the time-dependent viscoplastic effects during spudcan penetration, both a displacement-controlled and load-controlled model set-up is constructed in PLAXIS, as seen in figure 5.40 on the right, to compute the soil resistance and spudcan settlement as function of time, respectively.

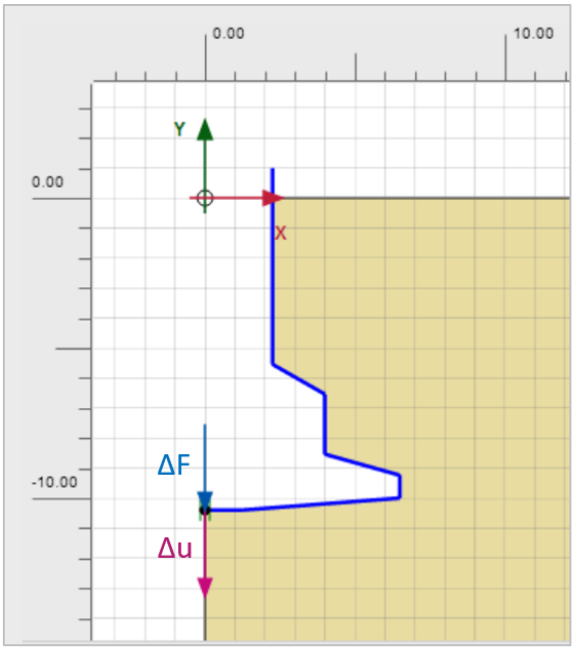

Figure 5.40 Model geometry: spudcan penetration analysis.

At first, the time-dependent viscoplastic effects on the soil resistance is investigated by conducting a series of displacement-controlled wished-in-place analyses at 10 meters depth, in which a prescribed displacement, Δu, of $0.10\ m$ is applied in a time interval of 1, 10, 30 and 60 minutes, respectively. This corresponds to a spudcan penetration rate of 6, 0.6, 0.2 and 0.1 m/hour, respectively. In this case, ΔF is zero, since only prescribed displacements are applied to the spudcan.

The results are shown in figure 5.41. It is seen that the soil shows a viscous increase in strength, i.e. higher peak penetration resistances are found for higher spudcan penetration rates. Thus, during rapid (pre)loading, the peak strength of the material would be higher than would be the case for slowly applied loads. Nevertheless, these peak resistances are only temporarily present, as long as the spudcan moves with a certain rate, in order to create a viscous drag (soil flow) around the spudcan. Once the target preload is reached, the spudcan is stopped and the additional viscous resistances will diminish as the there is no longer any spudcan strain rate present. It is seen that after the peak penetration resistance, the leg load reduces in time towards a certain critical state resitance. This is the static resistance as found in a rate-insensitive model. The faster the loading, the larger will be the difference between the peak resistance and critical state resistance. Consequently, this could result in rapid spudcan settlement afterwards.

The time-dependent viscoplastic effects on the spudcan settlement is investigated by conducting force-controlled wished-in-place analyses, in which the equilibrium leg load of 3750 ton is applied in a time interval of 1, 10, 30 and 60 minutes, respectively. In this case, the prescribed displacements are zero. The resulting spudcan settlement as function of time for different loading rates is plotted in figure 5.42. It is noted that the magnitude of total settlements is equal, regardless of the loading rate. It is just a matter of how these settlements evolve over time. After rapid application of the load, immediate settlements follow as the (pre)load is held constant. These settlements occur rapidly as the peak soil resistance also reduces rapidly towards a critical state soil resistance. The evolution of settlements over time changes with the (pre)loading rate. Settlements occur much more gradual for slower loading rates. The evolution of settlements can be subdivided into three stages. At first, settlements are small as the soil exhibits the additional effect of viscoplastic soil resistance. Until the point of peak resistance, the settlement gradient is then nearly horizontal. Next, post-peak behaviour shows significiant spudcan settlement as the viscoplastic resistances diminish, causing the soil strength to reduce. Eventually, the rate of settlement reduces as the soil is compacted and a new equilibrium bearing strengh is found.

In the long-term, it is noticed that the total spudcan settlement is more or less equal, irrespective of the loading rate. Thus, in order to reduce the risk of rapid leg penetration, a smaller loading rate can help to distribute the spudcan settlement more gradually over a certain time period.

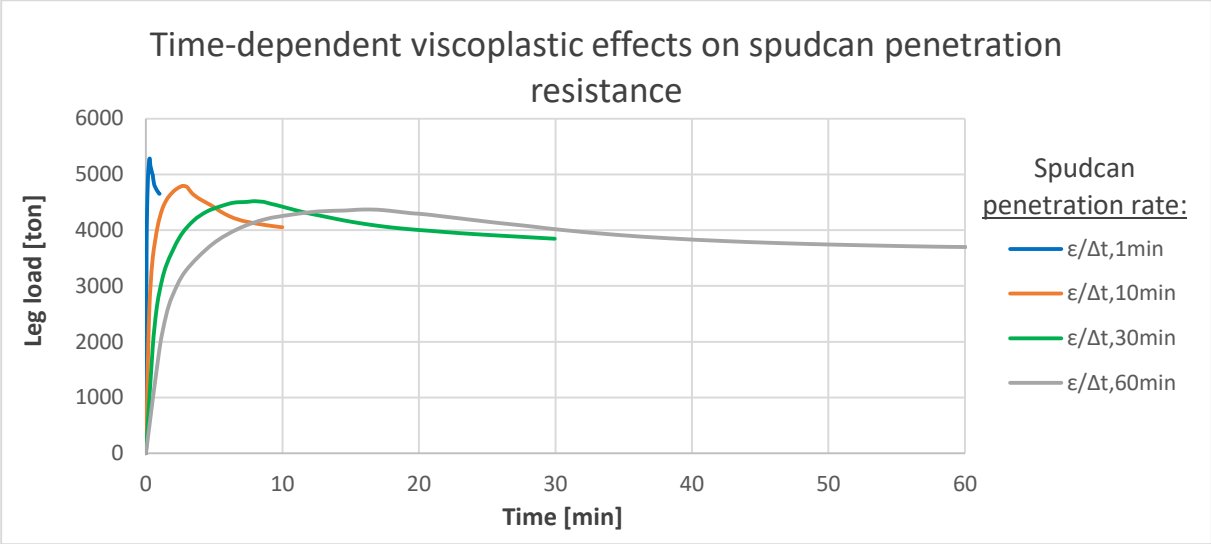

Figure 5.41 Time-dependent viscoplastic effects on spudcan penetration resistance

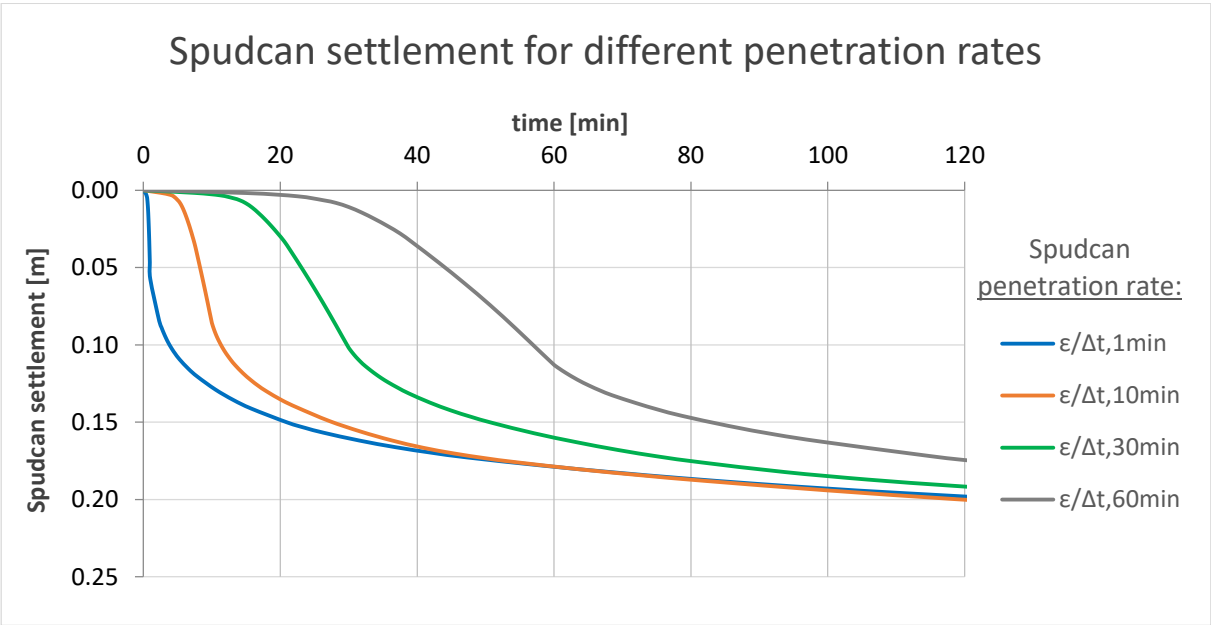

Figure 5.42 Spudcan settlement as function of time for different penetration rates

5.4.5 Standard and overshooting jacking procedure

When jacking-up in clay soils, the rate-dependency of the soil behaviour is observed when attempting to hold the target preload. During the final phases of the jacking process, when the preload is reached, a reduction of the leg load occurs, and the load must actively be brought back to the target preload value. In clay soils, this is expected to lead to further penetrations and multiple cycles are required, which results in large jacking times.

The phenomenon is well known and mentioned in the InSafeJIP (2011) guidelines, but detailed guidance on the causes and possible mitigation measures is not available. In order to gain more insight into this phenomenon, the rate-dependent Soft Soil Creep model is used to investigate the effect of spudcan penetration rate on the required preloading time and corresponding spudcan settlements by using the standard or overshooting jacking procedure. In Appendix J, the soil response of stiffer and softer clay materials in both jacking procedures are assessed in a sensitivity analysis.

Standard jacking procedure

Considering the SSF-SBD soil unit, a displacement-controlled modelling approach is used, in which prescribed displacements of 1.0 m and 0.10 m are applied in a time interval of one hour to represent spudcan penetration rates of 1.0 m/h and 0.10 m/h, respectively. The spudcan is stopped when a target preload is reached. In this case, an arbitrarily chosen value of 3500 ton is used as the target preload value. In practice, this value differs at each location and should be determined on a site-specific basis. After holding the preload for 15 minutes, a reduction in leg load occurs and the load is actively brought back to the target preload value by reloading the soil with the same spudcan penetration rate as before. Multiple 'iterative' preload hold cycles are performed until the preload criterion of 400 ton load reduction in 15 minutes is established. The resulting plot of leg load versus time for both spudcan penetration rates is shown in figure 5.43.

It can be seen that the faster the penetration rate, the larger will be the leg load reduction during 15 minutes of preload-hold duration. This is caused by the viscoplastic rate-dependency of soil strength. The faster the soil is sheared, the larger will be the additional viscous resistance, as seen in the previous section. As the preload is then hold, the spudcan stops (strain rate zero) and the addition viscous resistance term will diminish. This reduction is therefore higher for larger spudcan penetration rates. As seen in figure 5.43, four cycles are required to reach the preload criterion of 400 ton load reduction in 15 minutes when penetrating with a spudcan rate of 1.0 m/h, whereas only two cycles are needed for the slower penetration rate of 0.10 m/h. Penetrating in a slower rate will therefore contribute to reduced jacking times as less cycles are needed.

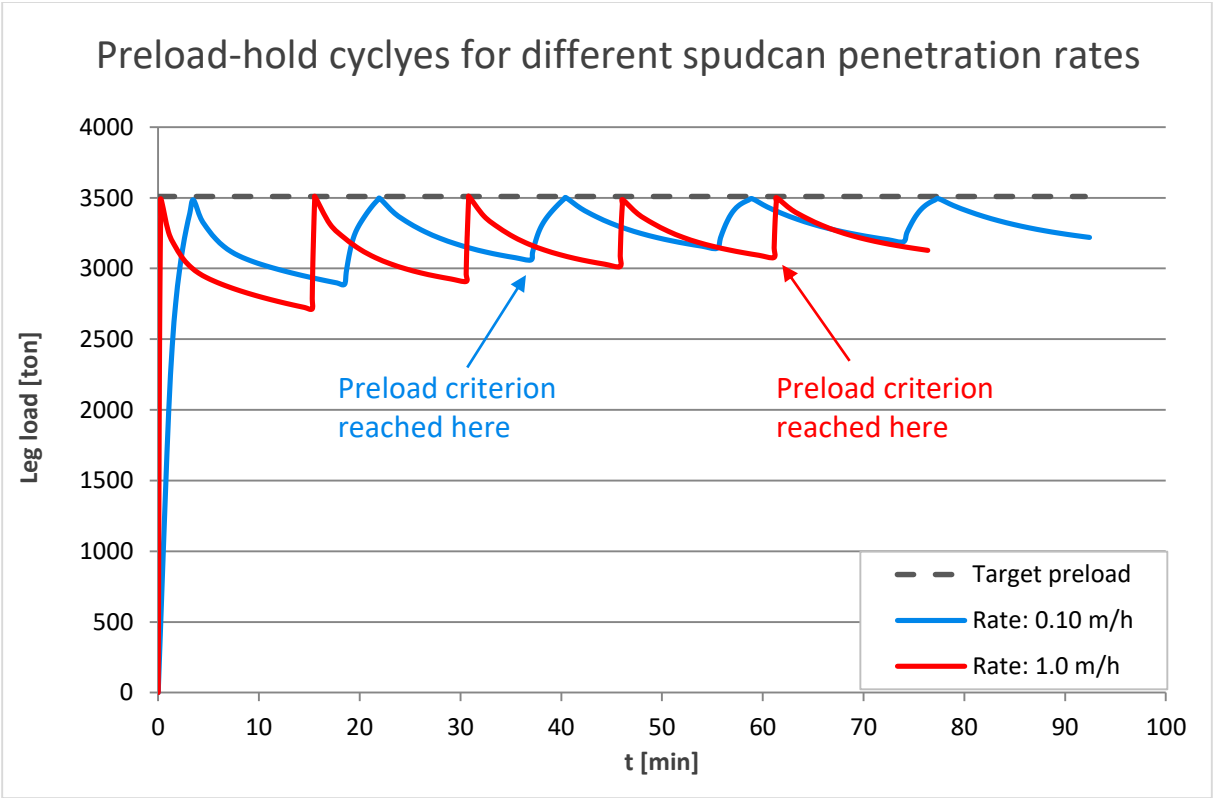

Figure 5.43 Preload-hold cycles for different spudcan penetration rates.

As for the settlements, a force-controlled modelling approach is used, in which the target preload force of 3500 ton is applied in a time interval corresponding to both penetration rates. Consider the spudcan penetration rate of 0.10 m/h, from figure 5.43 above, it is seen that the target preload is first reached in approximately 4 min. In the force-controlled model, the target preload is thus applied over this time interval. Next, it is seen that after the first cycle, the leg load has reduced towards approximately 2900 ton. In the next phase, a force of 2900 ton is applied and hold for 15 minutes. To start the next cycle, the spudcan is reloaded by again applying the target preload of 3500 ton in 4 minutes. This process needs to be repeated for as many cycles as necessary. The resulting plot of the spudcan settlements versus time for both spudcan penetration rates is shown in figure 5.44.

At first, it is noticed that the total settlements are more or less equal. That is, because you need to reach a certain depth where required bearing capacity is found. There is no other way around this. The loading rate does not seem to affect the total settlements, but it is more a matter of how to reach the settlements over time. During fast loading, the initial settlements are smaller compared to slower loading rates, because the soil is stronger when it is sheared faster (additional viscous resistances). After holding the preload, the strain rate is zero and the additional viscous resistance term diminishes, which leads to further penetrations until a stable equilibrium is found. Even some elasticity of the soil is noted as the leg load reduces, due to decreasing external loads. Further, the total amount of spudcan settlements depend on the amount of preload-hold cycles required. Each cycle leads to further additional, creep-like spudcan penetrations. When penetrating at a slower rate, less cycles are needed and thus, slightly less penetrations are expected in a much shorter jacking duration.

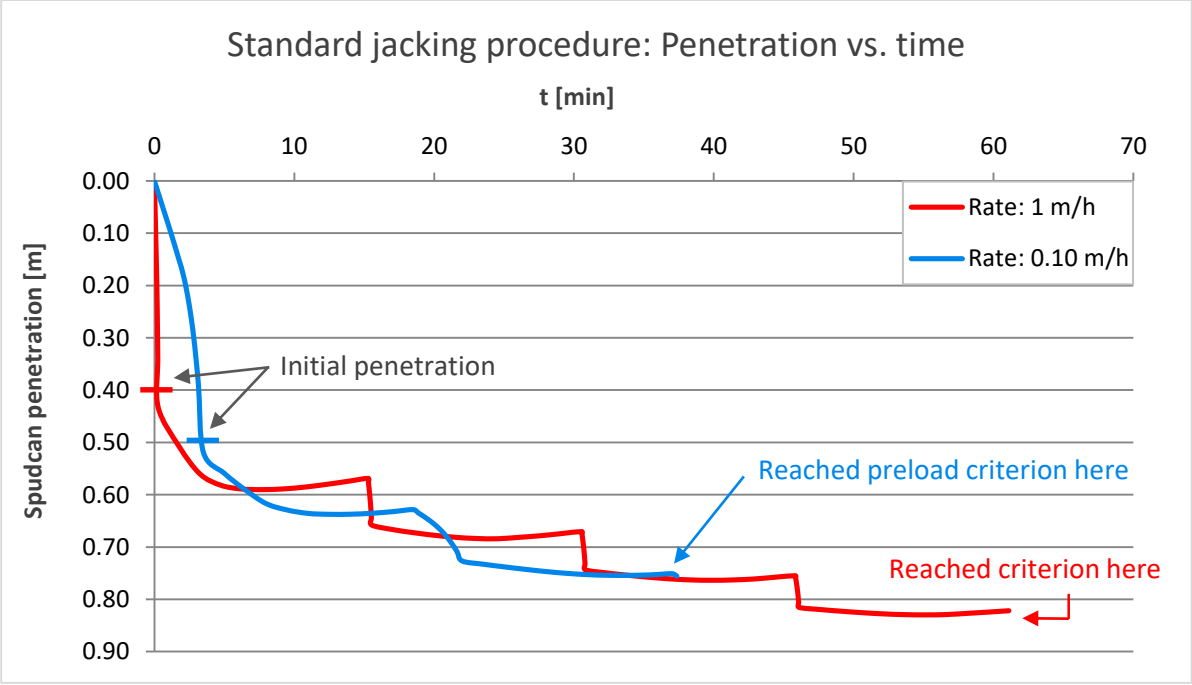

Figure 5.44 Plot spudcan penetration as function of time.

Overshooting jacking procedure

In this thesis, an alternative overshooting jacking procedure from Cathie et al. (2017) is proposed to reduce to the total time required for jacking in clay locations. The goal of this alternative strategy is to overshoot the target preload value by 10%, which makes it possible to reach the preload criterion of the standard jacking procedure more quickly. This method is explained in detail in section 2.8 – Alternative jacking procedure. The same model set-up as described above (section 5.4.5) is used to model the effects of spudcan penetration rate in the overshooting jacking procedure.

Applying the same penetration rates of 0.10 m/h and 1.0 m/h, the target preload value is overshot by 10%, after which the load-hold period is started. From figure 5.45, it is noted that for the fast loading rate (1.0 m/h), considerable time saving are gained, as the preload criterion is reached much quicker when using the overshooting jacking procedure. You don't have to go through all the preload-hold cycles. Considering the spudcan settlements, when using the overshooting method, an additional load is applied on top of the target preload, which brings the spudcan to the depth, which would have been reached by the creep-like additional penetrations under the standard jacking procedure, much quicker (see figure 5.46).

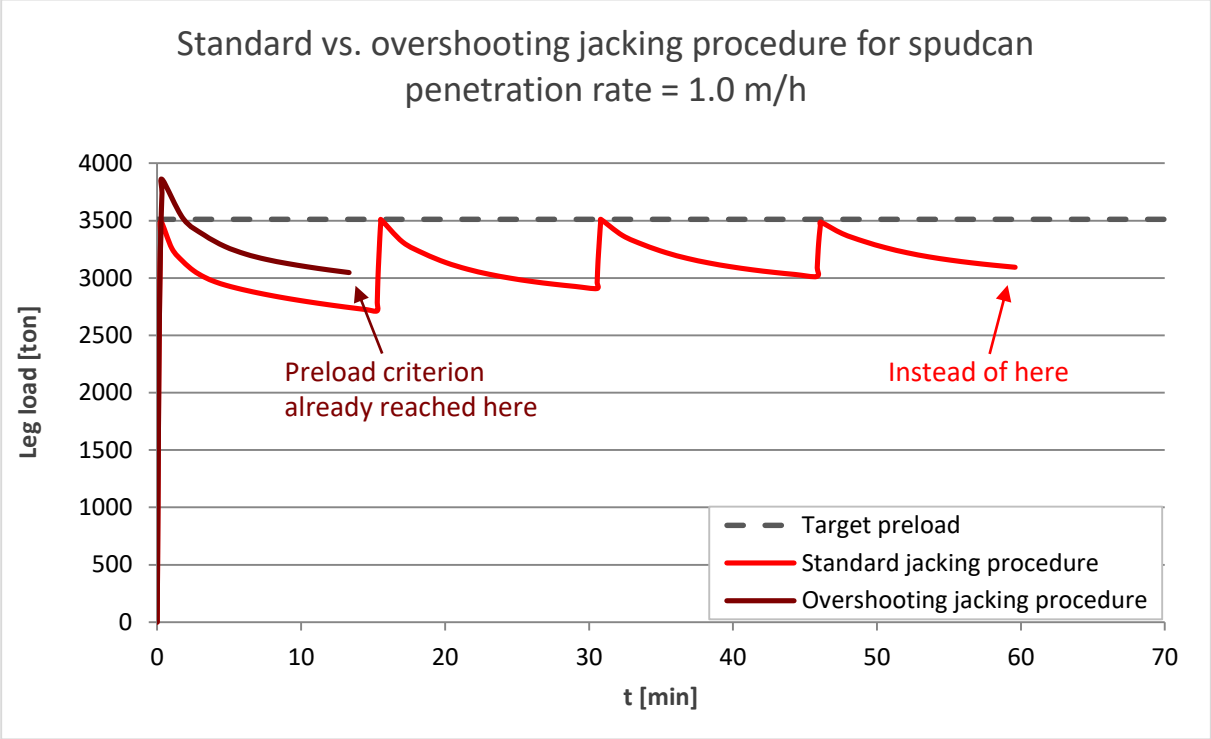

Figure 5.45 Standard vs. overshooting jacking procedure for spudcan penetration rate = 1.0 m/h.

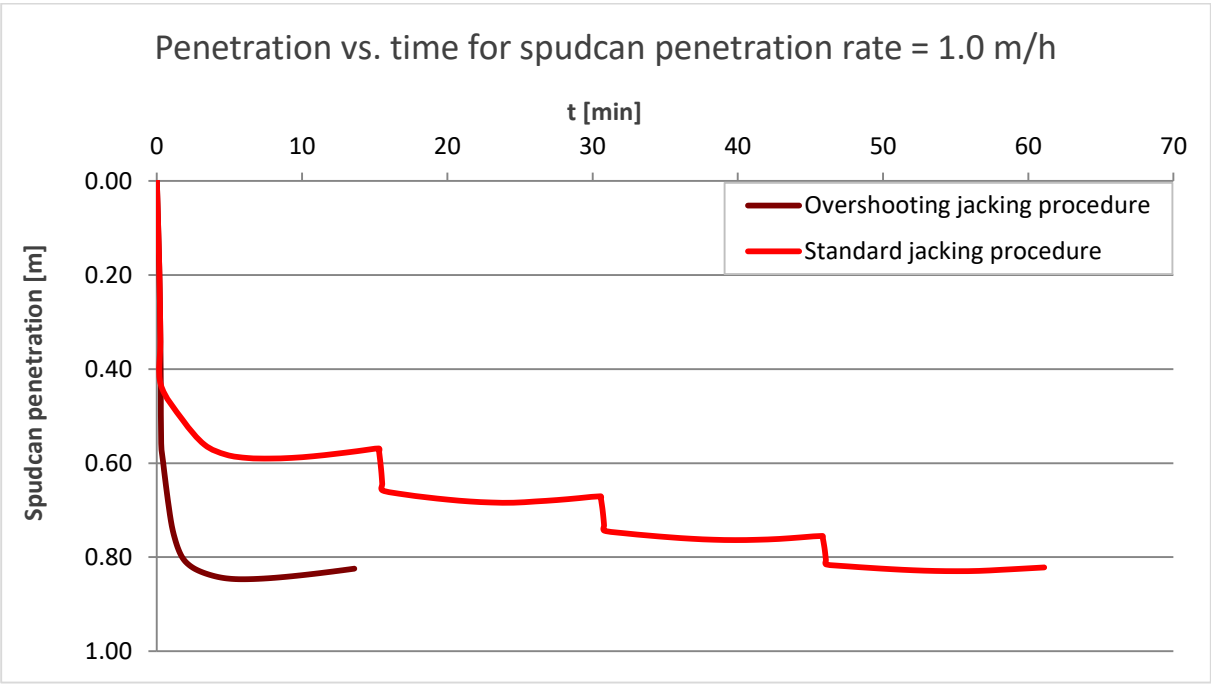

Figure 5.46. Spudcan penetration vs. time for both jacking procedures.

However, for the slower loading rate (0.10 m/h), different results are observed. As the spudcan penetrates with a slower rate, it takes a longer time before reaching the 10% overshot preload value. When holding the preload afterwards, the leg load reduces and intersects the target preload value after a certain time. From this point onwards, 15 minutes is waited and observed that the reduction in leg load remains within the 400 ton criterion. This is clearly illustrated in figure 5.47. By using the overshooting method with the slower spudcan penetration rate, it is seen that time saving are gained, but in a lesser degree compared to the faster spudcan penetration rate.

Considering the spudcan settlements for the slower loading rate in figure 5.48, the overshooting strategy would only lead to more settlements, as the spudcan is brought to a larger depth due to the additional load. In the standard jacking procedure, only two cycles are needed to reach the preload criterion, which makes the creep-like additional penetrations during these cycles relatively small. It can be concluded that for the slower loading rates, the overshooting method does contribute to time savings gained, yet it would lead to larger spudcan penetrations.

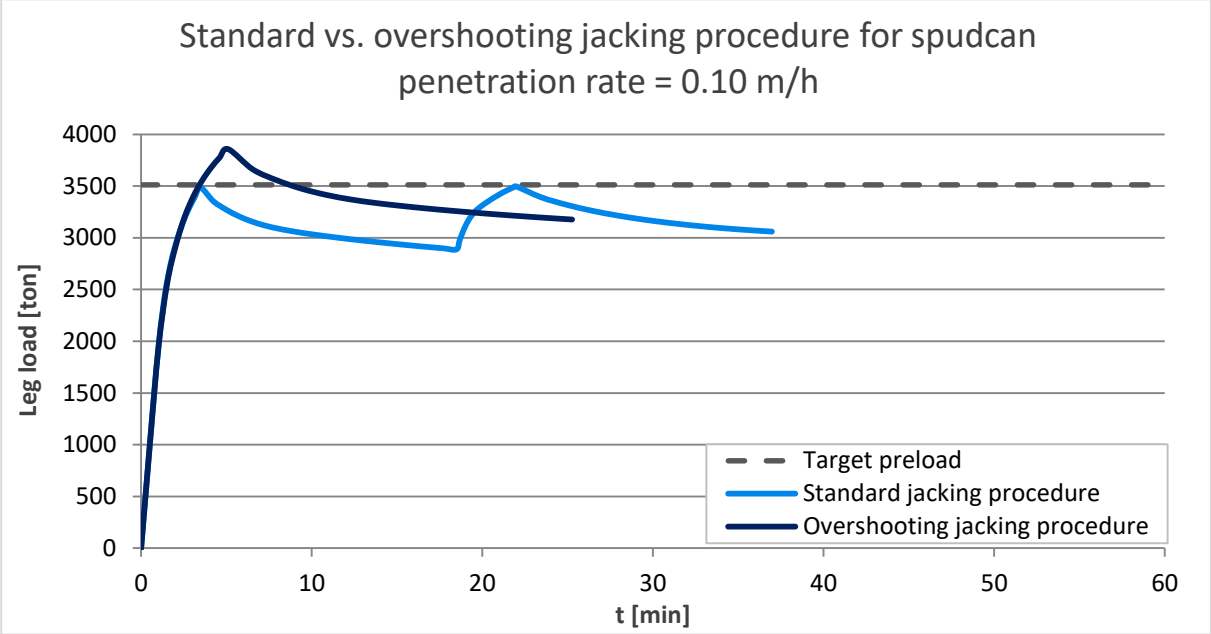

Figure 5.47 Standard vs. overshooting jacking procedure for spudcan penetration rate = 0.10 m/h

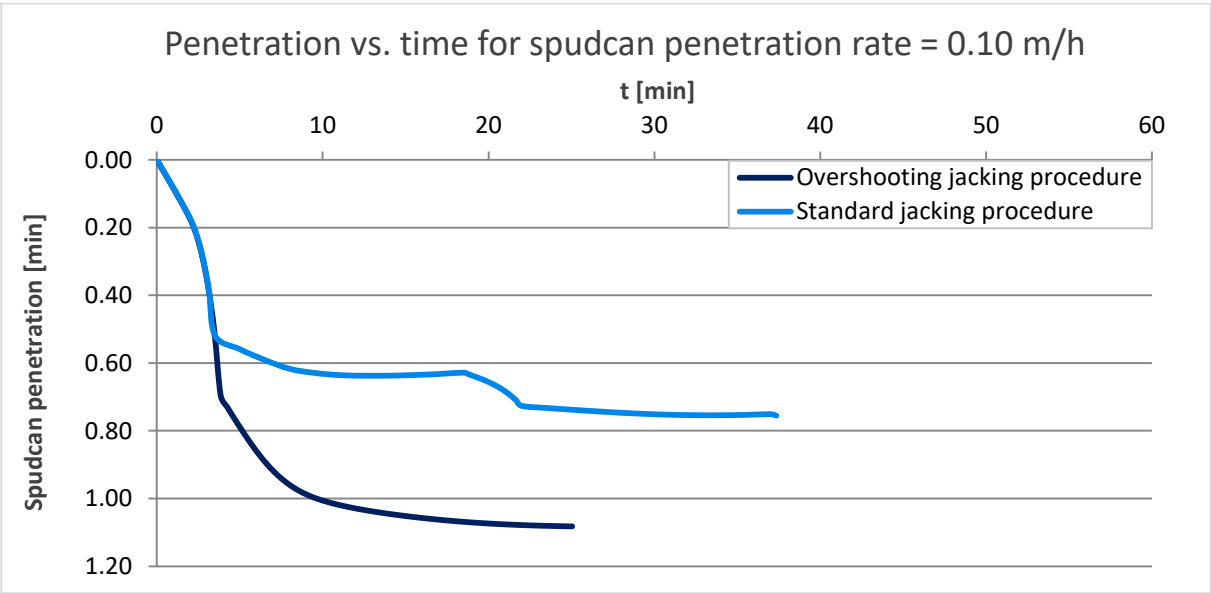

Figure 5.48 Spudcan penetration vs. time for both jacking procedures.

5.4.6 Conclusions

In this section, a PLAXIS model is constructed which is capable of modelling the viscous strain rate effects occurring during spudcan penetration in soft soils. This model can be seen as an extension of the current guidelines on spudcan penetration in cohesive soils, as numerical modelling is used to obtain a better understanding of the viscous increase in soil strength for different spudcan penetration rates. The following conclusions can be given:

- The Modified Cam-Clay model is a rate-independent (inviscid) material model, which does not account for viscous effects. Therefore, this material model cannot be used to model strain rate effects in soft soils. A different material model needs to be selected.
- The PLAXIS Soft Soil Creep model is a material model that does account for viscous effects, i.e. creep and stress relaxation. In this model, the irreversible strains are formulated by means of viscoplasticity rather than plasticity theory. The main difference between rate-independent plastic and viscoplastic material models is that the latter exhibit not only permanent deformations after the application of loads but continue to undergo a creep flow as a function of time under the influence of the applied load. The difference is clearly seen in figure 5.49. In the rate-sensitive SSC model, the faster the rate of shearing, the higher will be the soil resistance. In the rate-insenstive MCC model, the rate of shearing does not affect the soil resistance.
- The time-dependent viscoplastic FE modelling results are found to be compatible with the empirical relation for rate-dependent soil resistance as function of strain rate, as defined by Hossain and Randolph (2009a).

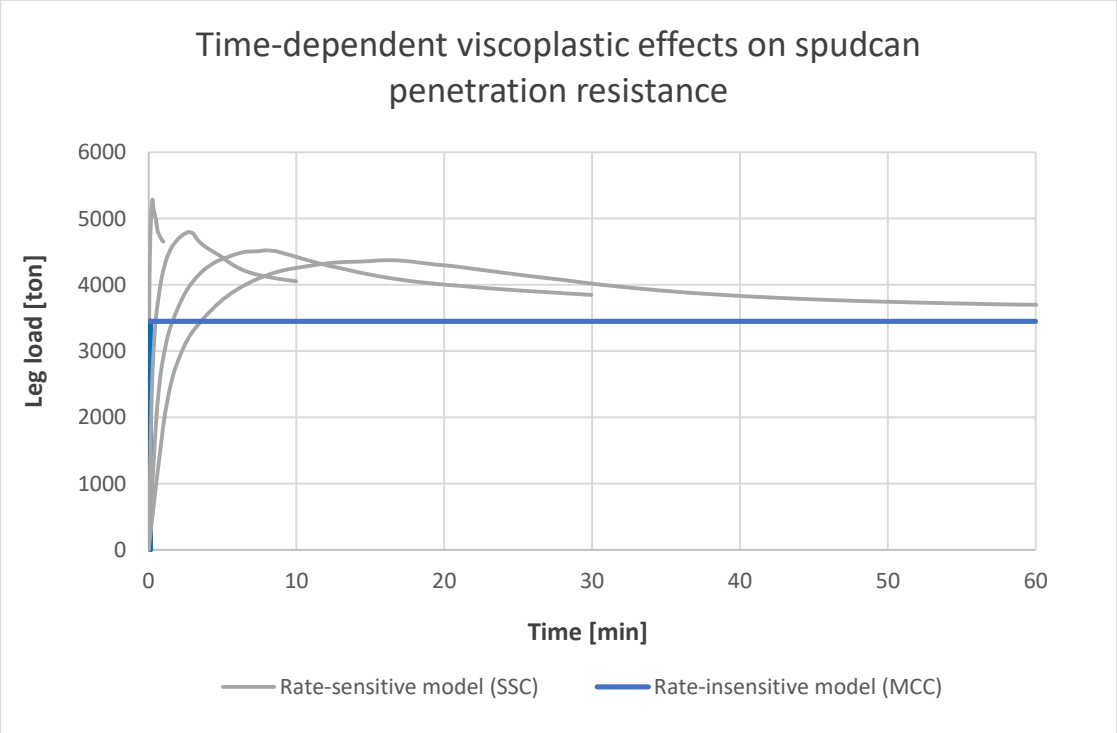

Figure 5.49 Comparison of rate-insenstive and rate-senstive model.

Based on the mechanism of strain rate dependent soil strength, both the standard and alternative overshooting jacking procedure is assessed numerically. Important conclusions are:

- When using the standard jacking procedure:
    - a slower spudcan penetration rate is beneficial, as less preload-hold cycles are required to reach the preload criterion of 400 ton load reduction in 15 minutes. This results in significant time savings in preloading durations.
    - the total settlements are not significantly affected by the spudcan penetration rate (more or less the same). It is just a matter of how to distribute the settlements over time.

- When using the overshooting jacking procedure:
    - the higher the spudcan penetration rate, the more beneficial this method becomes in terms of time savings, as the preload criterion is reached much quicker compared to the standard jacking procedure, as the number of required preload-hold cycles can be significantly reduced.
    - the slower spudcan penetration rate (here 0.10 m/h) leads to additional spudcan penetrations compared to the standard procedure. Retrieving the spudcan afterwards might become more difficult.

- Above conclusions are made based on the given soil properties and assumed spudcan penetration rates. It has to be noted that (slightly) different soil conditions may alter the soil behaviour and thus the effectiveness of both jacking procedures. For each set of soil conditions, it is recommended to perform this numerical assessment to be able to make a trade-off between spudcan penetration rate, time savings gained and (additional) spudcan penetrations when using both jacking procedures.

6. Conclusion and further research

6.1 Conclusion

This study is focussed on the investigation of spudcan penetration in cohesive soils. To assess the behaviour of cohesive soils during preloading, all relevant mechanisms that may contribute to the preload time were studied in more detail. Raw data is analysed to provide a proper soil characterisation, from which design parameters are derived. An axisymmetric finite element analysis in PLAXIS 2D is used to study the penetration of spudcan foundations subjected to vertical loading into cohesive soils. At first, the suitability of modelling a continuous spudcan penetration technique, called the Press Replace method (PR) is investigated by comparing its modelling achievements with a discontinuous Wished-in-Place method (WIP).

The Modified Cam-Clay soil constitutive model is used, because its modelling capabilities are based on the concept of critical state, rather than just a state of failure. In this way, both strain hardening and strain softening can be modelled, which represents both normally consolidated and overconsolidated clays. Both the PR and WIP model show similar results in terms of leg penetration predictions and the generations of excess pore water pressures below the spudcan footing. However, the PR method is found to be unstable during the geometry update phase. The change of penetrated soil material properties into spudcan material properties in the global stiffness matrix does not produce neat and reliable results. Yet, since the computational results are found to be similar, the relatively simple WIP method is used in all further spudcan penetration analyses.

Furthermore, the offshore industry has published guidelines for site specific assessment of mobile jack-up units. However, the conventional procedures to describe the geotechnical performance of spudcan penetration problems are inadequate in incorporating all relevant mechanism that contribute to the preload time in cohesive soils. The effect of consolidation on the soil strength and the viscous strain rate effects as a result of spudcan penetration are two important aspects which are poorly described. Using numerical modelling, a better understanding of these mechanisms is aimed for in order to evaluate spudcan bearing capacity in soft soils in a more detailed design. It can be concluded that consolidation effects are negligible during a relatively short installation duration of maximum 1 day.

On the other hand, viscous strain rate effects dominate as load application is fast during preloading and soil permeability is relatively low. The rate-effects of soil response are modelled by using the rate-sensitive Soft Soil Creep model. The faster the spudcan penetration rate, the higher will be the soil resistance observed. Note that these increases in soil resistances are only temporarily and diminish as the spudcan is stopped (no more strain rate present). The reduction in preload forces are then large and many preload-hold cycles are required to reach the preload criterion. Therefore, using the standard preload procedure, a slower penetration rate is beneficial, as the reduction in soil resistances are less and thus less cycles are required to reach the preload criterion. The total spudcan penetrations are unaffected by the spudcan penetration rate. The penetration rate just determines how these total penetrations are distributed over time.

Applying the alternative preloading strategy as proposed by Cathie et al. (2017), in which the target preload value is initially overshot by 10%, brings the spudcan to a depth, which would have been reached by the creep-like additional penetrations during multiple cycles, much quicker. The overshooting jacking procedure can be considered beneficial, as it reduces the required preloading time considerably for both the slow and the fast spudcan penetration rate. The benefits are highest for larger penetration rates. However, using this method, larger leg penetration predictions compared to the standard jacking procedure are observed for decreasing spudcan penetration rates. That is because in the standard jacking procedure, less creep-like additional penetrations are present when

using a slow spudcan penetration rate. The overshooting jacking procedure can thus be considered beneficial for relatively fast spudcan penetration rates, both in term of preloading duration and spudcan penetrations.

Note that the outcome of these preloading strategies might differ for slightly different soil conditions. For each given set of soil conditions, a correct trade-off should be made between the applied spudcan penetration rate, time savings gained and additional spudcan penetrations when using both jacking procedures.

Model limitations

An important model limitation of this study has to be taken into account when applying these modelling results into daily engineering practice. In the model of this thesis, the observed leg load is the effect of pure stress relaxation below the footing. In reality, the observed leg load during preloading comes from the combination of stress relaxation and the load transfer between the diagonally opposing leg pairs. Load redistribution from the active leg pair to the passive leg pair is a complex mechanism which cannot be modelled using a single spudcan in a 2-dimensional finite element domain. A complex 3D analysis would be required, in which all four spud legs are modelled simultaneously. For instance, the flexural rigidity of the vessel should be incorporated.

6.2 Recommendation for further research

There is still further optimisation possible when assessing spudcan penetration in cohesive soils. The following is recommended in further research:

- Investigate the problems arising by using the PR method.
    - Explore the numerical steps performed in the geometry update phase to make the model more stable.
    - Look into the interface elements more extensively to make the model more stable (interface elements and the relatively large deformations in clay does just not seem to go along properly).
- Realistic simulation of the whole spudcan penetration process should be investigated using large-deformation numerical analysis methods rather than small-deformation theory as done in this thesis. For instance, the large-deformation Material Point Method (MPM) can be used to simulate proper backflow mechanism, because in this method, material points can move through the mesh. However, MPM is not available yet in a user friendly software package.
- The given soil of this study is not a clean clay, but consists of a high degree of silt particles. Further site specific laboratory testing and FE modelling on other compositions of cohesive materials would be required to confirm the provisional conclusions reached in this study. For example, the following specific analyses could be considered:
    - Laboratory soil element testing (triaxial relaxation tests at high deviator stress) on representative clay samples.
    - Scale model testing of spudcan penetration in artificial or real clay specifically focussed on the active/passive character of loading of jack-up vessels.
    - Expanding the numerical model towards a full 3D analysis.
- Furthermore, the requirement to keep the preload on the spudcan for a specified time period (e.g. 15 minutes) without additional penetration could be re-evaluated in spudcan guidelines for spudcan penetration in cohesive soils. A systematic review of the dependency of the relaxation rates on the clay properties could provide a basis for establishing a suitable preload criterion for allowable rate of additional penetration or load relaxation of a specific holding period.

References

Akai, K., Yantamoto, J.-i. and Ozawa, Y. (1962) 'On behaviours of the pore pressure in saturated clays during shear', *Transactions of the Japan Society of Civil Engineers,* 1962(85), pp. 1-7.

Andersen, K. H., Andresen, L., Jostad, H. P. and Clukey, E. C. 'Effect of skirt-tip geometry on set-up outside suction anchors in soft clay.'. *Proceedings of the 23rd International Conference on Offshore Mechanics and Arctic Engineering, ASME: 2004 p. 1035-44.*, 20-25.

Atkinson, J. (2007) *The mechanics of soils and foundations.* CRC Press.

Augustesen, A., Liingaard, M. and Lade, P. V. (2004) 'Evaluation of time-dependent behavior of soils', *International Journal of Geomechanics,* 4(3), pp. 137-156.

Berre, T. and Bjerrum, L. (1973) 'Shear strength of normally consolidated clays', *ICSMFE,* vol. 1-1, pp. 39-49.

Bienen, B. and Cassidy, M. J. (2013) 'Set up and resulting punch-through risk of jack-up spudcans during installation', *Journal of Geotechnical and Geoenvironmental Engineering,* 139(12), pp. 2048-2059.

Bjerrum, L. (1967) 'Engineering geology of Norwegian normally-consolidated marine clays as related to settlements of buildings', *Geotechnique,* 17(2), pp. 83-118.

Bowles, J. E. (1988) *Foundation analysis and design.* 4th ed. edn. New York :: McGraw-Hill, p. xix, 1004 p. : ill. ; 25 cm.

Brennan, R., Diana, H., Stonor, R., Hoyle, M., Cheng, C.-P. and Roper, R. 'Installing jackups in punch-through-sensitive clays'. *Offshore Technology Conference*: Offshore Technology Conference.

Brinkgreve et al. (2017) 'PLAXIS 2D Reference Manual', *Delft University of Technology & PLAXIS BV*.

Brinkgreve, R. and Vermeer, P. (1998) 'Plaxis finite element code for soil and rock analysis-Version 7', *Plaxis BV, The Netherlands*.

Brinkgreve, R. and Vermeer, P. (2016) 'PLAXIS Material Model Manual', *Delft University of Technology & PLAXIS BV*.

Brinkgreve, R. B. J. and Post, M. (2013) 'On the use of finite element models for geotechnical design.', *Bernessen mit numerischen methoden Workshop (Veröffentlichungen des Institutes, 27)*, pp. 111-222.

British Standards Institute (2004) *British Standard EN ISO 14688-2, Geotechnical investigation and testing - identification and classification of soil, part 2: principles for a classification.*

Casagrande, A. (1932) 'Research on the Atterberg limits of soils', *Public roads,* 13(8), pp. 121-136.

Casagrande, A. and Fadum, R. E. (1940) 'Notes on soil testing for engineering purposes'.

Casagrande, A. and Wilson, S. (1951) 'Effect of rate of loading on the strength of clays and shales at constant water content', *Geotechnique,* 2(3), pp. 251-263.

Cathie, D. N., Versteele, H., Kuo, M. Y. K. and Raymackers, S. (2017) 'Planning the preloading procedure to account for rate-effects in clays'. *International Conference: The Jack-Up Platform*, London.

Cooke, R. and Price, G. 'Strains and displacements around friction piles'. Building Research Establishment, Department of the Environment.

Crawford, C. 'The influence of rate of strain on effective stresses in sensitive clay'. *Papers on Soils 1959 Meetings*: ASTM International.

Fugro (2013) *Offshore Wind Farm Geotechnical Site Investigation*.

Fugro Geoconsulting Ltd (2012-2014) *Part B (Geotechnical data), geotechnical site investigation at windfarm site, Main array, Irish Sea,* Report no J11186-3, Rev 3).

Geotechnical Interpretative Report (2015) *Geotechnical Interpretative Report at offshore wind farm location in Irish Sea*.

Hansen, J. B. (1970) 'A revised and extended formula for bearing capacity'.

Hill, R. (1950) 'The Mathematical Theory of Plasticity', *Oxford*.

Holt, J. 'The soils of Hong Kong's coastal waters'. *Proc Symp Hong Kong Soils*, 33-51.

Hossain, M., Randolph, M., Hu, Y. and White, D. 'Cavity stability and bearing capacity of spudcan foundations on clay.'. *Offshore Technology Conference*: Offshore Technology Conference.

Hossain, M. S. and Randolph, M. F. (2009a) 'Effect of strain rate and strain softening on the penetration resistance of spudcan foundations on clay', *International Journal of Geomechanics,* 9(3), pp. 122-132.

Hossain, M. S. and Randolph, M. F. (2009b) 'New Mechanism-Based Design Approach for Spudcan Foundations on Single Layer Clay', *Journal of Geotechnical and Geoenvironmental Engineering*, 135(9), pp. 1264-1274. WorldCat.org.

Houlsby, G. and Martin, C. (2003) 'Undrained bearing capacity factors for conical footings on clay', *Géotechnique,* 53(5), pp. 513-520.

InSafeJIP (2011) 'Improved Guidelines for the Prediction of Geotechnical Performance of Spudcan Foundations during Installation and Removal of Jack-up Units'.

ISO19905-1 (2012) 'International Standard Organisation', *Petroleum and natural gas industries -- Site-specific assessment of mobile offshore units -- Part 1: Jack-ups*.

Jamiolkowski, M., Ladd, C. C., Germaine, J. T. and Lancelotta, R. 'New Development in Field and Lab Testing of Soils'. *Proceedings, 11th International Conference on Soil Mechanics and Foundation Engineering*, 57-153.

Kimura, T. and Saitoh, K. (1983) 'The influence of strain rate on pore pressures in consolidated undrained triaxial tests on cohesive soils', *Soils and Foundations,* 23(1), pp. 80-90.

Koppula, S. (1981) 'Statistical estimation of compression index'.

Ladd, C. C. and Foott, R. 'New design procedure for stability of soft clays: 10F, 3T, 39R. J. GEOTECH. ENGNG. DIV. V100, N. GT7, JULY, 1974, P763–786'. *International Journal of Rock Mechanics and Mining Sciences & Geomechanics Abstracts*: Pergamon, A220.

Lee, K. K. (2009) 'Investigation of Potential Spudcan Punch-Through Failure on Sand Overlying Clay Soils', *The University of Western Australia*

Lehane, B., O'loughlin, C., Gaudin, C. and Randolph, M. (2009) 'Rate effects on penetrometer resistance in kaolin', *Géotechnique,* 59(1), pp. 41-52.

Lunne, T., Robertson, P. and Powell, J. (1997) 'Cone penetration testing', *Geotechnical Practice*.

Meyerhof, G. (1951) 'The ultimate bearing capacity of foundations', *Geotechnique,* 2(4), pp. 301-332.

Meyerhof, G. G. (1963) 'Some recent research on the bearing capacity of foundations', *Canadian Geotechnical Journal,* 1(1), pp. 16-26.

Mott, P. and Roland, C. (2009) 'Limits to Poisson's ratio in isotropic materials', *Physical review B,* 80(13), pp. 132104.

Prandtl, L. (1921) 'Hauptaufsätze: Über die eindringungsfestigkeit (härte) plastischer baustoffe und die festigkeit von schneiden', *ZAMM-Journal of Applied Mathematics and Mechanics/Zeitschrift für Angewandte Mathematik und Mechanik,* 1(1), pp. 15-20.

Randolph, M. and Gourvenec, S. (2011) *Offshore geotechnical engineering.* CRC Press.

Richardson, A. M. and Whitman, R. V. (1963) 'Effect of strain-rate upon undrained shear resistance of a saturated remoulded fat clay', *Geotechnique,* 13(4), pp. 310-324.

Robertson, P. (1990) 'Soil classification using the cone penetration test', *Canadian Geotechnical Journal,* 27(1), pp. 151-158.

Robertson, P. K., Campanella, R., Gillespie, D. and Greig, J. 'Use of piezometer cone data'. *Use of in situ tests in geotechnical engineering*: ASCE, 1263-1280.

Roscoe, K. H. and Burland, J. (1968) 'On the generalized stress-strain behaviour of wet clay'.

Roscoe, K. H., Schofield, A. and Wroth, C. (1958) 'On the yielding of soils', *Geotechnique,* 8(1), pp. 22-53.

Skempton, A. (1951) 'The bearing capacity of clays'.

Skempton, A. and Bishop, A. 1954. Soils. Chapter 10 of Building Materials, their Elasticity and Inelasticity.: North-Holland Publ. Co.

SNAME (2008) *Guideline For Site Specific Assessment of Mobile Jack-Up Units*: The Society of Naval Architects and Marine Engineers.

Stolle, D., Bonnier, P. and Vermeer, P. (1997) 'A soft soil model and experiences with two integration schemes', *Numerical Models in Geomechanics,* 1(12), pp. 123-128.
Taylor, D. (1948) *Fundamentals of soil mechanics.* Chapman And Hall, Limited.; New York.
Teh, K. L. (2007) *Punch-through of spudcan foundation in sand overlying clay.* National University of Singapore.
Tehrani, F. S., Nguyen, P., Brinkgreve, R. B. J. and van Tol, A. F. (2016) 'Comparison of Press-Replace Method and Material Point Method for analysis of jacked piles', *Computers and Geotechnics,* 78, pp. 38-53.
Terzaghi (1943) 'Theoretical soil mechanics'.
Terzaghi, K., Peck, R. B. and Mesri, G. (1996) *Soil mechanics in engineering practice.* John Wiley & Sons.
UK Government (2017) *UK Renewable Energy Roadmap 2017.* Department of Energy & Climate Change.
Van Langen, H. and Vermeer, P. (1991) 'Interface elements for singular plasticity points', *International journal for numerical and analytical methods in geomechanics,* 15(5), pp. 301-315.
Van Oord (2017) 'Equipment specifications Offshore Installation Vessel Aeolus'.
Vermeer, P. and Neher, H. (1999) 'A soft soil model that accounts for creep', *Proceedings of the international symposium "Beyond 2000 in Computational Geotechnics*, pp. 249-261.
Vesic, A. S. (1975) 'Bearing capacity of shallow foundations', *Foundation Engineering Handbook.*, pp. 121-147.
Waltham, T. (2009) *Foundations of engineering geology.* CRC Press.
Wesley, L. (1977) 'Shear strength properties of halloysite and allophane clays in Java, Indonesia', *Geotechnique,* 27(2), pp. 125-136.
Wood, D. M. (1990) *Soil behaviour and critical state soil mechanics.* Cambridge university press.
Yi, J. T., Lee, F. H., Goh, S. H., Zhang, X. Y. and Wu, J.-F. (2012) 'Eulerian finite element analysis of excess pore pressure generated by spudcan installation into soft clay', *Computers and Geotechnics,* 42, pp. 157-170.
Zeevaert, L. (1948) 'Discussion on effect of driving piles into soft clay', *ASCE,* 115, pp. 286-292.

Appendix

A. The general bearing capacity equation

The bearing capacity equation developed by Terzaghi (1943) for a strip footing under general shear failure has been modified by Meyerhof (1963) to take into account other types of foundations such as square, circular and rectangular footings by introducing shape factors. The general form of the bearing capacity equation (A.2) suggested by Meyerhof (1951) is given as:

Terzaghi (1943) $$q_u = cN_c + q'N_q + \frac{1}{2}\gamma B N_\gamma$$ *Eq. (A.1)*

Meyerhof (1963) $$q_u = c \cdot s_c \cdot d_c \cdot i_c \cdot N_c + q' \cdot s_q \cdot d_q \cdot i_q \cdot N_q + \frac{1}{2} \cdot \gamma' \cdot B \cdot s_\gamma \cdot d_\gamma \cdot i_\gamma \cdot N_\gamma$$ *Eq. (A.2)*

In which

$c = cohesion$
$q' = effective\ overburden\ pressure$
$\gamma' = effective\ unit\ weight\ of\ soil$
$B = width\ of\ foundation$
$N_c, N_q, N_\gamma = bearing\ capacity\ factors$
$s_c, s_q, s_\gamma = shape\ factors$
$d_c, d_q, d_\gamma = depth\ factors$
$i_c, i_q, i_\gamma = load\ inclination\ factors$

Hansen (1970) extended the work of Meyerhof (1963) by including two additional factors to take care of base tilt and foundations on slopes. Vesic (1975) used the same form of equation suggested by Hansen (1970). All three investigators use the equations as originally proposed by Prandtl (1921) for computing the values of N_c and N_q. However, the equations used by them for computing the values of N_γ are different. The bearing capacity factors N_c, N_q and N_γ are given in table A.1. Equations for shape, depth and inclination factors are given in table A.2.

Table A.1 The values of Nc, Nq, and Meyerhof (M), Hansen (H) and Vesic (V) Nγ factors

ϕ	N_c	N_q	N_γ (H)	N_γ (M)	N_γ (V)
0	5.14	1.0	0.0	0.0	0.0
5	6.49	1.6	0.1	0.1	0.4
10	8.34	2.5	0.4	0.4	1.2
15	10.97	3.9	1.2	1.1	2.6
20	14.83	6.4	2.9	2.9	5.4
25	20.71	10.7	6.8	6.8	10.9
26	22.25	11.8	7.9	8.0	12.5
28	25.79	14.7	10.9	11.2	16.7
30	30.13	18.4	15.1	15.7	22.4
32	35.47	23.2	20.8	22.0	30.2
34	42.14	29.4	28.7	31.1	41.0
36	50.55	37.7	40.0	44.4	56.2
38	61.31	48.9	56.1	64.0	77.9
40	72.25	64.1	79.4	93.6	109.4
45	133.73	134.7	200.5	262.3	271.3
50	266.50	318.50	567.4	871.7	762.84

Note: N_c and N_q are the same for all the three methods. Subscripts identify the author for N_γ.

Table A.2 Shape, depth and load inclination factors of Meyerhof, Hansen and Velsic

Factors	Meyerhof	Hansen	Vesic
s_c	$1+0.2N_\phi \frac{B}{L}$	$1+\frac{N_q}{N_c}\frac{B}{L}$	
s_q	$1+0.1N_\phi \frac{B}{L}$ for $\phi>10°$	$1+\frac{B}{L}\tan\phi$	
s_γ	$s_\gamma = s_q$ for $\phi>10°$ $s_\gamma = s_q = 1$ for $\phi=0$	$1-0.4\frac{B}{L}$	The shape and depth factors of Vesic are the same as those of Hansen.
d_c	$1+0.2\sqrt{N_\phi}\frac{D_f}{B}$	$1+0.4\frac{D_f}{B}$	
d_q	$1+0.1\sqrt{N_\phi}\frac{D_f}{B}$ for $\phi>10°$	$1+2\tan\phi(1-\sin\phi)^2\frac{D_f}{B}$	
d_γ	$d_\gamma = d_q$ for $\phi>10°$ $d_\gamma = d_q = 1$ for $\phi=0$	1 for all ϕ Note; Vesic's s and d factors = Hansen's s and d factors	
i_c	$1-\frac{\alpha°}{90}^2$ for any ϕ	$i_q-\frac{1-i_q}{N_q-1}$ for $\phi>0$	Same as Hansen for $\phi>0$
		$0.5\left(1-\frac{Q_h}{A_f c_a}\right)^{\frac{1}{2}}$ for $\phi=0$	$1-\frac{mQ_h}{A_f c_a N_c}$
i_q	$i_q = i_c$ for any ϕ	$\left(1-\frac{0.5Q_h}{Q_u+A_f c_a\cot\phi}\right)^5$	$\left(1-\frac{Q_h}{Q_u+A_f c_a\cot\phi}\right)^m$
i_γ	$1-\frac{\alpha°}{\phi°}^2$ for $\phi>0$ $i_\gamma=0$ for $\phi=0$	$\left(1-\frac{0.7Q_h}{Q_u+A_f c_a\cot\phi}\right)^5$	$\left(1-\frac{Q_h}{Q_u+A_f c_a\cot\phi}\right)^{m+1}$

$N_\gamma = (N_q-1)\tan(1.4\phi)$ (Meyerhof)

$N_\gamma = 1.5(N_q-1)\tan\phi$ (Hansen)

$N_\gamma = 2(N_q+1)\tan\phi$ (Vesic)

$N_q = e^{\pi\tan\phi}N_\phi$

$N_c = (N_q-1)\cot\phi$

B. Zone of influence around penetrating shaft

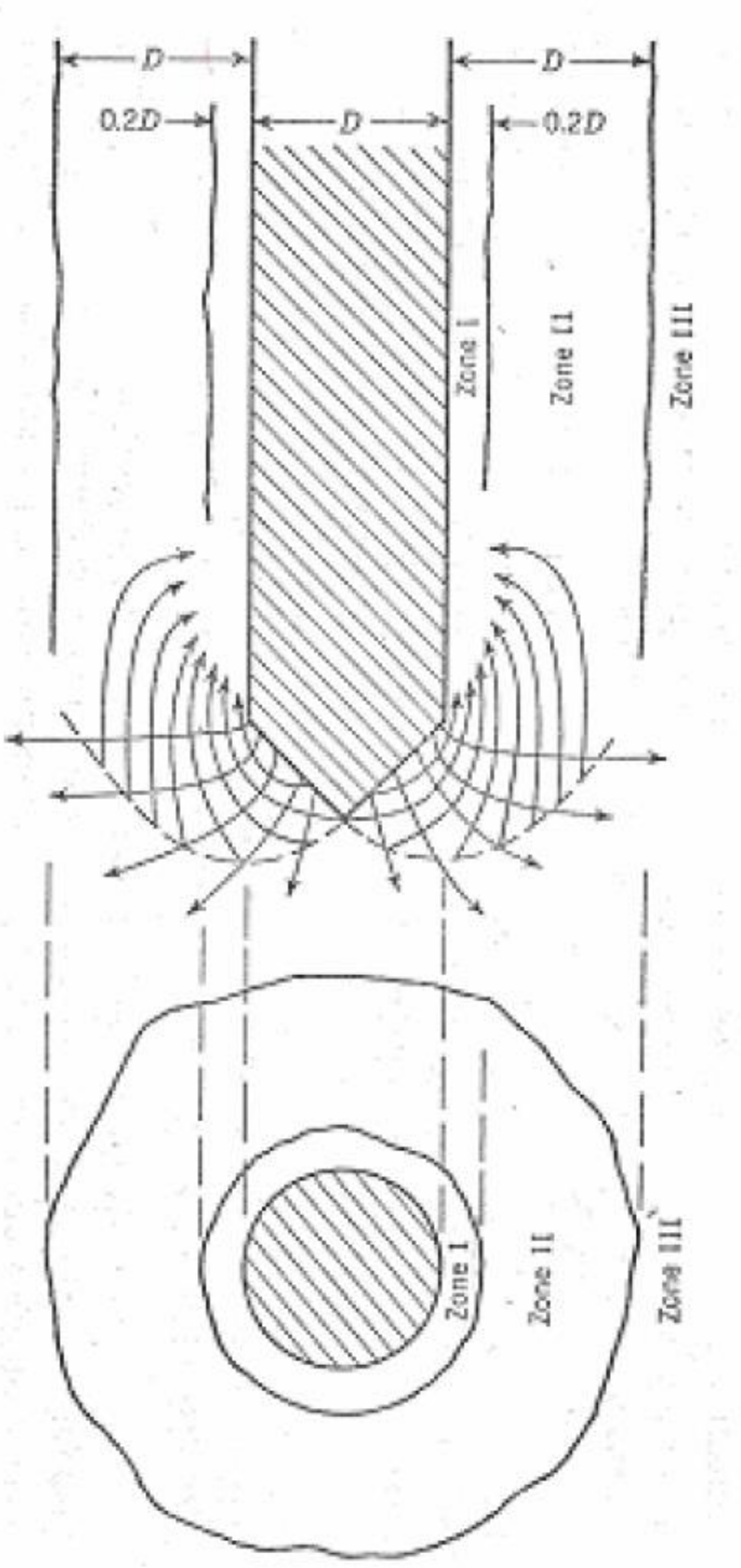

Figure B.1 Soil disturbance around penetrating shaft in soft clay (Zeevaert, 1948)

C. Geotechnical logs Offshore Wind Farm locations

A selection of some geotechnical logs from the offshore wind farm locations are presented below. The logs show CPT data, from which the soil stratification and characteristic values of soil parameters can be derived.

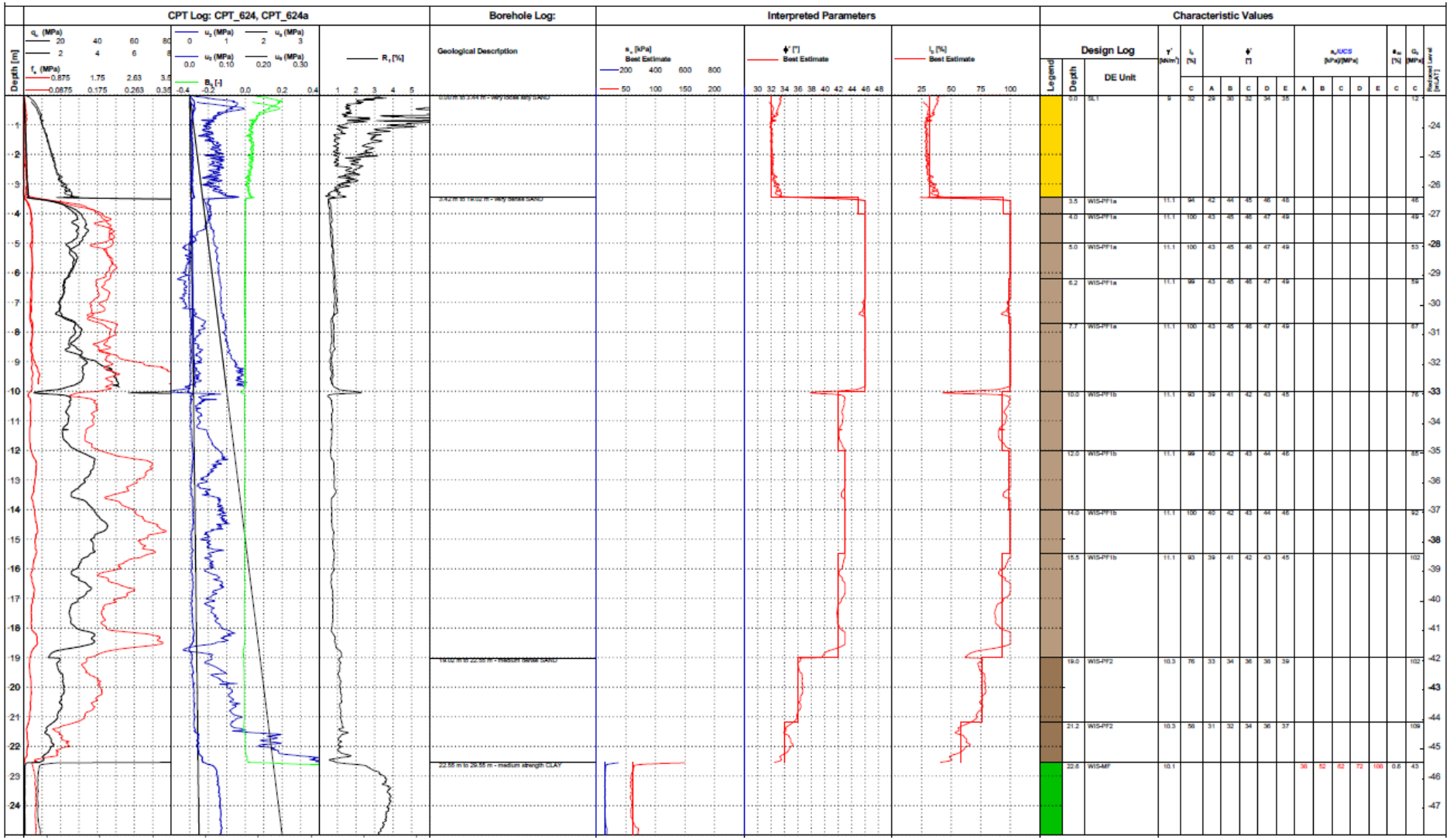
CPT Log: CPT_624, CPT_624a
Borehole Log:
Interpreted Parameters
Characteristic Values
Depth [m]
Geological Description
Design Log
Legend
Depth
DE Unit
0.0 SL1
3.5 WIS-PF1a
4.0 WIS-PF1a
5.0 WIS-PF1a
6.2 WIS-PF1a
7.7 WIS-PF1a
10.0 WIS-PF1b
12.0 WIS-PF1b
14.0 WIS-PF1b
15.5 WIS-PF1b
19.0 WIS-PF2
21.2 WIS-PF2
22.6 WIS-MF

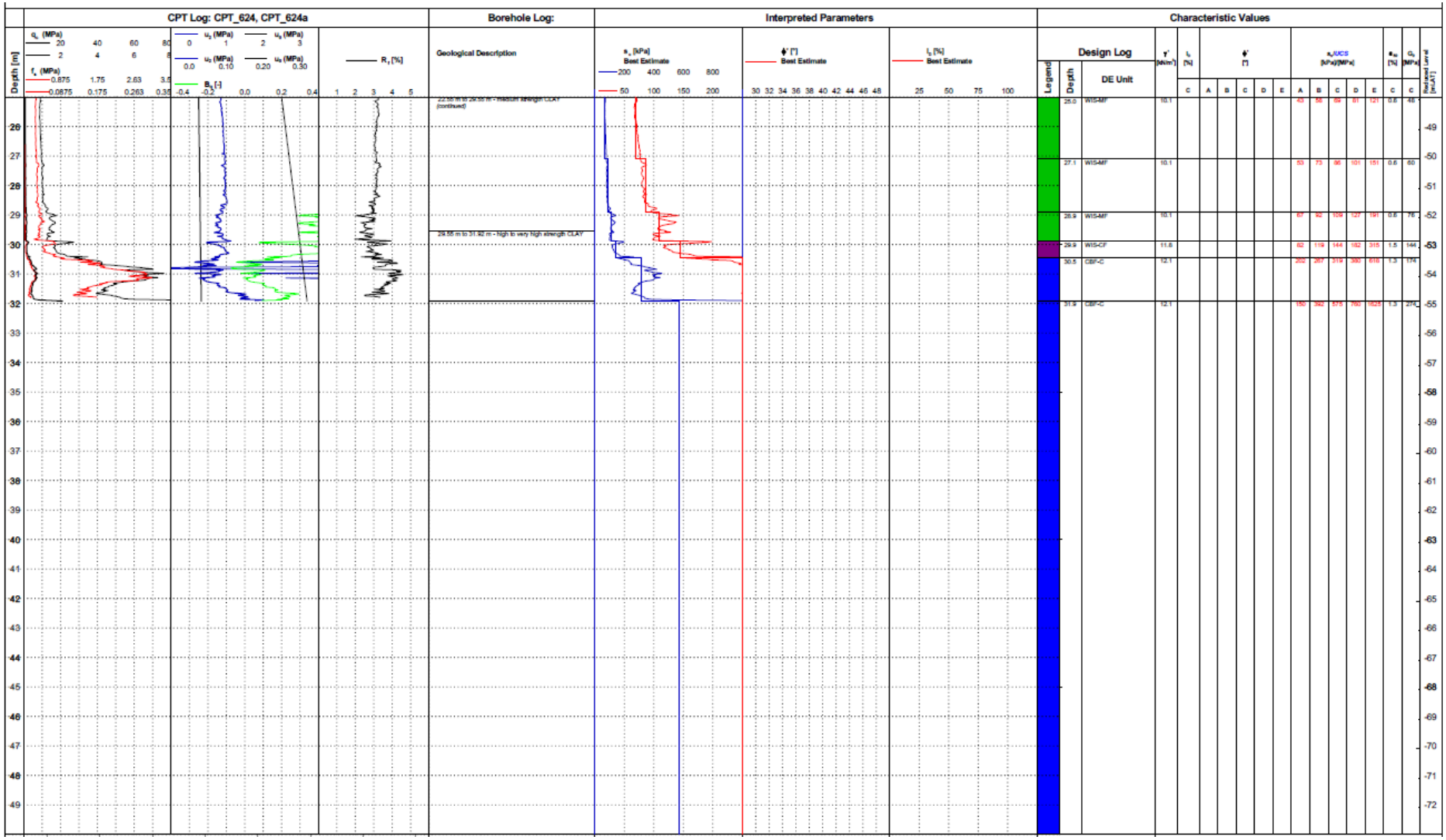

Figure C.1 Geotechnical log 1

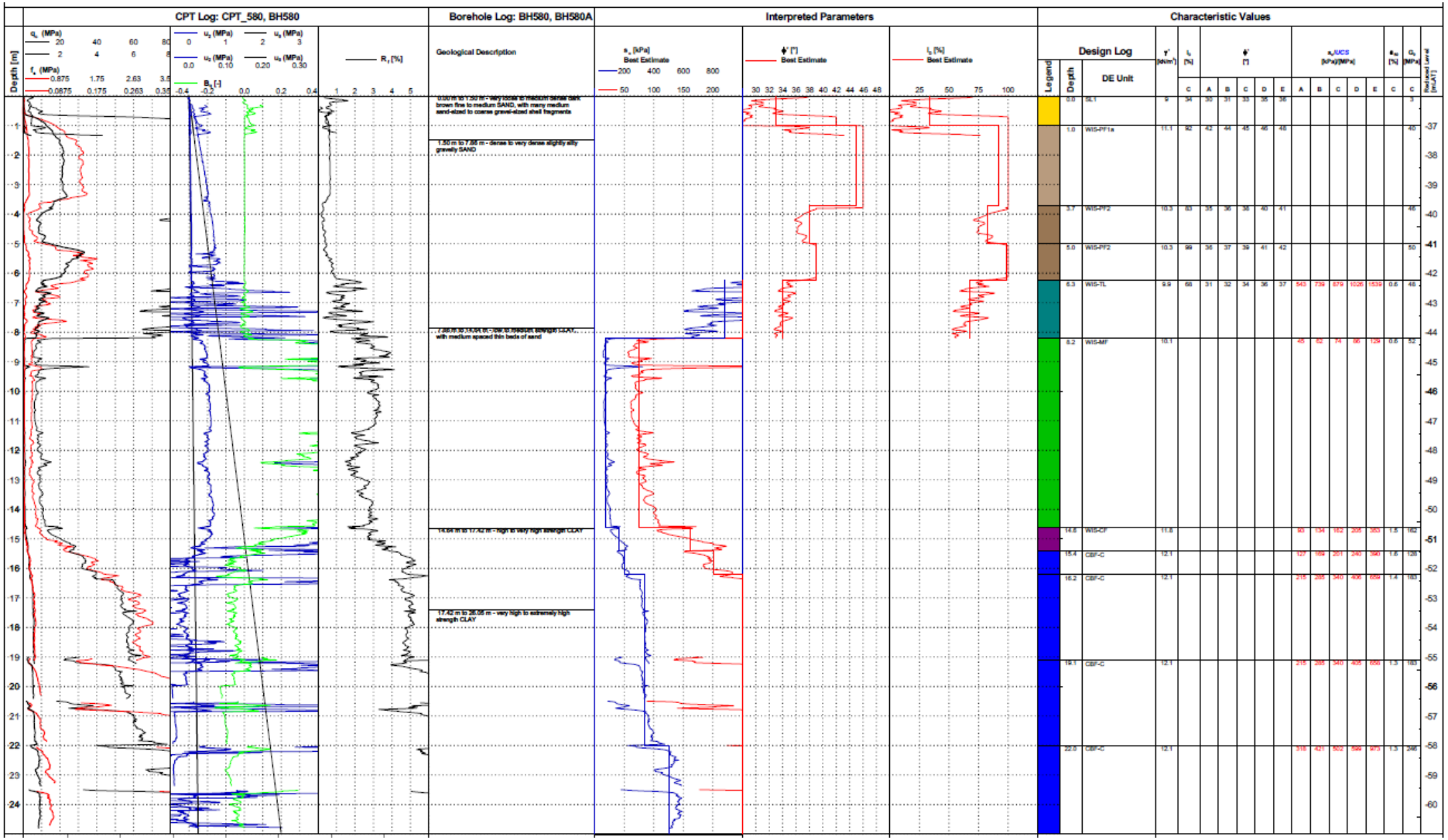
CPT Log: CPT_580, BH580
Borehole Log: BH580, BH580A
Interpreted Parameters
Characteristic Values
Design Log
Depth [m]
Geological Description
Legend
Depth
DE Unit
SL1
WIS-PF1a
WIS-PF2
WIS-TL
WIS-MF
WIS-CF
CBF-C

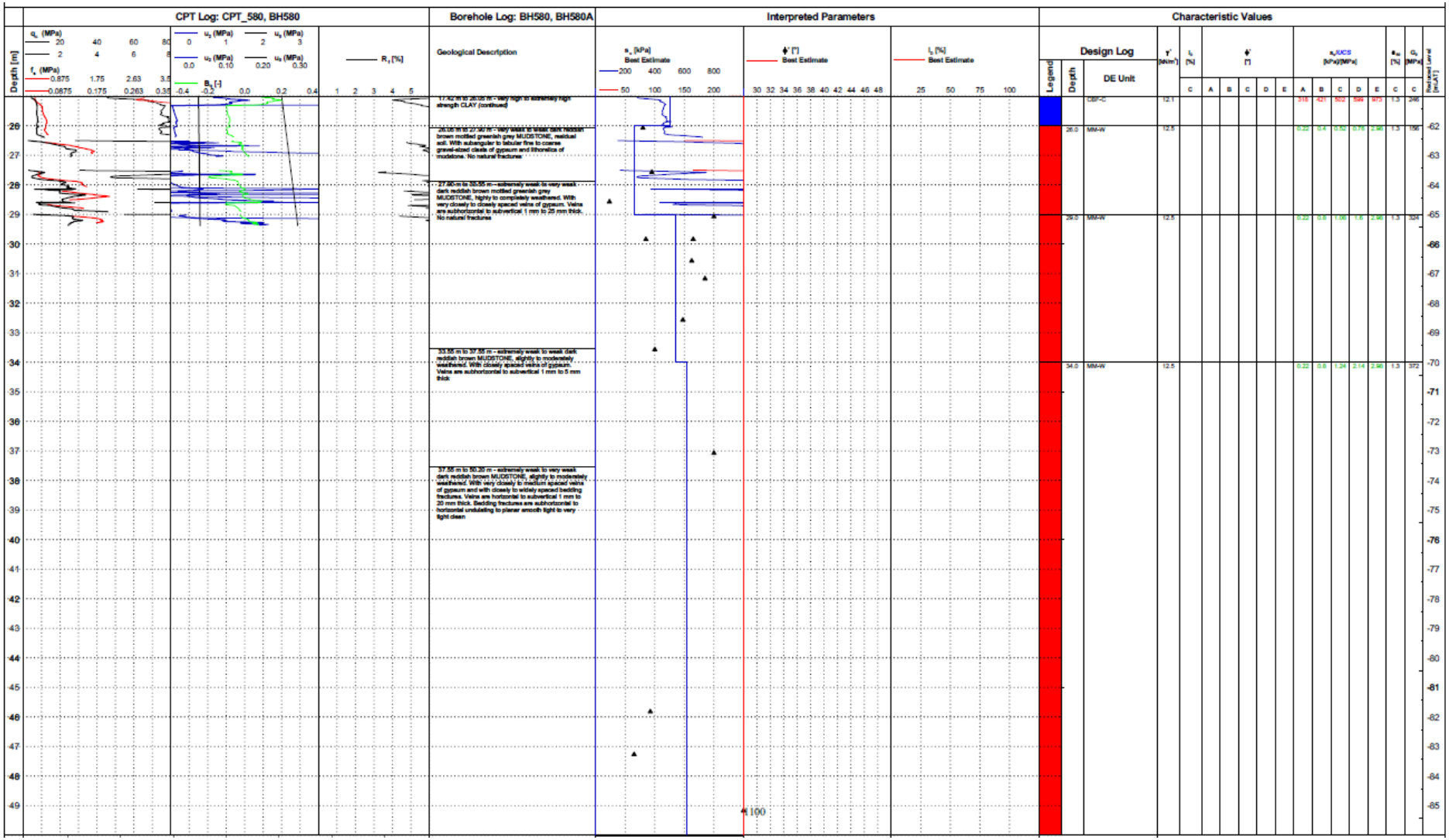

Figure C.2 Geotechnical log 2

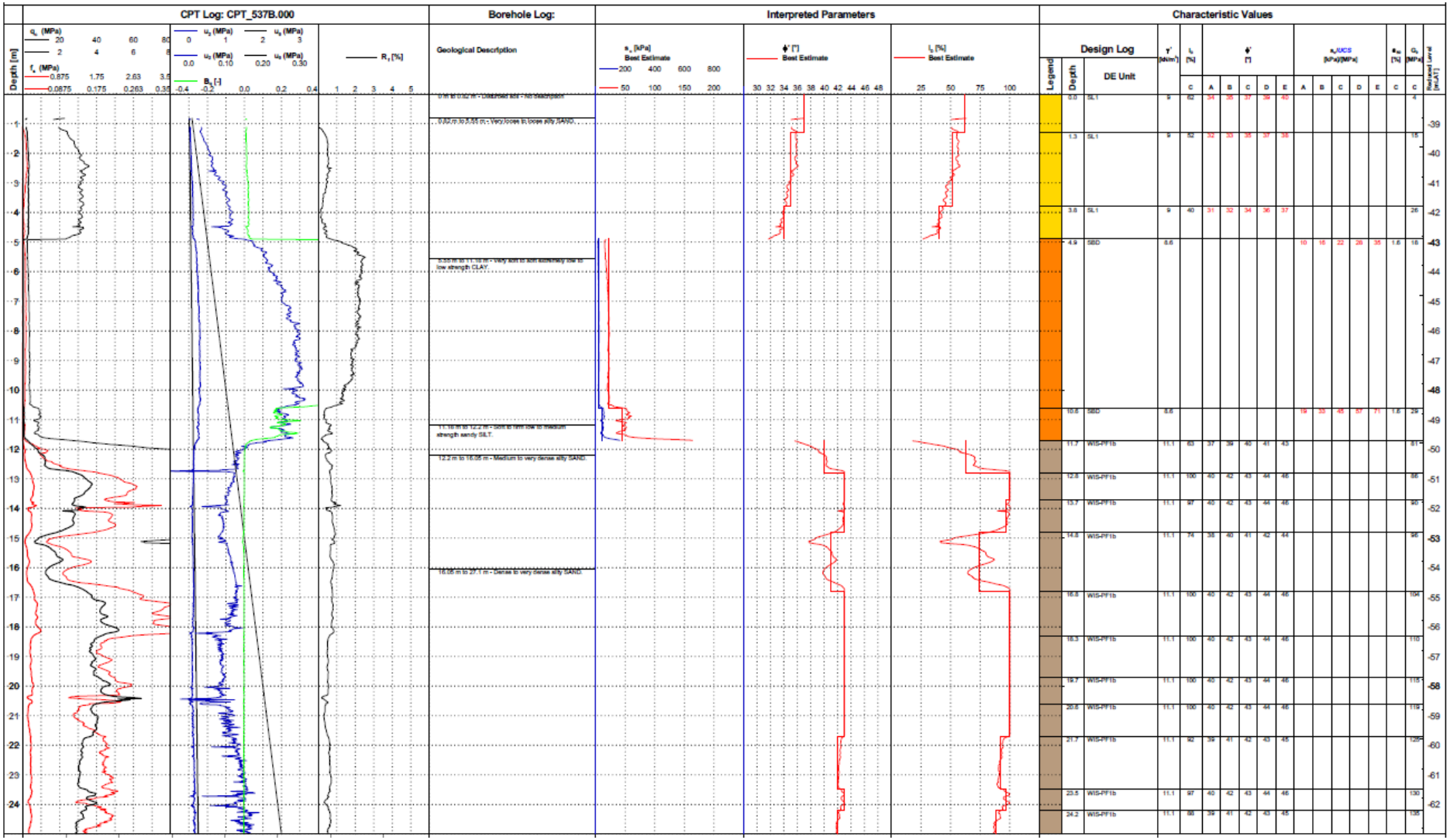
CPT Log: CPT_537B.000
Borehole Log:
Interpreted Parameters
Characteristic Values
Design Log
Depth [m]
Geological Description
Legend
Depth
DE Unit
0.0 SL1
1.3 SL1
3.8 SL1
4.9 SBD
10.8 SBD
11.7 WIS-PF1b
12.8 WIS-PF1b
13.7 WIS-PF1b
14.8 WIS-PF1b
16.8 WIS-PF1b
18.3 WIS-PF1b
19.7 WIS-PF1b
20.8 WIS-PF1b
21.7 WIS-PF1b
23.5 WIS-PF1b
24.2 WIS-PF1b

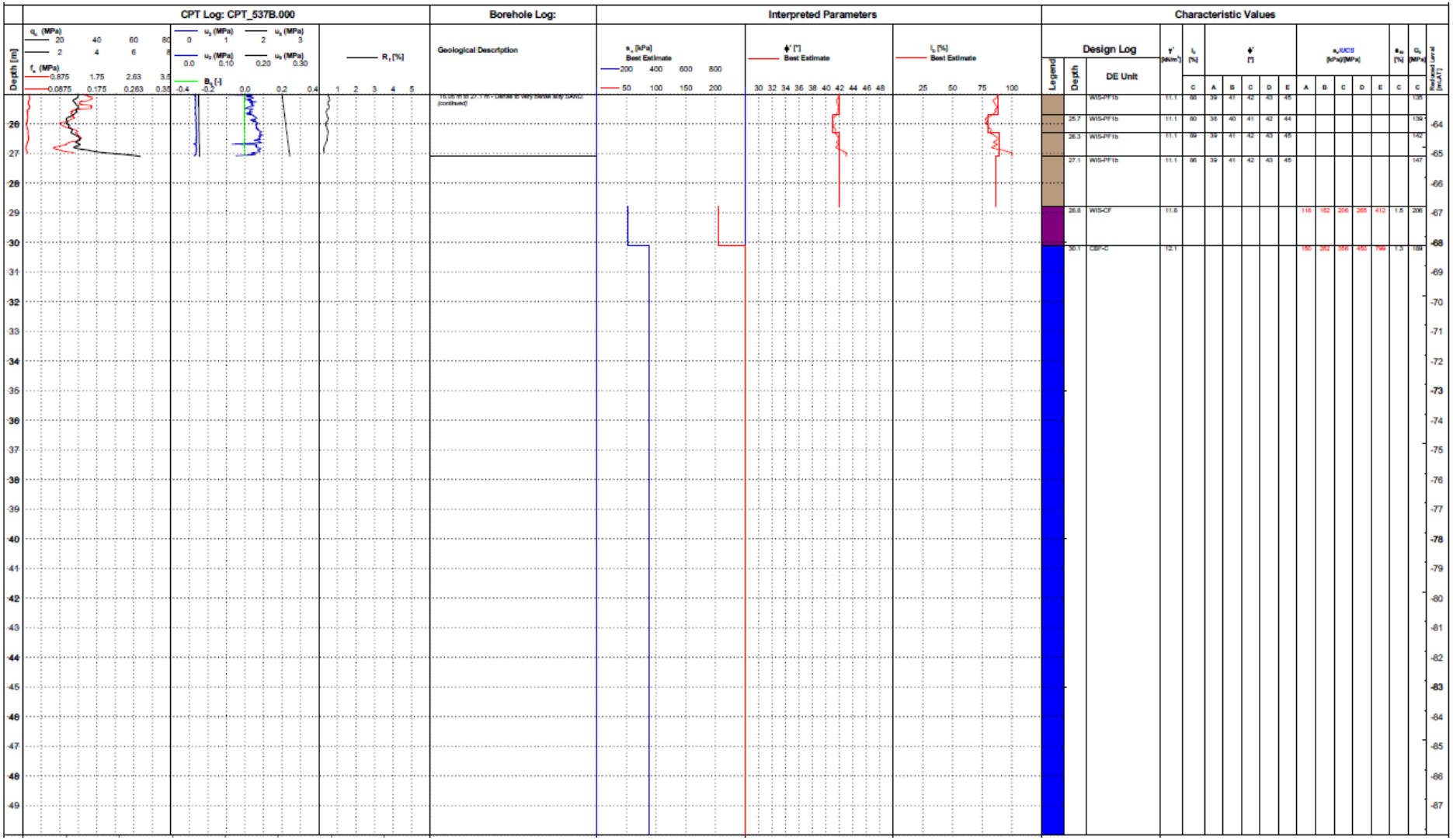

Figure C.3 Geotechnical log 3

D. Stiffness parameter estimates

Undisturbed incremental and continuous rate of strain oedometer tests were performed on clay specimens to determine the soil stiffness parameters. The stiffness parameters are represented by the compression (c_c) and swelling (c_s) indices and can be derived from the 1D compression test results in a semi-logarithmic stress - void ratio plot. An example is shown below.

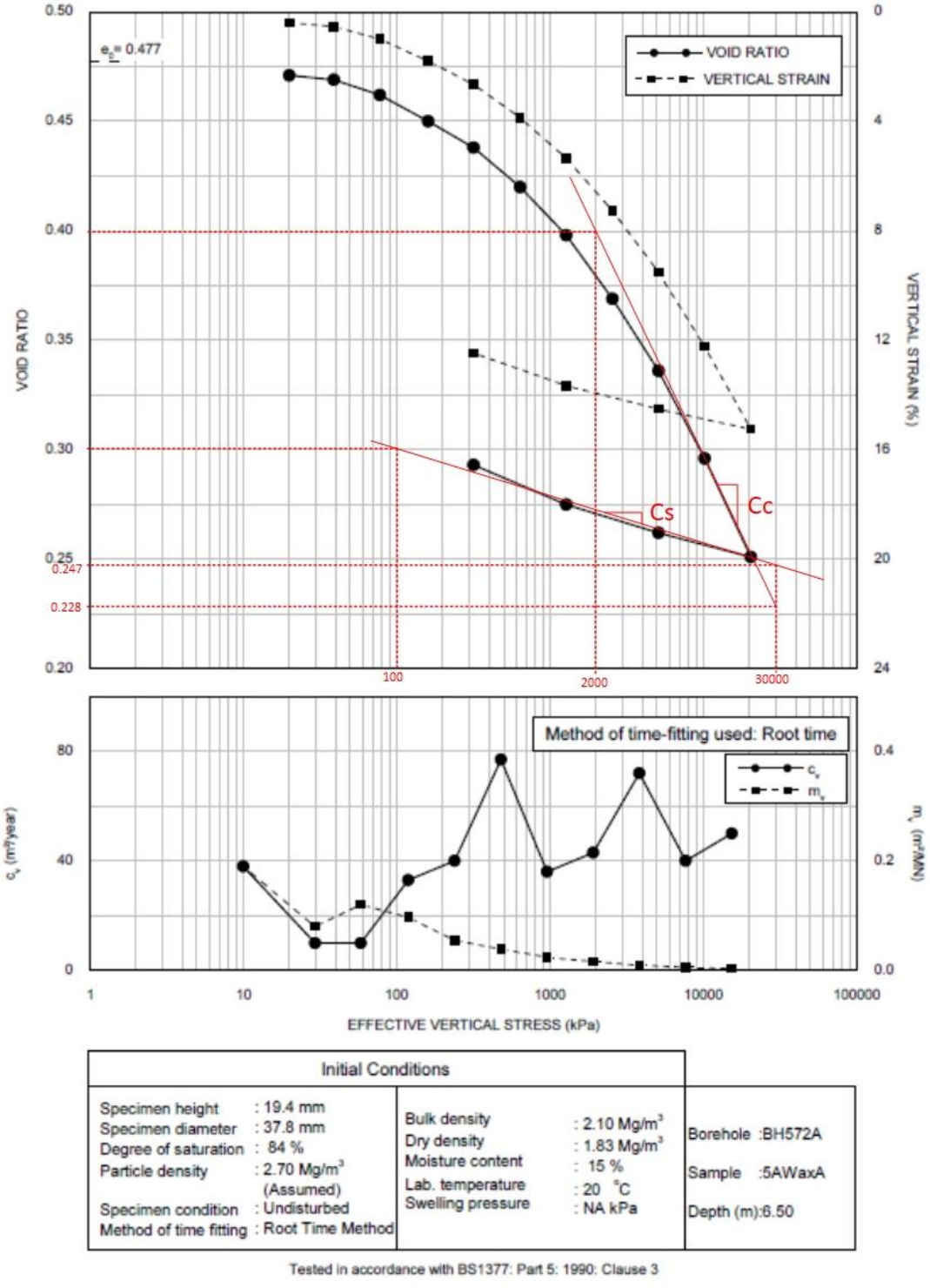

Figure D.1 Example of a 1D compression test result in a semi-logarithmic stress - void ratio plot, from which stiffness parameters Cc and Cs can be derived.

E. Characteristic values of Soils (NEN-EN1997-1:2005)

NEN-EN 1997-1:2005 Eurocode 7: Geotechnisch ontwerp Deel 1: Algemene regels, Nederlands Normalisatie-instituut, Delft.

Tabel 2.b — Karakteristieke waarden van grondeigenschappen

Grondsoort			Karakteristieke waarde [a] van grondeigenschap																	
Hoofd-naam	Bijmengsel	Consis-tentie [b]	γ [c] kN/m³		γ_{sat} kN/m³		q_c [d g] MPa	C'_p [g]		C'_s		$C_c/(1+e_0)$ [g] [-]		C_u [f] [-]		$C_{sw}/(1+e_0)$ [g] [-]		E_{100} [g h] MPa		φ' [g] Graden		c' kPa		c_u kPa	
Grind	Zwak siltig	Los	17		19		15	500		∞		0,004 6		0		0,001 5		45		32,5		0			
		Matig	18		20		25	1 000		∞		0,002 3		0		0,000 8		75		35,0		0		N.v.t.	
		Vast	19	20	21	22	30	1 200	1 400	∞		0,001 9	0,001 6	0		0,000 6	0,000 5	90	105	37,5	40,0	0			
	Sterk siltig	Los	18		20		10	400		∞		0,005 8		0		0,001 9		30		30,0		0			
		Matig	19		21		15	600		∞		0,003 8		0		0,001 3		45		32,5		0		N.v.t.	
		Vast	20	21	22	22,5	25	1 000	1 500	∞		0,002 3	0,001 5	0		0,000 8	0,000 5	75	110	35,0	40,0	0			
Zand	Schoon	Los	17		19		5	200		∞		0,011 5		0		0,003 8		15		30,0		0			
		Matig	18		20		15	600		∞		0,003 8		0		0,001 3		45		32,5		0		N.v.t.	
		Vast	19	20	21	22	25	1 000	1 500	∞		0,002 3	0,001 5	0		0,000 8	0,000 5	75	110	35,0	40,0	0			
	Zwak siltig, kleiig		18	19	20	21	12	450	650	∞		0,005 1	0,003 5	0		0,001 7	0,001 2	35	50	27,0	32,5	0		N.v.t.	
	Sterk siltig, kleiig		18	19	20	21	8	200	400	∞		0,011 5	0,005 8	0		0,003 8	0,001 9	15	30	25,0	30,0	0		N.v.t.	
Leem [e]	Zwak zandig	Slap	19		19		1	25		650		0,092 0		0,003 7		0,030 7		2		27,5	30,0	0		50	
		Matig	20		20		2	45		1 300		0,051 1		0,002 0		0,017 0		3		27,5	32,5	1		100	
		Vast	21	22	21	22	3	70	100	1 900	2 500	0,032 9	0,023 0	0,001 3	0,000 9	0,011 0	0,007 7	5	7	27,5	35,0	2,5	3,8	200	300
	Sterk zandig		19	20	19	20	2	45	70	1 300	2 000	0,051 1	0,032 9	0,002 0	0,001 3	0,017 0	0,011 0	3	5	27,5	35,0	0	1	50	100
Klei	Schoon	Slap	14		14		0,5	7		80		0,328 6		0,013 1		0,109 5		1		17,5		0		25	
		Matig	17		17		1,0	15		160		0,153 3		0,006 1		0,051 1		2		17,5		5		50	
		Vast	19	20	19	20	2,0	25	30	320	500	0,092 0	0,076 7	0,003 7	0,003 1	0,030 7	0,025 6	4	10	17,5	25,0	13	15	100	200
	Zwak zandig	Slap	15		15		0,7	10		110		0,230 0		0,009 2		0,076 7		1,5		22,5		0		40	
		Matig	18		18		1,5	20		240		0,115 0		0,004 6		0,038 3		3		22,5		5		80	
		Vast	20	21	20	21	2,5	30	50	400	600	0,076 7	0,046 0	0,003 1	0,001 8	0,025 6	0,015 3	5	10	22,5	27,5	13	15	120	170
	Sterk zandig	-	18	20	18	20	1,0	25	140	320	1 680	0,092 0	0,016 4	0,003 7	0,000 7	0,030 7	0,005 5	2	5	27,5	32,5	0	1	0	10
	Organisch	Slap	13		13		0,2	7,5		30		0,306 7		0,015 3		0,102 2		0,5		15,0		0	1	10	
		Matig	15	16	15	16	0,5	10	15	40	60	0,230 0	0,153 3	0,011 5	0,007 7	0,076 7	0,051 1	1,0	2,0	15,0		0	1	25	30
Veen	Niet voorbelast	Slap	10	12	10	12	0,1	5	7,5	20	30	0,460 0	0,306 7	0,023 0	0,015 3	0,153 3	0,102 2	0,2	0,5	15,0		1	2,5	10	20
	Matig voorbelast	Matig	12	13	12	13	0,2	7,5	10	30	40	0,306 7	0,230 0	0,015 3	0,011 5	0,102 2	0,076 7	0,5	1,0	15,0		2,5	5	20	30
Variatiecoëfficiënt v			0,05				–	0,25										0,10				0,20			

[a] De tabel geeft van de desbetreffende grondsoort de lage, respectievelijk de hoge karakteristieke waarde van gemiddelden. Binnen een gebied, vastgesteld door de rij van het bijmengsel en de kolom van de parameter (een cel), geldt:

— als een verhoging van de waarde van een van de grondeigenschappen tot een ongunstiger situatie leidt dan de toepassing van de in de tabel gepresenteerde lagere karakteristieke waarde, moet de rechterwaarde op dezelfde regel zijn gebruikt. Is er rechts geen waarde vermeld, dan moet de waarde er recht onder zijn toegepast;
OPMERKING Dit is bijvoorbeeld het geval bij negatieve kleef op een paal waar een hogere waarde van φ', c' en c_u ook een hogere waarde van de negatieve kleef oplevert.

— voor $C_c/(1+e_0)$, C_u en $C_{sw}/(1+e_0)$ zijn in de tabel de hoge karakteristieke gemiddelde waarden vermeld.

Table E.1 Characteristic values of Soils (NEN-EN1997-1:2005)

F. Estimation of clay permeability

Figure F.1 below shows an example of an estimation of clay permeability on one sample. An average value of permeability is taken over a certain range of effective stress.

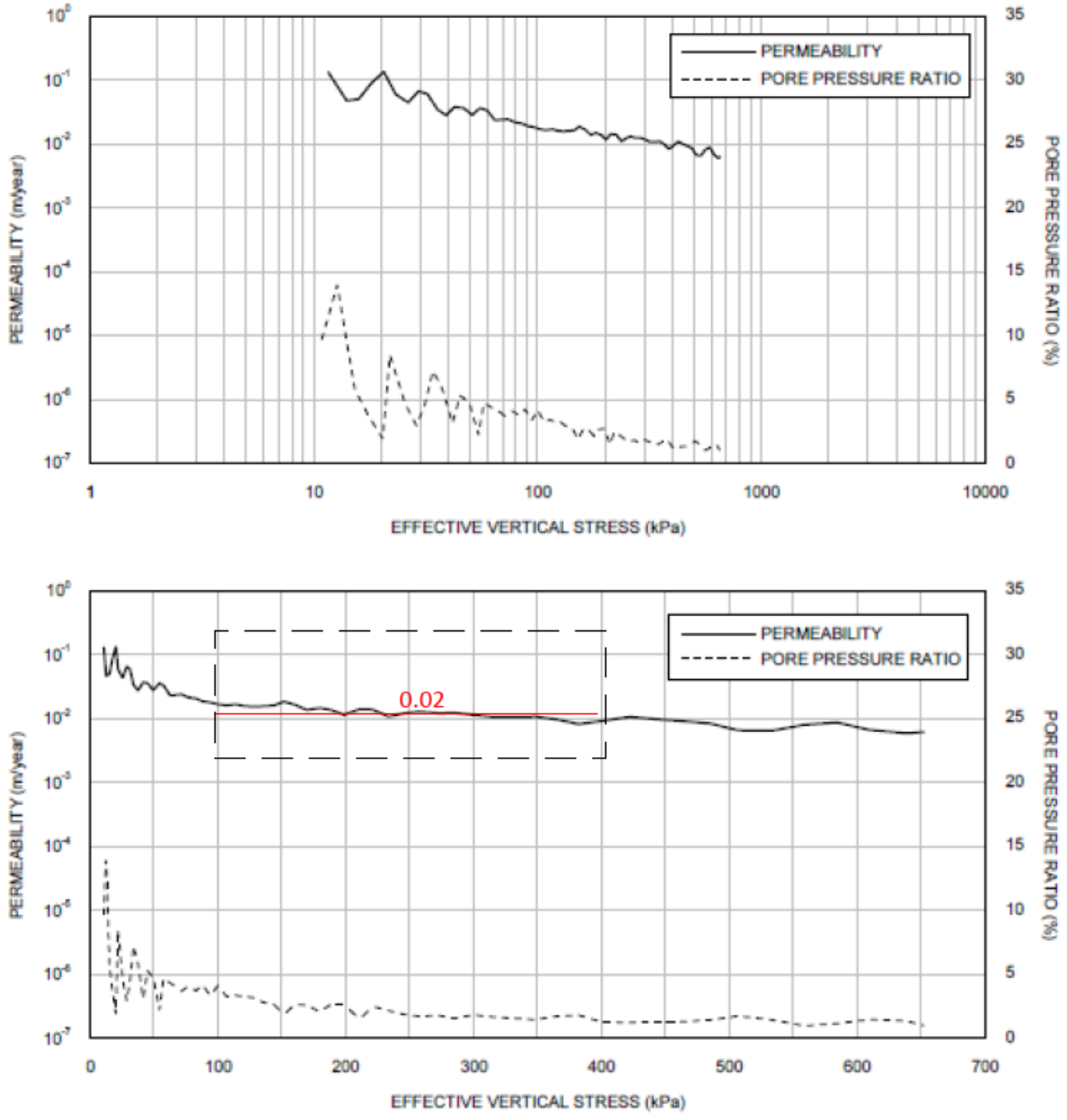

Borehole	Sample	Depth (m)
BH562	9WaxA	8.11

Initial void ratio	: 0.685
Particle Density	: 2.65 Mg/m^3
Strain rate (constant)	: 0.40 %/hour

Figure F.1 Estimation of clay permeability

G. Applicability of material models

The selection of a specific soil constitutive model can be based on the soil type, type of application and the type of soil loading. A full overview of the different possibilities of application is given below (PLAXIS Material Models Manual).

Considering different types of soils

Model	Concrete	Rock	Gravel	Sand	Silt	OC clay	NC clay	Peat (org)
Linear Elastic model	C	C						
Mohr-Coulomb model	A	B	C	C	C	C	C	C
Hardening Soil model			B	B	B	B	B	
HS small model			A	A	A	A	B	
Soft Soil Creep model							A*	A*
Soft Soil model							A*	A*
Jointed Rock model		A**						
Modified Cam-Clay model							C	C
NGI-ADP model							A*	A*
Hoek-Brown model		A**						

Considering different types of applications (consider also type of soil!)

Model	Foundation	Excavation	Tunnel	Embankment	Slope	Dam	Offshore	Other
Linear Elastic model			C					
Mohr-Coulomb model	C	C	C	C	C	C	C	C
Hardening Soil model	B	B	B	B	B	B	B	B
HS small model	A	A	A	A	A	A	A	A
Soft Soil Creep model	B	B	B	A	A	B	B	B
Soft Soil model	B	B	B	A	A	B	B	B
Jointed Rock model	B	B	B	B	B	B	B	B
Modified Cam-Clay model	C	C	C	C	C	C	C	C
NGI-ADP model	B	B	B	A	A	B	A	B
Hoek-Brown model	B	B	B	B	B	B	B	B

Considering different types of loading and soils (consider also type of soil!)

Model	Primary compression	Unloading / Reloading	Shear / Deviatoric loading	Undrained loading	Cyclic	Compression + Shear	Extension + Shear
Linear Elastic model	C	C					
Mohr-Coulomb model	C	B	C	C		C	C
Hardening Soil model	A	B	B	B	C	A	A
HS small model	A	A	A	B	B	A	A
Soft Soil Creep model	A	B	B	B	C	A	B
Soft Soil model	A	B	B	B	C	A	B
Jointed Rock model	B	B	B			B	B
Modified Cam-Clay model	C	C	C	C	C	C	C
NGI-ADP model	B	B	B	A	C	B	B
Hoek-Brown model	B	B	B			B	B

A : The best standard model in PLAXIS for this application

B : Reasonable modelling

C : First order (crude) approximation

* : Soft Soil Creep model in case time-dependent behaviour is important; NGI-ADP model for short-term analysis, in case only undrained strength is known

** : Jointed Rock model in case of anisotropy and stratification; Hoek-Brown model for rock in general

Figure G.1 Applicability of material models

H. The Press-Replace method

Introduction

Realistic simulation of the installation process is important in analysing the behaviour of jacked spudcans. Despite the promising performances of large deformation numerical methods, these methods are computationally expensive and relatively complicated, which decreases its attraction for practice engineers who look for practical and straight-forward methods in a daily engineering practice. The Press-Replace (PR) technique, on the other hand, is a simple method based on small deformation theory to model spudcan penetration in geotechnical engineering problems. Due to the application of small strain modelling, the installation process of jacked spudcans can be modelled as a staged construction process in any standard finite element software.

The PR technique, as first introduced by Andersen et al. (2004), benefits a displacement-controlled modelling scheme rather than a load-controlled scheme. The method involves a stepwise updated geometry, which consists of a straining phase (Press) followed by a geometry update (Replace). The initial mesh is preserved, while the material properties of the penetrated soil volume are replaced by the spudcan material at the end of each phase. This is achieved by changing the global stiffness matrix without the need for updating the mesh, which makes the calculations fast relative to large deformation analysis techniques. Despite its advantages, PR has its own limitations. Most importantly, it is unable to model the flow of soil from beneath the spudcan, around the sides towards to top; also known as backflow.

Figure H.1 illustrates three sequential phases in PR. The penetration path is divided into several slices of thickness t_s. When the spudcan base (in grey color) is resting on slice i, a Dirichlet boundary condition (displacement), u_i, equal to the summation of the previous displacement and an additional displacement increment, t_s, is applied on top to push the spudcan downwards. After completion of the loading stage, the soil material in slice i is replaced by a stiffer elastic material. This process continues until the spudcan reaches to the last slice on the penetration path.

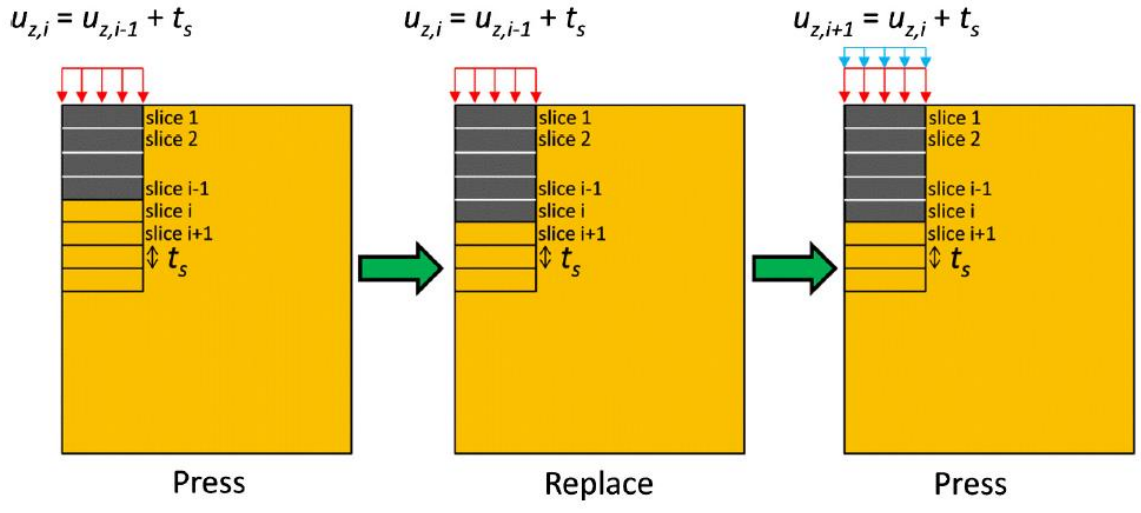

Figure H.1 Press-Replace technique (Tehrani et al., 2016)

Note that when applying the prescribed displacement at the top of the spudcan (instead of bottom), a part of the applied displacement is captured by the elasticity of the spud leg and thus, not imposed directly onto the soil. Although the stiffness of the spudcan is much higher than the soil stiffness, some straining inside the spud leg will occur as the material is not infinitely stiff. To overcome this problem, instead of applying the prescribed displacement at the top of the pile, in the PLAXIS model of this study, the prescribed line displacement is applied at the bottom of the spudcan. In this way, all load is directly imposed upon the soil and no compensation should be introduced for the deflection behaviour of the footing itself.

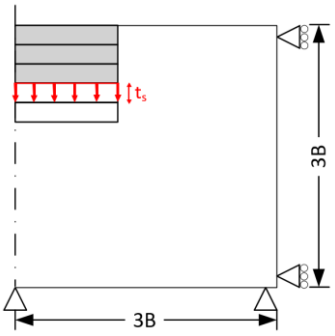

Figure H.2 PR model applying Dirichlet boundary condition at pile bottom

Leg penetration predictions

The load-penetration curve using the PR method is shown in figure H.4. At first sight, the graph looks somewhat messy. As a result of the geometry update in the analysis, very large stress oscillations occur below the footing, which alternate in sign; compression and tensional stresses. These oscillations reach values up to ± 2000 MN. During the loading phase (Press), a compressional force is found as the soil is being pushed downwards. Contrary, tensional forces are observed during the geometry update phase (Replace). Therefore, it can therefore be concluded that the method is found to be unstable after the geometry update phase and cannot be widely used. Because of the sudden change in global stiffness matrix, the model is unable to produce reliable results.

Plotting the Cartesian total vertical stresses around the spudcan shows that a significant amount of stress concentrations occur directly below the footing, as seen in figure H.3. This is exactly the location where PLAXIS automatically computes the soil reaction force, F_y, at each loading phase. In fact, F_y is the vertical component of the resulting reactions on the nodes where non-zero prescribed displacements are applied. Proper values for F_y could be calculated at a small distance below the footing where the stress concentrations are not present. However, this cannot be done in PLAXIS automatically. All results need to be processed manually, which is extremely time consuming. Doing this would require to draw a cross section 0.5m below the footing and calculate the incremental total vertical stresses at this level. The incremental total vertical stresses have to be calculated because the initial effective stresses and the pore pressures generated based on the phreatic level should not be part of the soil's bearing capacity. The incremental total stresses then need to be integrated to find the bearing capacity of the soil. This is very time consuming, which reduces the attractiveness of using this method.

However, between the stress oscillations, an underlying trend is visible, which shows the load-penetration resistance of the soil (figure H.4). This trend represents in fact WIP analyses as it only consists of points directly after the loading phases. A more detailed comparison can be seen in the next section. It is also noted that the trend matches reasonably with the ISO guidelines for soil bearing capacity in clay.

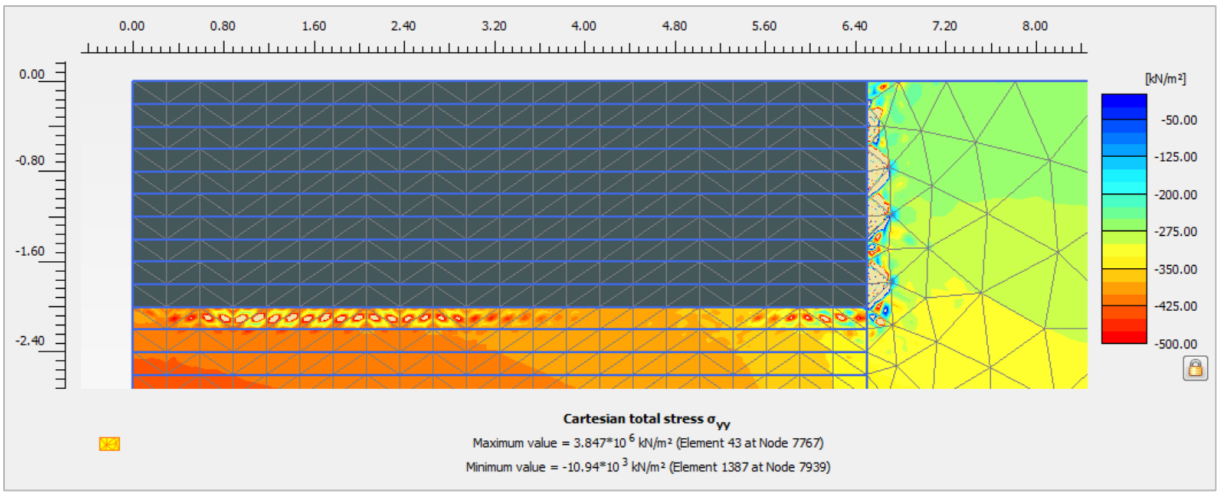

Figure H.3 Stress concentrations around spudcan footing. This gives unreliable results.

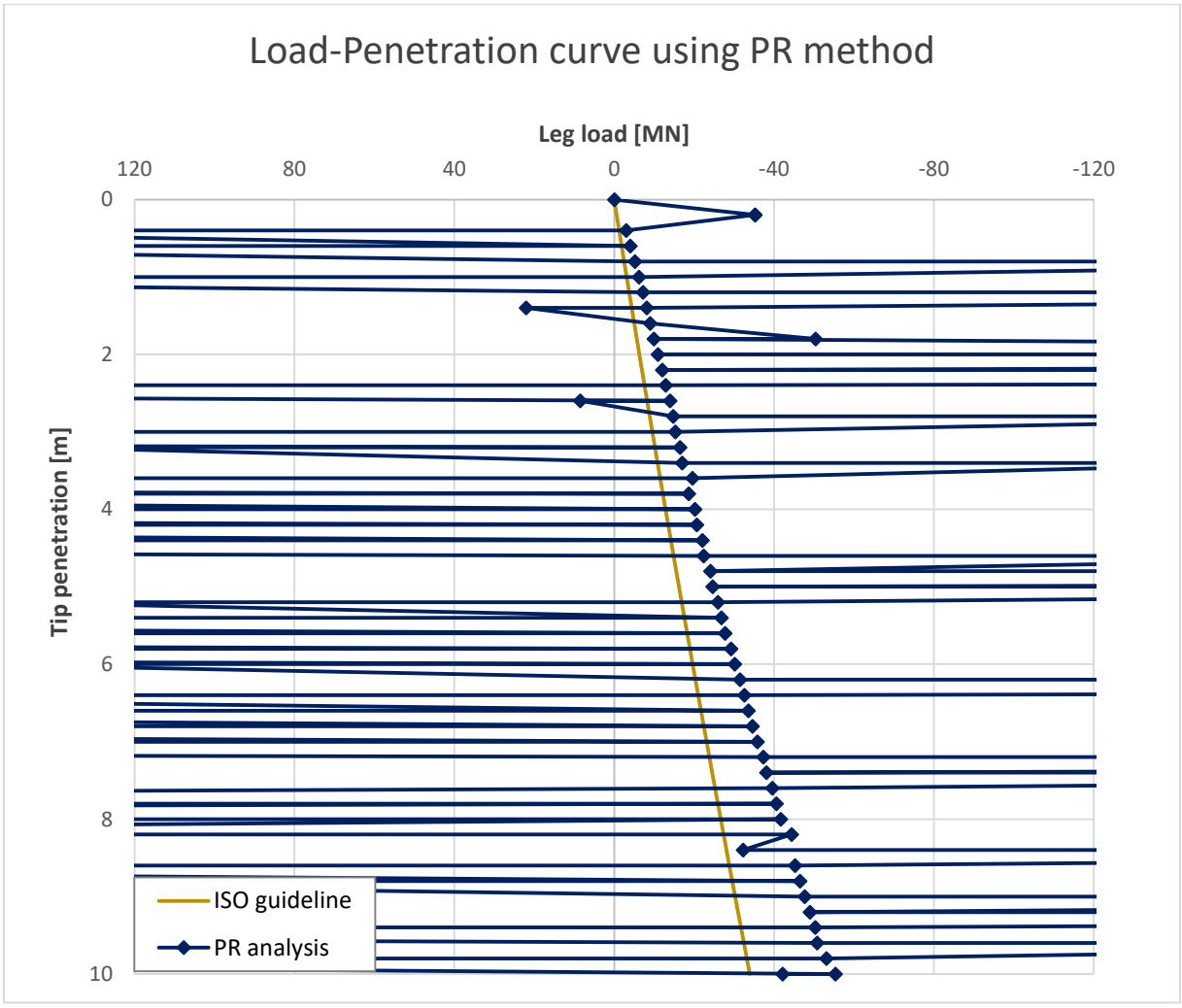

Figure H.4 Load-penetration curve using PR method

Excess pore water pressure

Using the PR-method, spudcan jacking is modelled as a continuous process by penetrating the footing and updating the geometry. The soil volume under the 6.5m wide spudcan footing is pushed down in consecutive steps of 0.20m. After each pushing step, the geometry is updated by replacing the displaced soil by the spudcan material. For a point under the foundation, the excess pore pressure is gradually accumulated by this sequential loading scheme.

Considering stress points below the spudcan at each slice increment, it can be seen that the excess pore water pressure is stepwise increased as the footing penetrates into the soil (figure H.6). During the geometry update phase, the stress state of the soil is kept at the previous level, which is illustrated by the horizontal dashed lines between the loading phases. When loading continues from the previous phase, the excess pore pressure starts from the previously reached value towards a higher value, as schematically illustrated in figure H.6. The excess pore water pressures are accumulating. Considering the first meter of spudcan penetration, i.e. at consecutive penetration depths of 0.20, 0.40, 0.60, 0.80 and 1.0 meter, model results in terms of excess pore water pressure accumulation are plotted in figure H.7. At one meter penetration, an excess pore water pressure of $80\ kPa$ is reached.

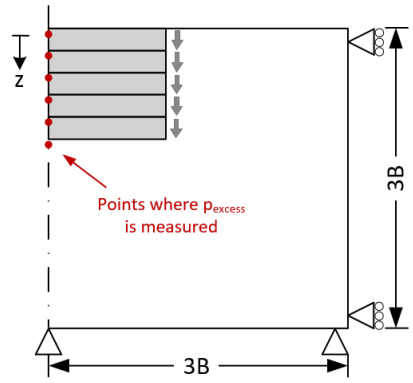

Figure H.5 Using PR, p_{excess} is measured at each slice increment

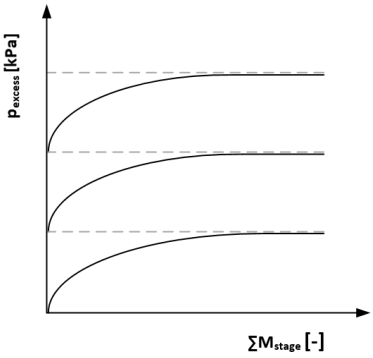

Figure H.6 Schematic representation of accumulation of excess pore water pressures directly below the footing.

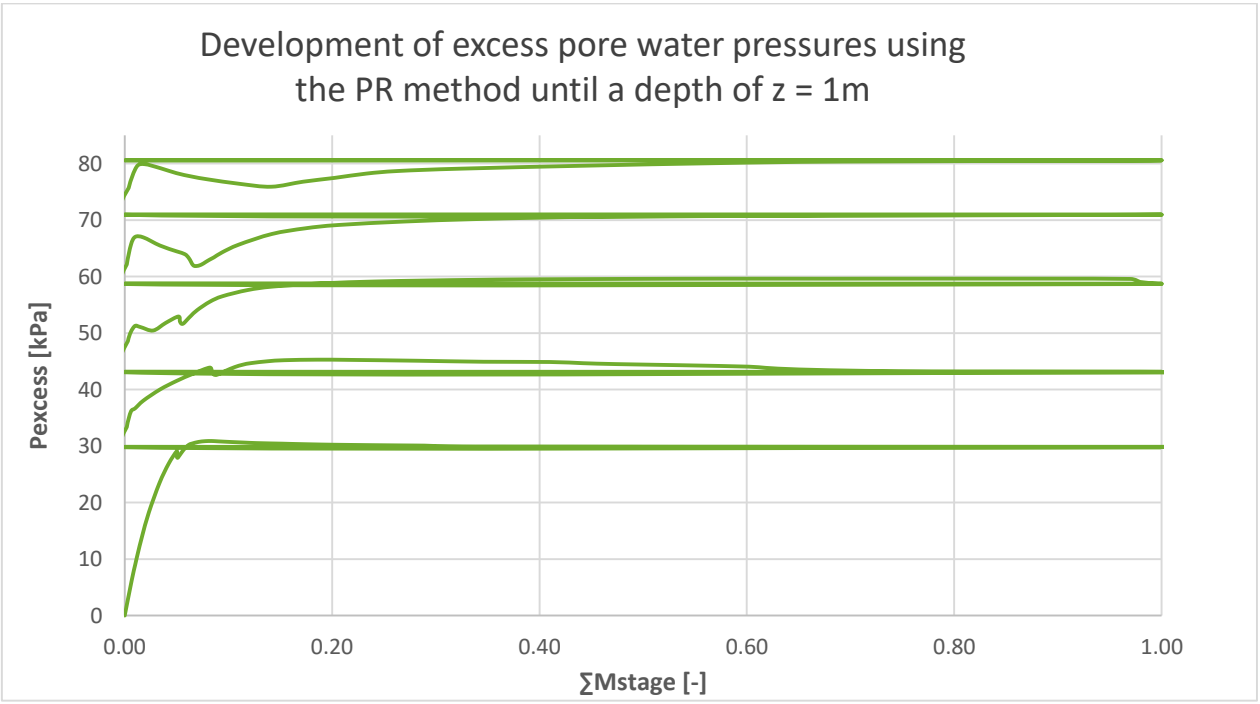

Figure H.7 Exess pore water pressure accumulation modelled using the PR method.

Comparison WIP and PR

Leg penetration predictions

Plotting the WIP analyses next to the PR curve shows that both methods show substantially similar results. The load-penetration trend observed from the PR method shows similar results compared to wished-in-place calculations, because it represents only points after the loading phase. In fact, the results are substantially similar, because you are pushing the same soil. Thus, the same resistances are found. The wide oscillations in the PR method occur as a result of the geometry update phases. The change of penetrated soil material properties into spudcan material properties in the global stiffness matrix does not produce neat and reliable results, which is shown by the large stress oscillations in figure H.8. After the geometry update has completed, in fact, a certain wished-in-place footing is obtained at the beginning of each loading phase. That is why both methods are producing similar results.

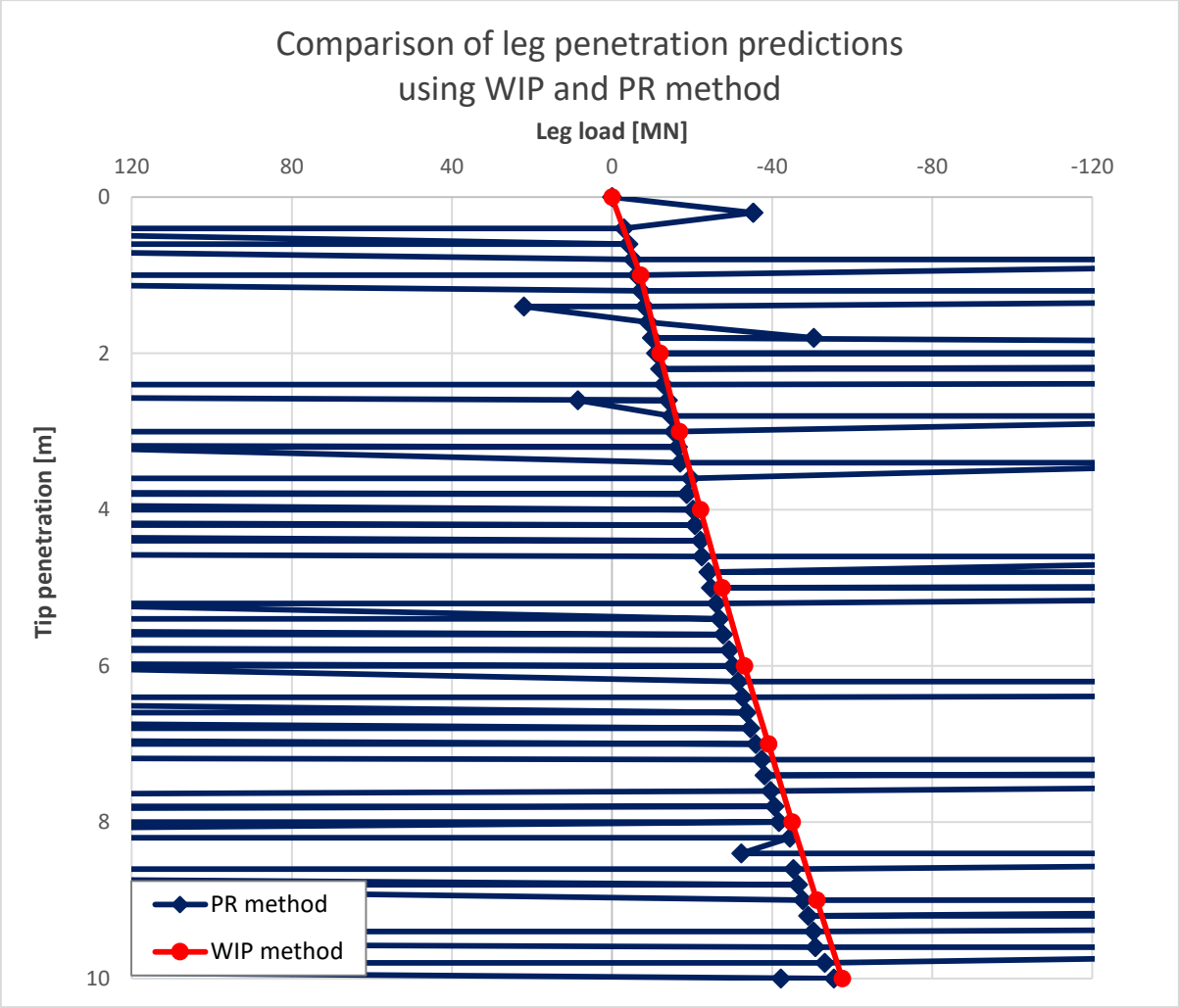

Figure H.8 Comparison of leg penetration predictions using WIP and PR method.

Excess pore water pressure

In terms of excess pore water pressure generation, a comparison is made between discontinuous loading as in the WIP method and continuous loading as in the PR method. As explained before, in the PR method, pore water pressures are maintained after each consecutive loading phase, hold constant during the geometry update phase and further increased at the next loading step. Using this approach, the accumulation of excess pore water pressures during continuous spudcan penetration is involved in the model. On the other hand, in the WIP analysis, the spudcan penetration is discontinuous and excess pore water pressures start from zero at each depth and increase to a certain equilibrium value. An investigation is done to verify whether the generation of excess pore water pressure under the spudcan is actually different in the PR and the WIP method.

At each meter penetration depth, a comparison is made by plotting the development of the excess pore water pressure using both the PR and WIP method, as seen in the graphs of figure H.10. From the resulting plot of p_{excess} as function of penetration depth, in figure H.9, it can be concluded that both methods compute similar results in terms of generating excess pore water pressures below the footing. Is does not matter if the excess pore water pressures are modelled by accumulation (PR) or not (WIP). Generally, results from the WIP method are just slightly below the results of the PR method. The deviation lies around 2% and is negligible when comparing the differences between both methods.

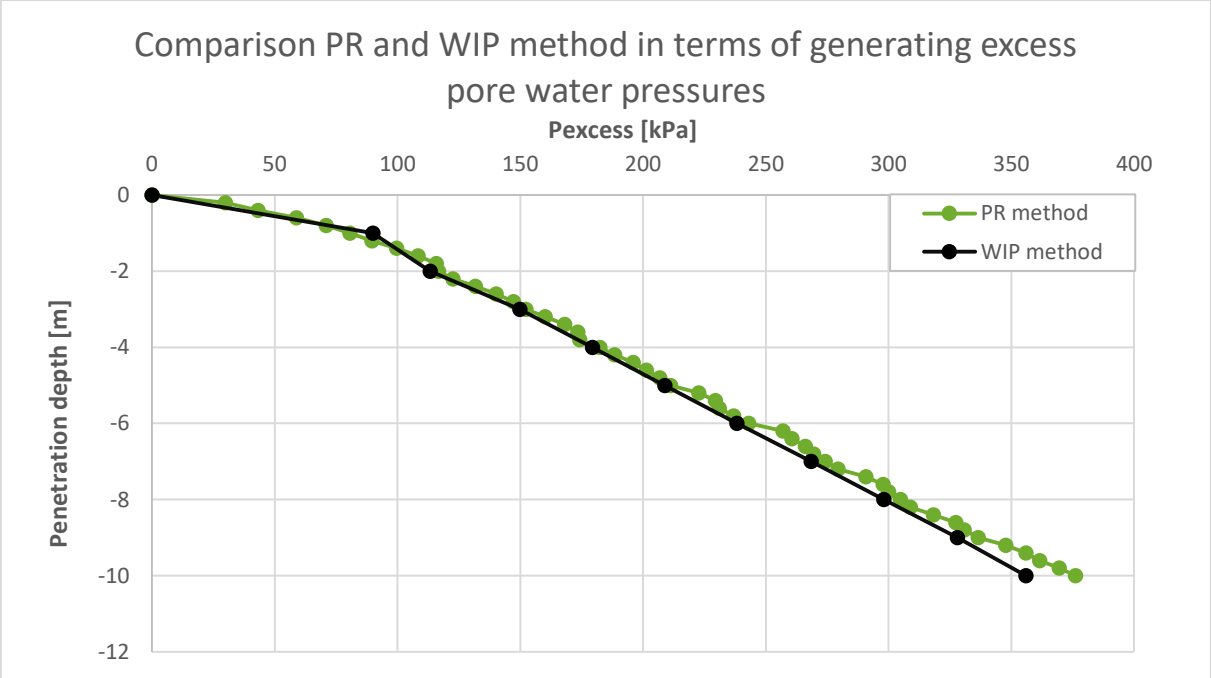

Figure H.9 Comparison PR and WIP method in terms of generating excess pore water pressures.

Generation of excess pore water pressures using the continuous (accumulating) PR method and discontinous (non-accummulating) WIP method

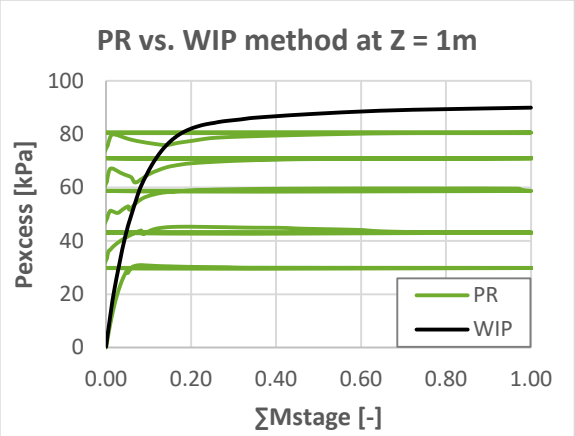

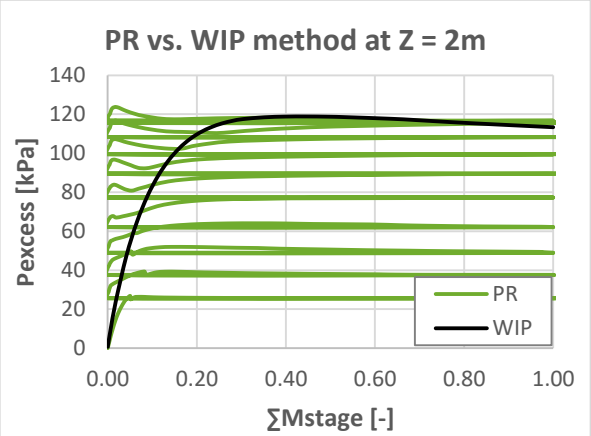

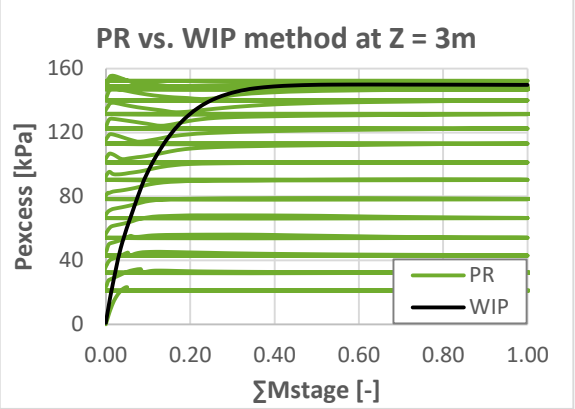

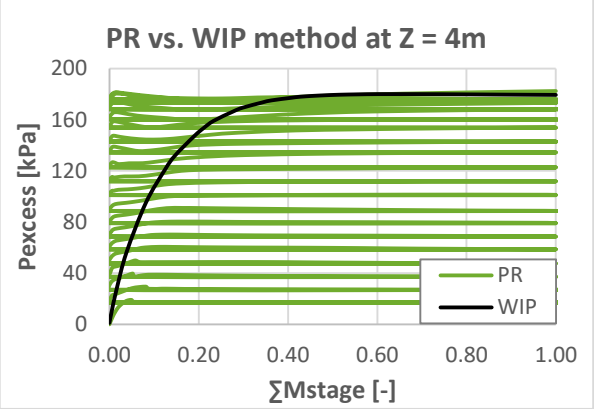

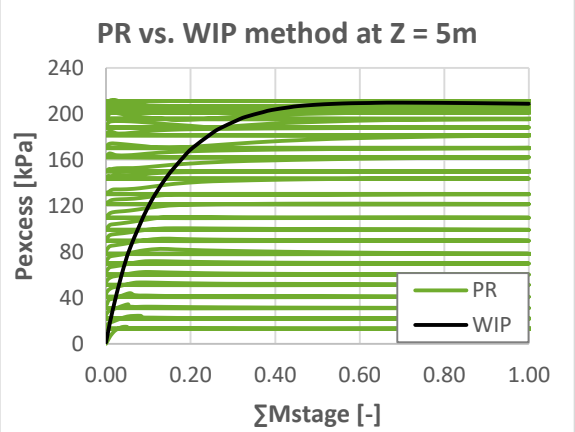

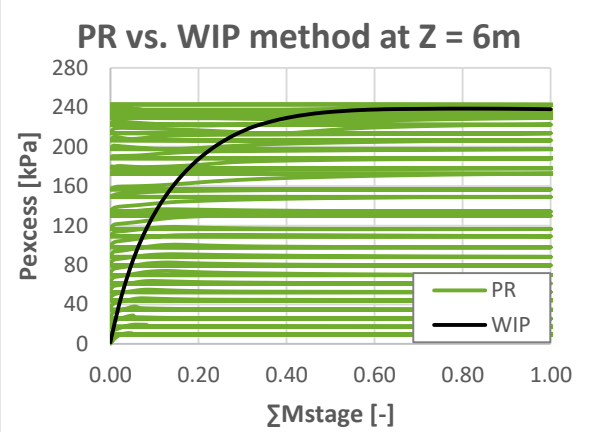

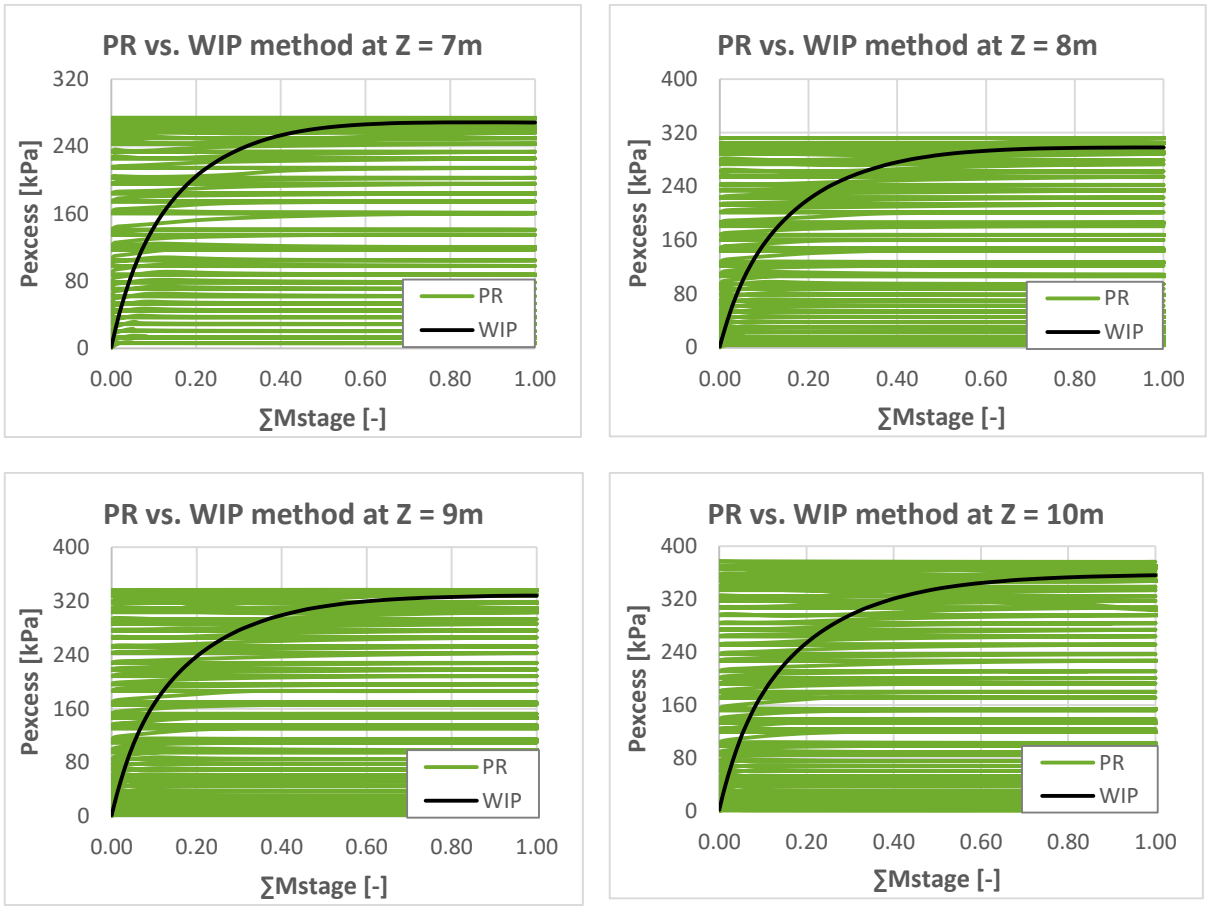

Figure H.10 Comparison of excess pore water pressure generation using both PR- and WIP method at each meter penetration depth.

Conclusion

In conclusion, the WIP and PR method show substantially similar results, both in terms of leg penetration predictions and generation of excess pore water pressure. The accumulating excess pore water pressure concept of the PR method does not differ from the non-accumulating concept in the WIP approach. Therefore, there is no extra benefit in using the PR method above the WIP method. On the contrary, the PR method is more complex to build, requires more computational effort (and time) and shows unreliable results when the model outcome, in terms of soil resistance, blows up after the geometry update phase. These are all undesirable ingredients for constructing numerical models.

Therefore, the more simple WIP method is selected in all further numerical analyses of this thesis, as this model is (1) more easier to implement and to use in a standard FE program and (2) shows substantially similar results compared to the complex PR model. Especially when considering consolidation analysis and soil failure in undrained conditions, proper and reliable modelling of excess pore water pressures are required, which is taken care of by the WIP method.

I. Effective stress paths in SSC-model

In section 5.4.2 – Simulation of triaxial tests, the viscous effect of time-dependent loading in the SSC-model on the soil resistance has been demonstrated. For increasing shear strain rates, higher effective stress paths will be followed, which will generate higher soil resistances. Convergence of the solution is found when soil samples are sheared to failure in a triaxial test simulation with a strain rate of 10,000 %/day (see figure I.1). This is the highest effective stress path computed by the SSC-model.

The rate-insensitive MCC-model is assumed to be the time-independent limit of the rate-sensitive Soft Soil Creep model. For very small strain rates, the undrained shear strength is considered to be independent of strain rate. Here, only the frictional resistance term is present (no additional viscous resistances). This limit corresponds to a strain rate of 0.01 %/day. The undrained shear strengths found by using both models are more or less equal, as more clearly shown in figure I.2.

For smaller shearing rates, it is noted that the model also produces stress states below this time-independent limit (below green line), which are assumed to be incorrect, as the soil resistance can never be lower than solely the frictional resistance of the soil. For very slow numerical loading rates, creep occurs in terms of irreversible volumetric strains as a result of initial stress states, which need to be compensated by elastic volumetric expansion, as in undrained conditions no total volumetric strains are allowed to occur (irreversible volumetric strains + elastic volumetric expansion = zero). Consequently, significant excess pore water pressures will arise, which inherently reduces the mean effective stress, p'. Therefore, for decreasing deviatoric loading rates, an abrupt pore pressure build-up is noted at q almost equal to zero.

Figure I.1 Full range of effective stress paths followed using SSC-model during different shearing durations.

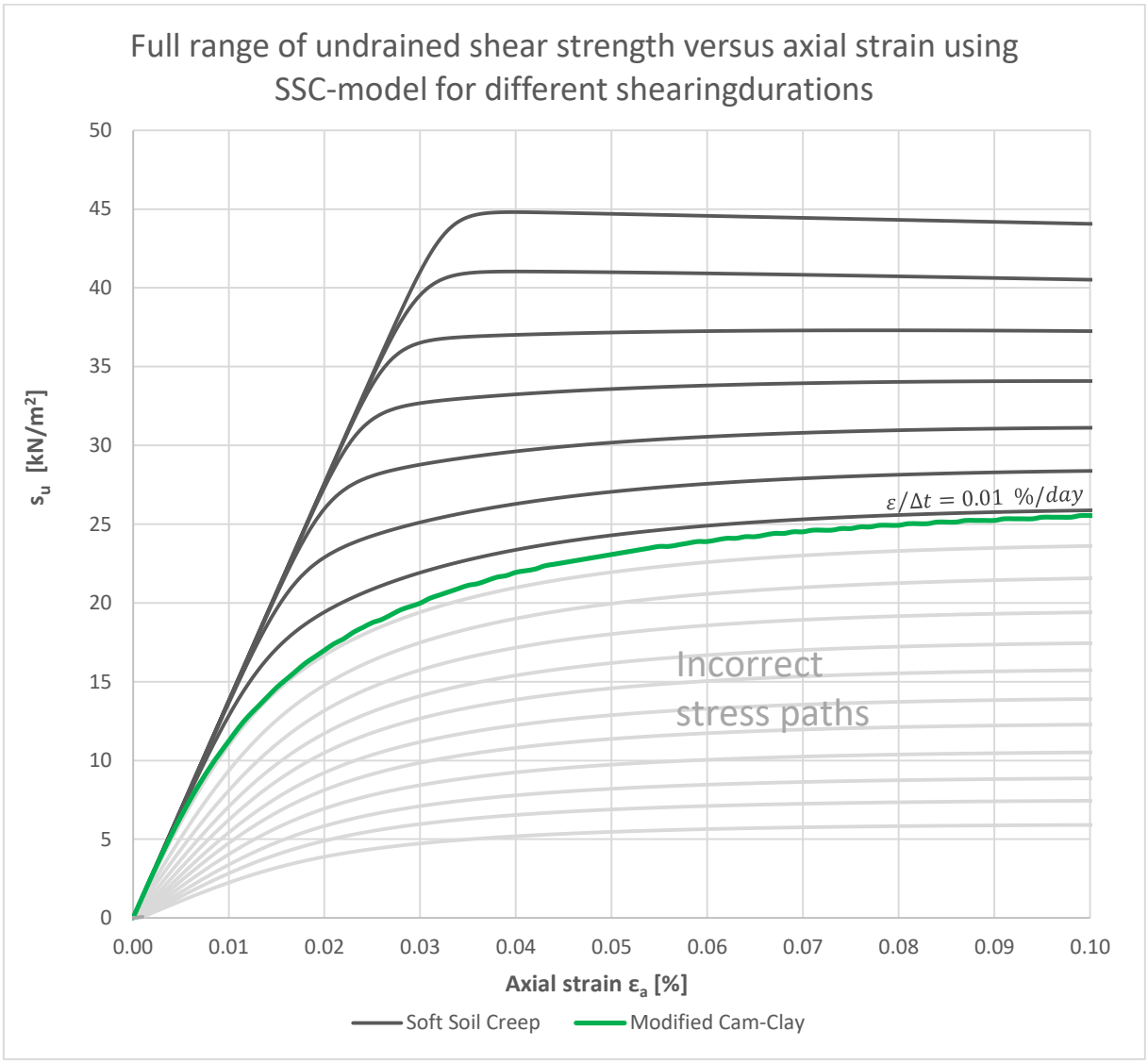

Figure I.2 Full range of undrained shear strength versus axial strain using SSC-model for different shearing durations.

J. Sensitivity analysis

Soil permeability

Permeability parameter (k)

In this analysis, the effect of permeability on the soil behaviour during preloading is investigated. Considering a uniform soil deposit, a relatively narrow probability density function of permeability, k, can be assumed. However, in reality, the subsoil is almost always inhomogeneous, which means that the material properties are spatially varying over the domain. Thus, a greater range of potential solutions is possible, which subjects the soil behaviour to considerable uncertainty. It is therefore unfair to assume that the characteristic value of permeability can be estimated based on one single hydraulic conductivity test on a specific clay specimen. To examine the impact of parameter uncertainty of soil permeability on the modelling results, a sensitivity analysis is performed by varying the input value of k over different order of magnitudes.

Using the standard preloading procedure, the value of permeability is varied over different orders of magnitude, ranging from $k = 10^{-6}$ until $10^{-9}\ cm/s$, to represent the soil behaviour over the full range of 'impervious' materials, as indicated in figure J.1. The resulting preload graph is shown in figure J.2 below. It is noted that the solution of the preload-hold cycles converges towards the same solution for $k < 10^{-7}\ cm/s$. For larger permeabilities (larger drainage potential), more dissipation of excess pore water pressure can occur during the 15 minutes of consolidation, which results in a larger reduction in leg load, as can be seen for values of $k > 10^{-7}\ cm/s$. As for the spudcan penetration, convergence of the solution is also found for values of permeability smaller than $10^{-7}\ cm/s$, as shown in figure J.3. For larger values of permeability, a larger spudcan penetration is observed, as more consolidation can take place.

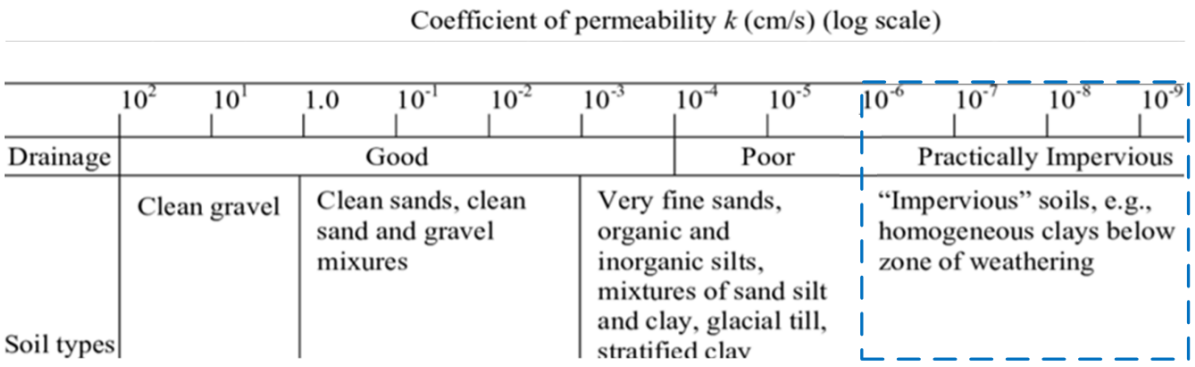

Figure J.1 Permeability and drainage characteristics by Casagrande and Fadum (1940).

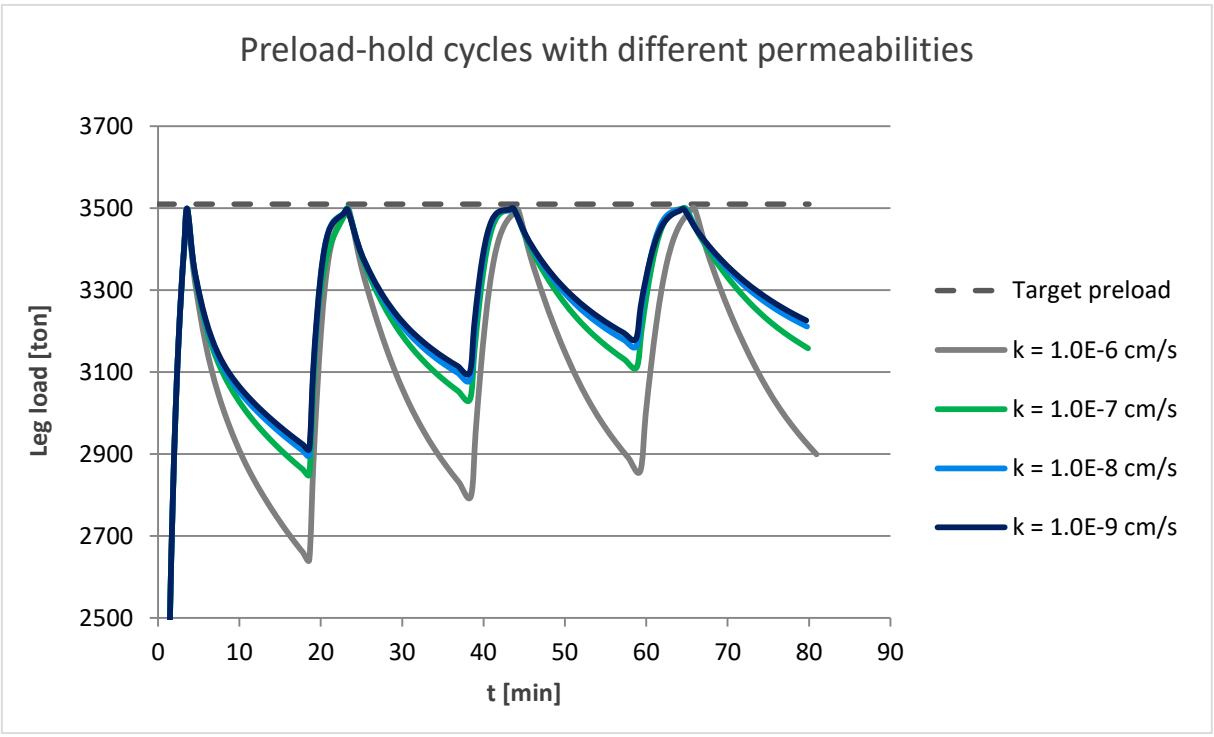

Figure J.2 Effect of soil permeability on preloading modelling results.

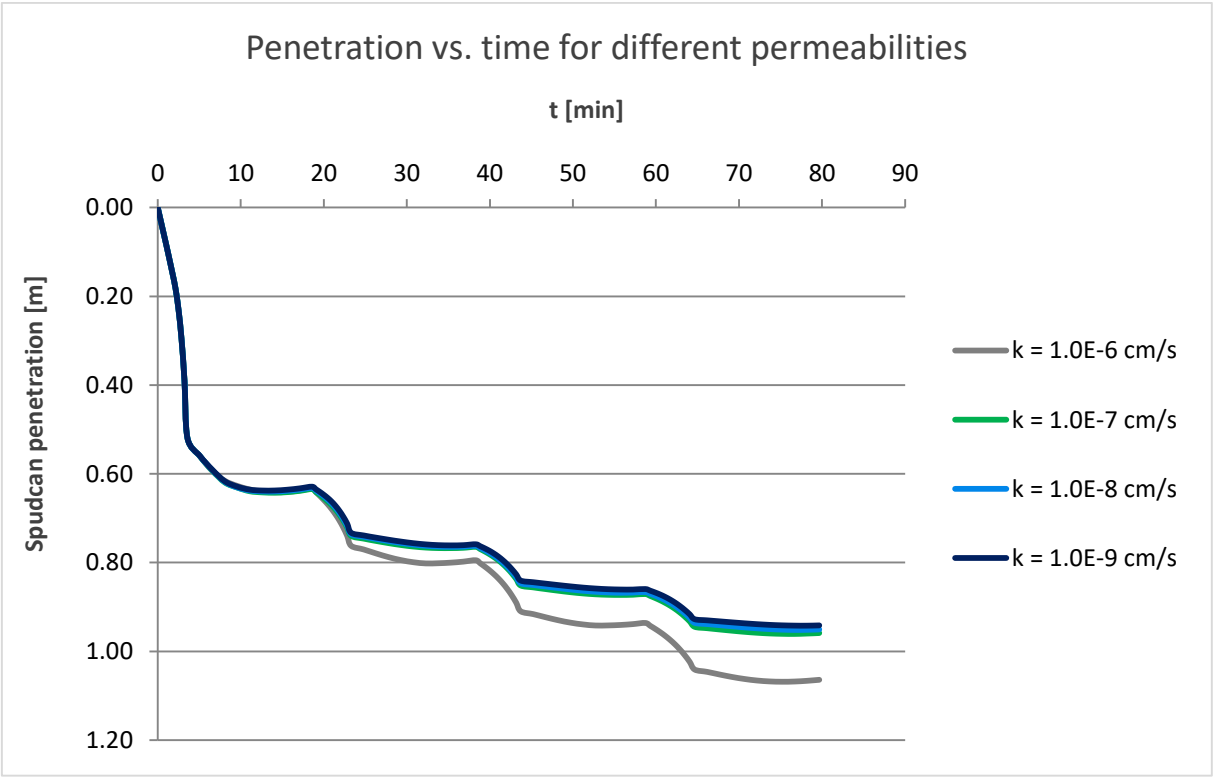

Figure J.3 Effect of soil permeability on spudcan penetration modelling results.

Soil stiffness

Stiffness parameters (λ^* and κ^*)

In this section, the effect of the stiffness parameters on the soil behaviour during preloading is investigated. Besides the SSF-SBD soil unit (in section 5.4.5), both the standard and overshooting preloading procedures are also modelled for the slightly stiffer WIS-MF material and an arbitrarily chosen softer material. An overview of the material parameters is given in table J.1.

Table J.1 Soft Soil Creep model input parameters

Soft Soil Creep model input parameters					
		softer material	SSF-SBD	Stiffer material: WIS-MF	
Stiffness	λ^*	0.052	0.026	0.012	$[-]$
	κ^*	0.0020	0.0010	0.0006	$[-]$
	μ^*	0.0026	0.00136	0.00063	$[-]$
	e_{init}	0.962	0.962	0.690	$[-]$
Strength	c	0	0	0	$[kN/m^2]$
	ϕ'	25.4	25.4	27.3	[°]
	ψ	0	0	0	[°]
Advanced	K_0^{NC}	0.7419	0.7419	0.7085	$[-]$
	M	1.0	1.0	1.08	$[-]$
	ν'_{ur}	0.15	0.15	0.15	$[-]$
	OCR	1.3	1.3	1.3	$[-]$

WIS-MF soil: standard jacking procedure

The WIS-MF soil unit is considered slightly stiffer compared to the SSF-SBD soil, as it consists of a higher unit weight, smaller void ratio and a slightly higher degree of silt particles, as seen in chapter 3 – Interpretation of site investigation data. Using the standard jacking procedure with both spudcan penetration rates of 0.10 and 1.0 m/h, it is noted that this material only requires two preload-hold cycles before reaching the preload criterion of 400 ton load reduction in 15 minutes, as can be seen in figure J.4. Additionally, since this material is more silty (and less clayey), less viscous resistances are being generated and thus, only a small variation in soil behaviour during preloading is noted between the different spudcan penetration rates. The frictional resistance term, rather than the viscous resistance term is dominating. This results in similar spudcan penetration behaviour, irrespective of the penetration rate, as seen in figure J.5. For this material, no time savings are gained when using different spudcan penetration rates in the standard jacking procedure.

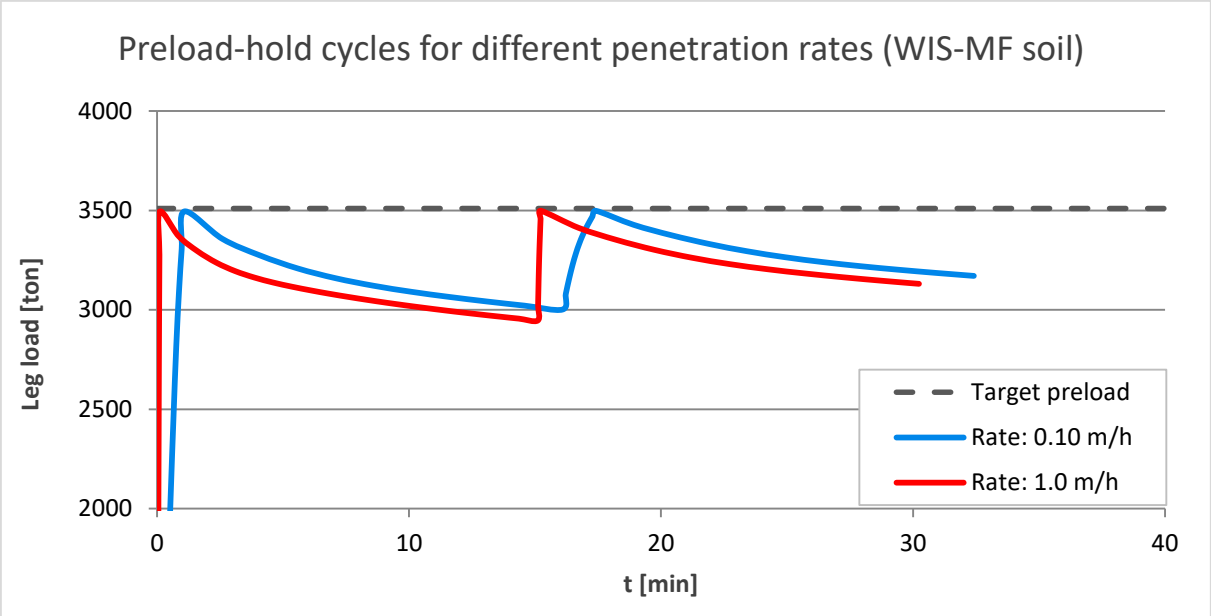

Figure J.4 Standard jacking procedure for WIS-MF soil.

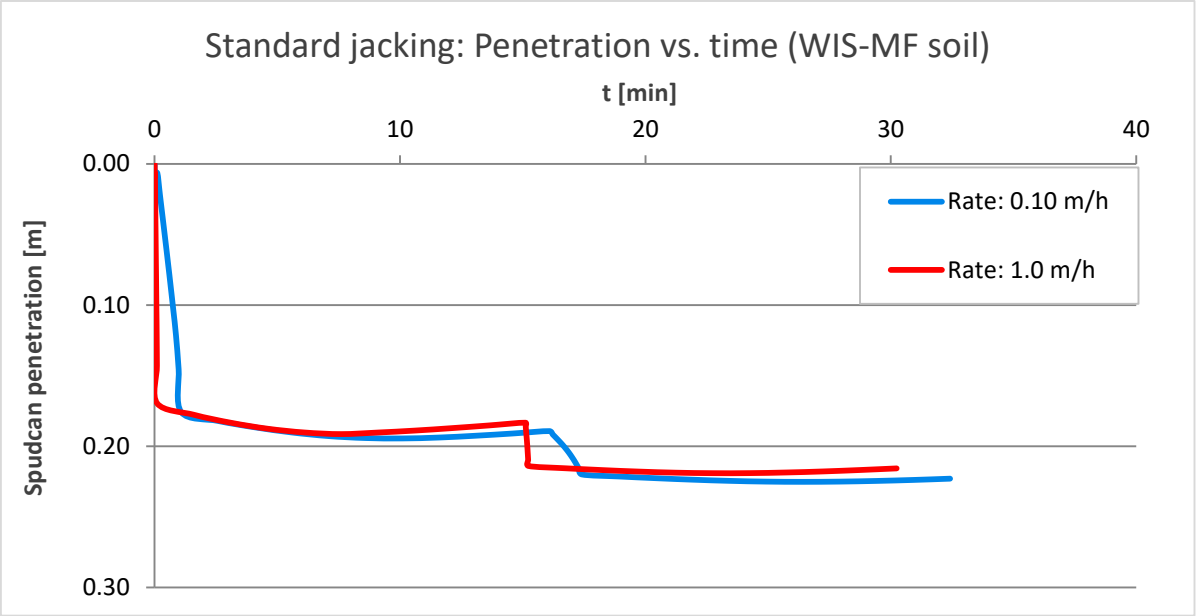

Figure J.5 Standard jacking spudcan penetrations for WIS-MF soil.

WIS-MF soil: overshooting jacking procedure

It is noted that for both spudcan penetration rates, the overshooting jacking procedure is still beneficial in terms of required preloading time. From figure J.6 and J.8, it can be seen that the required preloading criterion is reached earlier when the overshooting method is applied. In terms of spudcan settlements (figure J.7 and J.9), a slightly larger spudcan penetration is found for the relatively slow spudcan penetration rate of 0.10 m/h. Yet, this difference is marginal, as the material is relatively stiff. The difference in spudcan penetration becomes larger for weaker materials, as elaborated next.

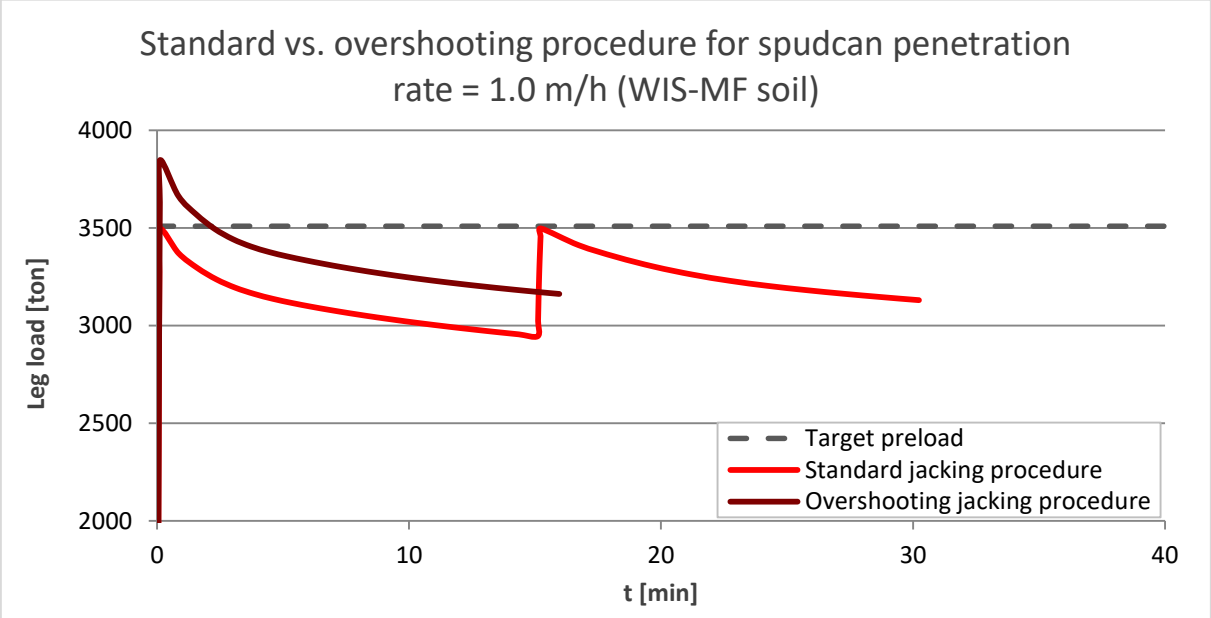

Figure J.6 Overshooting jacking procedure for fast spudcan penetration rate (WIS-MFsoil).

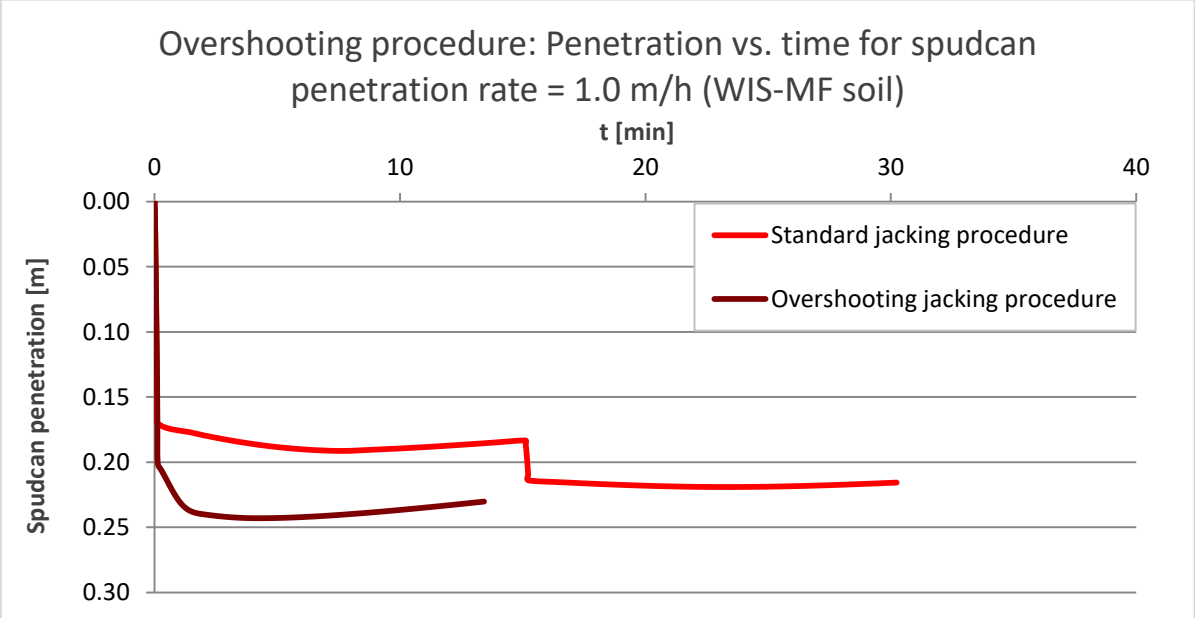

Figure J.7 Overshooting spudcan penetrations for fast spudcan penetration rate (WIS-MF soil).

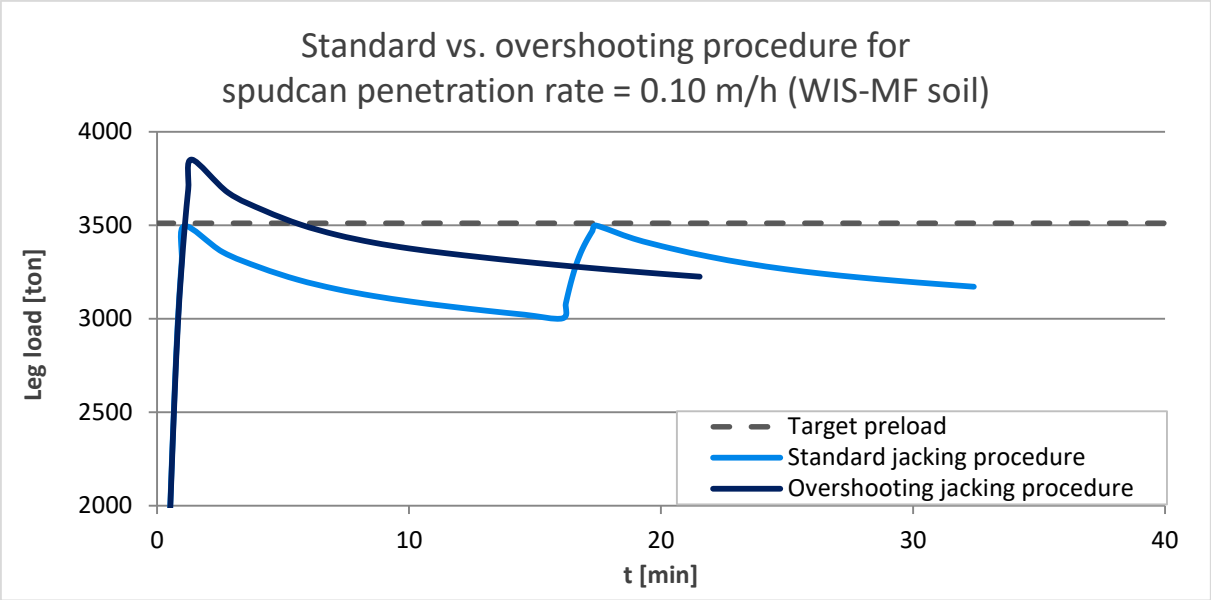

Figure J.8 Overshooting jacking procedure for slow spudcan penetration rate (WIS-MFsoil).

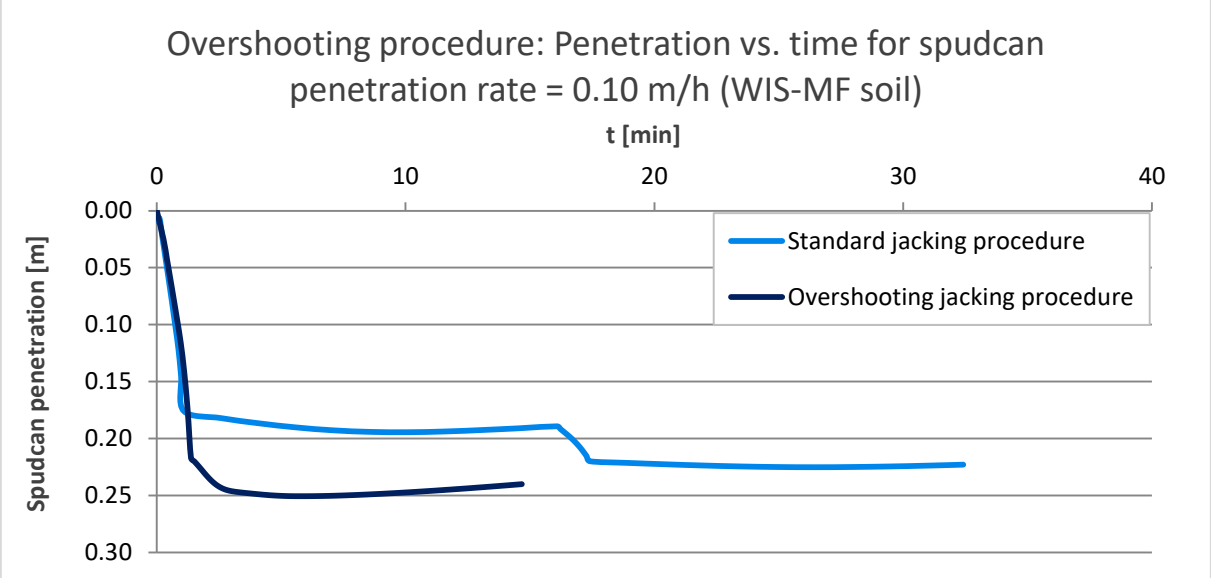

Figure J.9 Overshooting spudcan penetrations for slow spudcan penetration rate (WIS-MF soil).

Softer soil: standard jacking procedure

Considering a decrease in soil stiffness, the stiffness parameters, λ^* and κ^* (and correspondingly the modified creep index parameter μ^*), of the SSF-SBD soil are multiplied by a factor 2, in order to simulate a more clayey, and thus softer material. All other material parameters are unaltered. An overview of this softer soil is given in table J.1.

In this softer, clayey material, the leg load reduces significantly for the relatively faster spudcan penetration rate of 1.0 m/h. This means that the viscous resistances dominate and multiple preload cycles are required in order to reach the preload criterion. When applying a slower spudcan penetration rate, it initially takes a little longer time before reaching the target preload value. However, as the viscous resistance term is smaller for slower strain rates, the reduction in leg load during each preload cycle is less and thus, only two cycles are needed to reached to preload criterion (figure J.10). That means, a reduction in preload time is gained for slower spudcan penetration rates. No difference in terms of spudcan penetrations are found, as seen in figure J.11.

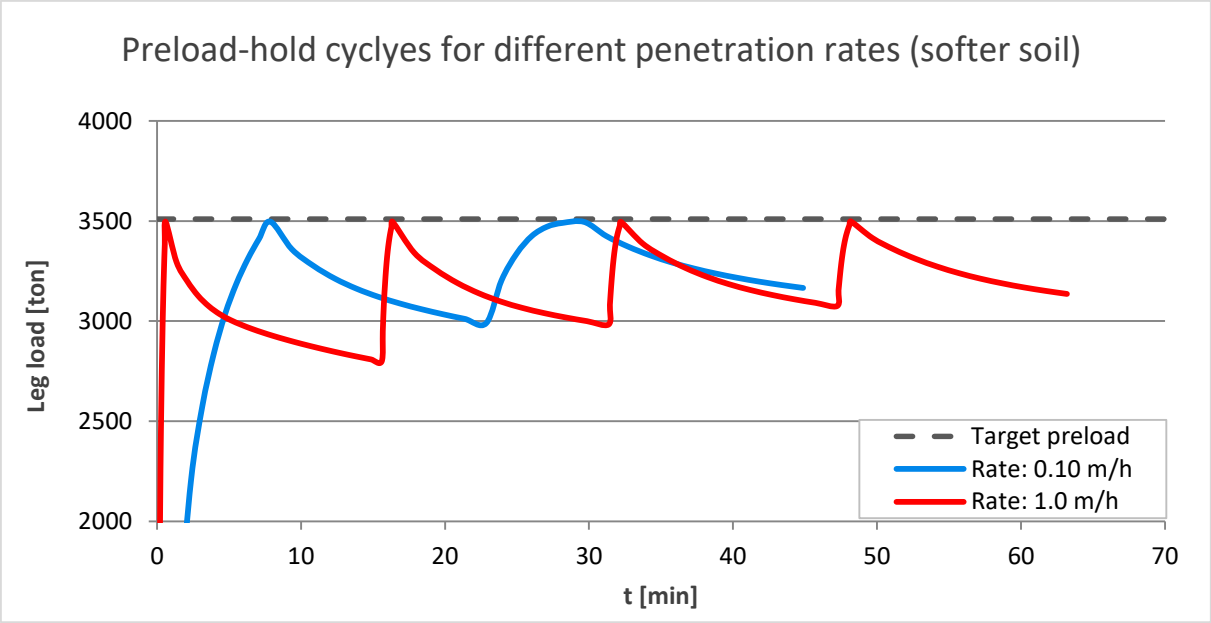

Figure J.10 Standard jacking procedure for softer soil.

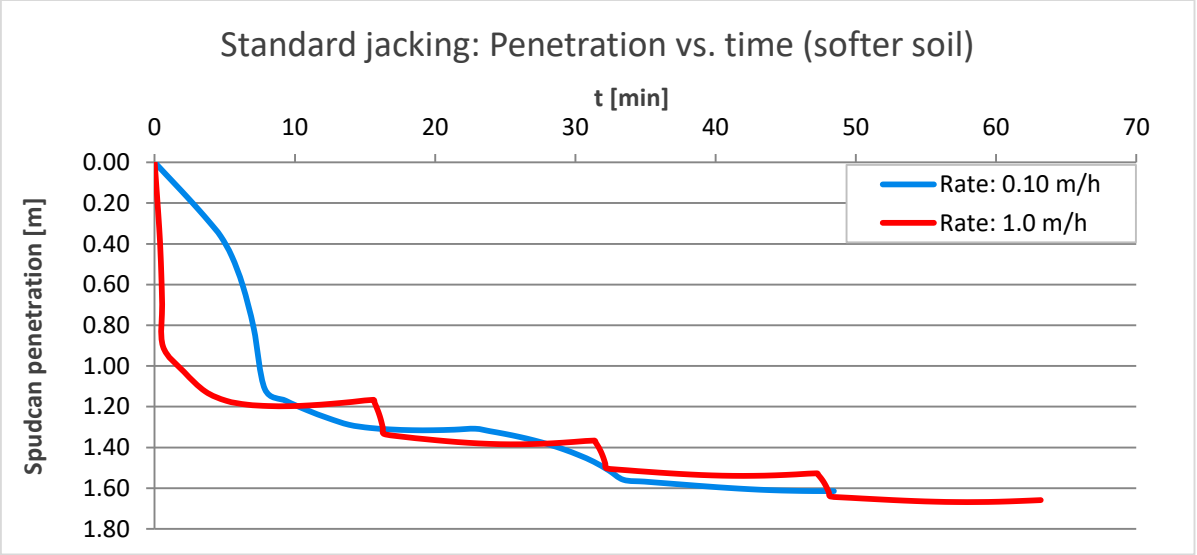

Figure J.11 Standard jacking spudcan penetrations for softer soil.

Softer soil: overshooting jacking procedure

When using the overshooting jacking procedure, significant time savings are gained for both the slow and fast spudcan penetration rate, as the preload criterion is reached much earlier relative to the standard jacking procedure. In the overshooting method, no additional preload cycles have to be followed, which reduces the total preload time considerably.

In terms of spudcan settlements, however, there is actually a difference in soil behaviour between both spudcan penetration rates. When using the fast spudcan penetration rate of 1.0 m/h, the spudcan is initially brought to a larger depth, which would have been reached by the creep-like additional penetrations. For the slower spudcan penetration rate of 0.10 m/h, the viscous resistances are of less importance and thus, overshooting would lead to additional penetrations under the influence of the additional load.

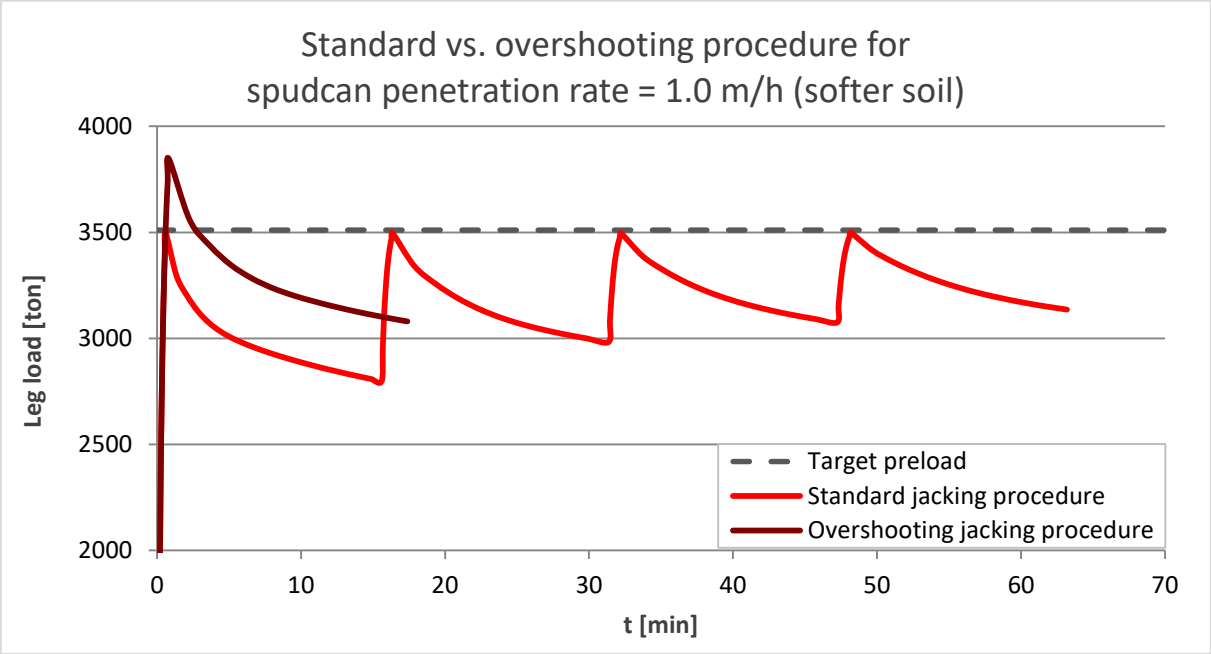

Figure J.12 Overshooting jacking procedure for fast spudcan penetration rate (softer soil).

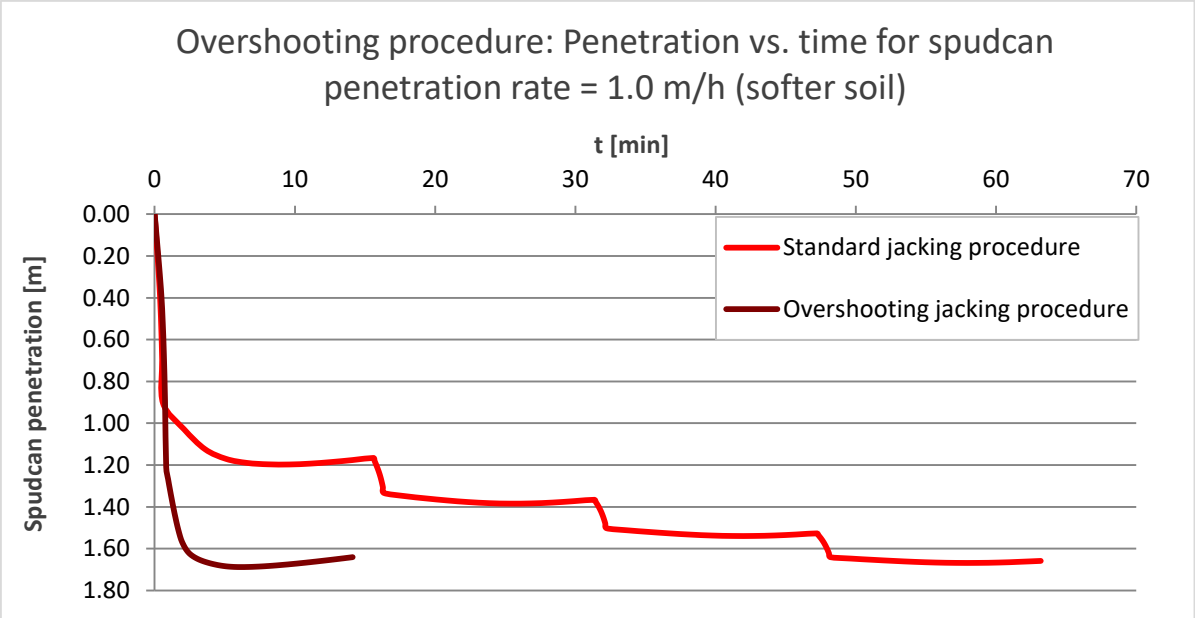

Figure J.13 Overshooting spudcan penetrations for fast spudcan penetration rate (softer soil).

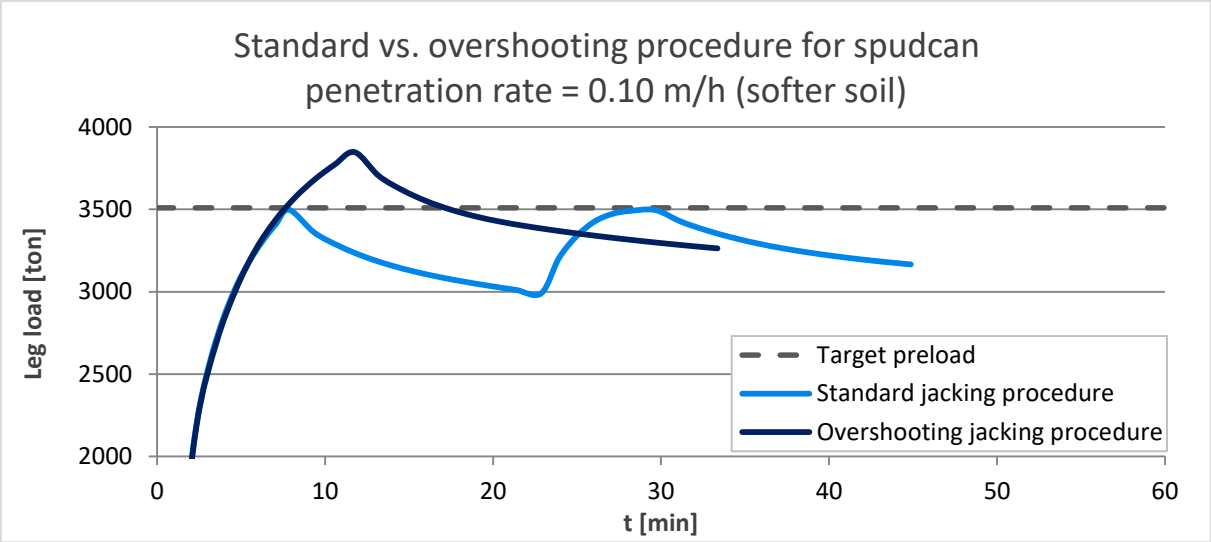

Figure J.14 Overshooting jacking procedure for slow spudcan penetration rate (softer soil).

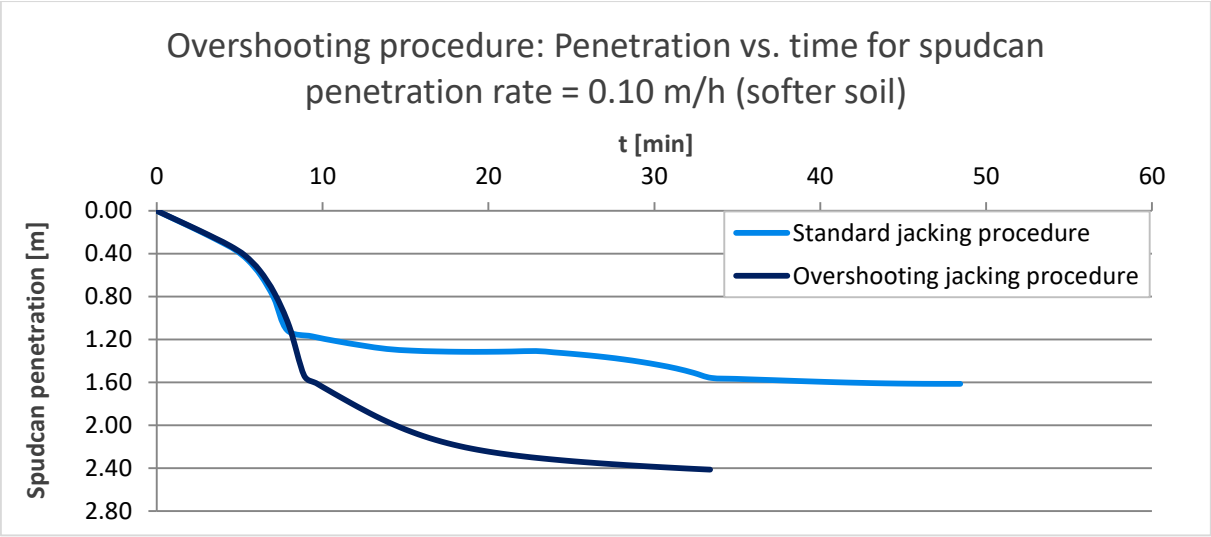

Figure J.15 Overshooting spudcan penetrations for slow spudcan penetration rate (softer soil).

Conclusions sensitivity analysis

The degree of permeability has an effect on the soil behaviour during preloading. The larger the soil permeability, the larger will be the degree of consolidation during the 15 minutes waiting cycles. This effect is largest for permeability values in the order of $10^{-6}\ cm/s$, which is close the permeability of very fine sands. As a result, larger spudcan penetration will occur, as more water is able to dissipate the soil. For increasing values of permeability, the soil becomes almost impervious and the soil behaviour can be considered unaffected by its permeability. The solution converges towards a similar solution.

Considering the soil stiffness, for stiffer materials, the required preloading time and the amount of spudcan penetrations in the standard jacking procedure is unaffected by the spudcan penetration rate, because the frictional resistances rather than the viscous resistances dominate. Contrary, for softer materials, the viscous resistance term is of greater importance and time savings can be gained by applying a slower spudcan penetration rate.

For any given soil, the overshooting method is beneficial in terms of time savings. However, this method leads to larger spudcan settlements for slower spudcan penetration rates, as there is a smaller contribution of viscous soil resistances.